

12/10/76

CHELATE CONFORMATION IN METAL COMPLEXES

A thesis submitted for the degree of  
Doctor of Philosophy

by RODNEY JAMES GEUE, B.Sc. (Hons.)

Department of Physical and Inorganic Chemistry  
The University of Adelaide

September 1975

<u>CONTENTS</u>	Page
SYNOPSIS	v
DECLARATION	vii
ACKNOWLEDGEMENTS	viii
INTRODUCTION	1
LIGAND TERMINOLOGY	9
<u>CHAPTER 1.</u> THE CRYSTAL STRUCTURE OF $(-)$ <sub>589</sub> - <i>S,S</i> -6,9-DIAZA-2,13-DITHIATETRADECANE-5,10-DICARBOXYLATO-COBALT(III) PERCHLORATE	13
1.1 ABSTRACT	13
1.2 PREAMBLE	13
1.3 EXPERIMENTAL AND DATA REDUCTION	17
1.4 REFINEMENT TERMINOLOGY	20
1.5 STRUCTURE SOLUTION AND REFINEMENT	23
1.6 TABLES AND PERSPECTIVE PROJECTIONS	25
1.7 STRUCTURAL FEATURES AND DISCUSSION	26
<u>CHAPTER 2.</u> THE CRYSTAL STRUCTURE OF BIS-(DIHYDRO-1 <i>H</i> ,3 <i>H</i> ,5 <i>H</i> -OXAZOLO[3,4- <i>c</i> ]OXAZOLE-7 <i>a</i> -CARBOXYLATO)COPPER(II)	40
2.1 ABSTRACT	40
2.2 PREAMBLE	40
2.3 EXPERIMENTAL AND DATA REDUCTION	43
2.4 STRUCTURE SOLUTION AND REFINEMENT	45
2.5 TABLES AND PERSPECTIVE PROJECTIONS	48

	Page
2.6 STRUCTURAL FEATURES AND DISCUSSION	48
<u>CHAPTER 3.</u> THE CRYSTAL STRUCTURE OF (+) <sub>589</sub> -BIS-(1,1,1-TRIS(AMINO-METHYL)ETHANE)COBALT(III) CHLORIDE (+) <sub>589</sub> -R,R-TARTRATE PENTAHYDRATE	72
3.1 ABSTRACT	72
3.2 EXPERIMENTAL AND DATA REDUCTION	73
3.3 STRUCTURE SOLUTION AND REFINEMENT	82
3.4 TABLES AND PERSPECTIVE PROJECTIONS	87
3.5 STRUCTURAL FEATURES AND DISCUSSION	88
<u>CHAPTER 4.</u> CORRELATION OF ABSOLUTE CONFIGURATION AND SIGNED ROTATORY STRENGTH IN DISSYMMETRIC Co(III) COMPLEXES	117
4.1 INTRODUCTION	117
4.2 OPTICAL ACTIVITY AND ROTATORY POWER	125
4.3 THE PIPER-KARIPÉDES THEORY FOR $D_3$ Co(III)L <sub>6</sub> CHROMOPHORES	129
4.3.1 The Crystal Field Model	132
4.3.2 Application to $\lambda\lambda$ -[Co(tame) <sub>2</sub> ] <sup>3+</sup>	137
4.4 THE RICHARDSON THEORY FOR DISSYMMETRIC Co(III) COMPLEXES	148
4.4.1 The Crystal Field Model for $D_3$ Complexes	150
4.4.2 Application to $\lambda\lambda$ -[Co(tame) <sub>2</sub> ] <sup>3+</sup>	155
<u>CHAPTER 5.</u> CONFORMATIONAL ANALYSIS OF METAL COMPLEXES	169
5.1 INTRODUCTION	169
5.2 ENERGY REPRESENTATION AND FORCE FIELD	173

	Page
5.3 THE MOLECULAR ENERGY MINIMIZATION PROCEDURE	182
5.4 THE REFINEMENT OF SYMMETRIC MOLECULES	189
5.4.1 Energy Minima and Saddle-points of Symmetric Configurations	190
5.4.2 Symmetry-dependent Refinement	193
5.4.3 Evasion of Saddle-point Convergence	197
5.5 ENERGY MINIMIZATION RESULTS AND DISCUSSION	200
5.5.1 Conformers of $[\text{Co}(\text{tame})_2]^{3+}$	201
5.5.2 Symmetric Conformers of $[\text{Co}(\text{tn})_3]^{3+}$	217
5.5.3 Chair Conformers of $[\text{Co}(\text{tn})_2\text{CO}_3]^+$	234
5.5.4 Discussion of the Geometric Isomers of $[\text{Co}(\text{dien})_2]^{3+}$	251
 <u>CHAPTER 6. ENERGY MINIMIZED CONFIGURATIONS AND THEIR SIGNED</u>	
ROTATORY STRENGTHS	258
6.1 INTRODUCTION	258
6.2 COMPARISON OF OBSERVED AND CALCULATED DATA	262
6.3 CONCLUDING DISCUSSION	274
 <u>APPENDICES</u>	
I CATALOGUE OF COMPUTER PROGRAMS	280
II MODIFICATIONS TO BOYD'S ENERGY MINIMIZATION PROGRAM	283
III SUPPLEMENTARY INFORMATION ON THE STRUCTURE ANALYSES	288
 <u>BIBLIOGRAPHY</u>	
	290



SYNOPSIS

The experimental investigation of chelate conformation included the determination of three crystal structures by X-ray analysis. The structures of  $(-)_589$ -*S,S*-6,9-diaza-2,13-dithiatetradecane-5,10-dicarboxylato-cobalt(III) perchlorate,  $[\text{Co}(\text{C}_{12}\text{H}_{22}\text{N}_2\text{O}_4\text{S}_2)]\text{ClO}_4$ , bis-(dihydro-1*H*,3*H*,5*H*-oxazolo[3,4-*c*]oxazole-7*a*-carboxylato)copper(II),  $\text{Cu}(\text{C}_6\text{H}_8\text{NO}_4)_2$ , and  $(+)_589$ -bis-(1,1,1-tris(aminomethyl)ethane)cobalt(III) chloride  $(+)_589$ -*R,R*-tartrate pentahydrate,  $(+)_589$ - $[\text{Co}(\text{C}_5\text{H}_{15}\text{N}_3)_2\text{Cl}-(+)_589$ - $(\text{C}_4\text{H}_4\text{O}_6) \cdot 5.4\text{H}_2\text{O}$  were determined and refined by full matrix least-squares techniques to conventional *R* indices of 0.060, 0.038 and 0.025 respectively. The absolute configuration of the complex cation in the first structure was designated skew chelate pairs,  $\Lambda\Lambda\Lambda$ . In the third structure, the helicity of the complex cation is a function of the ring conformations only and the absolute configuration was designated  $\lambda\lambda$ .

The  $\lambda\lambda$ -bis-(1,1,1-tris(aminomethyl)ethane)cobalt(III) ion was observed to have quasi- $D_3$  symmetry in the crystal, and parameters indicating the distortion of the mean  $D_3$  chromophore from  $O_h$  symmetry were computed from the crystal geometry. The signs of the *net* rotatory strengths of this ion for the  ${}^1A_{1g} \rightarrow {}^1T_{1g}$  and  ${}^1A_{1g} \rightarrow {}^1T_{2g}$  octahedral transitions were estimated by application of the one-electron static coupling model of Richardson for dissymmetric six-coordinate cobalt(III) complexes with  $D_3$  symmetry. The observed *net* rotatory strength for the complete manifold of *d-d* transitions was large and similar in sign to that predicted, and the model is empirically verified.

The molecular conformational analysis procedure of Boyd, based on the mathematical minimization of potential energy by a Newton-Raphson technique, has been extended to allow the exceptionally fast refinement of molecules possessing one or more symmetry elements in their final configurations. An artifice for evading symmetry saddle-points was also devised. Conformational mechanics was applied to the conformational isomers of bis-(1,1,1-tris(aminomethyl)ethane)cobalt(III), the symmetric conformers of tris-(1,3-diaminopropane)cobalt(III) and the chair configurations of *cis*-carbonatobis-(1,3-diaminopropane)-cobalt(III). Computations on these molecules, supplemented by other examples, verified the symmetry refinement procedure.

Finally, a qualitative assessment of the validity of applying energy minimized molecular configurations of metal complexes to the correlation between absolute configuration and the sign of the observed *d-d* transition rotatory strength, was effected. It is suggested that the agreement between observed and calculated data is generally sufficiently good to permit such applications.

DECLARATION

This thesis is founded on research undertaken by the candidate in the Department of Physical and Inorganic Chemistry at the University of Adelaide unless asserted otherwise.

To the best of the candidate's knowledge the text contains no material written or devised by another person, except where an appropriate reference is made. No work in the thesis has previously been submitted by the candidate for the award of any other degree.

The author accepts full responsibility for any errors present in the treatise, regardless of their nature.

Rodney Geue

September 1975

ACKNOWLEDGEMENTS

I extend genuine gratitude to my supervisor, Dr. M.R. Snow, who through his unflinching interest and patronising attitude, has contributed significantly to the essence of this research.

I sincerely thank Dr. M. Dwyer for his collaboration and encouragement in developments of the mechanics of conformational analysis and for the innumerable stimulating discussions which resulted therefrom. I am also indebted to Dr. G.B. Robertson of the Research School of Chemistry at the Australian National University, Canberra, for the collection of a set of diffractometer data.

Professors D.O. Jordan and D.R. Stranks have my gratitude for their acceptance of myself as a research student in the Department of Physical and Inorganic Chemistry.

I wish to thank the Department of Education and Science for supporting me with a Commonwealth Postgraduate award for the period of this work. My thanks are also due to the staff of the Computing Centre of the University of Adelaide for the continual use of their facilities. I acknowledge the use of computing facilities of the CSIRO Department of Computing Science and thank their staff who assisted in the development of control routines for the manipulation of paper tapes.

My final appreciation is directed to Mrs. Del Hewish who typed the manuscript.

## INTRODUCTION

The study of the conformations of coordinated chelates in transition metal complexes has soared in recent years.<sup>1-3</sup> Much of the current interest stems from the theoretical treatment of energetically preferred ring conformations in complex ions by Corey and Bailar,<sup>4</sup> and the experimental confirmation of their results by the equilibrium studies of Dwyer and co-workers<sup>5-8</sup> on the cobalt(III) complexes of ethylenediamine and (*R,S*)<sup>9</sup> propylenediamine. These works revealed the importance of steric interactions in establishing potential energy differences between conformers, and so, in effecting the stereospecific coordination of optically active chelates to transition metals. The concept of preferred chelate conformations and conformational analysis in metal chelate systems thus evolved.

Knowledge of conformer geometries and relative energies has since contributed immensely to the understanding of phenomena in many areas of metal chelate chemistry. Such knowledge has often been instrumental in the assignment of absolute configurations to components of equilibrium mixtures in which the ligands coordinate stereospecifically. Tris-bidentate complexes with both five and six-membered chelate rings, *e.g.* cobalt(III) complexes of ethylenediamine and (*R,S*)propylenediamine<sup>1,5,6,8</sup> and of (*RR,SS*)2,4-diaminopentane,<sup>10</sup> have been assigned absolute configurations on the basis of the known configurations of the optically active ligands, and these were supported by the solution  $d-d$  circular dichroism (CD) spectra of the complexes.<sup>10-12</sup> They have also been confirmed by several X-ray analyses<sup>13-17</sup> in which the effects of

the anomalous dispersion of X-rays<sup>18,19</sup> were used to determine the absolute configurations. Conformational energy differences have aided the interpretation of stereospecific influences in other tris-bidentate and polydentate complex<sup>1,20-24</sup> systems in addition to providing tentative assignments of complex or ligand configurations.

Nuclear magnetic resonance spectroscopy (NMR) has furnished considerable information on chelate ring conformation in solution. The tris-ethylenediamine complexes of several transition metals were studied extensively by NMR techniques<sup>25-28</sup> and rapid interchange between the  $\lambda$  and  $\delta$ <sup>29</sup> skew conformations of the chelate rings was evident in these studies. The equilibrium population ratios for the  $\delta \rightleftharpoons \lambda$  inversion were determined from effective chemical shift differences<sup>25,30</sup> and intra-ligand coupling constants.<sup>26,27</sup> An estimate of the relative standard free energies of the  $\Lambda(\delta\delta\delta)$  and  $\Lambda(\delta\delta\lambda)$ <sup>29</sup> conformers of tris-(ethylenediamine)cobalt(III) indicated the prevalence of the  $\Lambda(\delta\delta\lambda)$  conformer in solution.<sup>27</sup> Similar results were obtained for other tris-ethylenediamine complexes in solution,<sup>25,26</sup> and the  $\delta$  conformer was found to be stabilized over the  $\lambda$  conformer in the  $\Lambda$  configuration by 0.3-0.6 kcal mol<sup>-1</sup>, depending on the size of the metal atom. The prevalence of the  $\Lambda(\delta\delta\lambda)$  complex conformer was ascribed to a statistical preference for this isomer.<sup>25,27</sup> In interpreting the NMR spectra, it was necessary to assume that the  $\lambda$  and  $\delta$  ring conformers were present in solution and that the  $\Lambda(\delta\delta\delta)$  species was more stable than the  $\Lambda(\lambda\lambda\lambda)$  one.<sup>26,27</sup> The above conclusions are in agreement<sup>3,27,28</sup> with those determined for tris-(ethylenediamine)cobalt(III) conformer

proportions from the equilibrium data of Dwyer *et al.*<sup>6</sup> when the statistical entropy effect<sup>7</sup> is realized. Complexes of 2,4-diaminopentane,<sup>10,31</sup> 1,3-diaminopropane<sup>31,32</sup> and other six-membered ring complexes<sup>31,33</sup> studied by NMR methods, have all required an appreciation of the nature and stability of the possible conformational isomers present in solution for the analysis of their spectra.

The profound influence of ring conformation on the CD spectra of transition metal complexes is well exemplified in both bidentate<sup>12,34-36</sup> and polydentate<sup>21,37</sup> chelate complex systems. This effect was thought<sup>12,34,35</sup> to be especially important in the charge transfer region of the CD spectrum, and rules were devised for making assignments of conformation from the contributions of known rigid conformers in this region. However, the variable temperature study of the tris-(1,3-diaminopropane)cobalt(III) system in solution<sup>36</sup> has indicated the importance of conformational contributions in the visible CD spectral region. In fact it was argued<sup>15,38</sup> that the tris-(chair) and tris-(skew boat) conformers in this system had oppositely signed rotatory strengths for the same electronic transition and absolute configuration of the complex ion. This explanation was based on the solid state KBr disc spectrum<sup>36</sup> of the tris-(chair) complex, the single crystal CD spectrum<sup>39</sup> of  $\Delta(+)$ -tris-(1,3-diaminopropane)cobalt(III) chloride tetrahydrate, and the solution CD spectra of the conformationally rigid tris-(2,4-diaminopentane)cobalt(III) complex ions.<sup>10</sup> In these investigations, the knowledge of CD contributions from known conformers was correlated with the knowledge of the energetically favoured conformers

of the tris-(1,3-diaminopropane)cobalt(III) ion in solution, to yield an interpretation of the solution CD spectrum in terms of a conformational equilibrium. Here again information on conformer geometries and energies has proved to be of cardinal importance in the analysis of solution spectra.

Much of the data on metal chelate conformational geometries has derived from one or both of two sources. The solid state data, obtained by X-ray or neutron structural analysis, is essential for the direct observation of conformer configuration, *e.g.* the puckered nature of five<sup>40-42</sup> and six-membered<sup>16,17,43</sup> metal-diamine rings and the relatively flat metal- $\alpha$ -amino acidato rings.<sup>44</sup> Although this technique gives no explicit information on the conformers present in solution, it may, when combined with CD spectral analysis of both the known solid state conformers and the complex in solution, lead to an interpretation of the solution spectrum in terms of contributions from the various conformers.<sup>36,38</sup> If there are strong specific interactive forces, *e.g.* hydrogen bonds or van der Waals repulsion forces present in the crystal, the detailed conformer geometry in the solid state may differ from that in solution<sup>4</sup> or in other crystalline environments. Energetically unfavourable conformers<sup>45,46</sup> may also be stabilized by crystal force fields<sup>47</sup> or strongly hydrogen-bonding solvents.<sup>41</sup>

The detailed geometries and relative energies of the conformations of individual complex molecules may now be acquired with adequate reliability by theoretical techniques<sup>2,3,48-51</sup> far more advanced, but similar in purpose to the original calculations of Corey and Bailar.<sup>4</sup> The methods involve adjustment of the conformer geometry to determine the



configuration of minimum potential energy, an idea extensively developed in organic chemistry,<sup>52</sup> but only recently<sup>48-50</sup> applied to transition metal complex systems. The actual method of minimization has varied widely.<sup>48-51</sup> The most reliable and powerful of these techniques<sup>48,49</sup> involve the solution of a set of simultaneous equations in the independent molecular coordinates.<sup>53,54</sup> These equations define the inter-coordinate relationships existing at the minimum energy configuration. Search techniques<sup>52,55</sup> have proved less reliable for metal chelate complexes because of the large number of independent variables, and their convergence to local minima,<sup>51,52</sup> rather than the lowest point on the energy surface associated with a given conformational isomer. These difficulties do not arise in iterative minimization,<sup>52,56,57</sup> and for a chemically reasonable initial coordinate set, convergence is also more efficient than for search techniques.<sup>54,58,59</sup> A potential energy surface mapping procedure<sup>50</sup> has also been used to determine the configurations and energies of metal chelate conformers. The independent variables employed in this technique,<sup>50,60-62</sup> however, have been limited to a few selected parameters defining the metal chelate ring backbone. This was necessary to alleviate the enormous computational load associated with the procedure.

In this work, the crystal structure of  $(-)_589\text{-[Co}(S,S\text{-ebm)]ClO}_4^\dagger$  was first determined to elucidate the stereospecific coordination of  $S,S\text{-ebm}$  and to investigate the conformational preference of six-membered chelate rings containing sulphur. The disposition of the five-membered

---

<sup>†</sup> ligand terminology is described on page 9.

cobalt-amino-acidato rings with respect to the cobalt-diamine ring was also considered to be of interest in relation to the observed<sup>63,64</sup> relative strains of axially and equatorially arranged cobalt-amino-acidato rings in  $[\text{Co}(\text{EDTA})]^-$ .<sup>†</sup> A preliminary account of the structure has been published as a technical report.<sup>65</sup>

The complex  $\text{Cu}(\text{dioxc})_2$ <sup>†</sup> at first aroused interest through the suggested<sup>66</sup> presence of a six-membered, unsaturated copper-diamine chelate ring. This was predicted<sup>66</sup> from the synthetic procedure and the information then available on the system. Subsequent solution of the crystal structure indicated this to be untrue, but the novel attachment of four oxazolidine rings to the copper-amino-carboxylato rings and the crystallographically induced square pyramidal geometry of the complex stimulated the continuation and completion of the refinement. This also established the synthetic mechanism<sup>66</sup> and a preliminary note on the mechanistic details and the structure of the complex was published.<sup>67</sup>

As previously intimated, the importance of chelate ring conformation in relation to the visible CD spectra of metal chelate complexes is well illustrated, especially with regard to the saturated diamine complexes of cobalt(III).<sup>12,21,36</sup> However, this conformational effect has only been observed when associated with configurational and/or vicinal dissymmetry. The complex ion  $\text{Co}(\text{tame})_2$ <sup>3+†</sup>, if resolved into enantiomeric conformers, would owe its dissymmetry solely to the conformation of the chelate rings. Furthermore, the CD of the quasi- $D_3$  symmetric complex

---

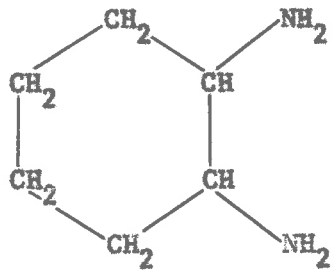
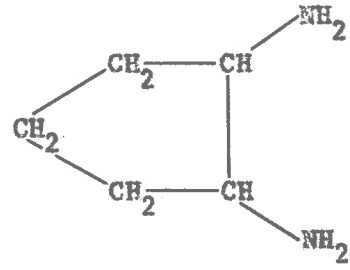
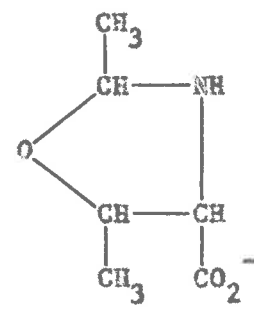
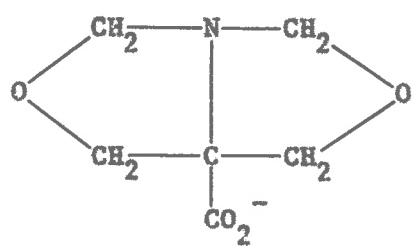
<sup>†</sup> ligand terminology is described on page 9.

would afford a novel test for the visible CD spectral theories of Piper and Karipades<sup>68,69</sup> and of Richardson,<sup>70-72</sup> if correlated with the observed conformation. Most of the previous theoretical correlations of CD with absolute configuration of  $D_3$  metal complexes were applied to tris-bidentate examples<sup>15,68-73</sup> in which the chelate ring atoms had polar dispositions<sup>15</sup> (with respect to the  $C_3$  axis and the metal origin) intermediate to those of the ligators. With these forethoughts, the preparation and X-ray crystal structural analysis of  $[\text{Co}(\text{tame})_2]\text{Cl}\cdot R,R\text{-tartrate}$  were undertaken. In this crystal the  $\text{Co}(\text{tame})_2^{3+}$  ion appears as the dissymmetric  $\lambda\lambda^{29}$  conformer (see Chapter 3). The solid state CD disc spectrum of the compound was also recorded for the above purposes.

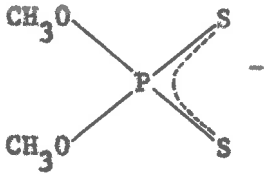
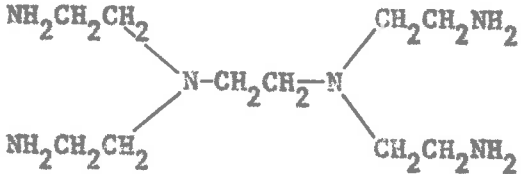
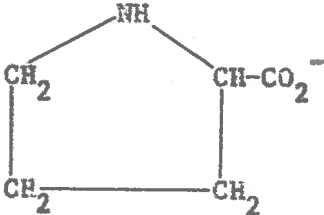
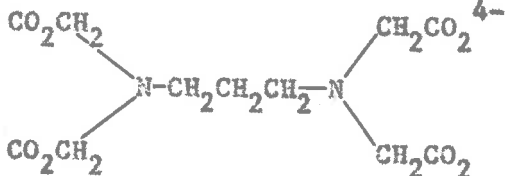
The detailed molecular geometries and relative energies of conformers of  $[\text{Co}(\text{tame})_2]^{3+}$ ,  $[\text{Co}(\text{tn})_3]^{3+}$  and  $[\text{Co}(\text{tn})_2\text{CO}_3]^+$  were determined by the energy minimization technique of Boyd<sup>54</sup> which was applied to metal chelate complexes by Snow<sup>48</sup> and Buckingham *et al.*<sup>49</sup> The purpose of this was two fold. Firstly, the conformers were employed as trial molecules in the extension of the Boyd method to the fast refinement of molecules with symmetry minima. Several results on the conformational analysis of the geometric isomers of  $[\text{Co}(\text{dien})_2]^{3+}$ <sup>74,75</sup> were also used in this respect. A paper on this symmetry refinement technique has been published.<sup>56</sup> In addition, the computations were designed to assess the predictive worth and reliability of the minimization procedure for six-membered metal-diamine ring complexes, and to obtain an estimate of the magnitude of lattice distortions in

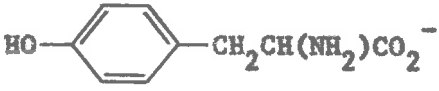
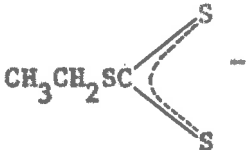
crystals of the conformers. These features are of interest in relation to the merits of using computed geometries for correlation between the sign of the CD spectrum and the absolute configuration of the complex, and if the chirality of the isomer is known, for testing correlation theories. Conformational calculations on the above trimethylene-diamine complexes and an analysis of conformer stabilities has been published.<sup>76</sup> The structure of one of these complexes, *cis*-[Co(tn)<sub>2</sub>CO<sub>3</sub>]<sup>+</sup>, also published in this paper, was determined prior to the work of this thesis.

LIGAND TERMINOLOGY

<i>Symbol</i>	<i>Systematic or Trivial Name</i>	<i>Structural Formula</i>
$\alpha$ -ala	alaninate	$\text{CH}_3\text{CH}(\text{NH}_2)\text{CO}_2^-$
asp	aspartate	$\text{CO}_2\text{CH}_2\text{CH}(\text{NH}_2)\text{CO}_2^{2-}$
bn	2,3-diaminobutane	$\text{CH}_3\text{CH}(\text{NH}_2)\text{CH}(\text{NH}_2)\text{CH}_3$
chxn	1,2-diaminocyclohexane	
cptn	1,2-diaminocyclopentane	
dien	diethylenetriamine	$\text{NH}_2\text{CH}_2\text{CH}_2\text{NHCH}_2\text{CH}_2\text{NH}_2$
dimgly	<i>N,N</i> -dimethylglycinate	$\text{N}(\text{CH}_3)_2\text{CH}_2\text{CO}_2^-$
dimoxc	2,5-dimethyloxazolidine-4-carboxylate	
dioxc	dihydro-1 <i>H</i> ,3 <i>H</i> ,5 <i>H</i> -oxazolo[3,4- <i>c</i> ]-oxazole-7 <i>a</i> -carboxylate	

Symbol	Systematic or Trivial Name	Structural Formula
dtc	<i>N,N</i> -diethyldithiocarbamate	$\text{N}(\text{C}_2\text{H}_5)_2\text{C} \begin{array}{l} \diagup \text{S} \\ \diagdown \text{S} \end{array}^-$
ebm	6,9-diaza-2,13-dithia-tetradecane-5,10-dicarboxylate	$\begin{array}{c} \text{CO}_2 \\ \diagdown \\ \text{CH}-\text{NHCH}_2\text{CH}_2\text{NH}-\text{CH} \\ \diagup \quad \quad \quad \diagdown \\ \text{CH}_3\text{SCH}_2\text{CH}_2 \quad \quad \quad \text{CH}_2\text{CH}_2\text{SCH}_3 \\ \text{CO}_2^{2-} \end{array}$
EDDS	<i>N,N'</i> -ethylenediamine-disuccinate	$\begin{array}{c} \text{CO}_2 \\ \diagdown \\ \text{CH}-\text{NHCH}_2\text{CH}_2\text{NH}-\text{CH} \\ \diagup \quad \quad \quad \diagdown \\ \text{CO}_2\text{CH}_2 \quad \quad \quad \text{CH}_2\text{CO}_2 \\ \text{CO}_2^{4-} \end{array}$
EDTA	<i>N,N,N',N'</i> -ethylenediamine-tetra-acetate	$\begin{array}{c} \text{CO}_2\text{CH}_2 \\ \diagdown \\ \text{N}-\text{CH}_2\text{CH}_2-\text{N} \\ \diagup \quad \quad \quad \diagdown \\ \text{CO}_2\text{CH}_2 \quad \quad \quad \text{CH}_2\text{CO}_2^{4-} \\ \text{CH}_2\text{CO}_2 \end{array}$
en	1,2-diaminoethane	$\text{NH}_2\text{CH}_2\text{CH}_2\text{NH}_2$
exan	<i>O</i> -ethylxanthate	$\text{CH}_3\text{CH}_2\text{OC} \begin{array}{l} \diagup \text{S} \\ \diagdown \text{S} \end{array}^-$
gly	glycinate	$\text{NH}_2\text{CH}_2\text{CO}_2^-$
Gly-Met	<i>N</i> -glycylmethioninate	$\begin{array}{c} \text{NH}_2\text{CH}_2\text{CO}-\text{NH} \\ \diagdown \\ \text{CH}-\text{CO}_2^- \\ \diagup \\ \text{CH}_3\text{SCH}_2\text{CH}_2 \end{array}$

<i>Symbol</i>	<i>Systematic or Trivial Name</i>	<i>Structural Formula</i>
Meth	methionine	$\text{CH}_3\text{SCH}_2\text{CH}_2\text{CH}(\text{NH}_2)\text{CO}_2\text{H}$
mtp	<i>O,O'</i> -dimethyldithiophosphate	
penten	<i>N,N,N',N'</i> -tetrakis(2'-aminoethyl)-1,2-diaminoethane	
pn	1,2-diaminopropane	$\text{CH}_3\text{CH}(\text{NH}_2)\text{CH}_2\text{NH}_2$
pro	prolinate	
ptn	2,4-diaminopentane	$\text{CH}_3\text{CH}(\text{NH}_2)\text{CH}_2\text{CH}(\text{NH}_2)\text{CH}_3$
sen	1,1,1-tris(2'-aminoethylamino-methyl)ethane	$(\text{NH}_2\text{CH}_2\text{CH}_2\text{NHCH}_2)_3\text{CCH}_3$
tame	1,1,1-tris(aminomethyl)ethane	$(\text{NH}_2\text{CH}_2)_3\text{CCH}_3$
tn	1,3-diaminopropane	$\text{NH}_2\text{CH}_2\text{CH}_2\text{CH}_2\text{NH}_2$
trdta	<i>N,N,N',N'</i> -trimethylenediamine-tetraacetate	

<i>Symbol</i>	<i>Systematic or Trivial Name</i>	<i>Structural Formula</i>
tyro	tyrosinate	
xan	<i>S</i> -ethylxanthate	



CHAPTER 1. THE CRYSTAL STRUCTURE OF  $(-)_589$ -*S,S*-6,9-DIAZA-2,13-DITHIATETRADECANE-5,10-DICARBOXYLATO-COBALT(III) PERCHLORATE,  $(-)_589$ -[Co(*S,S*-ebm)]ClO<sub>4</sub>

1.1 ABSTRACT

The structure of  $(-)_589$ -[Co(*S,S*-ebm)]ClO<sub>4</sub> has been determined from 2451 photographically collected reflections. The compound forms monoclinic crystals with space group *C*2 and  $a = 12.34(2)$ ,  $b = 7.94(1)$ ,  $c = 9.46(1)\text{\AA}$ ,  $\beta = 97.45(8)^\circ$  and  $Z = 2$ . The full matrix least-squares refinement of the structure yielded a conventional *R* value of 0.060. The complex cation has crystallographic *C*<sub>2</sub> symmetry. The six-membered chelate rings have distorted chair forms and assume equatorial orientations with respect to the five-membered cobalt-diamine ring which has the  $\delta$  conformation. The absolute configuration of the complex is  $\Lambda\Lambda\Lambda$  with respect to the skew chelate pairs and the cobalt- $\alpha$ -amino-carboxylato rings have the  $\lambda$  conformation. Both the configuration at the nitrogen and that at the sulphur is *R*.

1.2 PREAMBLE

*S,S*-ebm was synthesized from *S*-methionine and 1,2-dibromoethane by Mazurek and Phillip<sup>65,77</sup> according to a method similar to that used for the preparation of *S,S*-EDDS.<sup>78</sup> Both the *S,S*-EDDS<sup>79</sup> and the *S,S*-ebm<sup>65,77</sup> ligands have been shown to act as sexadentate chelates on coordination to cobalt(III). In addition only one optically active isomer has been isolated in the preparation of both the cobalt(III) complex of *S,S*-EDDS<sup>79</sup> and that of *S,S*-ebm.<sup>65,77</sup> Hence both ligands are stereospecific

sexadentate chelating agents for cobalt(III), the donor atom sets being  $N_2O_2S_2$  and  $N_2O_4$  for *S,S*-ebm and *S,S*-EDDS respectively.

When the configuration about the asymmetric carbon atom is *S*, Dreiding molecular models indicate that for each of the above ligands, there are two possible configurational isomers for the cobalt(III) complex.<sup>77,79</sup> (Figure 1.1) In the  $\Lambda\Lambda\Lambda$ <sup>29</sup> or  $\Lambda$  configuration, the six-membered rings span equatorial sites, whereas in the  $\Delta$  configuration they span axial coordination sites with respect to the cobalt-diamine ring. In view of the relatively strained nature of the equatorial five-membered cobalt-glycinato rings of  $[Co(EDTA)]^-$ <sup>63</sup> it was suggested<sup>79</sup> that the  $\Lambda$  configuration would be favoured for  $[Co(S,S-EDDS)]^-$ . Similar strain has been observed in the equatorially disposed five-membered rings of  $[Co(trdta)]^-$ <sup>80</sup> where the metal-diamine ring is six-membered. A recent X-ray structural analysis of a hydrate of  $NH_4-[Co(S,S-EDDS)]$  has revealed<sup>81</sup> the equatorial disposition of the six-membered rings in  $[Co(S,S-EDDS)]^-$ . These observations, correlated with the similarity<sup>77</sup> of the CD spectra of  $Na[Co(S,S-EDDS)]$ <sup>79</sup> and  $(-)_589-[Co(S,S-ebm)]ClO_4$ ,<sup>77</sup> indicate that the complex ion in the latter compound has the  $\Lambda$  configuration with the sulphur atoms occupying *cis* coordination sites. Several close non-bonded contacts in a molecular model of the  $\Delta$  configuration enhance the favourability of  $\Lambda$  for  $[Co(S,S-ebm)]^+$ .

The six-membered chelate rings may adopt the chair, skew-boat or boat conformation in the crystal, although the lower energy chair or skew-boat forms would be favoured in the molecular state unless they

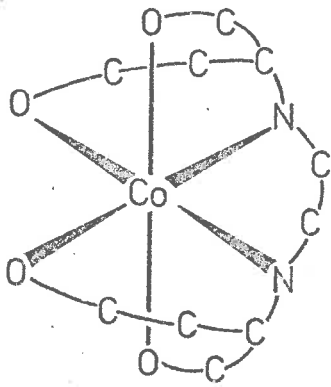
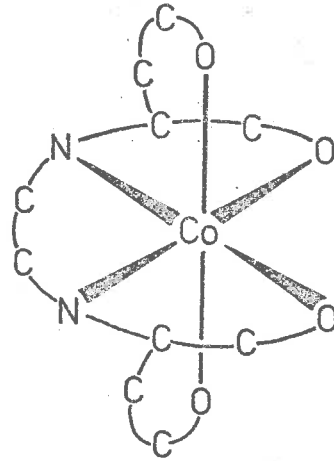
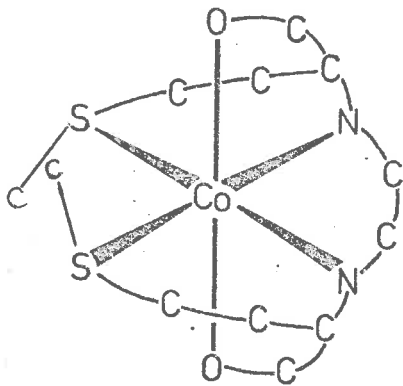
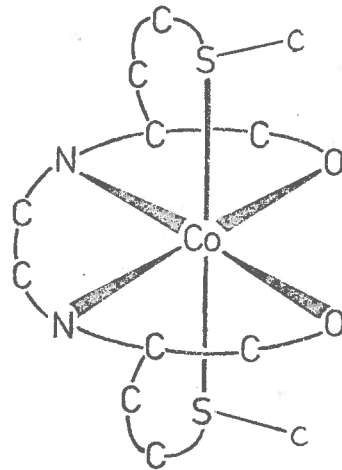

 $\Lambda$ -[Co(*S,S*-EDDS)]<sup>-</sup>

 $\Delta$ -[Co(*S,S*-EDDS)]<sup>-</sup>

 $\Lambda$ -[Co(*S,S*-ebm)]<sup>+</sup>

 $\Delta$ -[Co(*S,S*-ebm)]<sup>+</sup>

FIGURE 1.1. CONFIGURATIONAL ISOMERS OF [Co(*S,S*-ebm)]<sup>+</sup> AND [Co(*S,S*-EDDS)]<sup>-</sup>.

induce steric hindrance between chelate rings. Molecular models indicate no notable increase in inter-ring steric hindrance on changing from the boat to the chair or skew-boat conformation. In the crystal structures of  $\text{Pt}(R,S\text{-Meth})\text{Cl}_2$  and  $\text{Pt}(S\text{-Meth})\text{Cl}_2$ ,<sup>82</sup> the carboxylate oxygens are not coordinated, and the six-membered platinum-methionine rings have the chair conformation. However in the crystal structure of  $\text{Pt}(\text{Gly-}S\text{-Met})\text{Cl}\cdot\text{H}_2\text{O}$ ,<sup>82</sup> they are in the boat form. It was suggested<sup>82</sup> that this was due to steric hindrance induced by the chair conformation in this compound. It may then be anticipated that the six-membered rings of  $[\text{Co}(S,S\text{-abm})]^+$  would prefer the chair or skew-boat conformation in the crystal when there are no strong counteracting lattice forces.

Because of the strong connectivity between all chelate rings in this hexadentate complex, a Dreiding model of the A configuration of  $[\text{Co}(S,S\text{-abm})]^+$  also indicates conformational preferences for the cobalt-glycinato and cobalt-diamine rings. Thus, for a six-membered ring chair conformation, the  $\lambda$  and  $\delta$  conformations of cobalt-glycinato and cobalt-diamine rings respectively, appear to be favoured. For the skew-boat conformation of the six-membered rings, the  $\lambda$  conformation of the cobalt-diamine ring is favoured with the envelope conformation of the cobalt-glycinato rings.

Most of the presentiments discussed above have been confirmed by the X-ray structural analysis of  $(-)_589\text{-}[\text{Co}(S,S\text{-abm})]\text{ClO}_4$ .

### 1.3 EXPERIMENTAL AND DATA REDUCTION

Crystals of  $(-)_589\text{-[Co}(S,S\text{-ebm)]ClO}_4$  were prepared<sup>77</sup> and recrystallized from nitromethane solution by W. Mazurek and Dr. A.T. Phillip. The deep crimson crystals were pseudo-hexagonal platelets which exhibited the forms  $\{100\}$ ,  $\{010\}$ ,  $\{001\}$ ,  $\{0\bar{1}0\}$ ,  $\{110\}$  and  $\{1\bar{1}0\}$ . Preliminary precession photographs recorded with  $\text{MoK}\alpha$  radiation were used to determine the space group and unit cell dimensions. Errors in the cell constants were estimated from several measurements using the same crystal.

#### *Crystal Data*

$(-)_589\text{-Co}(\text{C}_{12}\text{H}_{22}\text{N}_2\text{O}_4\text{S}_2)\text{ClO}_4$ , F.W. 480.83,  $F(000) = 496$  electrons

Monoclinic, space group  $C2$  (No. 5)

$a = 12.34(2)$ ,  $b = 7.94(1)$ ,  $c = 9.46(1)\text{\AA}$ ,  $\beta = 97.45(8)^\circ$ ,  $V = 919(4)\text{\AA}^3$

$D_m = 1.73(2) \text{ g cm}^{-3}$ ,  $Z = 2$ ,  $D_x = 1.737 \text{ g cm}^{-3}$

$\text{MoK}\alpha$  ( $\lambda = 0.7107\text{\AA}$ ),  $\mu_{\text{MoK}\alpha} = 13.4 \text{ cm}^{-1}$

Integrated intensity data were recorded on X-ray film using a Supper Buerger precession camera for the reciprocal layers  $h0l\text{-}h\bar{3}l$  and  $hk0\text{-}hk4$ . Three photographs per layer were recorded with  $\text{MoK}\alpha$  using a Zr filter and exposure time ratios of 1:6:12 and 1:6:16. Triple film packs and a Nonius Weissenberg camera were used to record the layers  $0kl\text{-}10kl$  of integrated data by the equi-inclination Weissenberg technique. The films were separated by 0.0013(1) inch brass foil to increase the range of recorded reflections. The crystal used for intensity data collection measured  $0.45 \times 0.45 \times 0.15 \text{ mm}$ , and was mounted along the  $a^*$  axis for the precession photographs and the  $a$  axis for the Weissenberg

photographs.

Intensities were determined photometrically with a Nonius microdensitometer attached to a Time Systems Corp. digital panel meter, Model 711, and a Facit 4070 paper tape punch. The response linearity of the system was confirmed using intensity strips and silica discs of known optical density over a range of 0 → 2. For each observed reflection, a value for the relative intensity of the light transmitted by the plateau region of the spot was punched on paper tape, followed by an average value of the background intensity. A reflection which could not be detected on the film of maximum exposure was designated unobserved, and the background value only was recorded. Reflections which could not be measured reliably were also recorded. Both unobserved and unreliable reflections were assigned token identifiers and precluded from least-squares procedures. A computer program, DATA, (Appendix I) including a subroutine for conversion to ASCII from CSIRO "Typetronics" code, was written for the CSIRO 3200 computer to read and sort the paper tape data and finally record it on magnetic tape.

The inter-film scale factors were determined for each layer by a non-iterative least-squares procedure described by Rae<sup>83</sup> and modified by Paul. The method is incorporated in AUFAC, a local computer program developed from that described by Paul (Appendix I). The intensity for an observed reflection  $h$  on film  $i$  was determined as

$$I_{hi} = \left[ \ln \left( \frac{\text{Background}_i}{\text{Spot}_i} \right) \right] \times 100$$

The weight  $w_{hi}$  assigned to each reflection in the least-squares process

was determined from the scheme

$$\begin{aligned} \sigma_{hi} &= a_1(I_{hi}) + a_2 \times 100 \\ \sigma_{hi} &= a_3 \times 100 \text{ when } I_{hi} < a_4 \times 100 \\ \text{and } w_{hi} &= 1/(\sigma_{hi})^2 \end{aligned}$$

The mean intensity for each reflection was determined by least-squares as

$$\bar{I}_h = \frac{\sum_i (w_{hi}/k_i) I_{hi}}{\sum_i (w_{hi}/k_i^2)}$$

where  $k_i$  is the scale factor determined for film  $i$ . Assuming the weight  $w_{hi}$  to be proportional to the absolute value for  $1/(\sigma_{hi})^2$ , the standard deviation of the mean intensity,  $\bar{\sigma}_h$ , was obtained by a rigorous procedure described by Paul (Appendix I). AUFAC also checks the validity of the weighting scheme  $a_1$ ,  $a_2$ ,  $a_3$  and  $a_4$  by a least-squares procedure, in which new values for the scheme are estimated for each layer of data and also for the overall data of each axis. This was used as the basis of a recycling process to obtain improved values for the inter-film scale factors, the mean intensities and the standard deviations of the mean intensities. The intensity of an unobserved reflection was determined as

$$I_{unobs} = \left[ \ln \left( \frac{\text{Background}}{\text{Background}-BGF} \right) \right] \times 100 \times S$$

and its standard deviation as

$$\sigma_{unobs} = I_{unobs} \times T/S \times \sqrt{EOF}$$

where  $BGF$  is an estimate of the maximum background fluctuation,  $S$  and  $T$  have the values 0.500 and 0.346 for non-centric<sup>84</sup> data, and  $EOF$  is the error of fit to the equations of condition in the least-squares determination of the film factors. The weighted mean intensities,  $\bar{I}_h$ ,

were corrected for Lorentz and polarization effects but not for absorption ( $\mu_{\text{MoK}\alpha} = 13.4 \text{ cm}^{-1}$  and see Appendix III for sources of mass absorption coefficients). Reflections with large deviations of the individual scaled intensities  $k_i I_{hi}$ , from the mean intensities  $\bar{I}_h$ , were reexamined on all films  $i$  after the first cycle of AUFAC. The weighting scheme  $a_1 = 0.1104$ ,  $a_2 = -0.0191$ ,  $a_3 = 0.0100$  and  $a_4 = 0.2638$  was used in the final AUFAC determination of the  $k_i$ ,  $\bar{I}_h$  and  $\bar{\sigma}_h$  for all layers of data.

The inter-layer scale factors were computed by a similar procedure using program AULAC (Appendix I) and the output mean intensities and their standard deviations from AUFAC. Symmetry equivalent reflections, excluding non-equivalent Friedel pairs, were identified at this stage and included in the inter-layer meshing process. As in AUFAC, the final mean intensity,  $\bar{I}_h$ , and the standard deviation,  $\bar{\sigma}_h$ , were determined for each reflection. The relative observed structure factor magnitudes and their standard deviations were also calculated as

$$|F_o| = \sqrt{\bar{I}_h}$$

$$\sigma_{F_o} = \frac{\bar{\sigma}_h}{2 \times |F_o|}$$

The final data set included 2451 unique reflections with 265 non-equivalent Friedel pairs.

#### 1.4 REFINEMENT TERMINOLOGY

A full matrix least-squares<sup>85-88</sup> procedure was used to refine the initial parameter set of the determined structure. The function



$$D = \sum_{hkl} w_{hkl} (|F_o| - |F_c|)^2$$

where  $w_{hkl}$  is the weight assigned to  $|F_o|$ , and  $|F_c|$  is the scaled value of the calculated structure factor amplitude, was minimized by program FUORFLS (Appendix I) with respect to the independent parameters,  $p_i$ , defining the calculated structure factors. The sum was taken over all observed reflections,  $hkl$ , excluding those with unreliable values. Improved values for the  $p_i$  were then obtained by solution of the normal equations

$$\sum_{hkl} w_{hkl} (|F_o| - |F_c|) \frac{\partial |F_c|}{\partial p_i} = 0 \quad (i = 1, \dots, n)$$

where the  $|F_c|$  was made linear in the  $p_i$  by expression as a Taylor series expansion about the initial values of the  $n$  parameters. This led to an iterative refinement procedure for the  $p_i$ . For each cycle of refinement, the full matrix of the coefficients of the  $p_i$  in the normal equations was employed, and refinement for a given model was considered complete when the parameter change,  $\Delta p_i$ , was  $< 0.3 \times \sigma p_i$  for each parameter in the current cycle. Here,  $\sigma p_i$  is an estimated standard deviation (e.s.d.) of the variable parameter,  $p_i$ , and is determined<sup>87,88</sup> from the inverse matrix of the  $p_i$  coefficients as

$$\sigma p_i = (b_{ii} \cdot D / (m - n))^{1/2}$$

where  $b_{ii}$  is the  $i^{\text{th}}$  diagonal element of the inverse matrix and  $m$  is the number of observed reflections used in the above summation. If there are no systematic data errors, the function  $(D / (m - n))^{1/2}$  is an estimate<sup>88,89</sup> of the error in an observation of unit weight and has a unit value if

the weight  $w_{hkl}$  was chosen so that  $w_{hkl} = 1 / (\sigma F_o)^2$  where  $\sigma F_o$  is absolute.

It has been shown<sup>90</sup> however, that the estimated standard deviations derived

in this way are too optimistic by a factor of the order of two.

As refinement progresses, an indication of the reflection-by-reflection agreement between  $|F_o|$  and  $|F_c|$  is obtained from the conventional  $R$  factor

$$R_1 = \Sigma ||F_o| - |F_c|| / \Sigma |F_o|$$

On altering the model, *e.g.* changing the number or functional dependence of the parameters defining the  $|F_o|$ , meaningful changes in  $R_1$  may be identified<sup>85,91</sup> by significance tests based on the values of

$$R_2 = (\Sigma w(|F_o| - |F_c|)^2 / \Sigma w |F_o|^2)^{1/2}$$

for the converged refinements of the two models. FUORFLS also computes  $R_1$  and  $R_2$  in ranges of  $\sin\theta/\lambda$  and the average  $w(|F_o| - |F_c|)^2$  in ranges of  $|F_o|$ . An estimate of the relevance of the weighting scheme assigned to the  $|F_o|$  may be obtained from these distributions.

The variable parameters refined in the subsequent structures of this thesis were the scale factor(s), the atomic coordinates, the atomic thermal parameters and in some instances the atomic site occupancy factors or atom multipliers. For an isotropically vibrating atom, the scattering factor is<sup>86,88</sup>

$$f = f_o \exp[-B \cdot (\sin\theta_{hkl}/\lambda)^2]$$

where  $B = 8\pi^2 \bar{u}^2$

Here  $B$  is the isotropic thermal parameter,  $f_o$  is the scattering factor of the stationary atom and  $\bar{u}^2$  is the mean-square amplitude of atomic vibration.

For an anisotropic atom, the expression

$$f = f_o \exp[-(\beta_{11}h^2 + \beta_{22}k^2 + \beta_{33}l^2 + 2\beta_{12}hk + 2\beta_{13}hl + 2\beta_{23}kl)]$$

was used for the scattering factor, and the  $\beta_{ij}$  are the anisotropic

thermal parameters for the atom.

### 1.5 STRUCTURE SOLUTION AND REFINEMENT

The complex cation  $[\text{Co}(S,S\text{-eba})]^+$  has crystallographic site symmetry in the structure since  $Z = 2$  and  $C_2$  has four general asymmetric sites per cell.<sup>92</sup> Of the two possible independent sites with two-fold symmetry, the one on the  $C_2$  axis through the origin of the conventional<sup>92</sup> cell was chosen for the cation. Since the  $y$  coordinate for one atom may be assigned arbitrarily in this space group, the cobalt atom was placed at the origin of the cell, (0,0,0). A Patterson synthesis revealed the position of the sulphur atom. A subsequent Fourier map, phased on the cobalt and sulphur coordinates, located the nitrogen and oxygen positions in the coordination sphere around cobalt and the chlorine atom of the  $\text{ClO}_4$  anion. The anion resided on the  $C_2$  axis at  $x = 0$ ,  $z = 1/2$ , which is not symmetry related to that constraining the cation at  $x = 0$ ,  $z = 0$ . It was apparent at this stage that the oxygen donor atoms were *trans* and the sulphur atoms *cis* in the coordination sphere. A second Fourier synthesis established the sites of all other non-hydrogen atoms in the structure. The confirmation of the *S* configuration about the asymmetric carbon atoms revealed the  $\Lambda^{29}$  configuration for the complex cation as expected for *cis*-arranged sulphur atoms. The refinement by full matrix least-squares of the scale factor, positional parameters and individual isotropic thermal parameters converged with an  $R_1$  value of 0.109. Subsequent refinement with anisotropic thermal parameters for all atoms reduced  $R_1$  to 0.080 and incorporated the anomalous components in the

scattering factors of Co, Cl and S. A comparison of the observed and calculated values for the 265 Friedel pairs then established the *S* configuration for the asymmetric carbon atoms and the *A* configuration for the complex cation.

Hydrogen atom positions, with the exception of the methyl hydrogens, were calculated for C-H and N-H distances of 1.02 and 0.95Å assuming tetrahedral H-N-H and H-C-H angles. The hydrogen atoms were then included in the refinement with fixed coordinates and isotropic thermal parameters of 3.0Å<sup>2</sup>. Refinement of the scale factor and the non-hydrogen atom parameters finally converged with  $R_1 = 0.060$  and  $R_2 = 0.060$ . The weighting scheme employed in the refinement was derived from the standard deviations of the mean intensities as determined in the least-squares inter-film and inter-layer scaling process. The error in an observation of unit weight was estimated as 3.24 from a structure factor calculation after the final refinement cycle. This indicates that the  $\sigma_{F_o}$  and  $w_{hkl}$  are not on an absolute scale. The average  $w(|F_o| - |F_c|)^2$  determined in ranges of  $|F_o|$  varied from 3.6 to 8.6 (excluding the terminal ranges) in a random manner. The terminal ranges had lower values, suggesting that very strong and very weak reflections were not given enough weight relative to the others. A similar determination of average  $w(|F_o| - |F_c|)^2$  in ranges of  $\sin\theta/\lambda$  showed an analogous trend. Thus the weighting scheme was satisfactory for all reflections but those with high  $\sin\theta/\lambda$  and those with very high or very low intensities. A final difference Fourier map showed no peak heights larger than 0.5 e/Å<sup>3</sup>.

In view of the suggested<sup>93</sup> and confirmed<sup>94-96</sup> charge delocalization

in complex ions, the scattering factor curve for  $\text{Co}^{2+}$  was used in the structure factor calculations. For  $\text{Co}^{2+}$  and  $\text{Cl}^-$  the scattering factors of Doyle and Turner<sup>97</sup> were used. Values for O, N, C and S were obtained from International Tables for X-ray Crystallography,<sup>98</sup> and for H, the values of Stewart *et al.*<sup>99</sup> were used. The anomalous components  $\Delta f'$  and  $\Delta f''$  for Co (0.3, 1.0), Cl (0.1, 0.2) and S (0.1, 0.2) were acquired from International Tables.<sup>98</sup>

Zalkin's program FORDAPB for Fourier computations was used for structure solution. Program FUORFLS, a local modification of Busing, Martin and Levy's ORFLS, was used for refinement (see Appendix I for detailed descriptions). The derived structural parameters and their standard deviations were determined with program ORFFE by Busing, Martin and Levy. Hydrogen atom coordinates were calculated with PLANEH, a modification of Blount's PLANET. This was also used for the determination of least-squares planes. Blount's BLANDA was used for periodical checks on structural geometry during the refinement. Perspective ellipsoid plots were achieved with Johnson's ORTEPB.

#### 1.6 TABLES AND PERSPECTIVE PROJECTIONS

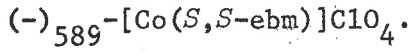
The subsequent tables and perspective projections are self-explained by the appropriate table headings, legends and foot-notes. Observed and calculated structure factors ( $\times 10$ ), with *U* and *F* designations for unobserved and unreliable values respectively, are listed in Table 1.1. Positional and thermal parameters appear in Table 1.2 and the internal geometry of the cation and anion in Table 1.3.

Tables 1.4, 1.5 and 1.6 contain least-squares planes, atom deviations and dihedral angles. Close intermolecular distances are presented in Table 1.7. All listed parameters were obtained or derived from the final least-squares cycle and their standard deviations are enclosed in parentheses.

### 1.7 STRUCTURAL FEATURES AND DISCUSSION

The crystal structure of  $(-)_589-[Co(S,S-ebm)]ClO_4$  is portrayed in Figure 1.2 as a projection down the  $-\underline{c}^*$  direction. Both the  $(-)_589-[Co(S,S-ebm)]^+$  cation and the perchlorate anion have rigorous  $C_2$  symmetry and lie on separate crystallographic two-fold axes parallel to  $b$ . Although the hydrogen atoms were not observed in this structure, the reliability with which the calculated N-H hydrogen position is defined by the relatively rigid non-hydrogen geometry should be adequate for an assessment of approximate hydrogen bonding parameters. The cation and anion interact through N-H...O hydrogen bonds to form chains parallel to  $a$ . There is only one independent interaction, the others being related by the crystal symmetry. This N(1)-H(8)...O(5) contact satisfies the distance criterion for hydrogen bonding suggested by Hamilton and Ibers,<sup>101</sup> if the calculated position for H(8) is approximately correct. The N...O distance of  $3.00(1)\text{\AA}$  and N-H...O angle of  $149^\circ$  (see Table 1.7) are well within the ranges  $2.87$  to  $3.07\text{\AA}$  and  $119$  to  $175^\circ$  established by neutron diffraction for unbranched N-H...O hydrogen bonds.<sup>101</sup> Intermolecular contact distances are listed in Table 1.7. If the van der Waals radii of carbon, nitrogen, oxygen and sulphur have the

TABLE 1.1. OBSERVED AND CALCULATED STRUCTURE FACTORS FOR



h	k	l	observed	calculated
0	0	0	100	100
1	0	0	100	100
2	0	0	100	100
3	0	0	100	100
4	0	0	100	100
5	0	0	100	100
6	0	0	100	100
7	0	0	100	100
8	0	0	100	100
9	0	0	100	100
10	0	0	100	100
11	0	0	100	100
12	0	0	100	100
13	0	0	100	100
14	0	0	100	100
15	0	0	100	100
16	0	0	100	100
17	0	0	100	100
18	0	0	100	100
19	0	0	100	100
20	0	0	100	100
21	0	0	100	100
22	0	0	100	100
23	0	0	100	100
24	0	0	100	100
25	0	0	100	100
26	0	0	100	100
27	0	0	100	100
28	0	0	100	100
29	0	0	100	100
30	0	0	100	100
31	0	0	100	100
32	0	0	100	100
33	0	0	100	100
34	0	0	100	100
35	0	0	100	100
36	0	0	100	100
37	0	0	100	100
38	0	0	100	100
39	0	0	100	100
40	0	0	100	100
41	0	0	100	100
42	0	0	100	100
43	0	0	100	100
44	0	0	100	100
45	0	0	100	100
46	0	0	100	100
47	0	0	100	100
48	0	0	100	100
49	0	0	100	100
50	0	0	100	100
51	0	0	100	100
52	0	0	100	100
53	0	0	100	100
54	0	0	100	100
55	0	0	100	100
56	0	0	100	100
57	0	0	100	100
58	0	0	100	100
59	0	0	100	100
60	0	0	100	100
61	0	0	100	100
62	0	0	100	100
63	0	0	100	100
64	0	0	100	100
65	0	0	100	100
66	0	0	100	100
67	0	0	100	100
68	0	0	100	100
69	0	0	100	100
70	0	0	100	100
71	0	0	100	100
72	0	0	100	100
73	0	0	100	100
74	0	0	100	100
75	0	0	100	100
76	0	0	100	100
77	0	0	100	100
78	0	0	100	100
79	0	0	100	100
80	0	0	100	100
81	0	0	100	100
82	0	0	100	100
83	0	0	100	100
84	0	0	100	100
85	0	0	100	100
86	0	0	100	100
87	0	0	100	100
88	0	0	100	100
89	0	0	100	100
90	0	0	100	100
91	0	0	100	100
92	0	0	100	100
93	0	0	100	100
94	0	0	100	100
95	0	0	100	100
96	0	0	100	100
97	0	0	100	100
98	0	0	100	100
99	0	0	100	100
100	0	0	100	100

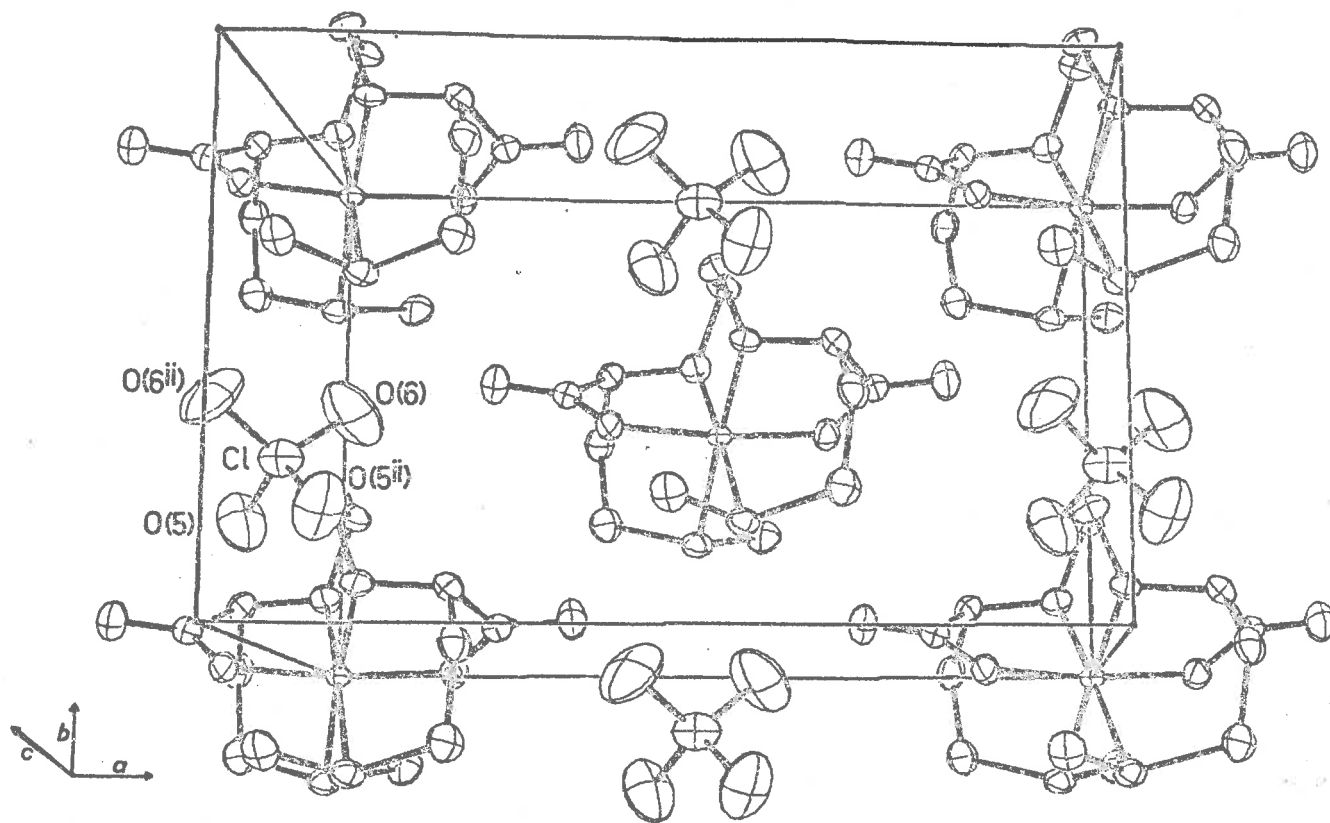


FIGURE 1.2. PROJECTION OF UNIT CELL OF  $(-)_589$ -[Co(*S,S*-ebm)]ClO<sub>4</sub> DOWN  $-c^*$ .  
 ii denotes an atom related by the 2-fold axis at  $x = 0, z = 1/2$ .  
 (Thermal ellipsoids enclose 50% probability.)



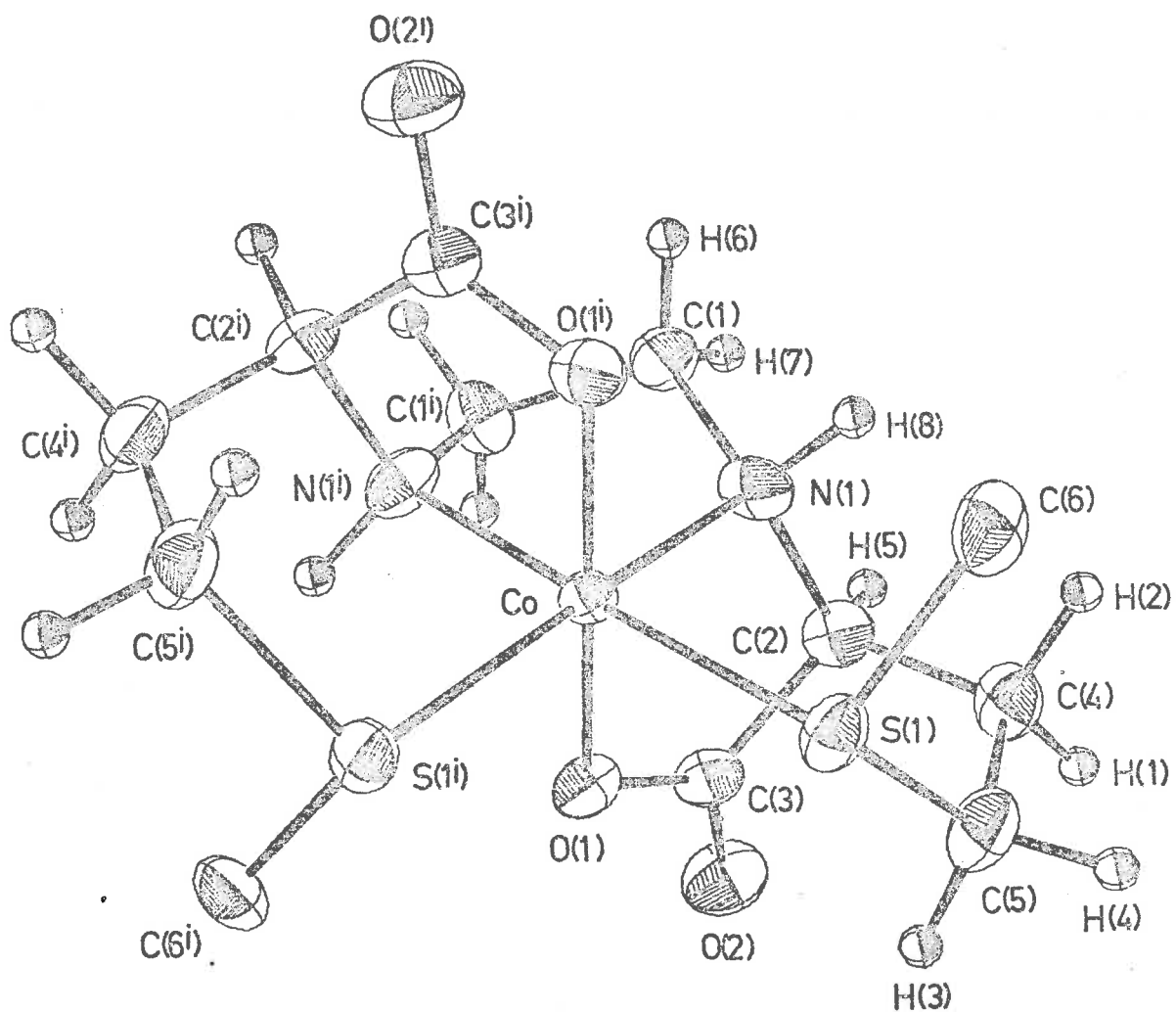


FIGURE 1.3. PERSPECTIVE VIEW OF  $(-)_589-[Co(S,S-ebm)]$ .

The labelling scheme is indicated and *i* denotes an atom related to the asymmetric unit by a 2-fold axis through the origin. (Non-hydrogen thermal ellipsoids enclose 50% probability.)

TABLE 1.2. POSITIONAL AND THERMAL PARAMETERS FOR  $(-)_589-[Co(S,S\text{-}ebm)]ClO_4$ .<sup>a</sup>

Atom	<i>x</i>	<i>y</i>	<i>z</i>	$\beta_{11}$	$\beta_{22}$	$\beta_{33}$	$\beta_{12}$	$\beta_{13}$	$\beta_{23}$
Co <sup>c</sup>	0	0	0	236(7)	389(18)	436(13)	0	35(7)	0
Cl	0	3571(4)	5000	723(19)	972(43)	662(28)	0	133(19)	0
S(1)	397(1)	-2036(3)	1665(2)	401(11)	610(28)	574(19)	-1(15)	-56(12)	106(24)
O(1)	1448(3)	130(8)	-425(5)	275(22)	852(80)	694(48)	23(48)	44(29)	206(74)
N(1)	407(5)	1731(9)	1370(8)	375(34)	644(99)	835(77)	-32(51)	14(44)	-340(79)
O(2)	3077(4)	1138(9)	387(6)	318(29)	1390(107)	1133(77)	-55(47)	116(42)	62(85)
C(1)	-6(5)	3379(10)	807(7)	469(44)	681(112)	729(75)	141(61)	75(51)	130(91)
C(2)	1629(5)	1615(10)	1767(8)	326(34)	725(106)	689(79)	-115(59)	26(47)	-134(98)
C(3)	2114(5)	953(10)	484(8)	308(37)	670(105)	746(80)	15(53)	63(47)	19(89)
C(4)	1874(5)	375(11)	3006(7)	323(34)	1213(166)	629(70)	-99(61)	-74(41)	-137(100)
C(5)	1733(6)	-1480(13)	2592(8)	420(41)	1103(133)	746(82)	3(70)	-138(49)	73(117)
C(6)	-475(6)	-1671(12)	3040(8)	442(43)	1181(156)	688(79)	-59(69)	73(49)	376(107)
O(5)	-636(6)	2539(13)	3983(8)	795(49)	2856(219)	1243(91)	-458(90)	107(57)	-1015(134)
O(6)	726(7)	4567(13)	4259(9)	1113(67)	2664(252)	1815(116)	-658(100)	122(73)	1120(149)

Positional parameters calculated for hydrogen atoms<sup>b</sup>

	<i>x</i>	<i>y</i>	<i>z</i>	<i>B</i>
H(1)	2648	552	3487	3.0Å <sup>2</sup>
H(2)	1337	618	3737	3.0
H(3)	2312	-1767	1947	3.0
H(4)	1875	-2197	3500	3.0
H(5)	1934	2776	2072	3.0
H(6)	-779	3574	1056	3.0
H(7)	493	4321	1280	3.0
H(8)	24	1540	2250	3.0

<sup>a</sup> Positional parameters ( $\times 10^4$ ).  
Anisotropic thermal parameters ( $\times 10^5$ ).

<sup>b</sup> Hydrogen atoms were assigned fixed isotropic thermal parameters.

<sup>c</sup>  $\beta_{12}$ ,  $\beta_{23}$  for Co, Cl are constrained by symmetry (see reference 100).

TABLE 1.3. INTRAMOLECULAR BOND LENGTHS AND ANGLES.

<i>Cation</i>			
Co-S(1)	2.267(3)Å	S(1)-Co-O(1 <sup>1</sup> )	90.92(19)°
Co-N(1)	1.912(7)	N(1)-Co-O(1)	86.12(27)
Co-O(1)	1.884(5)	N(1)-Co-O(1 <sup>1</sup> )	89.36(26)
S(1)-C(6)	1.815(8)	Co-S(1)-C(6)	106.82(29)
S(1)-C(5)	1.818(7)	Co-S(1)-C(5)	105.23(32)
C(5)-C(4)	1.529(12)	C(6)-S(1)-C(5)	101.50(41)
C(4)-C(2)	1.531(11)	S(1)-C(5)-C(4)	115.07(54)
C(2)-N(1)	1.508(9)	C(5)-C(4)-C(2)	114.79(59)
N(1)-C(1)	1.479(10)	C(4)-C(2)-N(1)	108.79(62)
C(1)-C(1 <sup>1</sup> ) <sup>a</sup>	1.529(14)	C(2)-N(1)-Co	106.91(47)
O(1)-C(3)	1.288(9)	Co-N(1)-C(1)	110.15(50)
C(3)-O(2)	1.213(8)	N(1)-C(1)-C(1 <sup>1</sup> )	108.21(46)
C(3)-C(2)	1.515(11)	N(1)-C(2)-C(3)	107.90(57)
S(1)-Co-S(1 <sup>1</sup> )	88.96 (15)°	C(4)-C(2)-C(3)	109.35(63)
N(1)-Co-N(1 <sup>1</sup> )	88.01 (46)	C(2)-N(1)-C(1)	115.50(61)
O(1)-Co-O(1 <sup>1</sup> )	173.72 (40)	C(2)-C(3)-O(2)	120.73(66)
S(1)-Co-N(1)	91.59 (25)	C(2)-C(3)-O(1)	115.32(54)
S(1)-Co-N(1 <sup>1</sup> )	177.02 (22)	O(2)-C(3)-O(1)	123.86(73)
S(1)-Co-O(1)	93.56 (18)	C(3)-O(1)-Co	115.16(44)
<i>Anion</i>			
Cl-O(5)	1.420(8)Å	O(5)-Cl-O(6 <sup>11</sup> )	108.82(48)°
Cl-O(6)	1.443(8)	O(5)-Cl-O(5 <sup>11</sup> )	109.49(86)
O(5)-Cl-O(6)	108.06 (49)°	O(6)-Cl-O(6 <sup>11</sup> )	113.55(91)

<sup>a</sup> Symmetry transformations are designated by the superscripts and are defined in Table 1.7.

TABLE 1.4. LEAST-SQUARES PLANES AND ATOM DEVIATIONS.

Planes equations are in the form  $LX + MY + NZ = P$ .  $X, Y, Z$  are orthogonal coordinates ( $\text{\AA}$ ) referred to an orthonormal base system with axes parallel to  $\underline{a}, \underline{b}$  and  $\underline{c}^*$ . The residuals were assigned unit weights.

Plane	L	M	N	P	Symbol
S(1),Co,N(1)	0.9759	-0.0358	-0.2153	0.0	1
S(1),N(1),C(2),C(5)	0.4080	-0.1677	-0.8974	-1.1192	2
C(2),C(4),C(5)	0.9860	-0.0402	-0.1617	1.4477	3
O(1),C(3),C(2),O(2)	-0.1621	0.8547	-0.4932	-0.0071	4
N(1),Co,N(1 <sup>1</sup> ) <sup>a</sup>	0.9679	0.0	-0.2515	0.0	5
S(1),Co,S(1 <sup>1</sup> )	0.9837	0.0	-0.1796	0.0	6
N(1),N(1 <sup>1</sup> ),S(1),S(1 <sup>1</sup> )	0.9779	0.0	-0.2093	0.0	7

*Distances from the Planes ( $\text{\AA}$ )*

Atom <sup>b</sup>	1	2	3	Atom	4	Atom	5	6	7
Co	0.0	1.119	-1.448	O(1)	-0.006	S(1)	-0.117	0.0	-0.048
S(1)	0.0	0.105	-1.354	C(3)	0.018	S(1 <sup>1</sup> )	0.117	0.0	0.048
N(1)	0.0	-0.129	-1.382	C(2)	-0.005	N(1)	0.0	0.098	0.058
C(2)	1.346	0.148	0.0	O(2)	-0.007	N(1 <sup>1</sup> )	0.0	-0.098	-0.058
C(4)	1.278	-0.669	0.0	N(1)	0.494	C(1)	-0.293		
C(5)	1.294	-0.124	0.0	Co	0.007	C(1 <sup>1</sup> )	0.293		

<sup>a</sup> See Table 1.7 for definitions of symmetry transformations.

<sup>b</sup> The mean isotropic e.s.d.'s for Co, S, N, O and C coords. are 0,  $2 \times 10^{-3}$ ,  $7 \times 10^{-3}$ ,  $5 \times 10^{-3}$  and  $8 \times 10^{-3} \text{\AA}$  respectively.

**TABLE 1.5. INTERPLANAR DIHEDRAL ANGLES.<sup>a</sup>**

<i>Planes</i>	<i>Angle</i>	<i>Planes</i>	<i>Angle</i>	<i>Planes</i>	<i>Angle</i>
1,2	53.3°	1,5	3.0°	5,6	4.2(3)°
1,3	3.1	1,6	2.9	5,7	2.5
2,3	56.3	1,7	2.1	6,7	1.7

<sup>a</sup> Standard deviations of angles between planes of four or more atoms were not computed (see Appendix III).

**TABLE 1.6. TORSION ANGLES IN THE CHELATE RINGS.**

<i>Defining Atoms<sup>a</sup></i>	<i>Torsion Angle</i>	<i>Defining Atoms</i>	<i>Torsion Angle</i>
Co-N(1)-C(1)-C(1 <sup>1</sup> )	-32.9(8)°	C(4)-C(5)-S(1)-Co	+45.4(6)°
N(1)-C(1)-C(1 <sup>1</sup> )-N(1 <sup>1</sup> )	+42.5(10)	Co-N(1)-C(2)-C(3)	+30.3(7)
Co-N(1)-C(2)-C(4)	-88.2(6)	N(1)-C(2)-C(3)-O(1)	-22.2(9)
N(1)-C(2)-C(4)-C(5)	+75.4(8)	C(2)-C(3)-O(1)-Co	+2.4(9)
C(2)-C(4)-C(5)-S(1)	-55.3(8)		

<sup>a</sup> The angle is that between the planes *i,j,k* and *j,k,l* in the chain *i-j-k-l*. If the skew lines *i → l* and *j → k* define a right-handed helix, the angle is positive. It is negative for a left-handed helix.

TABLE 1.7. INTERMOLECULAR DISTANCES TO 3.6Å.<sup>a</sup>*van der Waals Contacts*

N(1)...O(6)	3.525(13)Å	O(2)...O(1 <sup>iv</sup> )	3.223(10)Å
C(1)...O(5)	3.270(12)	O(2)...C(5 <sup>iv</sup> )	3.428(11)
C(1)...O(6)	3.408(13)	C(1)...O(2 <sup>iv</sup> )	3.527(10)
C(6)...O(5)	3.474(15)	O(2)...C(1 <sup>v</sup> )	3.211(10)
O(2)...S(1 <sup>iii</sup> )	3.295(6)	C(5)...O(5 <sup>v</sup> )	3.431(11)
O(2)...C(6 <sup>iii</sup> )	3.370(10)	C(6)...O(6 <sup>vi</sup> )	3.466(14)
O(2)...S(1 <sup>iv</sup> )	3.219(7)		

*Apparent Hydrogen Bond A-H...B*

Atoms	A...B	H...B	Angle A-H...B
N(1)-H(8)...O(5)	3.001(12)Å	2.080Å	149°

*Symmetry transformations designated by the superscripts in Tables 1.3, 1.4, 1.6 and 1.7*

i	$\bar{x}$	$y$	$\bar{z}$
ii	$\bar{x}$	$y$	$\bar{z} + 1$
iii	$x + 1/2$	$y + 1/2$	$z$
iv	$\bar{x} + 1/2$	$y + 1/2$	$\bar{z}$
v	$x + 1/2$	$y - 1/2$	$z$
vi	$x$	$y - 1$	$z$

<sup>a</sup> These involve non-hydrogen atoms only.

literature<sup>102,103</sup> values of 1.7, 1.5, 1.4 and 1.85Å, the only other close contact present is an inter-cation O...S contact of 3.22(1)Å, but this is not significantly less than the van der Waals radii sum of 3.25Å. If the methyl group on the sulphur has an effective van der Waals radius of 2.0Å<sup>103</sup> in its freely rotating state, there are no evident close contacts restricting such rotation in the crystal.

The complex cation  $(-)_589^-[\text{Co}(S,S\text{-ebm})]^+$  has the  $\Lambda^{29}$  absolute configuration and is shown in Figure 1.3. The configuration about the asymmetric carbon is *S*, whereas both the nitrogen and sulphur atoms are present in the *R* configurational arrangement. The six-membered sulphur containing rings are equatorially disposed with respect to the cobalt-diamine ring as is required by the  $\Lambda$  configuration of the complex with the *S* configuration at the asymmetric carbon (section 1.2). These stereochemical properties of the complex cation are in agreement with those predicted in section 1.2 by correlation with the observed CD<sup>79</sup> and six-membered ring disposition<sup>81</sup> of the  $[\text{Co}(S,S\text{-EDDS})]^-$  anion. They also support the observations<sup>63,80</sup> for  $[\text{Co}(\text{EDTA})]^-$  and  $[\text{Co}(\text{trdta})]^-$  that axially disposed cobalt-glycinato rings are less strained than those equatorially oriented.

The internal geometry of the cation is given in Table 1.3. The Co-S distance of 2.267(3)Å is similar to the mean values of 2.258(3)<sup>104</sup> and 2.267(3)Å<sup>105</sup> reported for the tris-dithiocarbamate complex  $\text{Co}(\text{dtc})_3$ , that of 2.266(1)Å<sup>106</sup> recently seen in tris-ethylthioxanthate cobalt(III) ( $\text{Co}(\text{xan})_3$ ) and that of 2.277(4)Å<sup>107</sup> in  $\text{Co}(\text{exan})_3$ , but shorter than the value of 2.322(3)Å<sup>108</sup> observed in the tris-dithiophosphato complex  $\text{Co}(\text{mtp})_3$ .

The mean Co(III)-S distances of 2.23(2)<sup>109,110</sup> and 2.244(5)<sup>15,111</sup> Å found in octahedral bis-dithiolato and tris-dithioxalato complexes of cobalt(III) are slightly shorter than that observed here. The value of 1.912(7)<sup>112</sup> Å for the Co-N bond length is comparable with the mean values of 1.926(5) and 1.902(5)<sup>112</sup> Å observed in the bis-S-aspartato complex ions, *cis(N)-trans(O<sub>5</sub>)-[Co(S-asp)<sub>2</sub>]<sup>-</sup>* and *cis(N)-trans(O<sub>6</sub>)-[Co(S-asp)<sub>2</sub>]<sup>-</sup>*. These ions have the same bonding structure as the [Co(S,S-EDDS)]<sup>-</sup> ion with the dimethylene linkage removed. In the former S-aspartato complex, the six-membered rings are equatorial with respect to the N-Co-N plane. These distances are similar to that of 1.925(5)<sup>63</sup> Å and significantly shorter than that of 1.966(9)<sup>80</sup> Å seen in [Co(EDTA)]<sup>-</sup> and [Co(trdta)]<sup>-</sup>, both of which have strained equatorial five-membered rings. Most other cobalt(III) complexes with Co-en rings have longer Co-N distances than that found here in [Co(S,S-ebm)]<sup>+</sup>. (See reference 15 for a recent review of tris-diaminacobalt(III) structures with pseudo-C<sub>3</sub> symmetry.) For example, in the complex ion [Co(penten)]<sup>3+</sup>, which has<sup>133</sup> six nitrogen donors and a similar ring structure to [Co(EDTA)]<sup>-</sup>, the Co-N distance in the equivalent Co-en ring is 1.964(11)<sup>133</sup> Å. In the structure of [Co(NH<sub>3</sub>)<sub>6</sub>]<sup>3+</sup>-[Co(CN)<sub>6</sub>]<sup>4-</sup> the Co-N bond length was observed<sup>96</sup> to be 1.972(1)<sup>96</sup> Å from an accurate structure analysis. The Co-O distance of 1.884(5)<sup>112</sup> Å is close to the mean distances of 1.885(15), 1.861(8) and 1.891(4)<sup>112</sup> Å found for the axial Co-O bonds in [Co(EDTA)]<sup>-</sup>,<sup>63</sup> [Co(trdta)]<sup>-</sup><sup>80</sup> and *cis(N)-trans(O<sub>5</sub>)-[Co(S-asp)<sub>2</sub>]<sup>-</sup>*.<sup>112</sup> The S-C bonds are similar and the mean distance of 1.817(5)<sup>112</sup> Å is that for a mercaptide single bond (1.82(1)<sup>98</sup> Å). The mean values for the C-C and N-C distances are 1.526(6) and 1.494(7)<sup>112</sup> Å. These



are only slightly shorter and longer than the respective paraffinic values (1.541(3) and 1.479(5)Å<sup>98</sup>). The carboxyl C-O length of 1.288(9)Å is significantly different from the carbonyl distance of 1.213(8)Å, and the values are in agreement with those of 1.276(7) and 1.219(7)Å for the averaged lengths of the equivalent bonds in<sup>112</sup> *cis(N)-trans(O<sub>5</sub>)-[Co(S-asp)<sub>2</sub>]<sup>-</sup>.*

The angular geometry of the cobalt-ethylenediamine ring is similar to that found<sup>63</sup> in [Co(EDTA)]<sup>-</sup> and that observed<sup>133</sup> in the equivalent Co-en ring of [Co(penten)]<sup>3+</sup>. The cobalt-glycinato ring has angular parameters closely matching those seen<sup>112</sup> for the equivalent rings in *cis(N)-trans(O<sub>5</sub>)-[Co(S-asp)<sub>2</sub>]<sup>-</sup>, and is broadly similar to the axial rings of [Co(EDTA)]<sup>-</sup><sup>63</sup> and [Co(trdta)]<sup>-</sup>.<sup>80</sup> Angular distortion of the coordination sphere from octahedral geometry is not marked except for the O(1)-Co-O(1<sup>1</sup>) angle of 173.7(4)° and the N(1)-Co-O(1) angle of 86.1(3)° in the cobalt-glycinato ring. The equivalent angles in the similar aspartato complex<sup>112</sup> have the values 176.7(2) and 85.5(2)°. In the N,N,S,S equatorial plane, the N(1)-Co-N(1<sup>1</sup>), N(1)-Co-S(1) and S(1)-Co-S(1<sup>1</sup>) angles of 88.0(5), 91.6(3) and 89.0(2)° approach octahedral values as closely as do the appropriate N-Co-N, N-Co-O and O-Co-O angles of 93.9(2), 89.7(2) and 87.0(2)° in<sup>112</sup> *cis(N)-trans(O<sub>5</sub>)-[Co(S-asp)<sub>2</sub>]<sup>-</sup>. The equivalent angles N-Co-O and O-Co-O in the strained equatorial geometry of [Co(EDTA)]<sup>-</sup> have<sup>63</sup> the mean values 83.2(4) and 104.0(7)° and indicate a much larger distortion than that observed here in [Co(S,S-ebm)]<sup>+</sup>. These distortions would contribute to the strain associated with<sup>63,80</sup> equatorially disposed cobalt-glycinato rings and provide an *a fortiori* reason for the equatorial coordination of the sulphur atoms in**

$[\text{Co}(\text{S},\text{S}\text{-ebm})]^+$ . A similar result was found<sup>81</sup> for  $[\text{Co}(\text{S},\text{S}\text{-EDDS})]^-$ . The N,N,S,S donor set in  $[\text{Co}(\text{S},\text{S}\text{-ebm})]^+$  is very closely planar as is revealed by the small distances of these atoms from their least-squares plane (see Table 1.4) and the small dihedral angles between the N,N,S,S, the N,Co,N and the S,Co,S planes (see Table 1.5).

The six-membered rings assume the chair conformation as seen in Figure 1.3. A distortion is evident, but this is probably due to differences in the covalent radii<sup>93</sup> of S and N, and the least-squares plane through N(1), C(2), C(5), S(1) makes similar angles with the closely coplanar S(1), Co, N(1) and C(2), C(4), C(5) planes (see Tables 1.4 and 1.5). A conclusive indication of the chair conformation and its distortion is obtained from the relative magnitudes and signs of the torsion angles of the six-membered ring (see Table 1.6).

The five-membered cobalt-ethylenediamine and cobalt-glycinato rings have the  $\delta$  and  $\lambda$ <sup>29</sup> conformations respectively. As suggested in Section 1.2 this is expected for six-membered chair rings. Alternatively, for a skew-boat six-membered ring conformation, the envelope conformation of the cobalt-glycinato ring is favoured (section 1.2). This combination was found<sup>112</sup> in *cis(N)-trans(O<sub>5</sub>)-[Co(S-asp)<sub>2</sub>]*<sup>-</sup> and further supports the Dreiding model predictions. The  $\delta$  and  $\lambda$  conformations found here for the above mentioned chelate rings are clearly indicated by the signed values of the torsion angles about the C-C bonds (see Table 1.6). The Co-O(1)-C(3)-C(2) torsion angle of  $+2.4(9)^\circ$  is not significantly different from zero and the Co, O(1), C(3), C(2) set is essentially planar. The results of Table 1.4 also indicate the accurately planar nature of the

atoms Co, O(1), O(2), C(3), C(2) in the cobalt-glycinato linkage.

The anion geometry is approximately tetrahedral. The mean Cl-O bond distance of 1.432(6)Å lies within the range 1.41-1.48(6)Å established<sup>98</sup> for Cl-O distances in ClO<sub>4</sub><sup>-</sup>. The O-Cl-O angles range from 108.1(5) to 113.5(9)°, the latter value being the only one significantly different from the tetrahedral value of 109.47°.

CHAPTER 2. THE CRYSTAL STRUCTURE OF BIS-(DIHYDRO-1H,3H,5H-OXAZOLO-  
[3,4-c]OXAZOLE-7a-CARBOXYLATO)COPPER(II), Cu(dioxc)<sub>2</sub>

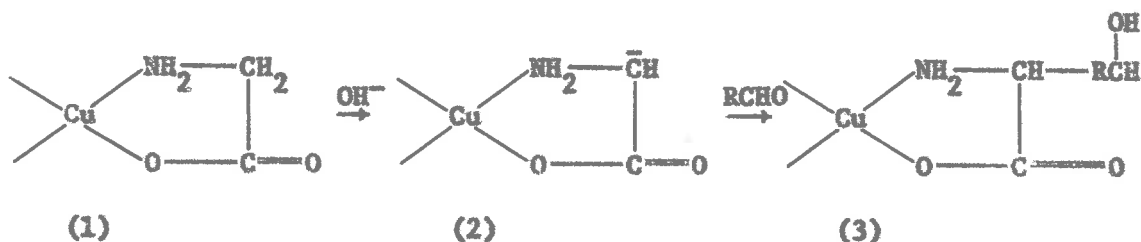
2.1 ABSTRACT

The structure of Cu(dioxc)<sub>2</sub> has been determined from 2395 diffractometer collected data and refined by full matrix least-squares to an *R* value of 0.038. The compound forms deep blue monoclinic crystals having space group  $P2_1/c$  with  $a = 18.559(1)$ ,  $b = 10.142(1)$ ,  $c = 7345(1)\text{\AA}$ ,  $\beta = 101.60(1)^\circ$  and  $Z = 4$ . The formula unit of the complex has approximate  $C_{2h}$  symmetry with the nitrogen atoms occupying *trans* positions in the pseudo-square planar coordination geometry. These sub-units are connected in the crystal by an apical bond between the copper atom and a glide related carbonyl oxygen to form infinite molecular chains parallel to *c*. The Cu-O distance for this bond is  $2.354(4)\text{\AA}$  compared with  $1.904(4)$  and  $1.939(4)\text{\AA}$  for the Cu-O bonds in the chelate rings. The complex has a distorted square pyramidal coordination geometry in the crystal. The two chelate rings have considerably different degrees of puckering because of the apical interaction. The substituted oxazolidine rings adopt envelope conformations which fold toward each other in each ligand.

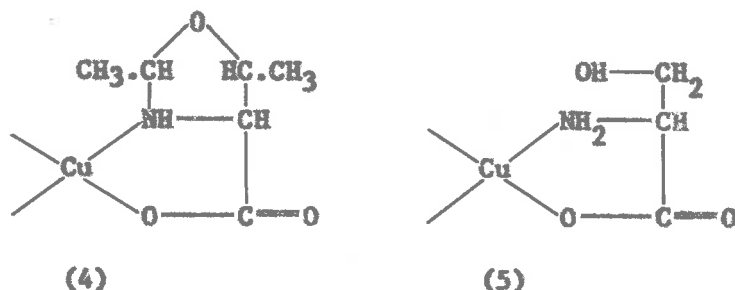
2.2 PREAMBLE

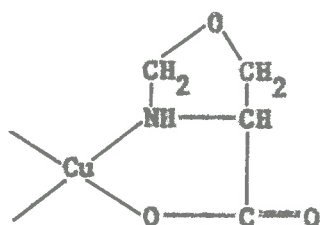
Bis-(*S*-serinato)copper(II) has been found<sup>67</sup> to react with excess formaldehyde under basic conditions (pH 7-9) to form Cu(dioxc)<sub>2</sub>. The X-ray structural analysis of the reaction product has established the nature of the reaction and indicated the reaction mechanism by interpolation of the structure of an optically active intermediate.

The condensation of bis-(glycinato)copper(II) with aldehydes in basic solution was thought<sup>113,114</sup> to occur as follows:

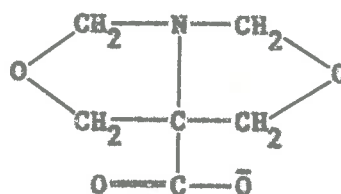


The exchange rate of the  $\alpha$ -carbon hydrogens in alkaline solution has been studied<sup>115,116</sup> for several  $\alpha$ -amino acidato complexes and found to be sufficiently high to indicate ready formation of the  $\alpha$ -carbanion under basic conditions. Treatment of (3) with  $\text{H}_2\text{S}$  under acid conditions releases the  $\alpha$ -hydroxyalkyl substituted amino acid in the aqueous solution and the copper is precipitated as  $\text{CuS}$ . The copper(II) ion may thus be employed as a catalyst in the preparation of  $\alpha$ -hydroxyalkyl substituted amino acids. Only recently<sup>117</sup> has the nature and structure of the intermediate (with  $\text{R} = \text{CH}_3$ ) been sufficiently characterized to suggest a scheme for the mechanism of the copper(II) catalyzed aldehyde-amino acid condensations in basic solution. Glycine was reacted with acetaldehyde in aqueous base in the presence of basic copper(II) carbonate and the product, (4), was treated with  $\text{H}_2\text{S}$  in an acid medium to produce  $R,S$ -threonine. The structure of the copper(II) intermediate, (4) was





(6)



(7)

determined<sup>117,118</sup> by an X-ray analysis and led to the suggestion<sup>117</sup> of a reaction mechanism for the threonine synthesis.

The copper(II) complex formed from the reaction of bis-(*S*-serinato)-copper(II), (5), with excess formaldehyde in base (pH 7-9) was isolated<sup>67</sup> by Brush, Magee, O'Connor and Teo. Both the composition,  $\text{Cu}(\text{C}_{12}\text{H}_{16}\text{N}_2\text{O}_8)$ , and the structure of the complex were determined by the X-ray structural analysis<sup>67</sup> described here, and it was found that two units of the bis-(oxazolidine)carboxylate, (7), were coordinated to copper(II). An optically active intermediate was isolated<sup>67</sup> in the initial phase of the reaction and interpolated to have the structure and composition of (6). This was substantiated by a satisfactory elemental analysis of the compound. Knowledge of the structures of these oxazolidine and bis-(oxazolidine)- $\alpha$ -amino acidatocopper(II) complexes established the mechanism for the reaction as being analogous to that for the preparation<sup>117</sup> of (4) in the threonine synthesis. However the initial formation of (6), which loses activity in base containing formaldehyde at 40°C, suggests that the formaldehyde first attacks the amino or the hydroxy group of (5), rather than the  $\alpha$ -carbanion. Subsequent cyclization then occurs to give (6). A further attack by formaldehyde on the  $\alpha$ -carbon atom and/or the secondary nitrogen, followed by a second cyclization results in the

formation of the bis-copper(II) complex of (7). Treatment of this complex with  $\text{H}_2\text{S}$  releases  $\alpha$ -hydroxymethyl-substituted serine as expected by analogy with the threonine synthesis.<sup>117</sup> Esters of (7) may also be prepared<sup>67</sup> by treatment of the complex with aqueous sodium borohydride solution and subsequent esterification.

### 2.3 EXPERIMENTAL AND DATA REDUCTION

Deep blue tabular crystals of  $\text{Cu}(\text{dioxc})_2$  were kindly supplied by Dr. M.J. O'Connor of La Trobe University, Victoria, Australia. The forms {100}, {010}, {001}, and {011} were evident from the crystal morphology. The crystal system and space group were determined from preliminary precession photographs using  $\text{MoK}\alpha$  radiation. Initial estimates of the unit-cell constants were also obtained from these photographs. The setting angles of 12 high-angle reflections, determined on a Picker four-circle diffractometer with monochromatic  $\text{CuK}\alpha$  radiation, were then used to refine these estimates and to assess errors in the cell constants.

#### *Crystal Data*

$\text{Cu}(\text{C}_6\text{H}_8\text{NO}_4)_2$ , F.W. 379.81,  $F(000) = 780$  electrons

Monoclinic, space group  $P2_1/c$  (No. 14)

$a = 18.559(1)$ ,  $b = 10.142(1)$ ,  $c = 7.345(1)\text{\AA}$ ,  $\beta = 101.60(1)^\circ$ ,  $U = 1354(1)\text{\AA}^3$

$D_m = 1.86(2) \text{ g cm}^{-3}$ ,  $Z = 4$ ,  $D_w = 1.863 \text{ g cm}^{-3}$

$\text{CuK}\alpha$  ( $\lambda = 1.5405\text{\AA}$ ),  $\mu_{\text{CuK}\alpha} = 27.0 \text{ cm}^{-1}$

Intensity data were collected on a Picker automated four-circle diffractometer fitted with a Furnas monochromator.  $\text{CuK}\alpha$  radiation was

used for the intensity measurements on a crystal specimen with the approximate dimensions  $0.12 \times 0.20 \times 0.25$  mm. These data were generously collected by G.B. Robertson and P.O. Whimp of the Research School of Chemistry, A.N.U., Canberra using the  $2\theta$  scan technique. A total of 2395 unique reflections were recorded out to  $2\theta = 127^\circ$ , and three standard reflections were counted after every 60 data measurements. The net counts of the standards showed no systematic change over the period of data measurement. The observed integrated intensity for a reflection,  $h$ , was determined as

$$I_h^{obs} = P - (t_P/t_B)(B_1 + B_2)$$

where  $P$  is the peak count,  $B_1$  and  $B_2$  are the background counts on either side of the peak,  $t_P$  is the peak scan time and  $t_B$  is the total background count time. Lorentz and polarization corrections were applied to these observed intensities and the relative structure factor amplitudes,  $|F_o|$ , were determined from the corrected intensities,  $I_h$ , as

$$|F_o| = +\sqrt{I_h}$$

The standard deviations in the observed structure factors were calculated from

$$\sigma F_o = L_p (P + (t_P/t_B)^2 (B_1 + B_2) + (0.001 I_h^{obs})^2)^{1/2} / 2 |F_o|$$

where  $L_p$  is the Lorentz-polarization factor applied to the  $I_h^{obs}$  and the  $(0.001 I_h^{obs})^2$  allows for machine instability. Of the total 2395 measured intensities, 2035 satisfied the criterion  $I_h^{obs} > 3\sigma(I_h^{obs})$  where  $\sigma(I_h^{obs})$  is the statistical counting error in the observed integrated intensity. The remaining 360 reflections were designated unobserved and precluded from least-squares refinement procedures. Absorption corrections were not applied to the intensity data ( $\mu_{CuK\alpha} = 27.0 \text{ cm}^{-1}$ ). The transmission



factor ranged from about 0.65 to 0.80 over all orientations of the crystal. Program SETUP by B. Foxman and P.O. Whimp of the A.N.U., Canberra, was used for the data reduction procedure described above (Appendix I).

Symmetry equivalent reflections, which were present in the original non-unique data set, were then averaged using programs CUPICK and AULAC (Appendix I). These were also necessary to correlate the output data from SETUP with the input required for the structure solution and refinement programs.

#### 2.4 STRUCTURE SOLUTION AND REFINEMENT

The copper atom was located from a Patterson synthesis based on the mean corrected observed intensities,  $I_h$ . A Fourier map, phased on the copper coordinates, subsequently revealed the positions of the nitrogen and oxygen ligators. One of these appeared to originate from a glide-related complex. The other four donors formed an approximate plane containing the copper atom, and the coordination geometry was observed to be that of a square pyramid. However the nitrogen and oxygen atoms could not be distinguished at this point. A second Fourier synthesis established the carbon atom positions in the copper- $\alpha$ -amino acidato rings, and indicated the *trans* configuration of the planar nitrogen and oxygen donors. The carbonyl oxygens, also determined from this map, allowed the nature of the donor atoms to be decided. The coordinates of the atoms determined above were then used to calculate phases for a third electron density map. The sites of all remaining non-hydrogen atoms in

the structure were located from this synthesis. Both the nitrogen and  $\alpha$ -carbon atoms of each chelate ring were found to be quaternarily substituted and formed a common N-C link for two oxazolidine rings. The calculated elemental analysis for C, N and H was similar to that observed<sup>66</sup> for the compound determined here as  $\text{Cu}(\text{dioxc})_2$ . A least-squares refinement (see Section 1.4 for refinement terminology) of the scale factor, atomic positional parameters and individual isotropic thermal parameters converged with a conventional  $R_1$  factor of 0.115. Anisotropic thermal parameters were included for all atoms in a subsequent refinement which resulted in an  $R_1$  value of 0.060.

The positions of the hydrogen atoms in the oxazolidine rings were calculated by assuming a shortened<sup>119</sup> C-H distance of  $1.02\text{\AA}$  and a tetrahedral H-C-H angle. The hydrogen atoms were included in the refinement with fixed isotropic thermal parameters of  $3.0\text{\AA}^2$ . The refinement was continued in blocks because of computer storage restrictions on the size of the matrix of parameter coefficients. All coordinates, including those for the hydrogens, were refined in one cycle, and the non-hydrogen coordinates and anisotropic temperature factors in the following cycle. The scale factor was always included. This mode of refinement converged with  $R_1 = 0.041$ . The weighting scheme, derived from statistical errors in the observed intensity counts and a machine instability factor, was at this stage adjudged to be unsatisfactory from an analysis of the average  $w(|F_o| - |F_c|)^2$  in ranges of  $|F_o|$ . A new relative weighting scheme designed to flatten the  $w(|F_o| - |F_c|)^2$  vs.  $|F_o|$  curve was devised. All reflections would then have weights differing from the absolute values by approximately the same scale factor. The function  $w(|F_o| - |F_c|)^2$  of

$|F_o|$  was fitted by a least-squares procedure to  $A + B|F_o| + C|F_o|^2$ .

All existing weights,  $w$ , were then multiplied by  $1/(A + B|F_o| + C|F_o|^2)$  to place them approximately on the same relative scale. A final two cycles of refinement incorporating the new weighting scheme reduced  $R_1$  to 0.038 and the final  $R_2$  was 0.050. The error in an observation of unit weight was estimated after the final coordinate refinement cycle to be 5.41 showing that the weights are not on an absolute scale. On introducing the new weighting scheme, errors in the positional parameters decreased by a factor of three. As required by the scheme, the curves of average  $w(|F_o| - |F_c|)^2$  vs.  $|F_o|$  and  $\sin\theta/\lambda$  were relatively flat showing no systematic variations.

Because of the expected<sup>93-96</sup> charge delocalization in the complex, the scattering curve for  $\text{Cu}^+$  was used in the structure factor calculations. The values used were those from International Tables for X-ray Crystallography.<sup>98</sup> For  $\text{Cl}^-$  the scattering factors of Doyle and Turner<sup>97</sup> were used. The values for O, N and C were drawn from International Tables<sup>98</sup> and those for H were obtained from Stewart *et al.*<sup>99</sup> The anomalous components  $\Delta f'$  and  $\Delta f''$ , appropriate for  $\text{CuK}\alpha$  radiation, were included in the scattering factors for Cu and Cl, and were obtained from International Tables.<sup>98</sup>

Fourier computations were performed with Zalkin's program FORDAPB. FUORFLS, a modification of ORFLS by Busing, Martin and Levy, was used for refinement of structural parameters and structure factor calculations. Program PLANEH, a modification of Blount's PLANET, was used to calculate hydrogen atom coordinates and to determine least-squares planes. Derived

structural parameters and their standard deviations were computed with ORFFE by Busing, Martin and Levy. Blount's BLANDA was also used for checks on structural geometry during the refinement. Johnson's ORTEPA was used for the perspective plots of atom ellipsoids, (see Appendix I for details).

## 2.5 TABLES AND PERSPECTIVE PROJECTIONS

The following set of tables and perspective projections are presented with self-explanatory headings, captions and footnotes. Table 2.1 lists the observed and final calculated structure factor amplitudes ( $\times 10$ ). Table 2.2 contains the positional and thermal parameters and Table 2.3, the internal geometry of the formula unit. Least-squares planes, atom distances from the planes, interplanar dihedral angles and torsion angles appear in Tables 2.4, 2.5 and 2.6. Torsion angles are positive if the skew lines  $i \rightarrow j$  and  $k \rightarrow l$ , formed by the atom chain  $i-j-k-l$ , define a right-handed helix. They are negative for a left-handed helix. Intra and interchain close contacts are presented in Tables 2.7 and 2.8. Table 2.9 lists the RMS components of thermal displacement along the principal axes of the thermal ellipsoids. All parameters in these tables were derived from the final least-squares cycle and the standard deviations are enclosed in parentheses. Appendix III contains some additional information on the derivation of standard deviations in the averaged parameters and the interplanar dihedral angles.

## 2.6 STRUCTURAL FEATURES AND DISCUSSION

A projection of the structure down the  $c$  direction is shown in

TABLE 2.1. OBSERVED AND CALCULATED STRUCTURE FACTORS FOR  $\text{Cu}(\text{diox})_2$ .

$h$	$k$	$l$	$F_o$	$F_c$	$F_o/F_c$
0	0	0	100	100	1.00
1	0	0	100	100	1.00
2	0	0	100	100	1.00
3	0	0	100	100	1.00
4	0	0	100	100	1.00
5	0	0	100	100	1.00
6	0	0	100	100	1.00
7	0	0	100	100	1.00
8	0	0	100	100	1.00
9	0	0	100	100	1.00
10	0	0	100	100	1.00
11	0	0	100	100	1.00
12	0	0	100	100	1.00
13	0	0	100	100	1.00
14	0	0	100	100	1.00
15	0	0	100	100	1.00
16	0	0	100	100	1.00
17	0	0	100	100	1.00
18	0	0	100	100	1.00
19	0	0	100	100	1.00
20	0	0	100	100	1.00
21	0	0	100	100	1.00
22	0	0	100	100	1.00
23	0	0	100	100	1.00
24	0	0	100	100	1.00
25	0	0	100	100	1.00
26	0	0	100	100	1.00
27	0	0	100	100	1.00
28	0	0	100	100	1.00
29	0	0	100	100	1.00
30	0	0	100	100	1.00
31	0	0	100	100	1.00
32	0	0	100	100	1.00
33	0	0	100	100	1.00
34	0	0	100	100	1.00
35	0	0	100	100	1.00
36	0	0	100	100	1.00
37	0	0	100	100	1.00
38	0	0	100	100	1.00
39	0	0	100	100	1.00
40	0	0	100	100	1.00
41	0	0	100	100	1.00
42	0	0	100	100	1.00
43	0	0	100	100	1.00
44	0	0	100	100	1.00
45	0	0	100	100	1.00
46	0	0	100	100	1.00
47	0	0	100	100	1.00
48	0	0	100	100	1.00
49	0	0	100	100	1.00
50	0	0	100	100	1.00
51	0	0	100	100	1.00
52	0	0	100	100	1.00
53	0	0	100	100	1.00
54	0	0	100	100	1.00
55	0	0	100	100	1.00
56	0	0	100	100	1.00
57	0	0	100	100	1.00
58	0	0	100	100	1.00
59	0	0	100	100	1.00
60	0	0	100	100	1.00
61	0	0	100	100	1.00
62	0	0	100	100	1.00
63	0	0	100	100	1.00
64	0	0	100	100	1.00
65	0	0	100	100	1.00
66	0	0	100	100	1.00
67	0	0	100	100	1.00
68	0	0	100	100	1.00
69	0	0	100	100	1.00
70	0	0	100	100	1.00
71	0	0	100	100	1.00
72	0	0	100	100	1.00
73	0	0	100	100	1.00
74	0	0	100	100	1.00
75	0	0	100	100	1.00
76	0	0	100	100	1.00
77	0	0	100	100	1.00
78	0	0	100	100	1.00
79	0	0	100	100	1.00
80	0	0	100	100	1.00
81	0	0	100	100	1.00
82	0	0	100	100	1.00
83	0	0	100	100	1.00
84	0	0	100	100	1.00
85	0	0	100	100	1.00
86	0	0	100	100	1.00
87	0	0	100	100	1.00
88	0	0	100	100	1.00
89	0	0	100	100	1.00
90	0	0	100	100	1.00
91	0	0	100	100	1.00
92	0	0	100	100	1.00
93	0	0	100	100	1.00
94	0	0	100	100	1.00
95	0	0	100	100	1.00
96	0	0	100	100	1.00
97	0	0	100	100	1.00
98	0	0	100	100	1.00
99	0	0	100	100	1.00
100	0	0	100	100	1.00

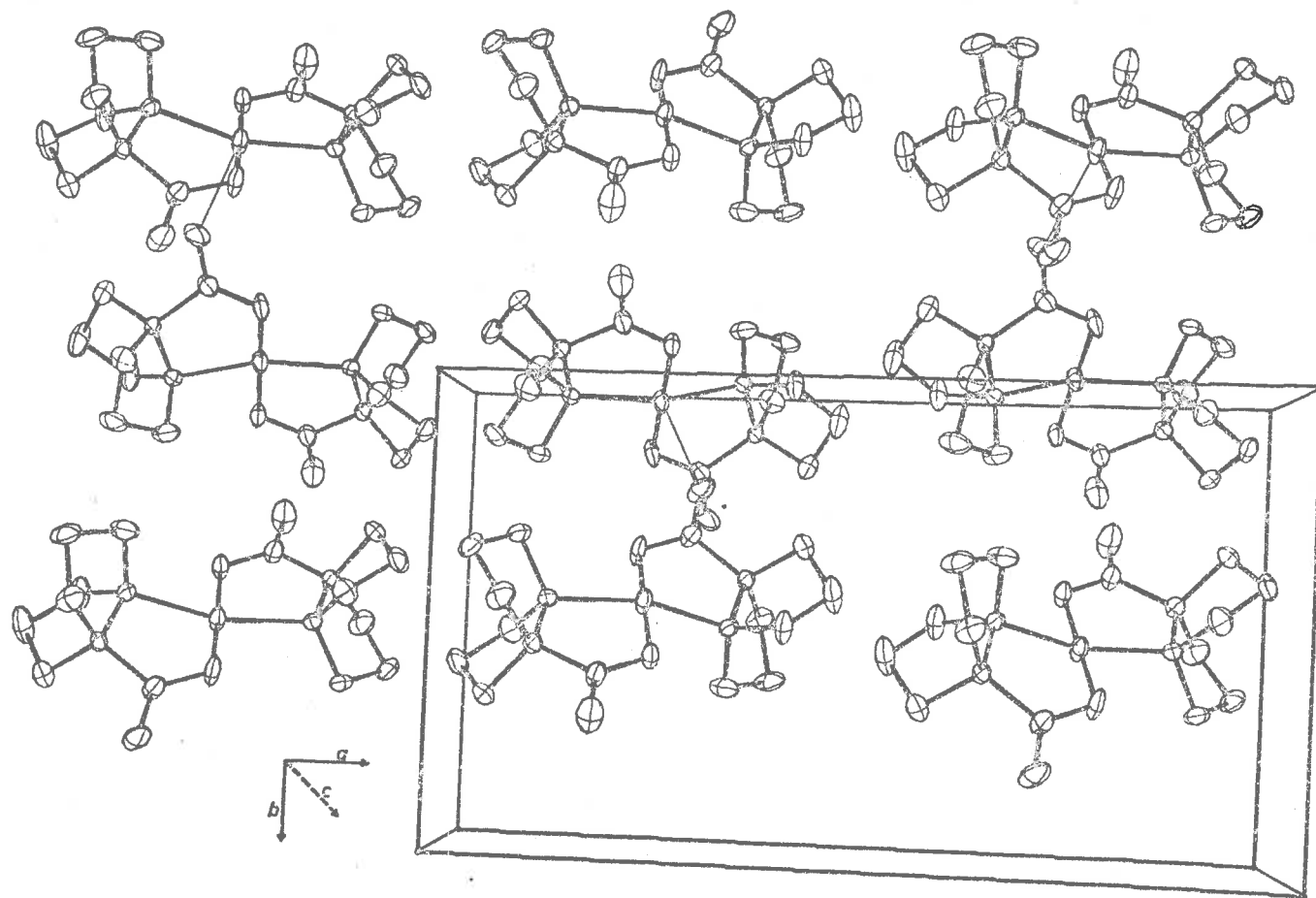


FIGURE 2.1. PROJECTION OF UNIT CELL OF  $\text{Cu}(\text{dioxc})_2$  DOWN  $\underline{c}$ .  
 (Thermal ellipsoids enclose 50% probability.)

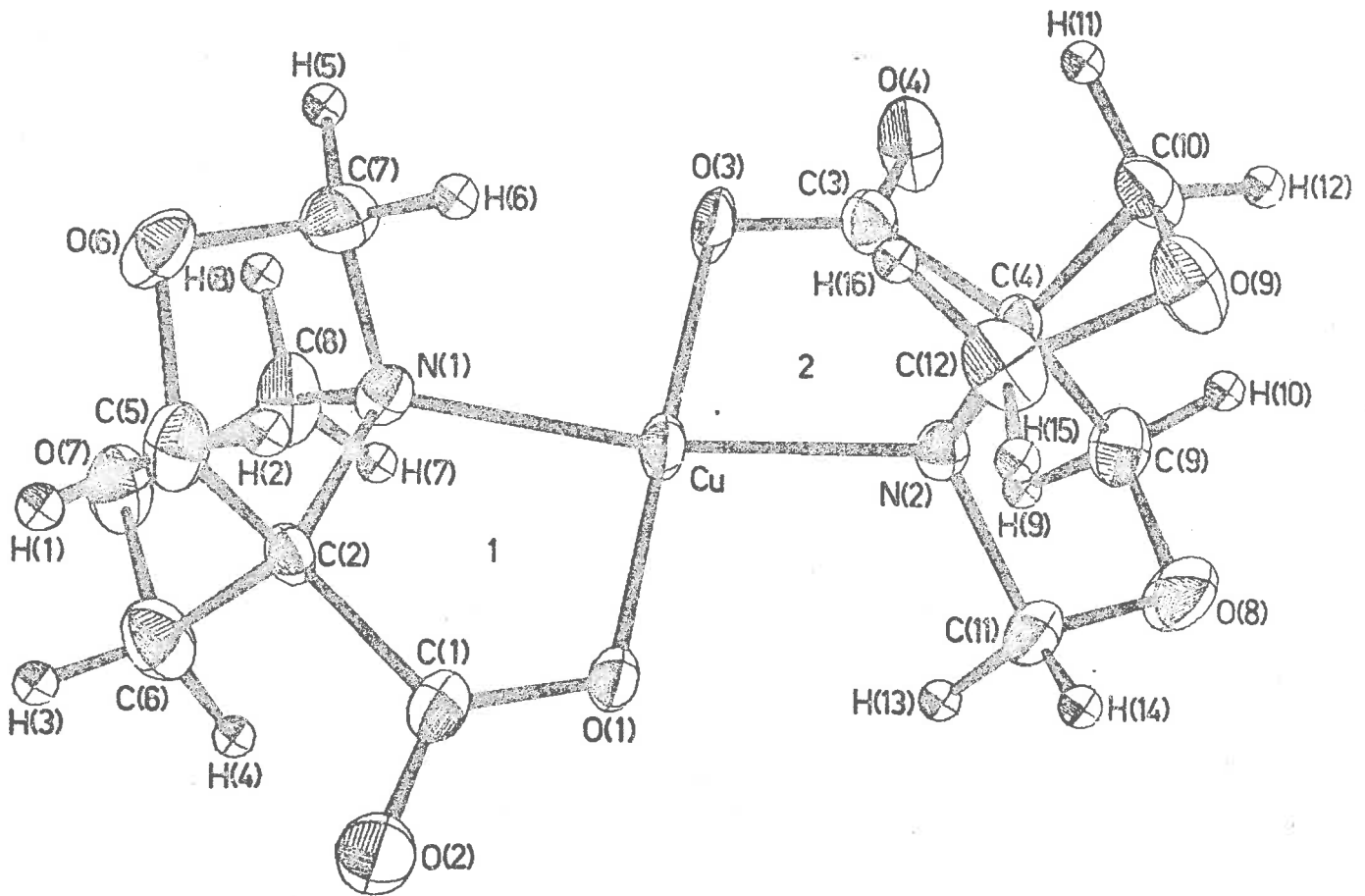


FIGURE 2.2. PERSPECTIVE VIEW OF THE  $\text{Cu}(\text{dioxc})_2$  FORMULA UNIT.

Atom labels are shown.

(Non-hydrogen thermal ellipsoids enclose 50% probability.)

TABLE 2.2. POSITIONAL AND THERMAL PARAMETERS FOR  $\text{Cu}(\text{dioxo})_2$ .

Atom <sup>a</sup>	x	y	z	$\beta_{11}$	$\beta_{22}$	$\beta_{33}$	$\beta_{12}$	$\beta_{13}$	$\beta_{23}$
Cu	2525(0)	335(1)	4927(1)	86(3)	589(10)	912(19)	33(3)	-33(6)	-233(10)
N(1)	1446(2)	326(4)	3705(6)	100(13)	345(44)	921(93)	-8(19)	34(29)	-116(53)
N(2)	3498(2)	-155(4)	6578(6)	101(13)	392(44)	743(88)	29(20)	13(28)	-49(53)
O(1)	2671(2)	-763(4)	2930(5)	83(11)	628(42)	1033(81)	7(18)	21(25)	-208(50)
O(2)	2081(2)	-1926(5)	509(6)	171(14)	1148(60)	1728(104)	67(23)	24(32)	-925(71)
O(3)	2386(2)	1392(4)	7029(6)	95(11)	852(50)	1383(94)	92(20)	-38(28)	-479(58)
O(4)	3079(2)	2749(4)	9026(6)	221(14)	568(47)	1738(103)	136(21)	-138(32)	-541(60)
O(6)	441(2)	-1026(4)	3746(6)	126(12)	663(45)	1760(101)	-89(19)	195(29)	-148(59)
O(7)	652(2)	1304(4)	1210(6)	173(13)	495(43)	1496(97)	109(19)	-69(30)	95(53)
O(8)	4699(2)	595(5)	6819(6)	116(12)	1320(64)	1721(107)	-93(23)	147(31)	-446(71)
O(9)	3978(2)	-1261(4)	9293(6)	282(15)	415(41)	1279(95)	83(20)	-87(32)	168(53)
C(1)	2092(3)	-1155(6)	1803(8)	106(16)	584(59)	1066(118)	42(26)	43(37)	69(76)
C(2)	1361(3)	-582(5)	2045(7)	97(15)	423(51)	734(103)	21(23)	-2(32)	-107(64)
C(3)	2991(3)	1762(5)	8047(8)	128(17)	531(60)	922(113)	55(25)	16(36)	-69(69)
C(4)	3660(3)	868(5)	8092(7)	94(15)	359(51)	741(102)	22(23)	3(32)	-95(63)
C(5)	812(3)	-1632(5)	2444(8)	139(17)	472(57)	1375(131)	-40(26)	21(39)	-103(74)
C(6)	1046(3)	329(6)	410(9)	198(21)	729(71)	1031(124)	61(31)	1(42)	107(79)
C(7)	999(3)	-318(6)	4939(9)	177(19)	712(69)	1168(125)	-43(29)	170(41)	-4(77)
C(8)	1117(3)	1606(5)	2931(9)	164(18)	345(54)	1680(142)	37(26)	-36(42)	-49(74)
C(9)	4335(3)	1577(6)	7695(8)	125(17)	668(63)	1426(136)	-77(28)	33(41)	-60(80)
C(10)	3823(3)	31(6)	9901(8)	207(21)	654(64)	836(119)	24(30)	10(40)	29(74)
C(11)	4143(3)	-110(7)	5633(8)	105(17)	979(76)	1165(131)	17(30)	104(40)	-25(84)
C(12)	3464(3)	-1407(5)	7607(9)	275(22)	338(55)	1379(138)	-38(28)	-32(45)	-33(73)

(contd.)



**TABLE 2.2.** (contd.)

*Positional parameters for the hydrogen atoms*

Atom <sup>b</sup>	<i>x</i>	<i>y</i>	<i>z</i>	Atom	<i>x</i>	<i>y</i>	<i>z</i>
H(1)	47(9)	-177(16)	131(22)	H(9)	414(8)	231(16)	669(21)
H(2)	109(8)	-242(16)	310(21)	H(10)	471(8)	189(16)	886(21)
H(3)	69(9)	-13(16)	-53(22)	H(1)	335(9)	-10(15)	1047(21)
H(4)	151(9)	77(16)	-7(21)	H(12)	427(9)	40(16)	1073(21)
H(5)	73(8)	43(16)	576(21)	H(13)	398(8)	48(16)	448(22)
H(6)	137(9)	-100(16)	578(21)	H(14)	433(8)	-111(16)	539(21)
H(7)	156(9)	220(16)	279(21)	H(15)	355(9)	-219(16)	703(21)
H(8)	77(8)	198(16)	383(21)	H(16)	291(9)	-145(16)	775(21)

<sup>a</sup> Positional parameters ( $\times 10^4$ ). Anisotropic thermal parameters ( $\times 10^5$ ).

<sup>b</sup> Positional parameters ( $\times 10^3$ ).

Hydrogen atoms were refined with fixed isotropic thermal parameters of  $3.0\text{\AA}^2$ .

TABLE 2.3. INTRAMOLECULAR BOND LENGTHS AND ANGLES.

<i>Ligand 1</i>		<i>Ligand 2</i>	
Cu-O(1)	1.904(4)Å	Cu-O(3)	1.939(4)Å
Cu-N(1)	2.024(4)	Cu-N(2)	2.024(4)
O(1)-C(1)	1.280(6)	O(3)-C(3)	1.274(6)
C(1)-O(2)	1.228(7)	C(3)-O(4)	1.225(7)
C(1)-C(2)	1.520(7)	C(3)-C(4)	1.532(7)
C(2)-N(1)	1.510(6)	C(4)-N(2)	1.506(6)
C(2)-C(5)	1.542(7)	C(4)-C(10)	1.554(7)
C(5)-O(6)	1.425(7)	C(10)-O(9)	1.430(7)
O(6)-C(7)	1.410(7)	O(9)-C(12)	1.411(7)
C(7)-N(1)	1.496(7)	C(12)-N(2)	1.485(7)
C(2)-C(6)	1.534(8)	C(4)-C(9)	1.523(7)
C(6)-O(7)	1.425(7)	C(9)-O(8)	1.427(7)
O(7)-C(8)	1.414(7)	O(8)-C(11)	1.405(7)
C(8)-N(1)	1.497(7)	C(11)-N(2)	1.499(7)
Cu-O(1)-C(1)	116.72(34)°	Cu-O(3)-C(3)	112.74(34)°
O(1)-C(1)-C(2)	117.28(48)	O(3)-C(3)-C(4)	116.98(47)
C(1)-C(2)-N(1)	112.09(42)	C(3)-C(4)-N(2)	110.56(40)
C(2)-N(1)-Cu	107.16(30)	C(4)-N(2)-Cu	107.13(29)
N(1)-Cu-O(1)	86.35(16)	N(2)-Cu-O(3)	84.52(16)
O(1)-C(1)-O(2)	125.45(51)	O(3)-C(3)-O(4)	125.61(52)
O(2)-C(1)-C(2)	117.23(49)	O(4)-C(3)-C(4)	117.38(48)
N(1)-C(2)-C(5)	103.50(42)	N(2)-C(4)-C(10)	103.35(40)
C(2)-C(5)-O(6)	104.82(43)	C(4)-C(10)-O(9)	104.57(44)
C(5)-O(6)-C(7)	104.10(41)	C(10)-O(9)-C(12)	103.31(42)
O(6)-C(7)-N(1)	105.85(46)	O(9)-C(12)-N(2)	105.44(43)
C(7)-N(1)-C(2)	104.02(39)	C(12)-N(2)-C(4)	103.65(41)
N(1)-C(2)-C(6)	103.11(41)	N(2)-C(4)-C(9)	103.47(42)
C(2)-C(6)-O(7)	103.96(47)	C(4)-C(9)-O(8)	103.83(44)
C(6)-O(7)-C(8)	104.29(41)	C(9)-O(8)-C(11)	106.25(42)
O(7)-C(8)-N(1)	106.30(42)	O(8)-C(11)-N(2)	106.46(46)

(contd.)

TABLE 2.3. (contd.)

<i>Ligand 1</i>		<i>Ligand 2</i>	
C(8)-N(1)-C(2)	104.68(41)°	C(11)-N(2)-C(4)	105.19(40)°
C(1)-C(2)-C(6)	110.30(47)	C(3)-C(4)-C(9)	114.25(44)
C(1)-C(2)-C(5)	113.43(45)	C(3)-C(4)-C(10)	111.37(45)
C(5)-C(2)-C(6)	113.76(46)	C(10)-C(4)-C(9)	112.96(44)
Cu-N(1)-C(8)	117.09(32)	Cu-N(2)-C(11)	114.45(35)
Cu-N(1)-C(7)	110.68(35)	Cu-N(2)-C(12)	112.99(34)
C(7)-N(1)-C(8)	112.06(43)	C(12)-N(2)-C(11)	112.36(45)
<i>Apical interaction with Cu</i>			
Cu-O(4 <sup>1</sup> ) <sup>a</sup>	2.354(4)Å		
<i>Interligand angles at Cu</i>			
O(1)-Cu-N(2)	94.03(16)°	O(4 <sup>1</sup> )-Cu-N(1)	109.16(16)°
O(3)-Cu-N(1)	94.44(16)	O(4 <sup>1</sup> )-Cu-O(1)	97.38(16)
N(1)-Cu-N(2)	161.58(18)	O(4 <sup>1</sup> )-Cu-N(2)	89.08(16)
O(1)-Cu-O(3)	177.66(17)	O(4 <sup>1</sup> )-Cu-O(3)	84.45(17)

<sup>a</sup> See Table 2.8 for definitions of symmetry transformations identified by superscripts.

**TABLE 2.4. LEAST-SQUARES PLANES AND ATOM DEVIATIONS.**

The form of the planes equations is described in Table 1.4.

The residuals were assigned weights based on the estimated standard deviations of positional parameters.

<i>Plane</i>	<i>L</i>	<i>M</i>	<i>N</i>	<i>P</i>	<i>Symbol</i>
N(1),O(1),Cu,O(3),N(2)	0.3884	0.8059	-0.4469	0.2075	1
N(1),Cu,O(1)	0.2506	0.8106	-0.5293	-0.6081	2
N(2),Cu,O(3)	0.5178	0.7778	-0.3563	1.0518	3
N(1),O(4 <sup>1</sup> ),N(2),Cu <sup>a</sup>	0.3978	-0.5011	-0.7686	-1.3233	4
O(1),O(4 <sup>1</sup> ),O(3),Cu	-0.7950	0.2988	-0.5280	-4.9195	5
Cu,N(1),C(2),C(1),O(1)	0.2414	0.7990	-0.5508	-0.7238	6
Cu,N(2),C(4),C(3),O(3)	0.4794	0.7399	-0.4719	0.4715	7
Cu,N(1),C(2)	0.2726	0.7719	-0.5743	-0.6942	8
C(2),C(1),O(1),O(2)	0.2290	0.7579	-0.6109	-0.8392	9
Cu,N(2),C(4)	0.6083	0.5531	-0.5693	0.5786	10
C(4),C(3),O(3),O(4)	0.3884	0.5165	-0.7631	-1.8113	11
N(1),C(2),C(5),C(7)	-0.7058	0.5533	-0.4424	-2.5912	12
C(5),O(6),C(7)	-0.0749	0.8004	-0.5948	-2.4566	13
N(1),C(2),C(6),C(8)	0.9532	0.2828	-0.1066	1.8225	14
C(6),O(7),C(8)	0.5382	0.7179	-0.4416	1.1191	15
N(2),C(4),C(10),C(12)	0.9923	-0.1184	-0.0368	5.2870	16
C(10),O(9),C(12)	0.7775	0.3847	-0.4975	0.8566	17
N(2),C(4),C(9),C(11)	-0.4174	0.6326	-0.6524	-5.5294	18
C(9),O(8),C(11)	0.2083	0.6367	-0.7424	-1.6521	19

(contd.)

TABLE 2.4. (contd.)

*Distances from the Planes (Å)*

*Chelate ring and metal, donor atom planes*

Atom <sup>b</sup>	1	2	3	4	5	6	7	8	9	10	11
Cu	0.020	0.0	0.0	0.003	0.002	-0.001	0.006	0.0	-0.162	0.0	0.820
N(1)	-0.304	0.0	-0.640	-0.042	1.915	0.035	-0.462	0.0	-0.050		
N(2)	-0.304	-0.640	0.0	-0.040	-2.017		-0.173			0.0	0.263
O(1)	-0.015	0.0	-0.061	1.890	-0.022	0.037	0.131	0.120	0.002		
O(2)						-0.124		0.009	0.003		
O(3)	-0.013	-0.074	0.0	-1.923	-0.024		-0.188			-0.614	-0.002
O(4)							0.629			-0.067	-0.002
C(1)		-0.121				-0.053		0.032	-0.012		
C(2)		-0.091				-0.021	-0.537	0.0	0.003		
C(3)			0.536				0.212			-0.230	0.011
C(4)			0.458				0.117			0.0	-0.003
O(4 <sup>1</sup> )	2.327			-0.010	-0.001	2.188	2.306				

*Oxazolidine ring planes*

Atom <sup>b</sup>	12	13	Atom	14	15	Atom	16	17	Atom	18	19
N(1)	0.017	0.976	N(1)	0.021	-0.911	N(2)	0.038	1.023	N(2)	0.037	-0.812
C(2)	-0.024	0.944	C(2)	-0.030	-0.997	C(4)	-0.049	0.939	C(4)	-0.050	-0.944
C(5)	0.019	0.0	C(6)	0.029	0.0	C(10)	0.048	0.0	C(9)	0.044	0.0
C(7)	-0.023	0.0	C(8)	-0.026	0.0	C(12)	-0.050	0.0	C(11)	-0.049	0.0
O(6)	0.564	0.0	O(7)	-0.560	0.0	O(9)	0.585	0.0	O(8)	-0.510	0.0

<sup>a</sup> See Table 2.8 for symmetry transformations.

<sup>b</sup> The mean isotropic e.s.d.'s for Cu, N, O and C coords. are  $8 \times 10^{-4}$ ,  $4 \times 10^{-3}$ ,  $4 \times 10^{-3}$  and  $6 \times 10^{-3}$  Å respectively.

TABLE 2.5. INTERPLANAR DIHEDRAL ANGLES.

Angles between planes defined in Table 2.4.<sup>a</sup>

Planes	Angle	Planes	Angle	Planes	Angle
1,2	9.2°	3,11	29.0°	12,14	118.0°
1,3	9.2	4,5	86.5	14,6	121.0
1,4	84.6	6,7	14.8	14,8	122.6
1,5	80.3	6,8	2.7	14,15	40.3
1,6	10.3	6,9	4.2	16,7	113.9
1,7	6.6	7,10	14.2	16,10	124.0
2,3	18.4(2)	7,11	21.8	16,17	41.9
2,4	84.3	8,9	3.4	16,18	117.7
2,5	71.2	10,11	17.0	18,7	125.2
2,9	5.7	12,6	121.0	18,10	117.9
3,4	84.8	12,8	119.3	18,19	36.9
3,5	89.5	12,13	40.6		

Angles between metal, donor atom planes of three atoms<sup>b,c</sup>

Plane 1	Plane 2	Angle
O(1),Cu,N(1)	N(1),Cu,O(3)	2.21(17) <sup>o</sup>
N(1),Cu,O(1)	O(1),Cu,N(2)	18.45(18)
O(3),Cu,N(2)	N(1),Cu,O(3)	18.46(18)
O(3),Cu,N(2)	N(2),Cu,O(1)	1.85(17)
N(1),Cu,O(3)	N(2),Cu,O(1)	18.72(18)
N(1),Cu,O(4 <sup>1</sup> )	O(3),Cu,O(4 <sup>1</sup> )	92.78(17)
N(1),Cu,O(4 <sup>1</sup> )	O(1),Cu,O(4 <sup>1</sup> )	88.69(18)
N(1),Cu,O(4 <sup>1</sup> )	O(4 <sup>1</sup> ),Cu,N(2)	2.64(19)
O(1),Cu,O(4 <sup>1</sup> )	O(4 <sup>1</sup> ),Cu,O(3)	1.47(15)
O(3),Cu,O(4 <sup>1</sup> )	N(2),Cu,O(4 <sup>1</sup> )	84.58(16)
O(1),Cu,O(4 <sup>1</sup> )	N(2),Cu,O(4 <sup>1</sup> )	93.95(17)

<sup>a</sup> For inter-ring angles where the planes bounded by the defining atoms meet at a common edge, the included angle is shown. For all other interplanar angles, the angle tabulated is that <90°.

<sup>b</sup> This excludes the interligand plane angle tabulated previously.

<sup>c</sup> The angle presented is that between the normals  $(\underline{1,2}) \times (\underline{1,3})$  and  $(\underline{4,5}) \times (\underline{4,6})$  where 1, 2, 3 and 4, 5, 6 refer to the atoms of planes 1 and 2 respectively.  $(\underline{1,2})$  etc. are interatom vectors.

**TABLE 2.6. TORSION ANGLES IN THE LIGANDS.**

<i>Defining Atoms</i>	<i>Torsion Angle</i>	<i>Defining Atoms</i>	<i>Torsion Angle</i>
N(1)-Cu-O(1)-C(1)	-6.1(4)°	N(2)-Cu-O(3)-C(3)	+27.1(4)°
Cu-O(1)-C(1)-C(2)	+6.8(7)	Cu-O(3)-C(3)-C(4)	-28.5(6)
O(1)-C(1)-C(2)-N(1)	-3.3(7)	O(3)-C(3)-C(4)-N(2)	+12.0(7)
C(1)-C(2)-N(1)-Cu	-1.3(5)	C(3)-C(4)-N(2)-Cu	+9.3(5)
C(2)-N(1)-Cu-O(1)	+3.6(3)	C(4)-N(2)-Cu-O(3)	-18.6(3)
N(1)-C(2)-C(5)-O(6)	+20.9(5)	N(2)-C(4)-C(10)-O(9)	+17.6(5)
C(2)-C(5)-O(6)-C(7)	-39.3(5)	C(4)-C(10)-O(9)-C(12)	-38.7(6)
C(5)-O(6)-C(7)-N(1)	+42.7(5)	C(10)-O(9)-C(12)-N(2)	+45.7(6)
O(6)-C(7)-N(1)-C(2)	-28.2(5)	O(9)-C(12)-N(2)-C(4)	-33.4(5)
C(7)-N(1)-C(2)-C(5)	+4.0(5)	C(12)-N(2)-C(4)-C(10)	+8.9(5)
N(1)-C(2)-C(6)-O(7)	-28.4(5)	N(2)-C(4)-C(9)-O(8)	-28.8(5)
C(2)-C(6)-O(7)-C(8)	+42.2(6)	C(4)-C(9)-O(8)-C(11)	+39.6(6)
C(6)-O(7)-C(8)-N(1)	-39.4(6)	C(9)-O(8)-C(11)-N(2)	-34.3(6)
O(7)-C(8)-N(1)-C(2)	+20.3(6)	O(8)-C(11)-N(2)-C(4)	+14.7(6)
C(8)-N(1)-C(2)-C(6)	+5.1(5)	C(11)-N(2)-C(4)-C(9)	+8.7(5)

TABLE 2.7. INTRACHAIN CLOSE CONTACTS TO 3.5Å.

*Inter-ring contacts*

O(6)...O(7)	3.083(6)Å	O(9)...O(8)	3.100(6)Å
O(6)...C(6)	3.203(8)	O(9)...C(9)	3.227(7)
O(6)...C(8)	3.060(7)	O(9)...C(11)	3.001(8)
O(7)...C(5)	3.110(7)	O(8)...C(10)	3.088(8)
O(7)...C(7)	3.149(7)	O(8)...C(12)	3.200(7)

*Intermolecular contacts<sup>a</sup>*

O(1)...O(4 <sup>1</sup> ) <sup>b</sup>	3.212(6)Å	C(9)...O(4 <sup>1</sup> )	3.262(7)Å
O(3)...O(4 <sup>1</sup> )	2.901(6)	C(11)...O(4 <sup>1</sup> )	3.176(7)
N(1)...O(4 <sup>1</sup> )	3.573(6)	Cu...C(3 <sup>1</sup> )	3.436(6)
H(2)...O(4 <sup>1</sup> )	3.080(6)	O(1)...C(10 <sup>11</sup> )	3.483(7)
C(3)...O(4 <sup>1</sup> )	3.031(7)	O(7)...C(8 <sup>1</sup> )	3.446(7)
C(4)...O(4 <sup>1</sup> )	3.279(7)	C(8)...O(3 <sup>1</sup> )	3.276(7)

*Contacts with hydrogen atoms to 2.8Å<sup>c</sup>*

H(9)...O(4 <sup>1</sup> )	2.49Å	H(7)...O(3 <sup>1</sup> )	2.25Å
H(13)...O(4 <sup>1</sup> )	2.43	O(7)...H(8 <sup>1</sup> )	2.51
H(7)...O(4 <sup>1</sup> )	2.78	O(1)...H(11 <sup>11</sup> )	2.50
H(9)...H(12 <sup>1</sup> )	2.45		

<sup>a</sup> A molecule is here defined as a formula unit of the molecular chain.

<sup>b</sup> See Table 2.8 for symmetry transformations.

<sup>c</sup> H...H contacts >2.6Å are not included.

The e.s.d's were not computed since the variance-covariance matrix from the final least-squares cycle did not involve the hydrogen atom parameters.



**TABLE 2.8. INTERCHAIN DISTANCES TO 3.5Å.***Non-hydrogen contacts*

O(7)...O(6 <sup>111</sup> )	3.387(5)Å	C(7)...O(2 <sup>v1</sup> )	3.418(8)Å
O(7)...C(5 <sup>1v</sup> )	3.430(7)	C(12)...O(1 <sup>v1</sup> )	3.257(7)
O(6)...O(6 <sup>v</sup> )	3.409(8)	C(12)...O(2 <sup>v1</sup> )	3.199(7)
O(6)...C(7 <sup>v</sup> )	3.313(7)	O(8)...O(8 <sup>v11</sup> )	3.324(9)
O(1)...O(2 <sup>v1</sup> )	3.334(6)	O(8)...C(11 <sup>v11</sup> )	3.109(7)
C(1)...O(2 <sup>v1</sup> )	3.350(7)	C(11)...C(11 <sup>v11</sup> )	3.498(11)
C(5)...O(2 <sup>v1</sup> )	3.260(7)		

*Contacts with hydrogen atoms to 2.8Å<sup>a</sup>*

O(7)...H(1 <sup>1v</sup> )	2.54Å	H(6)...O(2 <sup>v1</sup> )	2.52Å
O(7)...H(3 <sup>1v</sup> )	2.71	H(6)...H(7 <sup>v1</sup> )	2.47
O(6)...H(5 <sup>v</sup> )	2.36	H(16)...O(2 <sup>v1</sup> )	2.60
H(2)...O(2 <sup>v1</sup> )	2.38	O(8)...H(14 <sup>v11</sup> )	2.71

*Symmetry transformations described by the superscripts in Tables 2.3, 2.4, 2.5, 2.7 and 2.8.*

1	x	$\bar{y} + 1/2$	$z - 1/2$
11	x	y	$z - 1$
111	$\bar{x}$	$y + 1/2$	$\bar{z} + 1/2$
1v	$\bar{x}$	$\bar{y}$	$\bar{z}$
v	$\bar{x}$	$\bar{y}$	$\bar{z} + 1$
v1	x	$\bar{y} - 1/2$	$z + 1/2$
v11	$\bar{x} + 1$	$\bar{y}$	$\bar{z} + 1$

<sup>a</sup> H...H contacts >2.6Å are not included.  
As in Table 2.7 the e.s.d's were not computed.

TABLE 2.9. RMS COMPONENTS OF THERMAL DISPLACEMENT ALONG PRINCIPAL AXES.

<i>Atom</i>	<i>Axis 1</i>	<i>Axis 2</i>	<i>Axis 3</i>
Cu	0.112(2)Å	0.140(2)Å	0.199(1)Å
N(1)	0.123(9)	0.133(9)	0.164(8)
N(2)	0.123(9)	0.135(9)	0.157(8)
O(1)	0.117(8)	0.149(7)	0.197(6)
O(2)	0.131(9)	0.167(7)	0.302(7)
O(3)	0.116(8)	0.149(8)	0.253(6)
O(4)	0.123(9)	0.163(7)	0.279(6)
O(6)	0.125(8)	0.185(7)	0.223(6)
O(7)	0.121(8)	0.185(7)	0.224(6)
O(8)	0.132(8)	0.192(7)	0.279(7)
O(9)	0.124(9)	0.182(7)	0.244(6)
C(1)	0.129(11)	0.162(10)	0.184(9)
C(2)	0.120(11)	0.133(11)	0.165(9)
C(3)	0.136(10)	0.151(10)	0.183(9)
C(4)	0.120(11)	0.125(11)	0.159(9)
C(5)	0.138(10)	0.166(9)	0.198(9)
C(6)	0.149(11)	0.191(10)	0.205(9)
C(7)	0.151(10)	0.182(10)	0.198(9)
C(8)	0.130(11)	0.159(10)	0.226(9)
C(9)	0.133(11)	0.195(9)	0.198(9)
C(10)	0.144(11)	0.183(9)	0.196(9)
C(11)	0.127(11)	0.165(10)	0.234(9)
C(12)	0.130(11)	0.178(10)	0.235(9)

Figure 2.1. The copper atom is seen to be five-coordinate and the coordination geometry is pseudo-square pyramidal. The dioxc ligands coordinate in the basal plane of the square pyramid, and the apical bond occurs between the copper atom of one  $\text{Cu}(\text{dioxc})_2$  formula unit and the carbonyl oxygen of a glide-related unit along the  $c$  axis. The structure thus consists of infinite molecular chains of  $\text{Cu}(\text{dioxc})_2$  units along  $c$ . The apical Cu-O interaction has a distance of  $2.354(4)\text{\AA}$ . Similar coordination geometries and apical Cu-O distances have been observed in other bis-( $\alpha$ -amino acidato)copper(II) complex structures. The *cis*-bis-(*R*- $\alpha$ -alaninato)copper(II) structure<sup>120</sup> has such a square pyramidal coordination sphere around the copper atom. Here the *cis* arranged  $\alpha$ -amino acidato ligands coordinate in the basal plane and a screw-related carbonyl oxygen forms the apical bond with the copper atom, thus forming infinite spiral molecular chains similar to those of  $\text{Cu}(\text{dioxc})_2$ . The apical Cu-O distance in this structure is  $2.390(7)\text{\AA}$ . *Trans*-bis-(*S*-tyrosinato)copper(II)<sup>121</sup> also forms infinite chains coiled around crystallographic screw axes and the five-coordinate copper again has an apical bonding interaction of  $2.39\text{\AA}$  with the carbonyl oxygen of a screw-related  $\text{Cu}(\text{S-tyro})_2$  unit. In the aquobis-(*NH*-dimethylglycinato)copper(II) dihydrate structure,<sup>122</sup> the copper coordination sphere is square pyramidal but the apical Cu-O bond is between the copper atom and a water molecule ligand, and has the relatively short value of  $2.28(2)\text{\AA}$ . The complex *cis*-bis-(glycinato)-diaquocopper(II) in the structure<sup>123</sup> of  $\text{Cu}(\text{gly})_2\text{H}_2\text{O}$  has an essentially similar coordination geometry with the aquo ligand at the apex of the square pyramid and  $2.40(1)\text{\AA}$  from the copper atom. The

above values are within the ranges 2.30 to 2.74 and 2.30 to 2.53Å listed by Freeman<sup>124</sup> for Cu-O(carbonyl) and Cu-O(apical aquo) bond distances respectively.

Interchain distances for the Cu(dioxc)<sub>2</sub> structure are listed in Table 2.8. There are no non-hydrogen contacts less than the sum of the literature values<sup>102</sup> for the van der Waals (VDW) radii. The oxazolidine oxygens, O(6) and O(7), and the carbonyl oxygen, O(2), make close contacts with hydrogen atoms on neighbouring chains but these are only 0.1 to 0.2Å less than the VDW radii sum. In particular there is no obvious hydrogen bonding in the structure. This is a probable consequence of the absence of hydrogen substituents on the relatively electronegative atoms in the Cu(dioxc)<sub>2</sub> unit. In the Cu(gly)<sub>2</sub>H<sub>2</sub>O structure<sup>123</sup> no hydrogen bonding occurs with the chelated oxygen of the amino acid carboxylate group. This is also the case for the Cu(S-tyro)<sub>2</sub> structure,<sup>121</sup> whereas in both the Cu(R-α-ala)<sub>2</sub><sup>120</sup> and the Cu(NN-dingly)<sub>2</sub>H<sub>2</sub>O.2H<sub>2</sub>O<sup>122</sup> structures there is a hydrogen bond with the chelated oxygen of a carboxylate group. The apical Cu-O bond for the latter structure is significantly shorter than that for the other structures. Thus hydrogen bonding with chelated carboxyl oxygens does not appear to affect the strength of the apical Cu-O bond in these structures although other crystal packing forces may well determine the resultant coordination geometry. This is in contrast with the effect observed in NN'-ethylenbis-(salicylideneiminato)copper(II)<sup>125</sup> and its p-nitrophenol<sup>126</sup> and chloroform<sup>127</sup> adducts, where an increase in the strength of hydrogen bonding to one of the coordinated carboxyl oxygens

was accompanied by a decrease in the strength of the axial Cu-O bond between complex units.

There are no close non-hydrogen contacts between Cu(dioxc)<sub>2</sub> units in the same chain, other than the Cu-O(4<sup>1</sup>) apical interaction of the square pyramid. As is evident from Table 2.7 however, there is a close contact between the C(8) hydrogen, H(7), (see Figure 2.2 for the labelling scheme) and the chelated oxygen O(3<sup>1</sup>) of the glide-related carboxyl group containing the apical ligand O(4<sup>1</sup>). Several other contacts are only 0.09 to 0.17Å less than the sum of the VDW<sup>102</sup> radii for hydrogen and oxygen. The H(7)...O(3<sup>1</sup>) contact is 2.25(6)Å or shorter because of the reduction in the observed X-ray C(8)-H(7) distance, but such close contacts are not unusual.<sup>128</sup> In fact the C(8)-H(7)...O(3<sup>1</sup>) interaction, with a C...O distance of 3.276(7)Å, an O...H distance of less than 2.25(6)Å and a C-H...O angle of 169°, has a geometry which is very similar to that found<sup>101</sup> for previously postulated C-H...O hydrogen bonds.

The pseudo-square planar nature of the Cu(dioxc)<sub>2</sub> formula unit is illustrated in Figure 2.2. The dioxc ligands are chelated to copper in the *trans* configuration, and each consists of a glycinato substrate in which the N-C<sup>α</sup> bond is common to two oxazolidine rings formed by cyclization of the substituents on the N and C<sup>α</sup> atoms. The oxazolidine rings are similar to those found in *R,S*-bis-(2,5-dimethyloxazolidine-4-carboxylato)copper(II) dihydrate.<sup>117,118</sup>

Table 2.3 contains the internal geometry of the Cu(dioxc)<sub>2</sub> unit and the angular geometry of the square pyramidal coordination polyhedron. The Cu-O(chelate) bond lengths of 1.904(4) and 1.939(4)Å differ significantly, possibly because of changes in the bonding properties of

O(3) resulting from the function of O(4) as a ligator. A similar effect is found in  $\text{Cu}(S\text{-tyro})_2$ <sup>121</sup> but not in  $\text{cis-Cu}(R\text{-}\alpha\text{-ala})_2$ <sup>120</sup> both of these structures having a carbonyl oxygen functioning as a ligand. Hence the effect may be caused by the  $\text{H}(7)\dots\text{O}(3^{\text{i}})$  interaction in  $\text{Cu}(\text{dioxc})_2$  if  $\text{O}(3^{\text{i}})$  acts as a donor in a  $\text{C-H}\dots\text{O}$  hydrogen bond. A repulsive contact in this structure would decrease the  $\text{Cu-O}(3)$  distance relative to  $\text{Cu-O}(1)$ , whereas the converse is observed. In any case, the short  $\text{Cu-O}(\text{chelate})$  distance found here is significantly less than those of 1.925(3) and 1.973(3)Å for  $\text{Cu}(S\text{-tyro})_2$ <sup>121</sup> and the means of 1.947(5), 1.952(6) and 1.97(2)Å observed in the  $\text{cis-Cu}(R\text{-}\alpha\text{-ala})_2$ <sup>120</sup> the  $\text{Cu}(\text{gly})_2\text{H}_2\text{O}$ <sup>123</sup> and the  $\text{Cu}(\text{dingly})_2\text{H}_2\text{O}\cdot 0.2\text{H}_2\text{O}$ <sup>122</sup> structures respectively. The equivalent distances found in the  $\text{bis-}R,S\text{-}(\text{prolinato})\text{copper(II)}$  dihydrate<sup>129</sup> and the  $\text{Cu-}R,S\text{-}(\text{dimoxc})_2(\text{H}_2\text{O})_2$ <sup>118</sup> structures were 2.03(4) and 1.962(15)Å. The mean  $\text{Cu-O}(\text{chelate})$  distance given by Freeman<sup>124</sup> for copper-amino acid complexes is 1.98(1)Å and that by Muir<sup>130</sup> for 53 copper-carboxylato complexes is 1.96Å over a range of 1.89 to 2.02Å. In many of the latter complexes however, the  $\text{Cu-O}$  bond was not part of a copper-amino acid chelate ring. The square planar complex,  $\text{bis-}(1\text{-aminocyclopentanecarboxylato})\text{copper(II)}$ <sup>131</sup> has a  $\text{Cu-O}(\text{chelate})$  bond length of 1.91(1)Å, which is significantly shorter than most of the values listed above and similar to that found here for  $\text{Cu-O}(1)$ . The  $\text{Cu-N}$  distance of 2.024(4)Å found here in  $\text{Cu}(\text{dioxc})_2$  is similar to the mean literature values of 2.00(1)<sup>124</sup> and 2.01Å<sup>130</sup> for  $\text{Cu-N}(\text{amino})$  and  $\text{Cu-N}(\text{overall})$  bonds. It also compares well with the distances 2.013(14), 1.99(4), 2.003(3) and 2.05(2)Å found in the  $\text{trans}$  structures of  $\text{Cu-}R,S\text{-}(\text{dimoxc})_2(\text{H}_2\text{O})_2$ <sup>118</sup>

$\text{Cu-}R,S\text{-(pro)}_2(\text{H}_2\text{O})_2$ ,<sup>129</sup>  $\text{Cu}(S\text{-tyro})_2$ <sup>121</sup> and  $\text{Cu}(\text{dingly})_2\text{H}_2\text{O}\cdot 2\text{H}_2\text{O}$ .<sup>122</sup>

The comparison of Cu-N and Cu-O(chelate) bond lengths for these structures (including  $\text{Cu}(\text{dioxc})_2$ ) reveals some evidence for the decrease in axial bonding strength with increase in the basal plane ligand field strength.<sup>132</sup> The average chelate ring C-C bond length of 1.526(5)Å is slightly shorter than the paraffinic value<sup>98</sup> (1.541(3)Å), but is in agreement with the average value of 1.52(1)Å from the literature,<sup>124</sup> and is not significantly different from those found in the structures discussed above. In the oxazolidine rings, however, the mean C-C bond distance increases to a paraffinic<sup>98</sup> value of 1.538(4)Å. A similar increase occurs in the oxazolidine rings of  $\text{Cu-}R,S\text{-(dioxc)}_2(\text{H}_2\text{O})_2$ <sup>118</sup> and the pyrrolidine rings of  $\text{Cu-}R,S\text{-(pro)}_2(\text{H}_2\text{O})_2$ ,<sup>129</sup> although the large standard deviations in these structures probably nullify the significance of the increase. In the chelate ring, the N-C bond has a length of 1.508(4)Å which is similar to the mean literature value<sup>124</sup> of 1.49(1)Å, and slightly longer than the alkylamine value<sup>98</sup> of 1.479(5)Å. The mean distance for this bond in the oxazolidine rings has the slightly shorter value of 1.494(5) but this difference may not be significant.  $\text{Cu-}R,S\text{-(dioxc)}_2(\text{H}_2\text{O})_2$ <sup>118</sup> and  $\text{Cu-}R,S\text{-(pro)}_2(\text{H}_2\text{O})_2$ <sup>129</sup> show no such effect. The average C-O(chelate) and C-O(carbonyl) bond lengths of 1.277(4) and 1.227(5)Å differ as expected.<sup>124</sup> If the C-O(carbonyl) distance is corrected for thermal motion of the carbonyl oxygen (see Table 2.9) the value becomes 1.251(5)Å and the significant difference is reduced. C-O distances in the oxazolidine rings average to 1.418(3)Å and the similar bonds in  $\text{Cu-}R,S\text{-(dioxc)}_2(\text{H}_2\text{O})_2$ <sup>118</sup> have a mean value of 1.44(3)Å. These compare well with the paraffinic value

of  $1.43(1)\text{\AA}$ .<sup>98</sup> All C-H bond lengths were observed to be similar to within  $3\sigma$  and the mean C-H distance was  $1.04(2)\text{\AA}$ . This is significantly larger than the optimal value of  $0.95\text{\AA}$  determined by Churchill<sup>119</sup> over a very limited range of metal complexes, and justifies the earlier inclusion of the hydrogen atoms at the positions calculated by assuming a C-H distance of  $1.02\text{\AA}$ .

Apart from the Cu-O-C and the N-Cu-O(chelate) angles, the two ligands have identical angular geometries to within the accuracy of the structural determination. The difference in Cu-O-C and N-Cu-O(chelate) angles is probably induced by the ligating function of O(4) and the close contacts with O(3) as inferred above. The remaining chelate ring angles compare well with those found in the copper- $\alpha$ -amino acidato structures cited above, although the large standard deviations in some cases make detailed comparisons somewhat tenuous. The angular dimensions of the four oxazolidine rings do not differ significantly from each other or from those observed for the analogous rings in the Cu-R,S-(dimoxc)<sub>2</sub>-(H<sub>2</sub>O)<sub>2</sub><sup>118</sup> structure.

The coordination polyhedron is distorted significantly from square pyramidal geometry with the O(4<sup>i</sup>) apical donor atom being displaced toward ligand 2 (Figure 2.2), as indicated by the inter-donor atom angles at the copper atom (Table 2.3). This is a consequence of the H(7)...O(3<sup>i</sup>) interaction previously mentioned. Two further results of the close contacts between O(3<sup>i</sup>) and O(4<sup>i</sup>) and the oxazolidine ring hydrogens are the distorted N-Co-N angle of  $161.58(18)^\circ$  and the large distances of the nitrogen atoms ( $0.304\text{\AA}$ ) from the weighted least-squares basal plane



through Cu, N(1), O(1), N(2) and O(3) (plane 1 in Table 2.4). O(4<sup>1</sup>) is 2.327Å from this plane and 2.631Å from the parallel plane through the nitrogen atoms. Similar steric distortions occur in other pseudo-square pyramidal complexes of copper(II) and α-amino acids,<sup>120-123</sup> and generally increase with increasing substitution on the nitrogen and α-carbon atoms of the amino acid chelates. Atom deviations from planes 1 to 5 (Table 2.4), the interplanar dihedral angles, and the angles between metal, donor atom planes (Table 2.5), further illustrate the nature of the distortion observed here.

There is a considerable difference in planarity between the chelate ring planes 6 and 7 of ligands 1 and 2. The chelate ring of ligand 1 is relatively planar, as seen by the small deviations of the ring atoms from least-squares plane 6, and the small values of the torsion angles (Table 2.6). Particularly evident is the value of  $-1.3(5)^\circ$  for the C(1)-C(2)-N(1)-Cu torsion angle, which is not significantly different from zero. This closely planar nature of the Cu-N-C-C section of the ring is probably imposed by the envelope conformations of the oxazolidine rings. The apical bonding requirements for O(4) induce the anomalously large Cu-O-C-C torsion angle of  $-28.5(6)^\circ$  in the chelate ring of ligand 2, but as for ligand 1 the Cu-N-C-C torsion angle is the lowest in the ring. These observations indicate the high stability of the envelope conformation of the oxazolidine rings in the ligands, where the C-O-C linkage forms the envelope tip. The relative twist of the chelate rings, caused by the steric distortions associated with the apical bond, is evident from the dihedral angle of  $14.8^\circ$  between planes 6 and 7 or that of  $18.4(2)^\circ$  between planes N(1), Cu,

O(1) and N(2), Cu, O(3) (Table 2.5). This twist leads to a reduction of the distance between oxazolidine rings below the basal plane of the square pyramid, and may block access to the sixth coordination site. A similar effect has been noted in the  $\text{Cu}(\text{dimgly})_2\text{H}_2\text{O}\cdot 0.2\text{H}_2\text{O}$ <sup>122</sup> structure. The C(1), C(2), O(1), O(2) and C(3), C(4), O(3), O(4) sets are essentially planar (planes 9 and 11) with the maximum deviations from their least-squares planes being 0.012(6) and 0.011(6)Å for C(1) and C(3) respectively.

The four oxazolidine rings adopt envelope conformations as described above, and in each ligand the two C-O-C envelope tips fold toward each other (Figure 2.2). The small atom deviations from the least-squares planes 12, 14, 16 and 18 through the C-C-N-C sections of the rings illustrate their closely planar nature. The dihedral angles between these planes and the envelope tips range from 36.9° to 41.9°. The torsion angles in the oxazolidine rings (Table 2.6) provide an alternative description of the envelope conformations. These conformations are probably assumed by minimizing inter- and intra-oxazolidine ring non-bonded interactions. Either half-chair or alternative envelope conformations would introduce much closer C...H and/or H...H repulsive contacts between the rings, as revealed by an examination of a Dreiding molecular model of the complex. In the observed structure, these inter-ring C...H and H...H close contacts (those less than the VDW radii sum) range from 2.48 to 2.70Å and 2.13 to 2.33Å.

The RMS components of thermal displacement along the principal axes of thermal motion are given in Table 2.9 for the non-hydrogen atoms. A visual representation of the relative magnitudes of these, and their

orientations with respect to molecular planes, bonds or the unit cell axes, may be obtained from Figures 2.1 and 2.2. There are no obvious anomalies present, and as expected, the largest components are those corresponding to the out-of-plane vibrations of the carbonyl oxygens and the atoms of the C-O-C sections in the oxazolidine rings. The motion of O(4) perpendicular to the chelate ring plane is significantly less than that of O(3) and this correlates with the apical bonding function of O(4). The Cu, O(1), O(3), C(1) and C(3) chelate ring atoms also have relatively large components of motion perpendicular to the basal plane.

CHAPTER 3. THE CRYSTAL STRUCTURE OF (+)<sub>589</sub>-BIS-(1,1,1-TRIS(AMINOMETHYL)-ETHANE)COBALT(III) CHLORIDE (+)<sub>589</sub>-R,R-TARTRATE PENTAHYDRATE,  
 (+)<sub>589</sub>-[Co(tame)<sub>2</sub>]Cl(+)<sub>589</sub>-R,R-tartrate.5.4H<sub>2</sub>O

3.1 ABSTRACT

Crystals of (+)<sub>589</sub>-[Co(tame)<sub>2</sub>]Cl(+)<sub>589</sub>-R,R-tartrate.5.4H<sub>2</sub>O are monoclinic with space group  $P2_1$ :  $a = 14.6306(4)$ ,  $b = 16.8896(30)$ ,  $c = 8.7199(10)\text{\AA}$ ,  $\beta = 143.95(2)^\circ$  and  $Z = 2$ . The structure has been determined from 2692 reflections collected by counter methods and refined by full matrix least-squares to give a conventional  $R$  value of 0.025. The complex cation has approximate  $D_3$  symmetry. The conformation of the six-membered chelate rings formed by both of the tridentate chelate caps is  $\lambda$  and the absolute configuration of the complex is designated  $\lambda\lambda$ . The chelate rings have an asymmetric twisted-boat conformation. The  $\text{CoN}_6$  coordination sphere deviates significantly from  $O_h$  symmetry and shows a trigonal twist distortion with a small polar elongation along the pseudo- $C_3$  axis of the complex. The hydrogen atoms of the methyl groups were found to adopt staggered positions with respect to the opposing C-C bonds of the quaternary carbon atoms. The cation, two water molecules, and the tartrate ion, form an intricate planar network in which the molecular sub-units are connected by apparent hydrogen bonds. Other close contacts involving the chloride ion and the remaining water molecules are indicative of weak hydrogen bonding between molecular planes.

### 3.2 EXPERIMENTAL AND DATA REDUCTION

#### *Ligand Preparation*

The ligand, 1,1,1-tris(aminomethyl)ethane (tame) was prepared by a modification of the method of Stetter and Bockmann.<sup>134</sup>

Para-toluenesulphonylchloride (p-TSC, 572 g, 3.0 mole) was dissolved in A.R. pyridine (800 cm<sup>3</sup> redistilled over KOH), and placed in two separating funnels (500 cm<sup>3</sup>) fitted to a 3-necked round-bottomed flask (2000 cm<sup>3</sup>) containing 1,1,1-tris(hydroxymethyl)ethane (120 g, 1.0 mole) in A.R. pyridine (400 cm<sup>3</sup>). The flask was equipped with an electric stirrer and cooled in an ice bath. The p-TSC solution was admitted over a period of three hours with constant stirring. After standing (24 hr), the pyridine was distilled off (under vacuum with a cold trap to collect the pyridine) leaving the white crystalline residue. This was taken up in water (2000 cm<sup>3</sup>) and chloroform (1000 cm<sup>3</sup>), and the water fraction was separated, washed with chloroform (300 cm<sup>3</sup>), re-separated and discarded. The chloroform fractions were then washed with dilute sulphuric acid (1.5M, 500 cm<sup>3</sup>), separated and washed four times with water (1000 cm<sup>3</sup>). The resulting chloroform solution was dried over magnesium sulphate (12 hr) and the chloroform distilled off at room temperature using a water pump. The residue (a gum) was ground with methanol (250 cm<sup>3</sup>) and the mixture allowed to crystallize in an ice bath (24 hr). The white crystals of neo-pentyltris(para-toluenesulphonate), (NP(p-TSO)<sub>3</sub>), were filtered off and air dried (302 g, 52%).

Crystals of NP(p-TSO)<sub>3</sub> (194 g, 0.033 mole) were dissolved in dimethylformamide (600 cm<sup>3</sup>) and mixed with potassium phthalimide (250 g,

1.35 mole) in a round-bottomed flask (2000 cm<sup>3</sup>) fitted with a reflux condenser. The mixture was refluxed (2 hr) and the dimethylformamide distilled off (150°C) leaving a brown-green mass. This was mixed with water (1200 cm<sup>3</sup>) and filtered, giving a yellow-grey gum which was dried to a clay. The clay was triturated with methanol (400 cm<sup>3</sup>), filtered, washed with methanol and dried in a desiccator. This product was then recrystallized from glacial acetic acid to yield white crystals of 1,1,1-tris(phthalimidomethyl)ethane (69 g, 41%).

The 1,1,1-tris(phthalimidomethyl)ethane crystals (69 g, 0.14 mole) were shaken with potassium hydroxide (94 g, 1.68 mole) in water (250 cm<sup>3</sup>) over a period of twenty four hours. The mixture was distilled to dryness (temperature <150°C) and the tame distillate collected and neutralized with hydrochloric acid to yield the tame hydrochloride. Water (50 cm<sup>3</sup>) was then added to the residue in the distilling flask and the procedure repeated. The tame hydrochloride solutions were combined and evaporated to dryness over a steam bath. The white crystals were rubbed with methanol (50 cm<sup>3</sup>), filtered off and washed with methanol. The resulting leaf-like crystals (6 g, 20%) decomposed above about 270°C.

*Preparation of the [Co(tame)<sub>2</sub>]Cl<sub>3</sub> Complex*

Tame hydrochloride (4.5 g, 0.02 mole) was dissolved in water (10 cm<sup>3</sup>) and triturated with silver oxide (9.3 g, 0.04 mole) to release the amine and precipitate silver chloride. The mixture was filtered and the water solution of tame collected. Cobalt chloride (1.66 g, 0.007 mole) was dissolved in water (5 cm<sup>3</sup>), to which hydrochloric acid (0.6 cm<sup>3</sup> of 35%, 0.007 mole) and active charcoal (0.2 g) were added. The tame solution was

added to this mixture and air was slowly drawn through the resulting solution (2 hr) which turned an orange-brown colour. It was then filtered into dilute hydrochloric acid (5 cm<sup>3</sup>, 1M) to prevent subsequent decomposition of the complex which occurred at room temperature for pH greater than 7. The solution was then concentrated on a rotary evaporator (60°C and reduced pressure) and cooled in an ice bath to deposit bright orange hexagonal platelets. The crystals of [Co(tame)<sub>2</sub>]Cl<sub>3</sub> (1.45 g, 55%) were washed with ethanol and acetone and dried in an oven (70-80°C).

The visible solution absorption spectrum (see Figure 4.3) was determined for the complex using a Perkin-Elmer 402 ultraviolet-visible spectrophotometer.  $\epsilon_{\max}$  for the  ${}^1A_{1g} + {}^1T_{1g}$  electronic transition was 81 cm<sup>2</sup> mole<sup>-1</sup> and occurred at 472 nm which is similar to that for other Co(III)-amine complexes with a CoN<sub>6</sub> core. NMR (60 MHz) spectra of tame hydrochloride and [Co(tame)<sub>2</sub>]Cl<sub>3</sub> in D<sub>2</sub>O solution were recorded. The CH<sub>2</sub> and CH<sub>3</sub> proton resonance peaks were observed in both cases and the peak areas were in the ratio 2:1 respectively, in accord with the 2:1 ratio of CH<sub>2</sub> to CH<sub>3</sub> protons.

Attempts were made to detect isomers (optical and diastereo) of [Co(tame)<sub>2</sub>]Cl<sub>3</sub> by elution of the complex ion from a Sephadex (C25) cation exchange column using acid solutions containing various optically active anions. No isomer separations were effected, and it was thought that if optical and diastereo conformers were present, they may be rapidly interconverting at room temperature and no distinct separation would then be possible at this temperature. The NMR spectra above are consistent with rapid conformational interconversion on the NMR time scale.

*The [Co(tame)<sub>2</sub>]Cl(+)<sub>589</sub>-R,R-tartrate Complex*

The three possible conformational isomers for the [Co(tame)<sub>2</sub>]<sup>3+</sup> ion are the λλ, the δδ and the λδ forms, where the λ and δ refer to the conformations<sup>29</sup> of the three skew-boat six-membered chelate rings formed by the coordination of the tame ligand to cobalt(III) (as seen from a Dreiding model). The trichloride compound prepared above may then be composed of one of the following; the λδ, the λλ and δδ (equimolar amounts since both are equally favourable in an equilibrium mixture) or a mixture of all three. The latter two possibilities are more favourable because of the relatively large conformational strain energy of the λδ form (Chapter 5). Statistically, this form is not obviously favoured over the total λλ and δδ concentration. If then the λδ isomer is not present uniquely, the above resolution and separation attempts indicate the rapid interconversion of the isomers (either λλ ⇌ δδ or λλ ⇌ λδ ⇌ δδ) in a room temperature solution. From these considerations, it was thought that it may be possible to crystallize one of the optically active conformers (λλ or δδ) by means of an asymmetric synthesis using an optically active anion.

As a preliminary investigation of this possibility, the optical activity of the [Co(tame)<sub>2</sub>]<sup>3+</sup> ion in solutions of potassium (+)<sub>589</sub>-tartrate was observed for several complex and tartrate ion concentrations. This was done by determining the optical rotation over the 400 + 600 nm range of visible wavelengths using a Perkin-Elmer 141MC Spectropolarimeter with a quartz-iodine cycle tungsten lamp and an RCA IP28A photomultiplier detector. The [Co(tame)<sub>2</sub>]<sup>3+</sup> complex was found to exhibit a *net* positive



Cotton effect (Chapter 4) for the optically active  ${}^1A_{1g} \rightarrow {}^1T_{1g}$  transition which occurs at 472 nm (see above). The ORD curve is shown in Figure 4.3. To test for tartrate coordination to cobalt(III) as opposed to ion association, a visible absorption spectrum (Figure 4.3) was determined for a solution containing a 3:2 molar ratio of tartrate to complex ion. This was identical to that determined previously for the  $[\text{Co}(\text{tame})_2]\text{Cl}_3$  solution and  $\epsilon_{\text{max}}$  for the 472 nm  ${}^1A_{1g} \rightarrow {}^1T_{1g}$  transition was again  $81 \text{ cm}^2 \text{ mole}^{-1}$ . Thus the optical activity in the  $[\text{Co}(\text{tame})_2]^{3+}$  ion is induced by ion association with the (+)<sub>589</sub>-tartrate ion. The molecular rotation for the complex (+)<sub>589</sub>-tartrate solution was found to increase with an increase in the ratio of tartrate to complex concentration, but the data was not sufficient to determine the ion association ratio. Although it was realized that the optical activity induced here may have been caused by dissymmetric<sup>21,135-137</sup> perturbation of the  $[\text{Co}(\text{tame})_2]^{3+}$  conformers by the optically active (+)<sub>589</sub>-tartrate ions, the large magnitude of the observed effect suggested it may have been due to the preferential formation of either the  $\lambda\lambda$  or the  $\delta\delta$  optically active conformer. These observations strengthened the possibility of an asymmetric crystallization with (+)<sub>589</sub>-tartrate ion.

*Preparation of  $[\text{Co}(\text{tame})_2]\text{Cl} \cdot (+)_{589}\text{-R,R-tartrate} \cdot 5.4\text{H}_2\text{O}$*

Silver (+)<sub>589</sub>-tartrate was freshly precipitated by mixing silver nitrate (1 g, 0.0059 mole) in water (5 cm<sup>3</sup>) with potassium (+)<sub>589</sub>-tartrate (1.39 g, 0.0059 mole) in water (5 cm<sup>3</sup>). The precipitate was filtered off, washed with water and acetone and air dried.

$[\text{Co}(\text{tame})_2]\text{Cl}_3$  (0.22 g, ca. 0.00055 mole) was dissolved in water

(10 cm<sup>3</sup>) and triturated with fresh silver (+)<sub>589</sub>-tartrate (0.2 g, 0.00055 mole) for 15 min. The mixture was filtered to remove silver chloride and the filtrate (ca. 0.027M in complex, tartrate and chloride) was collected. This solution was reduced by evaporation in a desiccator under reduced pressure (water pump). Ethanol (1:4 volume ratio) was added to the reduced solution which was then further reduced by slow drying in a desiccator for two days. Large, well-formed, orange-red crystals were deposited. These were tested for tartrate by redissolving some and measuring the optical rotation. A non-zero rotation would confirm the presence of (+)<sub>589</sub>-tartrate ion, since [Co(tame)<sub>2</sub>]<sup>3+</sup> was found not to retain its optical activity in the absence of active tartrate (this also provides further evidence for the fast interconversion of the optical  $\lambda\lambda$  and  $\delta\delta$  isomers). The ORD curve of the solution was similar in shape to those obtained previously for complex (+)<sub>589</sub>-tartrate solutions and the large observed rotations indicated the presence of the (+)<sub>589</sub>-tartrate ion. The presence of chloride was tested by dissolution of several crystals in water, followed by the addition of silver nitrate and then dilute nitric acid to dissolve the silver tartrate.<sup>138</sup> Some precipitate still remained and must have been silver chloride<sup>138</sup> since the chloride was the only anion besides (+)<sub>589</sub>-tartrate to be introduced into the system. The crystals obtained above were then used for the X-ray analysis.

#### *Crystallographic Experimental and Data Reduction*

The deep orange-red crystals of [Co(tame)<sub>2</sub>Cl(+)<sub>589</sub>-tartrate.5.4H<sub>2</sub>O], obtained in the manner described above, were large chunky blocks elongated slightly along the *c* axis. Many were twins and the morphology showed the forms {1 $\bar{1}$ 0}, {010} and {10 $\bar{1}$ }. Preliminary precession photographs using

CuK $\alpha$  radiation were used to determine the space group and approximate unit cell constants. The crystal density was determined by flotation in 1,2-dibromopropane and ethanol. The observed and calculated densities were consistent with two formula units of [Co(tame) $_2$ ]Cl(+) $_{589}$ -tartrate.5H $_2$ O per cell. No other chloride to tartrate to complex ratio would fit the experimental results and preserve charge neutralization (unless the structure was disordered). Hence the space group and initial unit cell data established the composition of the crystals to within one H $_2$ O (assuming ethanol was not present). The crystal used for the accurate determination of cell constants and the collection of intensity data measured approximately 0.30, 0.30 and 0.50 mm along the *a*, *b* and *c* axes respectively. The  $2\theta$  and  $\mu$  values for 52 high angle reflections were measured on a STOE automatic Weissenberg diffractometer fitted with a graphite monochromator and using MoK $\alpha$  radiation. These were used to refine the cell constants by least-squares using program SUUCLS by Barnett (see Appendix I). The crystal was mounted along a pseudo-*c* axis associated with a non-conventional *B*-centred unit cell which was defined for convenience.

#### *Crystal Data*

CoC $_{14}$ H $_{34}$ N $_6$ O $_6$ Cl.H $_{10.87}$ O $_{5.43}$ , F.W. 574.73, F(000) = 613 electrons

Monoclinic, space group  $P2_1$  (No. 4)

$a = 14.6306(4)$ ,  $b = 16.8896(30)$ ,  $c = 8.7199(10)\text{\AA}$ ,  $\beta = 143.95(2)^\circ$ ,

$U = 1268(1)\text{\AA}^3$

$D_m = 1.50(1) \text{ g cm}^{-3}$ ,  $Z = 2$ ,  $D_x = 1.505 \text{ g cm}^{-3}$

MoK $\alpha$  ( $\lambda = 0.7107\text{\AA}$ ),  $\mu_{\text{MoK}\alpha} = 8.4 \text{ cm}^{-1}$

The calculated crystal data above were determined on the basis of 5.43 water molecules per asymmetric unit as observed in the subsequent structural analysis.

Reflection intensities using monochromated  $\text{MoK}\alpha$  radiation were measured with a STOE automatic Weissenberg diffractometer on line to a Digital Equipment Corporation PDP8/E mini-computer and a Teletype Corporation Model 33TBP teleprinter and paper tape punch. The crystal was aligned along the pseudo- $c$  axis as described above. The equi-inclination geometry and measuring technique<sup>139</sup> is similar to that described by Freeman *et al.*<sup>140</sup> The  $\omega$  scan technique (with the counter stationary) was used for collecting integrated reflection counts and the X-ray beam had a  $4^\circ$  takeoff angle. Before measuring each reflection, an automatic peak count was effected (STOE control program) and attenuators were inserted for more than 4000 counts/sec. If insufficient counts were obtained, the count times were increased by multiples of 2 up to a factor of 8. The  $\Delta\omega$  scan range of  $1.6^\circ$  for the zero  $hk0$  layer and  $A + B(\sin\mu/\tan(\Psi/2))$  for the upper reflection layers was traversed in steps of  $0.01^\circ$ . Here  $A$  and  $B$  are constants for the layer,  $\mu$  is the equi-inclination angle and  $\Psi$  is the detector angle. This expression allows for the increase in the angular reflection range for upper level equi-inclination reflections.<sup>141</sup> The  $hk0$  and  $hk1$  data were measured with a step count time of 0.5 sec and this was reduced to 0.25 sec for  $hk2 - hk4$ . For layers  $hk5 - hk12$ , a step counting time of 0.2 sec was used. Backgrounds were counted for 12.5 sec on either side of each peak count. Values of  $A$  ranged from 1.5 to 2.0 and  $B$  was set at 0.8. Crossed slits, chosen to

give aperture dimensions of  $2 \times 2$  or  $3 \times 3 \text{ mm}^2$  depending on beam divergence, were used to isolate the diffracted beams. A total of 2692 unique reflections were recorded about the pseudo- $c$  axis (layers  $hk0 - hk12$ ) out to  $50^\circ$  in  $2\theta$ . A standard reflection, chosen on each layer, was measured after every 30 reflections and showed no systematic change.

Program AUPTP by Hill (Appendix I) was used to process and reduce the observed intensity data after recording the intensities on magnetic tape, with the aid of a CDC 3600 computer system (CSIRO Canberra) to read the paper tapes. The observed integrated intensity for each reflection,  $I_h$ , was corrected for Lorentz and polarization effects<sup>142</sup> and the corrected intensity was determined as

$$I_h = \overline{L}_p (P - (t_p/t_B)(B_1 + B_2)) \times SCS \times ATT^{-1}$$

where  $P$  is the peak count,  $B_1$  and  $B_2$  are background counts on either side of the peak,  $t_p$  is the peak scan time,  $t_B$  is the total background count time,  $\overline{L}_p$  is the product of the Lorentz and polarization corrections to the observed intensities,  $SCS$  is the scan speed and  $ATT$  is the appropriate attenuation factor. The standard deviation in  $I_h$  was computed from

$$\sigma I_h = \overline{L}_p ((P + (t_p/t_B)^2(B_1 + B_2)) SCS^2 ATT^{-2} + PF I_h^2)^{1/2}$$

where  $PF$  allows for errors associated with instrumental fluctuation, and may be determined empirically during the structure refinement by adjustment to give the correct relative weighting scheme for the observed structure factors. Reflections were designated unobserved for  $I_h^{obs} < 2\sigma(I_h^{obs})$  where  $I_h^{obs}$  is the non-corrected observed intensity, and unreliable for  $|BD| > 6\sigma(BD)$  where  $BD$  is the difference in the

background counts. Of the total 2692 unique intensities measured, 41 were unobserved by the above criterion. A zero layer ( $hk0$ ) data set determined after the normal data collection was also processed, and by comparison with the initial  $hk0$  set showed no significant crystal decomposition. Absorption corrections were not applied to the observed intensities because of the low absorption coefficient ( $\mu_{\text{MoK}\alpha} = 8.4 \text{ cm}^{-1}$ ) and the approximate equilateral triangular cross-section of the crystal normal to the rotation axis (the transmission factor varied from 0.84 to 0.86 about the pseudo- $c$  axis of rotation).

Equivalent reflections in the data set were then averaged by a non-iterative least-squares procedure<sup>83</sup> using program AULAC (Appendix I). The structure factor amplitudes,  $|F_o|$ , and their standard deviations,  $\sigma F_o$ , were also determined from the mean intensities,  $\bar{I}_h$ , and the standard deviations,  $\bar{\sigma}_h$ .

### 3.3 STRUCTURE SOLUTION AND REFINEMENT

The cobalt and chlorine atom positions were found from a Patterson synthesis. These were then refined by a least-squares minimization of  $\Sigma(|F_o| - |F_c|)^2$  (see Section 1.4 for refinement terminology), where  $|F_c|$  is the calculated structure factor amplitude and the sum was taken over all reliable observed reflections. Besides the positional parameters and isotropic thermal parameters for the Co and Cl atoms, ten scale factors were refined for correct relative scaling of the single axis layers of data. A Fourier difference synthesis, phased on the refined cobalt and chlorine positions revealed the presence of two superimposed

mirror image structures in the cell, a consequence of the pseudo-centre introduced by the Co and Cl atoms having similar  $y$  coordinates. The correct image was determined unambiguously from stereochemical considerations and the relative weights of the mirror image peaks. The sites of all other non-hydrogen atoms in the  $[\text{Co}(\text{tame})_2]^{3+}$  and  $(+)\text{}_{589}\text{-tartrate}$  ions, as well as the oxygen positions of four ordered water molecules, were then located from this map. At this stage the tartrate ion was observed to be in the  $S,S$  configuration. The correct configuration for the structure was then obtained by inversion of all  $y$  coordinates to give the known<sup>18,143</sup>  $R,R$  configuration for the  $(+)\text{}_{589}\text{-tartrate}$  ion. A least-squares refinement of the scale factors, the atomic coordinates and the individual isotropic thermal parameters converged with a conventional  $R_1$  index of 0.074. Anisotropic thermal parameters were then included in the refinement for all atoms, and the imaginary components of the scattering factors for Co and Cl were also introduced. Subsequent refinement involving these modifications was continued in alternate cycles of coordinate and anisotropic thermal parameter blocks, and gave an  $R_1$  value of 0.053.

A second Fourier difference map then revealed the oxygen positions of three disordered water sites and the positions of all hydrogen atoms in the  $[\text{Co}(\text{tame})_2]^{3+}$  and tartrate ions. The three disordered oxygens were initially given atom multipliers based on the rough integration of electron density over  $1\text{\AA}$  radius spheres surrounding the observed peak height positions. At this point the hydrogen atoms were included in the refinement with coordinates fixed in their observed positions and with

fixed isotropic thermal parameters of  $5.0\text{\AA}^2$  for the methyl and hydroxyl hydrogens and  $4.0\text{\AA}^2$  for all others. The refinement blocks incorporated the scale factors and the atomic coordinates of all non-hydrogen atoms (including the disordered oxygens) in one cycle, and the scale factors and thermal parameters of all non-hydrogen atoms (isotropic for the disordered oxygens, anisotropic for all others) in the following cycle. The multipliers of the disordered oxygens were also refined with the scale factor and atomic coordinate block. This procedure gave  $R_1 = 0.037$ . The hydrogen atom coordinates were then included in the refinement and the disordered oxygens were given anisotropic thermal parameters and fixed atom multipliers. Refinement was continued in cycles of three blocks comprising; (1) coordinates and anisotropic thermal parameters of all non-hydrogen atoms in  $[\text{Co}(\text{tame})_2]^{3+}$ , (2) coordinates and anisotropic thermal parameters of all non-hydrogen atoms in the tartrate and chloride ions and the water molecules, and (3) all hydrogen atom coordinates. The scale factors were included in all cycles and the refinement converged with  $R_1 = 0.029$ .

Finally, the hydrogen atom positions in all of the water molecules were determined from a third Fourier difference synthesis phased on the refined positions of all other atoms. The extensive hydrogen bonding in the structure proved a considerable aid in the search for their locations. The three water sites with reduced site occupancy factors showed no obvious positional or rotational disorder about the oxygen positions, although the hydrogen positions for two of these sites are not inconsistent with such an effect. A final two sequences of least-squares refinement



cycles were computed. Each sequence consisted of five blocks composed of (1) coordinates and anisotropic thermal parameters of all non-hydrogen atoms in  $[\text{Co}(\text{tame})_2]^{3+}$ , (2) scale factors and coordinates of all atoms in  $[\text{Co}(\text{tame})_2]^{3+}$ , (3) coordinates and anisotropic thermal parameters of all non-hydrogen atoms in the tartrate and chloride ions and the water molecules, (4) scale factors and coordinates of all atoms in the tartrate, chloride and water entities, and (5) scale factors and coordinates of all non-hydrogen atoms in the structure. These blocks were necessary to obtain the appropriate final covariance data for the calculation of errors in the computed functions of structural coordinates and thermal parameters. This final refinement sequence reduced  $R_1$  to 0.025 at convergence. The value of  $R_2$  was 0.027. Unit weights were used in all refinements, i.e. the function  $\sum w(|F_o| - |F_c|)^2$  was minimized with  $w = 1$  for all  $hkl$ . The estimated error in an observation of unit weight was 0.77 from all refinement blocks in the final sequence. The average  $w(|F_o| - |F_c|)^2$ , determined in ranges of  $|F_o|$ , was plotted vs.  $|F_o|$  and  $\sin\theta/\lambda$ . The curves indicate a relative over-weighting of the very strong and very weak reflections. The former curve varied randomly from 0.21 to 0.35 in the centre ranges and had average values of 0.46 and 0.70 for the two terminal ranges. The latter curve showed a relatively flattened distribution over the  $\sin\theta/\lambda$  ranges, with a variation from 0.20 to 0.56 over the complete curve and 0.20 to 0.25 over the central angular ranges. These results indicated a satisfactory relative weighting scheme for the majority of reflections.

A final difference map showed no peak height values larger than 0.2

$e/\text{\AA}^3$  except for the region in the immediate vicinity of the cobalt atom, which showed several peaks from 0.2 to 0.35  $e/\text{\AA}^3$  in height in the directions of the Co-N bonds. Typical water hydrogens appeared in earlier maps with peak heights of 0.25 to 0.35  $e/\text{\AA}^3$ , whereas hydrogens in the more rigid  $[\text{Co}(\text{tame})_2]^{3+}$  ion had peak heights varying from 0.30 to 0.55  $e/\text{\AA}^3$ .

In view of the observed<sup>94-96</sup> charge delocalization over the whole complex ion in metal complexes,  $\text{Co}^+$  scattering factors were used from International Tables for X-ray Crystallography.<sup>98</sup> The  $\text{Cl}^-$  scattering factors were taken from Doyle and Turner.<sup>97</sup> For the O, N and C atoms, the values used were those given in International Tables.<sup>98</sup> The values for the H atoms were those of Stewart *et al.*<sup>99</sup> Values of the anomalous components  $\Delta f'$  and  $\Delta f''$  in the scattering factors of Co (0.299, 0.973) and Cl (0.132, 0.159) were acquired from Cromer and Liberman.<sup>144</sup>

Program FORDAPB, a modification of Zalkin's original program was used for Patterson and Fourier difference summations. FUORFLS, a modification of ORFLS by Busing, Martin and Levy, was used for the least-squares refinements. All parameters derived from the final positional coordinates and thermal parameters were computed with program ORFFE by Busing, Martin and Levy. Standard deviations in the derived parameters were also determined by this program. Structural geometry was periodically checked during the refinement with the aid of Blount's program BLANDA. Johnson's ORTEPB was used for the perspective atomic ellipsoid plots. (See Appendix I for program descriptions and authors.)

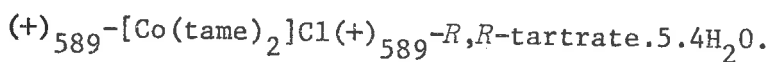
### 3.4 TABLES AND PERSPECTIVE PROJECTIONS

The subsequent tables and perspective projections are generally self-explanatory. A brief synopsis of table contents is given here. Observed and calculated structure factor magnitudes ( $\times 10$ ) are presented in Table 3.1. These and all other calculated quantities were determined from the structural and thermal parameters of the final least-squares refinement block. Table 3.2 contains the final positional and thermal parameters of all atoms. The internal geometry of the  $[\text{Co}(\text{tame})_2]^{3+}$  ion (including H atoms) is given in Table 3.3, and that of the water molecules and the tartrate ion appears in Table 3.4. Table 3.5 contains the interplanar dihedral angles in the cation, and Tables 3.6 and 3.7 present the torsion angles in the cation and tartrate ion, and the interplanar dihedral angles in the tartrate ion respectively. Intracation close contacts are found in Table 3.8. Tables 3.9 and 3.10 list the N-H...B and O-H...B hydrogen bonds found in the structure. Close intermolecular distances appear in Tables 3.11 and 3.12. Finally, Table 3.13 presents the RMS components of thermal displacement along the principal axes of thermal motion. All estimated standard deviations are enclosed in parentheses. Torsion angles were assigned positive or negative signs in accordance with the right or left-handed helix formed by the skew lines  $i \rightarrow l$  and  $j \rightarrow k$  of the atom chain  $i-j-k-l$  defining the torsion angle. The estimation of standard deviations in the mean parameters is described in Appendix III in addition to other general notes on the structure analyses and data presentation.

### 3.5 STRUCTURAL FEATURES AND DISCUSSION

Figures 3.1 and 3.2 show the structure projected down the  $c^*$  and  $-b$  directions respectively. It is apparent from these diagrams that the pseudo- $C_3$  axis of  $[\text{Co}(\text{tame})_2]^{3+}$  is aligned approximately along the  $b$  axis, and the plane of the four carbons in the  $(+)_589$ -tartrate ion is approximately parallel to the  $ac$  plane. These ions interact through an intricate planar hydrogen-bond network which also entails the water molecules whose oxygens are O(7), O(8) and O(9). This molecular plane is parallel to the  $ac$  plane and is shown in projection in Figure 3.2. The two O(7)-H...O and two O(8)-H...O hydrogen bonds between the water molecules and the carboxylate oxygens of the tartrate ions engender chains of end-to-end connected tartrate ions. These chains are bonded through the  $[\text{Co}(\text{tame})_2]^{3+}$  ion which forms numerous N-H...O hydrogen bonds with the water oxygens O(7), O(8) and O(9) and the carboxylate and hydroxyl oxygens of the tartrate ions. The  $[\text{Co}(\text{tame})_2]^{3+}$  ion also forms two N-H...Cl hydrogen bonds with the chloride ion. In fact every N-H hydrogen is involved in some close interaction with an oxygen atom or chloride ion. Only one bifurcated N-H hydrogen interaction is evident, and this is the N(6)-H(11) interaction with Cl(<sup>ii</sup>) and O(5<sup>iii</sup>). The hydrogen bonding in the molecular plane parallel to  $ac$  is clearly indicated in Figure 3.2 and the dotted lines represent relatively weak hydrogen bond interactions. The N-H...O interactions of the complex cation are parametrized in Table 3.9. The N...O distances range from 2.835(4) to 3.301(4)Å, a slightly larger range than that of the neutron diffraction distances listed by Hamilton and Ibers<sup>101</sup> (2.87 to 3.07Å for unbranched bonds) but similar

TABLE 3.1. OBSERVED AND CALCULATED STRUCTURE FACTORS FOR



h	k	l	F <sub>o</sub>	F <sub>c</sub>	F <sub>o</sub> /F <sub>c</sub>
0	0	0	100	100	1.00
1	0	0	100	100	1.00
2	0	0	100	100	1.00
3	0	0	100	100	1.00
4	0	0	100	100	1.00
5	0	0	100	100	1.00
6	0	0	100	100	1.00
7	0	0	100	100	1.00
8	0	0	100	100	1.00
9	0	0	100	100	1.00
10	0	0	100	100	1.00
11	0	0	100	100	1.00
12	0	0	100	100	1.00
13	0	0	100	100	1.00
14	0	0	100	100	1.00
15	0	0	100	100	1.00
16	0	0	100	100	1.00
17	0	0	100	100	1.00
18	0	0	100	100	1.00
19	0	0	100	100	1.00
20	0	0	100	100	1.00
21	0	0	100	100	1.00
22	0	0	100	100	1.00
23	0	0	100	100	1.00
24	0	0	100	100	1.00
25	0	0	100	100	1.00
26	0	0	100	100	1.00
27	0	0	100	100	1.00
28	0	0	100	100	1.00
29	0	0	100	100	1.00
30	0	0	100	100	1.00
31	0	0	100	100	1.00
32	0	0	100	100	1.00
33	0	0	100	100	1.00
34	0	0	100	100	1.00
35	0	0	100	100	1.00
36	0	0	100	100	1.00
37	0	0	100	100	1.00
38	0	0	100	100	1.00
39	0	0	100	100	1.00
40	0	0	100	100	1.00
41	0	0	100	100	1.00
42	0	0	100	100	1.00
43	0	0	100	100	1.00
44	0	0	100	100	1.00
45	0	0	100	100	1.00
46	0	0	100	100	1.00
47	0	0	100	100	1.00
48	0	0	100	100	1.00
49	0	0	100	100	1.00
50	0	0	100	100	1.00
51	0	0	100	100	1.00
52	0	0	100	100	1.00
53	0	0	100	100	1.00
54	0	0	100	100	1.00
55	0	0	100	100	1.00
56	0	0	100	100	1.00
57	0	0	100	100	1.00
58	0	0	100	100	1.00
59	0	0	100	100	1.00
60	0	0	100	100	1.00
61	0	0	100	100	1.00
62	0	0	100	100	1.00
63	0	0	100	100	1.00
64	0	0	100	100	1.00
65	0	0	100	100	1.00
66	0	0	100	100	1.00
67	0	0	100	100	1.00
68	0	0	100	100	1.00
69	0	0	100	100	1.00
70	0	0	100	100	1.00
71	0	0	100	100	1.00
72	0	0	100	100	1.00
73	0	0	100	100	1.00
74	0	0	100	100	1.00
75	0	0	100	100	1.00
76	0	0	100	100	1.00
77	0	0	100	100	1.00
78	0	0	100	100	1.00
79	0	0	100	100	1.00
80	0	0	100	100	1.00
81	0	0	100	100	1.00
82	0	0	100	100	1.00
83	0	0	100	100	1.00
84	0	0	100	100	1.00
85	0	0	100	100	1.00
86	0	0	100	100	1.00
87	0	0	100	100	1.00
88	0	0	100	100	1.00
89	0	0	100	100	1.00
90	0	0	100	100	1.00
91	0	0	100	100	1.00
92	0	0	100	100	1.00
93	0	0	100	100	1.00
94	0	0	100	100	1.00
95	0	0	100	100	1.00
96	0	0	100	100	1.00
97	0	0	100	100	1.00
98	0	0	100	100	1.00
99	0	0	100	100	1.00
100	0	0	100	100	1.00

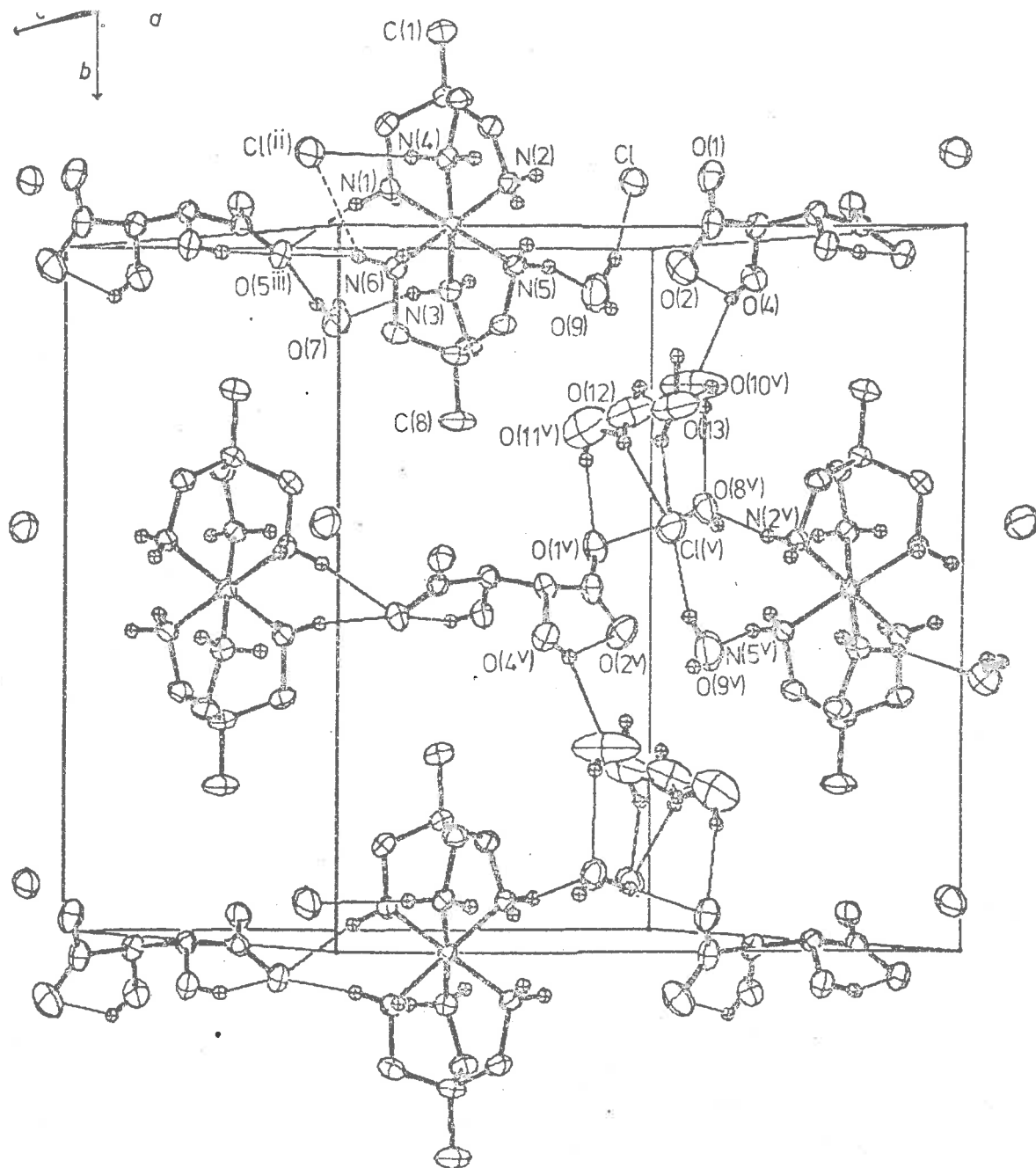


FIGURE 3.1. VIEW OF THE UNIT CELL OF  $(+)^{589}\text{-}[\text{Co}(\text{tame})_2]\text{Cl}(\text{+})^{589}\text{-}R,R\text{-tartrate}\cdot 5.4\text{H}_2\text{O}$  PROJECTED DOWN  $c^*$ . Thermal ellipsoids contain 50% probability for non-hydrogen atoms. Symmetry transformations defined by the superscripts are given in Table 3.11.

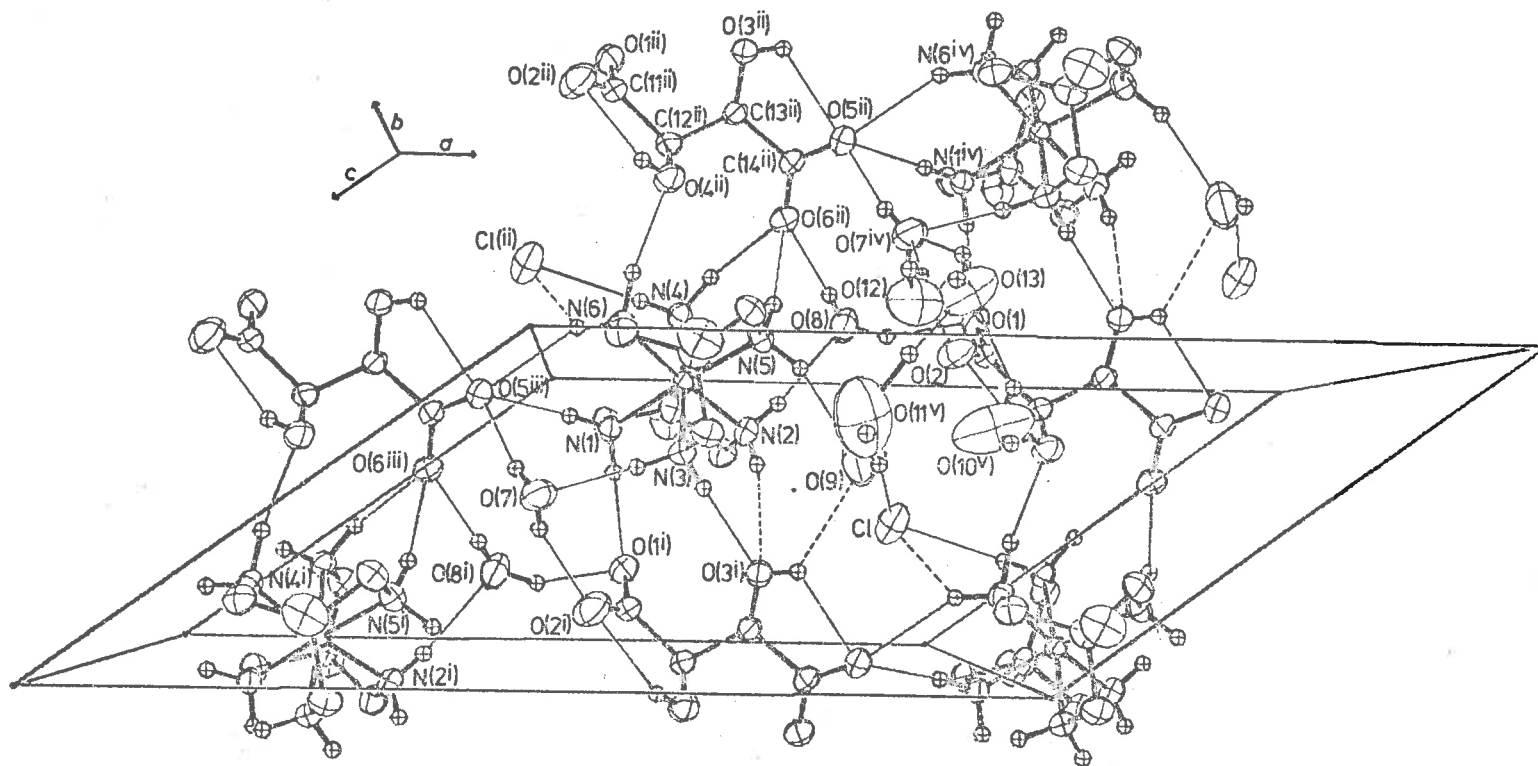


FIGURE 3.2. PROJECTION OF THE UNIT CELL OF  $(+)_589\text{-}[\text{Co}(\text{tame})_2]\text{Cl}(+)_589\text{-}R,R\text{-tartrate}\cdot 5.4\text{H}_2\text{O}$  DOWN  $\underline{-b}$ . Thermal ellipsoids enclose 50% probability for non-hydrogen atoms. Symmetry transformations defined by the superscripts are given in Table 3.11.

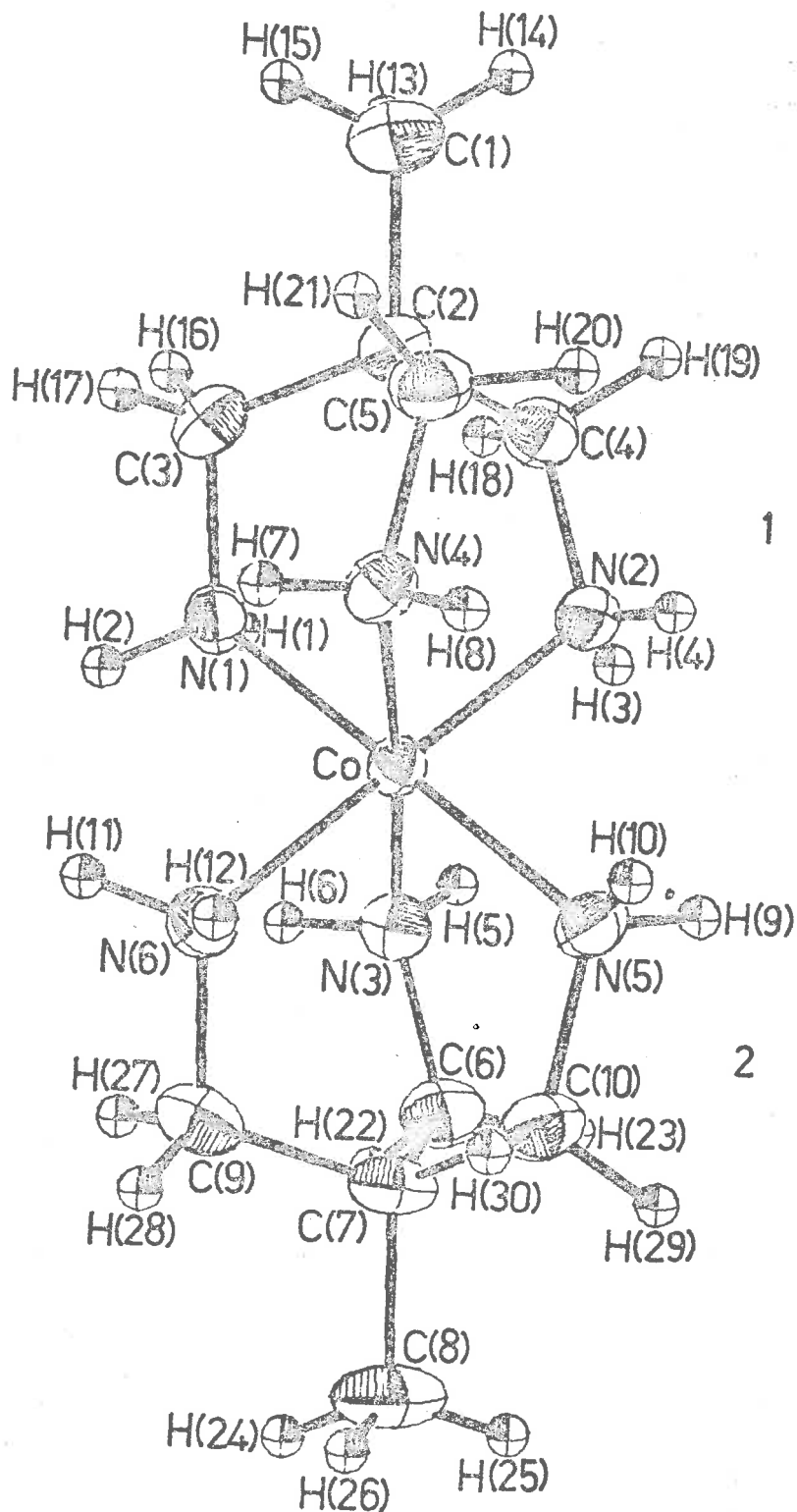
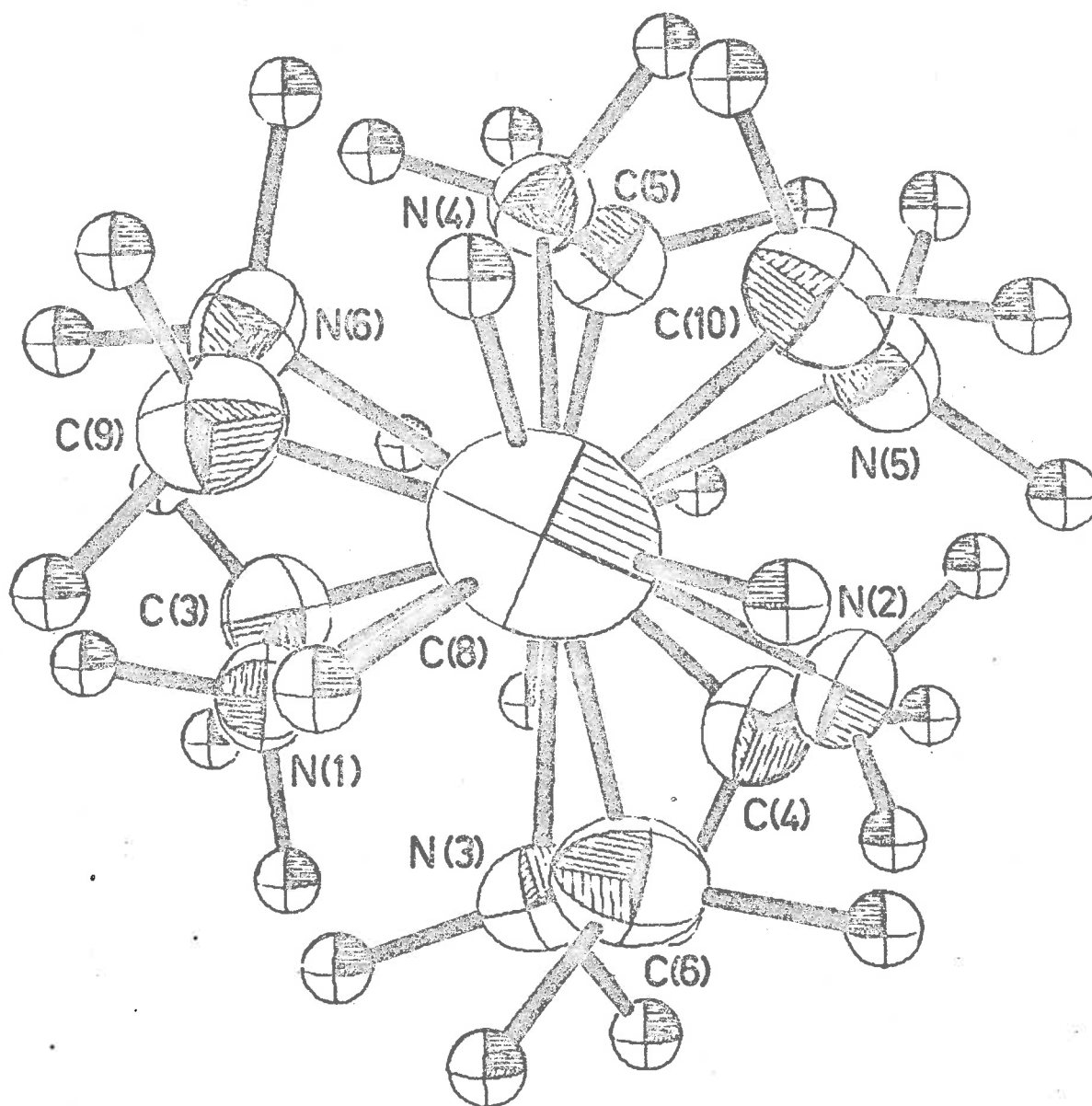


FIGURE 3.3. PERSPECTIVE OF  $[\text{Co}(\text{tame})_2]^{3+}$   $\perp$  TO THE PSEUDO- $C_3$  AXIS. The atom labelling scheme is indicated. Thermal ellipsoids of non-hydrogen atoms enclose 50% probability.





**FIGURE 3.4.** PERSPECTIVE OF  $[\text{Co}(\text{tame})_2]^{3+}$  DOWN THE PSEUDO- $C_3$  AXIS.  
Thermal ellipsoids of non-hydrogen atoms enclose 50% probability.

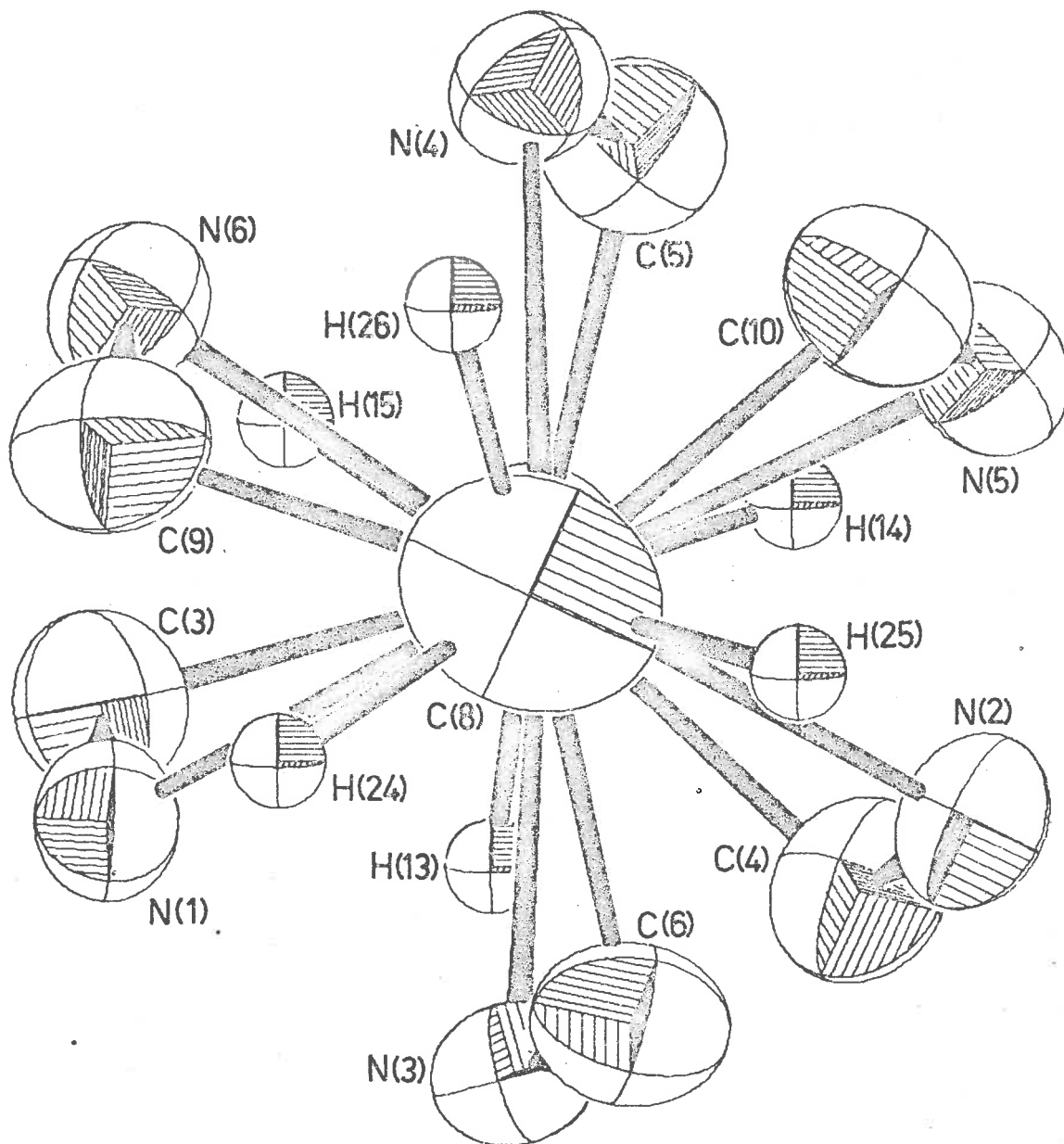


FIGURE 3.5. PROJECTION OF  $[\text{Co}(\text{tame})_2]^{3+}$  ONTO THE PLANE  $\perp$  TO THE PSEUDO- $C_3$  AXIS. The staggered hydrogen positions are clearly indicated. Thermal ellipsoids of non-hydrogen atoms enclose 50% probability.

TABLE 3.2. POSITIONAL AND THERMAL PARAMETERS FOR (+)<sub>589</sub>-[Co(tame)<sub>2</sub>]Cl(*R,R*-tartrate)·5.4H<sub>2</sub>O: λλ CONFORMATION.

Atom <sup>a</sup>	<i>x</i>	<i>y</i>	<i>z</i>	$\beta_{11}$	$\beta_{22}$	$\beta_{33}$	$\beta_{12}$	$\beta_{13}$	$\beta_{23}$
Co	1810(0)	0	38(1)	524(3)	152(1)	1551(10)	-4(3)	721(6)	12(4)
Cl	7368(1)	-813(1)	5363(3)	1204(14)	356(5)	5475(59)	-91(7)	2132(27)	-282(13)
N(1)	1687(3)	-569(2)	1841(5)	698(34)	206(12)	2130(103)	35(16)	1022(56)	61(25)
N(2)	3600(3)	-659(2)	1859(6)	707(34)	175(12)	2577(113)	6(16)	1105(59)	36(26)
N(3)	3125(3)	809(2)	2817(5)	617(33)	195(12)	1714(97)	-4(15)	755(53)	-14(24)
N(4)	423(3)	-808(2)	-2714(5)	642(32)	195(11)	1952(100)	-56(16)	874(54)	-52(24)
N(5)	2034(4)	590(2)	-1597(6)	983(40)	168(11)	2545(111)	-60(17)	1360(63)	-49(26)
N(6)	-41(3)	644(2)	-2001(5)	678(34)	198(12)	2225(106)	38(16)	967(56)	90(26)
C(1)	2258(6)	-2710(3)	1302(9)	1611(71)	201(17)	4652(212)	35(28)	2295(116)	164(45)
C(2)	2102(4)	-1806(2)	884(7)	891(46)	167(14)	2790(151)	-22(20)	1312(78)	17(33)
C(3)	1464(4)	-1446(2)	1493(7)	1006(48)	216(15)	2795(138)	-45(21)	1411(77)	63(33)
C(4)	3705(4)	-1469(2)	2682(8)	863(47)	203(15)	2784(147)	97(22)	1231(79)	195(34)
C(5)	969(5)	-1647(2)	-1965(8)	970(50)	171(14)	2654(143)	-70(20)	1288(80)	-115(32)
C(6)	3085(5)	1627(2)	2120(8)	1001(53)	189(15)	2420(142)	-98(22)	1202(82)	-171(32)
C(7)	1507(5)	1810(2)	-756(8)	1106(55)	139(14)	2597(153)	50(21)	1339(85)	58(33)
C(8)	1356(6)	2715(3)	-1140(10)	1975(84)	152(16)	4603(216)	38(29)	2434(126)	86(44)
C(9)	195(4)	1516(2)	-1516(7)	877(45)	199(15)	2492(135)	111(20)	1096(73)	104(32)
C(10)	1431(4)	1425(2)	-2442(7)	1138(51)	175(13)	2663(136)	-4(21)	1455(79)	64(31)
O(1)	4568(3)	-586(2)	-2679(5)	812(34)	412(14)	3651(113)	-179(18)	1156(59)	-237(30)
O(2)	4844(3)	605(2)	-1237(6)	944(39)	472(17)	3737(145)	113(21)	1354(70)	-85(38)
O(3)	6401(3)	360(2)	-2672(5)	704(30)	319(11)	2109(91)	111(15)	963(49)	298(24)
O(4)	7863(3)	648(2)	2422(5)	811(33)	326(12)	2398(100)	-73(16)	1051(54)	-257(26)
O(5)	9379(3)	378(2)	696(5)	788(32)	317(12)	2706(104)	-45(16)	1190(54)	8(26)

(contd.)

TABLE 3.2. (contd.)

Atom	<i>x</i>	<i>y</i>	<i>z</i>	$\beta_{11}$	$\beta_{22}$	$\beta_{33}$	$\beta_{12}$	$\beta_{13}$	$\beta_{23}$
O(6)	10041(3)	-405(2)	3541(5)	754(32)	286(12)	2285(96)	123(15)	983(52)	200(25)
C(11)	5345(3)	1(4)	-1206(5)	596(33)	379(15)	1804(99)	20(31)	810(54)	81(50)
C(12)	7091(4)	-33(3)	833(6)	646(33)	259(13)	1741(92)	-63(26)	821(53)	-46(42)
C(13)	7355(3)	-160(2)	-506(6)	584(34)	202(18)	1937(110)	4(16)	827(59)	40(25)
C(14)	9068(3)	-50(3)	1402(5)	589(30)	176(12)	2010(97)	15(22)	847(51)	-15(35)
<i>Water oxygens</i>									
O(7)	2059(3)	1212(2)	4513(6)	980(38)	379(14)	2966(119)	-80(19)	1231(63)	-67(31)
O(8)	2865(3)	-1127(2)	-2502(6)	1037(39)	408(15)	4173(139)	157(19)	1746(70)	459(35)
O(9)	5600(5)	835(3)	3050(8)	2255(68)	594(21)	6754(206)	133(32)	3538(113)	338(54)
O(10)	3407(6)	-2839(3)	-1806(11)	2575(100)	343(19)	7062(294)	-6(35)	1878(146)	17(57)
O(11) <sup>b</sup>	5275(21)	-2244(9)	-1559(36)	564(44)	70(7)	1702(139)	53(15)	872(73)	60(26)
O(12)	3352(8)	2605(4)	-2632(13)	2581(154)	391(31)	6101(350)	-210(55)	2959(208)	61(76)
O(13)	3835(15)	2534(8)	-3086(29)	1586(192)	314(55)	6600(812)	-67(82)	2059(328)	107(166)
<i>Positional parameters for the hydrogen atoms<sup>c</sup></i>									
Atom	<i>x</i>	<i>y</i>	<i>z</i>	Atom	<i>x</i>	<i>y</i>	<i>z</i>	<i>B</i>	
<i>Cation hydrogens</i>									
H(1)	258(6)	-50(3)	355(10)	H(2)	92(5)	-34(3)	139(9)	4.0Å <sup>2</sup>	
H(3)	436(6)	-43(3)	315(10)	H(4)	349(5)	-72(3)	73(10)	4.0	
H(5)	406(6)	65(3)	414(10)	H(6)	280(5)	84(3)	339(9)	4.0	
H(7)	-38(6)	-81(3)	-323(10)	H(8)	13(5)	-76(3)	-420(10)	4.0	
H(9)	310(6)	58(3)	-49(10)	H(10)	157(6)	35(3)	-293(10)	4.0	
H(11)	-57(5)	48(3)	-187(10)	H(12)	-88(6)	54(3)	-400(10)	4.0	
H(13)	306(6)	-284(3)	317(11)	H(14)	263(6)	-300(3)	91(10)	5.0	

(contd.)

TABLE 3.2. (contd.)

Atom	x	y	z	Atom	x	y	z	B
<i>Cation hydrogens (contd.)</i>								
H(15)	125(6)	-290(3)	36(10)	H(24)	127(6)	298(3)	-19(11)	5.0 <sup>a</sup>
H(25)	215(6)	289(3)	-73(10)	H(26)	29(6)	281(3)	-302(10)	5.0
H(16)	187(5)	-166(3)	288(10)	H(17)	44(6)	-156(3)	22(10)	4.0
H(18)	429(5)	-144(3)	457(9)	H(19)	436(5)	-183(3)	279(10)	4.0
H(20)	143(6)	-174(3)	-245(9)	H(21)	5(5)	-199(3)	-315(9)	4.0
H(22)	330(5)	196(3)	336(9)	H(23)	394(6)	171(3)	245(10)	4.0
H(27)	37(6)	159(3)	-21(10)	H(28)	-73(5)	174(3)	-297(10)	4.0
H(29)	203(5)	174(3)	-238(9)	H(30)	35(6)	145(3)	-421(10)	4.0
<i>Tartrate and water hydrogens</i>								
H(31)	687(6)	45(3)	-275(10)	H(32)	722(6)	93(3)	187(10)	5.0
H(33)	745(5)	-48(3)	174(10)	H(34)	699(5)	-69(3)	-125(9)	4.0
H(35)	269(7)	94(4)	577(11)	H(36)	127(7)	99(4)	352(11)	6.0
H(37)	366(7)	-93(4)	-208(11)	H(38)	208(6)	-90(4)	-365(11)	6.0
H(39)	590(8)	105(4)	315(13)	H(40)	578(7)	37(4)	278(12)	7.0
H(41)	387(9)	-279(5)	-33(15)	H(42)	296(9)	-254(5)	-236(16)	9.0
H(43)	580(21)	-211(12)	69(42)	H(44)	496(21)	-180(11)	-219(37)	10.0
H(45)	347(13)	300(7)	-337(22)	H(46)	299(13)	229(7)	-363(22)	8.0
H(47)	273(29)	304(18)	-367(53)	H(48)	310(24)	189(14)	-458(42)	8.0

<sup>a</sup> Positional parameters ( $\times 10^4$ ). Anisotropic thermal parameters ( $\times 10^5$ ) except for O(11), ( $\times 10^4$ ).

<sup>b</sup> O(11), O(12), O(13) are partially occupied water sites (see text). They, as well as their hydrogens (43-48), were refined with site occupancy factors of 0.433, 0.686, 0.314 respectively.

<sup>c</sup> Positional parameters ( $\times 10^3$ ). Hydrogens were assigned fixed isotropic thermal parameters.

TABLE 3.3. BOND LENGTHS AND ANGLES WITHIN THE COMPLEX CATION.

*Non-hydrogen atoms*

<i>Ligand 1</i>		<i>Ligand 2</i>	
Co-N(1)	1.970(3)Å	Co-N(3)	1.975(3)Å
Co-N(2)	1.974(3)	Co-N(6)	1.973(3)
Co-N(4)	1.966(3)	Co-N(5)	1.972(3)
N(1)-C(3)	1.495(5)	N(3)-C(6)	1.492(5)
N(2)-C(4)	1.495(5)	N(6)-C(9)	1.493(5)
N(4)-C(5)	1.493(5)	N(5)-C(10)	1.504(5)
C(3)-C(2)	1.524(6)	C(6)-C(7)	1.535(5)
C(4)-C(2)	1.529(5)	C(9)-C(7)	1.521(6)
C(5)-C(2)	1.528(5)	C(10)-C(7)	1.526(6)
C(2)-C(1)	1.544(6)	C(7)-C(8)	1.542(6)
N(1)-Co-N(2)	90.07(14)°	N(3)-Co-N(6)	89.44(13)°
N(1)-Co-N(4)	88.03(13)	N(3)-Co-N(5)	88.34(13)
N(2)-Co-N(4)	88.81(14)	N(6)-Co-N(5)	88.80(14)
Co-N(1)-C(3)	117.82(24)	Co-N(3)-C(6)	117.51(22)
Co-N(2)-C(4)	117.17(24)	Co-N(6)-C(9)	116.96(23)
Co-N(4)-C(5)	117.77(22)	Co-N(5)-C(10)	117.01(25)
N(1)-C(3)-C(2)	111.82(31)	N(3)-C(6)-C(7)	111.35(31)
N(2)-C(4)-C(2)	111.78(30)	N(6)-C(9)-C(7)	111.53(32)
N(4)-C(5)-C(2)	111.78(31)	N(5)-C(10)-C(7)	111.70(30)
C(3)-C(2)-C(4)	111.00(33)	C(6)-C(7)-C(9)	110.32(34)
C(3)-C(2)-C(5)	109.34(32)	C(6)-C(7)-C(10)	109.28(34)
C(4)-C(2)-C(5)	110.54(32)	C(9)-C(7)-C(10)	111.03(34)
C(3)-C(2)-C(1)	109.12(36)	C(6)-C(7)-C(8)	108.43(37)
C(4)-C(2)-C(1)	108.33(35)	C(9)-C(7)-C(8)	108.67(39)
C(5)-C(2)-C(1)	108.46(35)	C(10)-C(7)-C(8)	109.06(37)
<i>Interligand angles at Co</i>			
N(1)-Co-N(6)	92.53(13)°	N(3)-Co-N(2)	93.46(14)°
N(1)-Co-N(5)	177.15(14)	N(3)-Co-N(4)	176.39(14)
N(2)-Co-N(5)	88.73(14)	N(6)-Co-N(4)	88.42(13)
N(1)-Co-N(3)	89.16(13)	N(4)-Co-N(5)	94.53(13)
N(2)-Co-N(6)	176.14(14)		(contd.)

TABLE 3.3. (contd.)

Lengths and angles involving hydrogen atoms<sup>a</sup>

## Ligand 1

N(1)-H(1)	0.89(5) Å	N(2)-H(4)	0.87(5) Å	N(4)-H(7)	0.85(5) Å
N(1)-H(2)	0.92(5)	N(2)-H(3)	0.79(5)	N(4)-H(8)	0.99(5)
C(3)-H(16)	0.89(5)	C(4)-H(19)	1.08(5)	C(5)-H(21)	0.98(5)
C(3)-H(17)	0.91(5)	C(4)-H(18)	1.08(5)	C(5)-H(20)	1.05(5)
C(1)-H(13)	1.00(6)	C(1)-H(14)	0.98(6)	C(1)-H(15)	0.99(5)
Co-N(1)-H(1)	108(3)°	Co-N(2)-H(4)	104(3)°	Co-N(4)-H(7)	105(3)°
Co-N(1)-H(2)	109(3)	Co-N(2)-H(3)	107(3)	Co-N(4)-H(8)	118(3)
C(3)-N(1)-H(1)	105(3)	C(4)-N(2)-H(4)	107(3)	C(5)-N(4)-H(7)	105(3)
C(3)-N(1)-H(2)	110(3)	C(4)-N(2)-H(3)	106(4)	C(5)-N(4)-H(8)	99(3)
N(1)-C(3)-H(16)	109(3)	N(2)-C(4)-H(19)	107(3)	N(4)-C(5)-H(21)	108(3)
N(1)-C(3)-H(17)	110(3)	N(2)-C(4)-H(18)	110(3)	N(4)-C(5)-H(20)	105(3)
C(2)-C(3)-H(16)	113(3)	C(2)-C(4)-H(19)	114(3)	C(2)-C(5)-H(21)	112(3)
C(2)-C(3)-H(17)	111(3)	C(2)-C(4)-H(18)	105(2)	C(2)-C(5)-H(20)	115(3)
C(2)-C(1)-H(13)	111(3)	C(2)-C(1)-H(14)	116(3)	C(2)-C(1)-H(15)	107(3)

## Ligand 2

N(3)-H(6)	0.93(5) Å	N(6)-H(12)	1.06(5) Å	N(5)-H(9)	0.97(5) Å
N(3)-H(5)	0.85(5)	N(6)-H(11)	0.91(5)	N(5)-H(10)	0.83(5)
C(6)-H(22)	1.02(5)	C(9)-H(28)	0.90(5)	C(10)-H(29)	0.99(5)
C(6)-H(23)	1.04(5)	C(9)-H(27)	0.95(5)	C(10)-H(30)	0.97(5)
C(8)-H(26)	1.00(5)	C(8)-H(25)	0.95(5)	C(8)-H(24)	1.04(6)
Co-N(3)-H(6)	106(3)°	Co-N(6)-H(12)	108(3)°	Co-N(5)-H(9)	110(3)°
Co-N(3)-H(5)	110(3)	Co-N(6)-H(11)	114(3)	Co-N(5)-H(10)	110(3)
C(6)-N(3)-H(6)	108(3)	C(9)-N(6)-H(12)	109(3)	C(10)-N(5)-H(9)	110(3)
C(6)-N(3)-H(5)	109(3)	C(9)-N(6)-H(11)	107(3)	C(10)-N(5)-H(10)	106(3)
N(3)-C(6)-H(22)	102(3)	N(6)-C(9)-H(28)	106(3)	N(5)-C(10)-H(29)	110(3)
N(3)-C(6)-H(23)	111(3)	N(6)-C(9)-H(27)	104(3)	N(5)-C(10)-H(30)	112(3)
C(7)-C(6)-H(22)	113(3)	C(7)-C(9)-H(28)	114(3)	C(7)-C(10)-H(29)	110(3)
C(7)-C(6)-H(23)	108(3)	C(7)-C(9)-H(27)	114(3)	C(7)-C(10)-H(30)	105(3)
C(7)-C(8)-H(26)	106(3)	C(7)-C(8)-H(25)	108(3)	C(7)-C(8)-H(24)	110(3)

<sup>a</sup> H-N-H and H-C-H angles are not listed. All have tetrahedral values to within two standard deviations of (4°).

**TABLE 3.4. BOND LENGTHS AND ANGLES WITHIN THE TARTRATE ION AND WATER MOLECULES.**

*Tartrate ion*

*Non-hydrogen atoms*

C(11)-O(1)	1.250(6)Å	O(1)-C(11)-C(12)	116.15(42)°
C(11)-O(2)	1.244(6)	O(2)-C(11)-C(12)	117.15(41)
C(14)-O(5)	1.249(4)	O(5)-C(14)-C(13)	117.60(28)
C(14)-O(6)	1.254(4)	O(6)-C(14)-C(13)	116.75(30)
C(11)-C(12)	1.531(4)	C(11)-C(12)-C(13)	109.66(26)
C(13)-C(14)	1.531(4)	C(12)-C(13)-C(14)	111.10(25)
C(12)-C(13)	1.513(5)	C(11)-C(12)-O(4)	111.67(37)
C(12)-O(4)	1.411(5)	C(13)-C(12)-O(4)	111.86(31)
C(13)-O(3)	1.423(4)	C(12)-C(13)-O(3)	110.41(29)
O(1)-C(11)-O(2)	126.69(30)°	C(14)-C(13)-O(3)	110.78(28)
O(5)-C(14)-O(6)	125.65(27)		

*Lengths and angles involving hydrogen atoms*

O(3)-H(31)	0.77(5)Å	C(13)-C(12)-H(33)	104(3)°
O(4)-H(32)	0.78(5)	C(14)-C(13)-H(34)	112(3)
C(12)-H(33)	0.89(5)	O(3)-C(13)-H(34)	105(3)
C(13)-H(34)	0.97(5)	C(12)-C(13)-H(34)	107(3)
C(11)-C(12)-H(33)	107(3)°	C(12)-O(4)-H(32)	106(4)
O(4)-C(12)-H(33)	113(3)	C(13)-O(3)-H(31)	105(4)

*Water molecules*

O(7)-H(35)	0.80(6)Å	O(12)-H(46)	0.76(12)Å
O(7)-H(36)	0.78(6)	O(13)-H(45)	0.87(12)
O(8)-H(37)	0.95(6)	O(13)-H(48)	1.33(23)
O(8)-H(38)	0.78(6)	H(35)-O(7)-H(36)	105(5)°
O(9)-H(39)	0.52(6)	H(37)-O(8)-H(38)	113(5)
O(9)-H(40)	0.92(6)	H(39)-O(9)-H(40)	105(8)
O(10)-H(41)	0.84(7)	H(41)-O(10)-H(42)	99(8)
O(10)-H(42)	0.63(8)	H(43)-O(11)-H(44)	100(15)
O(11)-H(43)	1.44(21)	H(47)-O(12)-H(46)	102(13)
O(11)-H(44)	0.82(18)	H(45)-O(13)-H(48)	130(14)
O(12)-H(47)	0.92(27)		



**TABLE 3.5. INTERPLANAR DIHEDRAL ANGLES WITHIN THE COMPLEX CATION.<sup>a</sup>**

*Angles between metal, ligator planes of three atoms*

<i>Plane 1</i>	<i>Plane 2</i>	<i>Angle</i>	<i>Plane 1</i>	<i>Plane 2</i>	<i>Angle</i>
N(1),Co,N(2)	N(1),Co,N(4)	88.81(14) <sup>o</sup>	N(3),Co,N(6)	N(3),Co,N(5)	88.82(14) <sup>o</sup>
N(1),Co,N(2)	N(4),Co,N(2)	88.03(13)	N(3),Co,N(6)	N(5),Co,N(6)	88.35(13)
N(1),Co,N(4)	N(2),Co,N(4)	90.11(14)	N(3),Co,N(5)	N(6),Co,N(5)	89.48(13)
N(1),Co,N(6)	N(4),Co,N(5)	88.38(13)	N(2),Co,N(3)	N(4),Co,N(5)	88.69(14)
N(1),Co,N(6)	N(2),Co,N(3)	89.16(13)	N(4),Co,N(6)	N(2),Co,N(5)	94.49(13)
N(1),Co,N(3)	N(4),Co,N(6)	92.51(13)	N(1),Co,N(3)	N(2),Co,N(5)	93.46(14)
N(1),Co,N(6)	N(2),Co,N(5)	176.14(14)	N(2),Co,N(3)	N(4),Co,N(6)	176.15(14)
N(1),Co,N(3)	N(4),Co,N(5)	177.45(14)	N(1),N(2),N(4)	N(3),N(5),N(6)	0.75(15)

*Angles between planes approximately parallel to pseudo-C<sub>3</sub> axis*

Co,N(1),C(2)	Co,N(2),C(2)	121.96(19) <sup>o</sup>	Co,N(3),C(7)	Co,N(6),C(7)	121.32(19) <sup>o</sup>
Co,N(1),C(2)	Co,N(4),C(2)	118.40(18)	Co,N(3),C(7)	Co,N(5),C(7)	118.79(19)
Co,N(2),C(2)	Co,N(4),C(2)	119.65(19)	Co,N(6),C(7)	Co,N(5),C(7)	119.89(19)
Co,N(1),C(2)	C(7),N(6),Co	63.48(17)	C(7),N(3),Co	Co,N(2),C(2)	64.12(19)
Co,N(4),C(2)	C(7),N(5),Co	64.97(18)	Co,N(1),C(2)	C(7),N(3),Co	57.85(17)
Co,N(2),C(2)	C(7),N(5),Co	54.68(18)	Co,N(4),C(2)	C(7),N(6),Co	54.93(18)

*Angles between planes approximately normal to pseudo-C<sub>3</sub> axis<sup>b</sup>*

C(3),C(4),C(5)	N(1),N(2),N(4)	0.22(16) <sup>o</sup>	C(6),C(10),C(9)	N(3),N(5),N(6)	0.40(16) <sup>o</sup>
C(3),C(4),C(5)	N(3),N(5),N(6)	0.60(16)	C(6),C(10),C(9)	N(1),N(2),N(4)	1.14(16)
C(3),C(4),C(5)	C(6),C(10),C(9)	0.96(19)			

<sup>a</sup> The angles are catalogued in pairs. The pseudo-C<sub>2</sub> axis coincident with the N(1),Co,N(3) plane connects the members of each pair except where planes 1,2 are coincident with or related by the C<sub>2</sub>. In this case the pair tabulated is not a C<sub>2</sub> pair.

The definition of the tabulated angle is the same as that in Table 2.5; footnote c.

<sup>b</sup> The methyl hydrogen planes are parallel to each other and to the C,C,C atom planes listed above to within two standard deviations of the dihedral angles.

**TABLE 3.6. TORSION ANGLES.***Complex cation*

<i>Defining Atoms</i>	<i>Torsion Angle</i>	<i>Defining Atoms</i>	<i>Torsion Angle</i>
Co-N(1)-C(3)-C(2)	+26.7(4)°	Co-N(3)-C(6)-C(7)	+29.3(4)°
Co-N(2)-C(4)-C(2)	+29.0(4)	Co-N(6)-C(9)-C(7)	+31.4(4)
Co-N(4)-C(5)-C(2)	+27.6(4)	Co-N(5)-C(10)-C(7)	+29.0(4)
N(1)-C(3)-C(2)-C(1)	+164.4(3)	N(3)-C(6)-C(7)-C(8)	+162.6(4)
N(2)-C(4)-C(2)-C(1)	+162.5(4)	N(6)-C(9)-C(7)-C(8)	+162.1(3)
N(4)-C(5)-C(2)-C(1)	+164.7(4)	N(5)-C(10)-C(7)-C(8)	+163.1(4)
C(3)-C(2)-C(1)-H(13)	-66(3)	C(6)-C(7)-C(8)-H(24)	-68(3)
C(4)-C(2)-C(1)-H(14)	-61(4)	C(9)-C(7)-C(8)-H(26)	-57(3)
C(5)-C(2)-C(1)-H(15)	-69(3)	C(10)-C(7)-C(8)-H(25)	-57(3)
C(3)-C(2)-C(1)-H(15)	+50(3)	C(6)-C(7)-C(8)-H(25)	+62(3)
C(4)-C(2)-C(1)-H(13)	+55(3)	C(9)-C(7)-C(8)-H(24)	+52(3)
C(5)-C(2)-C(1)-H(14)	+59(4)	C(10)-C(7)-C(8)-H(26)	+64(3)
<i>Tartrate ion</i>			
O(1)-C(11)-C(12)-C(13)	+56.6(5)°	O(6)-C(14)-C(13)-C(12)	+48.5(5)°
O(2)-C(11)-C(12)-O(4)	+1.3(5)	O(6)-C(14)-C(13)-O(3)	+171.6(3)
C(11)-C(12)-C(13)-C(14)	+169.9(4)		

**TABLE 3.7. INTERPLANAR DIHEDRAL ANGLES IN THE TARTRATE ION.**

<i>Plane 1</i>	<i>Plane 2</i>	<i>Angle</i>
O(1),C(11),O(2)	C(12),O(4),H(32)	3(4)°
O(5),C(14),O(6)	C(13),O(3),H(31)	22(4)
O(1),C(11),O(2)	O(5),C(14),O(6)	78.3(2)

**TABLE 3.8. INTRACATION CLOSE CONTACTS.**

<i>Ligand 1</i>		<i>Ligand 2</i>	
N(1)...C(4)	2.840(5)Å	N(3)...C(9)	2.808(5)Å
N(2)...C(5)	2.823(5)	N(6)...C(10)	2.805(5)
N(4)...C(3)	2.811(5)	N(5)...C(6)	2.806(5)
H(1)...H(18)	2.45(6)	H(6)...H(27)	2.46(7)
H(4)...H(20)	2.49(7)	H(12)...H(30)	2.47(7)
H(7)...H(17)	2.51(7)	H(9)...H(23)	2.57(7)
H(1)...H(16)	2.08(7)	H(6)...H(22)	2.04(7)
H(2)...H(17)	2.16(7)	H(5)...H(23)	2.22(7)
H(3)...H(18)	2.15(7)	H(11)...H(27)	2.06(7)
H(4)...H(19)	2.16(7)	H(12)...H(28)	2.15(7)
H(7)...H(21)	2.08(7)	H(9)...H(29)	2.20(7)
H(8)...H(20)	2.00(7)	H(10)...H(30)	2.16(7)
<i>Interligand contacts</i>			
H(2)...H(11)	2.18(7)Å	H(3)...H(5)	2.21(7)Å
H(8)...H(10)	2.32(7)		

**TABLE 3.9. APPARENT N-H...B HYDROGEN BONDS WITH THE COMPLEX CATION.**

<i>Atoms</i>	<i>N...B</i>	<i>H...B</i>	<i>Angle N-H...B</i>
N(1)-H(1)...O(1 <sup>1</sup> ) <sup>a</sup>	2.835(4)Å	1.96(5)Å	168(4)°
N(1)-H(2)...O(5 <sup>111</sup> )	3.083(4)	2.17(5)	170(4)
N(2)-H(3)...O(3 <sup>1</sup> )	3.301(4)	2.53(5)	165(4)
N(2)-H(4)...O(8)	3.103(5)	2.25(5)	166(4)
N(3)-H(5)...O(3 <sup>1</sup> )	2.922(4)	2.07(5)	175(4)
N(3)-H(6)...O(7)	2.967(4)	2.06(5)	165(4)
N(4)-H(7)...Cl(1 <sup>11</sup> )	3.267(3)	2.42(5)	179(4)
N(4)-H(8)...O(6 <sup>11</sup> )	2.913(4)	1.95(5)	162(4)
N(5)-H(9)...O(9)	3.103(5)	2.20(5)	155(4)
N(5)-H(10)...O(6 <sup>11</sup> )	3.052(4)	2.23(5)	167(4)
N(6)-H(11)...O(5 <sup>111</sup> )	3.111(4)	2.31(5)	147(4)
N(6)-H(11)...Cl(1 <sup>11</sup> )	3.409(3)	2.81(5)	124(4)
N(6)-H(12)...O(4 <sup>11</sup> )	2.990(4)	1.97(5)	163(4)

<sup>a</sup> See Table 3.11 for definitions of symmetry transformations identified by the superscripts.

TABLE 3.10. APPARENT O-H...B HYDROGEN BONDS.

<i>Atoms</i>	<i>O...B</i>	<i>H...B</i>	<i>Angle O-H...B</i>
O(3)-H(31)...O(5) <sup>a</sup>	2.630(4)Å	2.16(5)Å	120(5)°
O(3)-H(31)...O(9 <sup>iv</sup> )	2.978(5)	2.50(5)	122(5)
O(4)-H(32)...O(2)	2.628(4)	2.12(5)	123(5)
O(4)-H(32)...O(10 <sup>v</sup> )	2.942(6)	2.26(5)	147(5)
O(7)-H(35)...O(2 <sup>i</sup> )	2.641(4)	1.94(6)	146(6)
O(7)-H(36)...O(5 <sup>ii</sup> )	2.709(4)	1.94(6)	168(6)
O(8)-H(37)...O(1)	2.772(4)	1.87(6)	157(5)
O(8)-H(38)...O(6 <sup>ii</sup> )	2.723(4)	1.94(6)	174(6)
O(9)-H(39)...O(10 <sup>v</sup> )	3.293(8)	2.80(6) <sup>b</sup>	160(9)
O(9)-H(40)...Cl	3.174(6)	2.45(6)	136(5)
O(10)-H(41)...O(13 <sup>vi</sup> )	2.654(14)	2.07(7)	126(6)
O(10)-H(42)...O(8)	2.930(6)	2.40(8)	144(9)
O(11)-H(43)...O(13 <sup>vi</sup> )	3.117(24)	1.79(21)	151(14)
O(11)-H(44)...O(1)	2.870(16)	2.08(18)	163(19)
O(12)-H(47)...Cl <sup>v</sup>	3.141(6)	2.37(25)	141(14)
O(12)-H(46)...O(7 <sup>iv</sup> )	2.774(7)	2.05(12)	158(10)
O(13)-H(45)...Cl <sup>v</sup>	3.031(13)	2.25(11)	149(10)
O(13)-H(48)...O(7 <sup>iv</sup> )	2.705(13)	1.52(23)	143(14)

<sup>a</sup> See Table 3.11 for symmetry transformations.

<sup>b</sup> The large value here results from the inordinately short O(9)-H(39) distance. In any case, the hydrogen bond would be very weak and possibly non-existent.

**TABLE 3.11. INTERMOLECULAR DISTANCES TO 3.5Å.<sup>a</sup>**

N(2)...O(9)	3.331(5)Å	N(3)...O(2 <sup>i</sup> )	3.498(5)Å
N(3)...O(9)	3.460(5)	N(3)...C(11 <sup>i</sup> )	3.493(4)
N(4)...O(8)	3.468(4)	C(3)...O(1 <sup>i</sup> )	3.354(5)
N(5)...O(8)	3.473(5)	C(4)...O(1 <sup>i</sup> )	3.454(5)
C(5)...O(8)	3.284(5)	O(7)...C(10 <sup>i</sup> )	3.460(5)
C(6)...O(7)	3.487(5)	O(7)...C(11 <sup>i</sup> )	3.495(5)
C(6)...O(9)	3.341(6)	C(6)...O(11 <sup>v</sup> )	3.396(14)
C(9)...O(7)	3.486(5)	C(8)...O(6 <sup>v</sup> )	3.424(5)
O(2)...O(9)	2.944(5)	C(8)...O(11 <sup>v</sup> )	3.329(17)
O(2)...O(13)	3.397(14)	O(2)...O(10 <sup>v</sup> )	3.084(6)
C(11)...O(8)	3.382(5)	O(3)...C(1 <sup>v</sup> )	3.480(5)
O(8)...O(11)	3.461(14)	O(9)...O(11 <sup>v</sup> )	3.341(17)
O(10)...O(11)	2.751(17)	O(12)...O(10 <sup>v</sup> )	2.890(8)
C1...O(5 <sup>i</sup> )	3.494(3)	O(7)...C(14 <sup>iii</sup> )	3.444(5)
N(3)...O(1 <sup>i</sup> )	3.467(4)	C(10)...O(4 <sup>ii</sup> )	3.351(5)

*Symmetry transformations described by the superscripts in Tables 3.9, 3.10, 3.11 and 3.12*

i	x	y	z + 1
ii	x - 1	y	z - 1
iii	x - 1	y	z
iv	x	y	z - 1
v	$\bar{x} + 1$	$y + 1/2$	$\bar{z}$
vi	$\bar{x} + 1$	$y - 1/2$	$\bar{z}$

<sup>a</sup> The distances in Tables 3.9, 3.10 and 3.12 are not included.

TABLE 3.12. INTERMOLECULAR HYDROGEN CONTACTS TO 2.8Å.<sup>a,b</sup>

O(2)...H(40)	2.56(6)Å	H(6)...H(48 <sup>i</sup> )	2.28(22)Å
C(11)...H(37)	2.47(6)	H(18)...O(1 <sup>i</sup> )	2.54(5)
O(7)...E(27)	2.65(5)	H(18)...O(11 <sup>i</sup> )	2.74(5)
O(8)...H(20)	2.37(5)	H(18)...H(44 <sup>i</sup> )	2.21(20)
O(9)...H(23)	2.51(5)	H(22)...O(13 <sup>i</sup> )	2.69(6)
O(10)...H(43)	2.48(18)	H(22)...H(48 <sup>i</sup> )	2.04(22) <sup>c</sup>
O(12)...H(29)	2.57(5)	H(35)...H(46 <sup>i</sup> )	2.30(13)
H(4)...H(38)	2.48(6)	H(35)...H(48 <sup>i</sup> )	1.83(23) <sup>c</sup>
H(6)...H(35)	2.22(6)	H(36)...H(48 <sup>i</sup> )	2.25(22)
H(6)...H(36)	2.35(5)	H(26)...H(20 <sup>viii</sup> )	2.54(6)
H(8)...H(38)	2.49(5)	H(28)...O(10 <sup>viii</sup> )	2.79(5)
H(9)...H(39)	2.54(6)	H(47)...H(21 <sup>viii</sup> )	2.45(26)
H(9)...H(40)	2.36(6)	O(13)...H(19 <sup>v</sup> )	2.66(6)
H(10)...H(38)	2.49(6)	H(23)...O(11 <sup>v</sup> )	2.56(5)
H(20)...H(38)	2.37(6)	H(25)...O(11 <sup>v</sup> )	2.46(6)
H(20)...H(42)	2.57(8)	H(32)...H(41 <sup>v</sup> )	2.35(7)
H(27)...H(36)	2.53(6)	H(45)...H(43 <sup>v</sup> )	1.61(23) <sup>c</sup>
H(29)...H(46)	2.55(11)	H(2)...C(14 <sup>iii</sup> )	2.76(5)
H(37)...H(44)	2.47(20)	H(36)...C(14 <sup>iii</sup> )	2.69(6)
H(41)...H(43)	2.45(18)	H(8)...H(33 <sup>ii</sup> )	2.38(6)
H(24)...H(17 <sup>vii</sup> )	2.59(6)	H(12)...H(32 <sup>ii</sup> )	2.22(5)
H(27)...H(15 <sup>vii</sup> )	2.43(6)	H(17)...C1( <sup>ii</sup> )	3.00(5)
H(5)...H(31 <sup>i</sup> )	2.52(5)	H(30)...O(4 <sup>ii</sup> )	2.53(5)

<sup>a</sup> H...H contacts >2.6Å are not included.  
H...Cl contacts ≤3.0Å are included.

<sup>b</sup> See Table 3.11 for symmetry transformations.

<sup>c</sup> These extremely short contacts are not realistic and occur because of the long O(11)-H(43) and O(13)-H(48) bonds. They are, however, consistent with their very large e.s.d's.

TABLE 3.13. RMS COMPONENTS OF THERMAL DISPLACEMENT ALONG PRINCIPAL AXES.<sup>a</sup>

<i>Atom</i>	<i>Axis 1</i>	<i>Axis 2</i>	<i>Axis 3</i>	<i>Atom</i>	<i>Axis 1</i>	<i>Axis 2</i>	<i>Axis 3</i>
Co	140(1)	144(1)	152(1)	O(1)	159(4)	198(4)	254(4)
Cl	189(1)	216(2)	297(2)	O(2)	179(4)	233(4)	295(5)
N(1)	150(5)	163(4)	179(4)	O(3)	146(4)	167(4)	232(4)
N(2)	153(5)	159(5)	193(4)	O(4)	161(4)	188(4)	237(4)
N(3)	148(4)	168(5)	179(5)	O(5)	160(4)	193(4)	219(4)
N(4)	146(5)	169(4)	178(5)	O(6)	153(4)	197(4)	215(4)
N(5)	146(6)	165(4)	196(4)	C(11)	149(4)	163(5)	236(5)
N(6)	154(4)	167(5)	187(4)	C(12)	150(5)	163(6)	199(6)
C(1)	162(7)	231(6)	252(6)	C(13)	148(4)	164(6)	179(5)
C(2)	149(7)	177(6)	194(5)	C(14)	145(6)	159(6)	179(5)
C(3)	146(7)	195(5)	203(6)	O(7)	186(4)	228(4)	245(4)
C(4)	152(6)	189(6)	210(5)	O(8)	176(4)	194(4)	285(4)
C(5)	150(6)	191(5)	196(5)	O(9)	203(5)	276(5)	322(5)
C(6)	148(6)	192(5)	211(6)	O(10)	223(6)	276(6)	528(8)
C(7)	140(7)	184(5)	216(6)	O(11)	284(17)	370(17)	488(19)
C(8)	147(8)	241(6)	282(6)	O(12)	212(9)	286(8)	368(10)
C(9)	150(6)	190(5)	216(6)	O(13)	206(19)	246(15)	392(23)
C(10)	149(6)	182(5)	209(5)				

<sup>a</sup> Values are  $\times 10^3$  and in Å.

to that of 2.73(10) to 3.22(10)Å given in International Tables.<sup>98</sup> Some of the N-H...O bonds observed here may be weakened by the multiple hydrogen bonding interactions of the tartrate and water oxygens, or the optimum packing-hydrogen bond arrangements which may not favour strong hydrogen bonds in all N-H...O encounters. The N-H...O angles for unbranched bonds range from 155(4) to 175(4)° and lie well within the range 119 to 175° determined from the neutron diffraction studies tabulated by Hamilton and Ibers.<sup>101</sup> The N-H...O and N-H...Cl angles of the bifurcated interaction are 147(4) and 124(4)°. For the N-H...Cl interactions, the N...Cl distances of 3.267(3) and 3.409(3)Å lie within the range 3.15 to 3.48Å established by the neutron diffraction results.<sup>101</sup> The N-H...Cl angles of 124(4) and 179(4)° lie on the outskirts of the literature<sup>101</sup> range (122-171°).

The O-H...O hydrogen bonds are listed in Table 3.10. The unforked interactions involving the tartrate ions and the water oxygens O(7) and O(8) (Figure 3.2) have O...O distances and O-H...O angles ranging from 2.641(4) to 2.772(4)Å and 146(6) to 174(6)° respectively. The corresponding literature ranges<sup>101</sup> are 2.49 to 3.00Å and 132 to 180° for unsymmetric unbranched O-H...O bonds. The tartrate hydroxyl groups appear to form bifurcated O-H...O bonds with an internal carboxylate oxygen and a water oxygen (O(9) and O(10) and see Figures 3.1 and 3.2). The internal O...O distances of 2.630(4) and 2.628(4)Å and the O...O(water) distances of 2.978(5) and 2.94(2)Å lie within the literature range above. The O-H...O angles of 120(5) to 147(5)° are similar to those observed<sup>101</sup> by neutron diffraction in other bifurcated systems. The other O-H...O hydrogen bonds involve the O-H bonds of the water whose oxygen is O(10) and the



disordered waters with oxygens O(11), O(12) and O(13). As seen from Figures 3.1 and 3.2 and Table 3.10 these oxygens are O-H...O bonded between themselves, to a carboxylate oxygen of the tartrate ion and to the water oxygens O(7) and O(8). Together with the O-H...Cl bonds formed by O(12) and O(13), each of the water oxygens O(10)-O(13) provides a direct or indirect hydrogen bonded link between the molecular planes discussed above. The O...O distances vary from 2.654(14) to 3.117(24)Å and the O-H...O angles from 126(6) to 163(19)° and these are not significantly outside the corresponding literature<sup>101</sup> ranges above. The O-H...Cl interactions listed in Table 3.10 also have O...Cl distances and O-H...Cl angles not significantly different from the literature values of 3.09 to 3.18Å and 153 to 166° tabulated by Hamilton and Ibers.<sup>101</sup>

If the chloride ion has an ionic radius<sup>103</sup> of 1.81Å and the C, N and O atoms have VDW radii<sup>102,103</sup> of 1.7, 1.5 and 1.4Å, there are no intermolecular non-bonded distances between non-hydrogen atoms less than the sum of the VDW or VDW and ionic radii. Intermolecular non-hydrogen contacts to 3.5Å are given in Table 3.11. For a hydrogen van der Waal radius of 1.2Å,<sup>102,103</sup> Table 3.12 indicates only two intermolecular non-bonded contacts involving H atoms which are significantly less than the VDW radii sum. One of these is a C...H contact of 2.47(6)Å (VDW radii sum is 2.9Å) imposed on the carboxylate carbon, C(11), of the tartrate ion by the O(8)-H...O(1) (carboxylate oxygen) hydrogen bond. The other contact involves the same water oxygen O(8) and a methylene hydrogen on [Co(tame)<sub>2</sub>]<sup>3+</sup> and is probably imposed by N-H...O(8) hydrogen bonding (see Figure 3.2). The contact O(8)...H(20) of 2.37(5)Å is not however

inordinately<sup>128</sup> less than the VDW radii sum of 2.6Å.

The  $[\text{Co}(\text{tame})_2]^{3+}$  ion exhibits a positive optical rotation in solution at 589 nm when in association with  $(+)\text{}_{589}\text{-tartrate}$  ion. The  $\lambda\lambda$  conformer, where  $\lambda$  refers to the conformation<sup>29</sup> of the skew-boat rings in the Co-tame moiety, is observed here (Figure 3.3) in the structure of the crystal formed with  $(+)\text{}_{589}\text{-tartrate}$ . A solution of this crystal in water also shows a positive optical rotation at 589 nm for the  $[\text{Co}(\text{tame})_2]^{3+}$  ion. Thus the  $\lambda\lambda$  optical isomer may be phenomenologically described as  $(+)\text{}_{589}\text{-}[\text{Co}(\text{tame})_2]^{3+}$  if it is remembered that the rotation observed in solution is induced by the  $(+)\text{}_{589}\text{-tartrate}$  ion and that the crystal and preferred solution conformers may not be the same. The latter phenomenon is unlikely however, since both the solution and solid state polystyrene disc CD spectra of the crystals show a relatively large *net* positive Cotton effect as asserted in Chapter 4. Because the intramolecular contribution to the dissymmetry of  $[\text{Co}(\text{tame})_2]^{3+}$  in this structure is imposed entirely by the chelate ring conformation, the absolute configuration is designated  $\lambda\lambda$ . The  $[\text{Co}(\text{tame})_2]^{3+}$  ion has approximate  $D_3$  symmetry as discussed in the following analysis of the internal geometry and illustrated in Figures 3.3 and 3.4.

The internal bond length and angle geometry of the complex cation is presented in Table 3.3. The Co-N bond distances do not differ significantly and the mean value of 1.972(1)Å is identical to that observed<sup>96</sup> in  $[\text{Co}(\text{NH}_3)_6]^{3+}$  in the accurate structure determination of  $[\text{Co}(\text{NH}_3)_6]\text{-}[\text{Co}(\text{CN})_6]$  where the complex ions have crystallographic  $\bar{3}$  symmetry. The average distances of 1.985(5)<sup>17</sup> and 1.99(2)Å<sup>16</sup> found in the structures of

(-)<sub>546</sub><sup>-</sup>[Co(*R,R*-ptn)<sub>3</sub>]Cl<sub>3</sub>·2H<sub>2</sub>O and (+)<sub>546</sub><sup>-</sup>[Co(*R,R*-ptn)<sub>3</sub>]Cl<sub>3</sub>·H<sub>2</sub>O, where the cations are approximately *D*<sub>3</sub> symmetric and have six-membered skew-boat chelate rings, are not significantly different from the value seen here. Most other tris(diamine)cobalt(III) complexes have similar Co-N bond lengths.<sup>15</sup> The N-C bonds in the structure are equivalent and the average length of 1.495(2)Å is only slightly longer than the paraffinic distance<sup>98</sup> of 1.479(5)Å. The C-C bonds in the chelate rings are similar with a mean distance of 1.527(2)Å which is shorter than the paraffinic<sup>98</sup> length (1.541(3)Å). However, the two terminal C-C bonds are significantly longer with a mean length of 1.543(4)Å and when corrected for the thermal motion effect this increases to 1.560(4), a value significantly longer than the paraffinic one. The mean N-H distance of 0.91(2)Å observed here is slightly longer than the "optimal" value of 0.87Å determined by Churchill<sup>119</sup> for X-ray N-H distances. The mean C-H length (excluding the methyl values which were not corrected for thermal motion) is found to be 0.99(2)Å, again slightly longer than Churchill's<sup>119</sup> "optimal" value of 0.95Å.

The angular geometries of the two rane ligands are almost identical for angles related by the pseudo-*C*<sub>2</sub> axis bisecting the N(1)-Co-N(3), N(4)-Co-N(5) and N(2)-Co-N(6) angles (see Figure 3.3). These *C*<sub>2</sub> related angles are tabulated in juxtaposition (Table 3.3) for the non-hydrogen angles of the two ligands and all, except the N(1)-Co-N(2) and N(3)-Co-N(6) angles, are similar to within three standard deviations. Similarly, with the possible exception of the N-Co-N angles, the pseudo-*C*<sub>3</sub> related angles of each ligand are equivalent, and the total non-hydrogen angular geometry

of the complex conforms closely with  $D_3$  symmetry. The mean angles N-Co-N, Co-N-C, N-C-C and C-C-C of the chelate rings are 88.92(6), 117.37(10), 111.66(13) and 110.25(14) $^\circ$  respectively. The equivalent angles in the quasi- $D_3$  complex<sup>17</sup>  $(-)_546-[Co(R,R\text{-ptn})_3]^{3+}$ , which has similar six-membered chelate rings to those of  $[Co(\text{tame})_2]^{3+}$ , have the mean values 89.0(3), 118.0(4), 112.0(6) and 117.2(7) $^\circ$ . Only the C-C-C angles differ significantly from those observed in  $[Co(\text{tame})_2]^{3+}$  and the closely tetrahedral value of 110.25(14) $^\circ$  found here is probably imposed by the quaternary carbons. All angles in the  $[Co(\text{tame})_2]^{3+}$  complex involving hydrogen atoms are tetrahedral to within three standard deviations (Table 3.3).

The  $CoN_6$  core of the complex is distorted significantly from octahedral geometry, the main distortion being a relative trigonal twist of the donor groups N(1), N(2), N(4) and N(3), N(5), N(6). This is probably caused by the repulsive hydrogen contacts H(2)...H(11), H(8)...H(10) and H(3)...H(5) (see Figure 3.3 and Table 3.8) and is in the correct sense to relieve such interactions. This twist increases the N(1)-Co-N(6), N(2)-Co-N(3) and N(4)-Co-N(5) angles to 92.53(13), 93.46(14) and 94.53(13) $^\circ$  respectively from the octahedral value of 90 $^\circ$  and correspondingly decreases the N(2)-Co-N(5), N(1)-Co-N(3) and N(6)-Co-N(4) angles. An indication of the magnitude of the trigonal twist may be obtained from the interligand angles between Co-N...C(quaternary carbon) planes (Table 3.5). Because of the quasi- $D_3$  symmetry of the  $[Co(\text{tame})_2]^{3+}$  ion, these planes are approximately coincident with a pseudo- $C_3$  axis passing through the cobalt and perpendicular to the mean of the N,N,N ligand planes. The mean

trigonal twist expanded interligand angle between the Co-N...C(quaternary) planes (*i.e.* angles between Co, N(1), C(2) and Co, N(6), C(7) *etc.*) has the value  $64.19(11)^\circ$  and the corresponding mean twist-contracted angle is  $55.82(11)^\circ$  (*i.e.* angles between Co, N(2), C(2) and Co, N(5), C(7) *etc.*). These angles are similar in nature and magnitude to the trigonal twist angle defined by Butler and Snow<sup>15,38</sup> and discussed in Section 4.3.2. The  $\text{CoN}_6$  core has a configurational arrangement about the  $C_3$  axis which is the mirror image of that observed in the  $(+)_{589}^-[\text{Co}(\text{en})_3]^{3+}$  and  $(+)_{546}^-[\text{Co}(\text{R,R-ptn})_3]^{3+}$  structures listed in reference 15. As seen from Figures 3.4 and 3.5 the N(1)...N(3), N(2)...N(5) and N(4)...N(6) skew lines define a right-handed helix, whereas the N...N skew lines spanning the twist-contracted angle<sup>15</sup> in the  $(+)_{589}^-[\text{Co}(\text{en})_3]^{3+}$  and  $(+)_{546}^-[\text{Co}(\text{R,R-ptn})_3]^{3+}$  structures define a left-handed helix. All N-Co-N angles are slightly less than  $90^\circ$  except for the N(1)-Co-N(2) angle, which is not significantly different from  $90^\circ$ . This indicates a small mean polar elongation<sup>15</sup> of the  $\text{CoN}_6$  core along the  $C_3$  axis and is discussed in terms of the polar angle  $\theta$  (w.r.t. the pseudo- $C_3$  axis) in Section 4.3.2.

The intraligand Co-N...C(quaternary) planes are close to  $120^\circ$  apart (Table 3.5), a further indication of the pseudo- $C_3$  symmetry observed in the  $[\text{Co}(\text{tams})_2]^{3+}$  ion. The angles between N-Co-N planes (Table 3.5) also conform relatively closely with  $D_3$  symmetry and very closely with  $C_2$  symmetry where the  $C_2$  axis, as mentioned above, is that bisecting the N(1)-Co-N(3) angle (see footnote a in Table 3.5). The C,C,C- (methylene carbon) and N,N,N planes are quite closely parallel with

each other and the H,H,H(methyl) planes as suggested by the interplanar dihedral angles of Table 3.5.

As previously intimated the six-membered chelate rings all have the  $\lambda$  conformation, describing the right-handed helix defined by the C...C(methylene) and N...N skew lines.<sup>29</sup> The conformation is intermediate between that of a regular skew-boat and a boat ring and may be described as asymmetric skew-boat. Torsion angles are given in Table 3.6 and the skew-boat conformation is clearly indicated by the fact that all Co-N-C-C torsion angles have the same sign. The magnitudes of the C-C-C-H torsion are all  $60^\circ$  to within  $3\sigma$  and indicate almost complete staggering of the methyl groups with respect to the opposing C-C bonds. The staggered conformation is also stabilized by minimizing H...H repulsive contacts with the methylene hydrogens, and is illustrated in Figures 3.4 and 3.5. The intraligand close contacts given in Table 3.8 are symptomatic of the skew-boat conformations adopted here. Thus the close H...H contacts are the result of the incomplete staggering about the N-C bonds (Co-N-C-C angles range from  $+26.7(4)$  to  $+31.4(4)^\circ$ ). The three close interligand H...H contacts appear to have induced the relative twist of the same ligands about the  $C_3$  axis.

The (+)<sub>589</sub>-tartrate ion is well illustrated in Figures 3.1 and 3.2. The mean carboxylate C-O bond length is  $1.249(3)\text{\AA}$  and  $1.266(3)\text{\AA}$  when corrected for thermal motion effects. As observed in the structure of ammonium tartrate,<sup>145</sup> the chemically equivalent bond lengths in the tartrate ion are similar to within three standard deviations. The mean C-O(carboxylate) distance found in the ammonium tartrate structure<sup>145</sup>

was 1.252(7)Å, uncorrected for thermal motion. The average C-C(carboxylate) distance of 1.531(3)Å seen here is slightly longer than the C(12)-C(13) value of 1.513(5)Å. A similar effect was observed<sup>145</sup> in the ammonium tartrate structure, the respective lengths being 1.542(9) and 1.528(13)Å, but the difference here is not significant. The mean value of 1.417(3)Å for the C-O(hydroxyl) bond is similar to the paraffinic value<sup>98</sup> (1.43(1)Å) and that of 1.413(9)Å in ammonium tartrate.<sup>145</sup> In other tartrate structures<sup>146,147</sup> chemically equivalent bond lengths have sometimes been found to differ.

The chemically equivalent bond angles found here in (+)<sub>589</sub>-tartrate are similar to within 4σ, and not significantly different from those in ammonium tartrate.<sup>145</sup> Angles involving hydrogen atoms do not differ significantly from the tetrahedral value. The mean O-H bond distance found in this structure is 0.79(2)Å (averaged over O-H bonds in the tartrate and water molecules with oxygens O(7), O(8) and O(9)), and shows the expected shortening with respect to the H-H distance of 0.91(2)Å. An analysis of the torsion angles (Table 3.6) and interplanar dihedral angles (Table 3.7) indicates that the CO-CO<sub>2</sub> sections of the tartrate ion are closely planar and twisted with respect to each other by about 78°. The ammonium tartrate structure<sup>145</sup> showed a similar effect.

The RMS components of thermal displacement are listed in Table 3.13. The atoms of [Co(tame)<sub>2</sub>]<sup>3+</sup> show the expected variations with the methyl carbons having the largest components approximately perpendicular to the pseudo-C<sub>3</sub> axis of the cation (as seen in Figures 3.3 and 3.4). In the (+)<sub>589</sub>-tartrate ion the largest components are approximately normal

to the CO-CO<sub>2</sub> planes as expected (Figures 3.1 and 3.2). The water oxygens O(9)-O(13) have the largest vibration amplitudes and the weakly hydrogen bonded oxygens O(10) and O(11) show exceptionally large values.



CHAPTER 4. CORRELATION OF ABSOLUTE CONFIGURATION AND SIGNED ROTATORY  
STRENGTH IN DISSYMMETRIC Co(III) COMPLEXES

4.1 INTRODUCTION

The theoretical connection between the observed optical activity associated with the  $d-d$  electronic transitions of chiral transition metal complexes, and their absolute stereochemistries, has received considerable attention in recent years.<sup>68-73,148-160</sup> In several of these proposed models,<sup>68,70,71,73,148-150,155,157-159</sup> an independent systems, perturbation approach<sup>161</sup> has been employed to develop the molecular electronic state wave functions required in the general "one-electron" theory of optical activity<sup>162</sup> for the calculation of  $d-d$  transition rotatory strengths (Section 4.2). The zeroth order wave functions for this approach are constructed on a model in which the metal complex is represented as an ensemble of isolated sub-groups free from inter-group Coulombic and electron exchange interactions. The molecular state wave functions are then obtained by quantum mechanical perturbation theory in which inter-group interactions are incorporated as perturbation potential energy functions. The rotatory strengths of electronic transitions within the sub-groups may be computed from these resultant wave functions. In the static coupling "one-electron" model,<sup>161</sup> terms involving the dynamic coupling between electrons located in different sub-groups are not included in the expressions for the rotatory strengths. These terms arise in a more general independent systems, perturbation approach which was developed by Tinoco<sup>163</sup> and applied to organic systems by Hohn and Weigang<sup>164</sup> and transition metal complexes by Mason<sup>160</sup> and Richardson.<sup>157</sup>

In accord with the above approaches, a pseudo-octahedral Co(III) complex may be partitioned to zeroth order into<sup>70,71,158</sup> an octahedral  $\text{CoL}_6$  (L = ligator atom) chromophore and a number of non-ligating sub-groups. For a magnetic-dipole allowed chromophore transition (e.g. a metal ion  $d-d$  transition), the expression for the rotatory strength (Section 4.2) includes non-zero electric-dipole terms which derive from both electric-dipole allowed transitions of the chromophore ("one-electron" static coupling)<sup>157,160,161</sup> and those of the ligand sub-groups ("two-electron" dynamic coupling).<sup>157,160,164</sup> These electric-dipole allowed components occur as a result of the dissymmetric perturbing interactions between the  $\text{CoL}_6$  chromophore and the ligand atoms and their subsequent incorporation in the expressions for the perturbed molecular wave functions.

In the one-electron models above,<sup>68,70,71,73,148-150,155,157-159</sup> electric-dipole contributions from the two-electron dynamic coupling mechanism (or electric-dipole magnetic-dipole coupled oscillator mechanism for  $d + d$  transitions) were not considered, and the zeroth and higher order chromophoric states involved in the metal ion  $d-d$  transitions were assumed to be constructed solely from metal orbitals according to the crystal-field theory of transition metal complexes. These models<sup>68,70,73,155</sup> have been applied to the calculation of *net* rotatory strengths for the single-electron transitions  ${}^1A_{1g} \rightarrow {}^1T_{1g}$  and  ${}^1A_{1g} \rightarrow {}^1T_{2g}$  of the  $\text{CoL}_6$  chromophore, where the group theoretical symbolism describes the symmetry species of the appropriate states of the unperturbed  $O_h$  symmetric chromophore in a dissymmetric pseudo-octahedral Co(III) complex.

The Co(III) complexes in these relatively formal estimations of the one-electron rotatory strengths were considered to have  $D_3$  symmetry. The rotatory strength for the  ${}^1A_{1g} \rightarrow {}^1T_{1g}$  transition has been developed by considering both first order<sup>68,70,73,150,155</sup> and second order<sup>70,155</sup> contributions to the wave functions for the perturbed  ${}^1A_{1g}$  and  ${}^1T_{1g}$  states. The net first order contribution to the rotatory strength for this transition was shown<sup>70,71,148-150,157,158</sup> to be zero on a crystal-field one-electron model unless the perturbed  ${}^1A_{1g}$  and  ${}^1T_{1g}$  wave functions included first order terms involving metal basis orbitals with  $l \geq 7$ . This required mixing of the metal  $3d$  orbitals with those for which  $l \geq 7$  by a perturbation potential function with an  $R_p^{-10}$  dependence on the metal-perturber distance,  $R_p$ , and was considered<sup>70,71</sup> unimportant if electron-exchange and charge-transfer interactions between the metal and ligand atoms were neglected. When developed to second order, the net rotatory strengths for the  ${}^1A_{1g} \rightarrow {}^1T_{1g}$  and  ${}^1A_{1g} \rightarrow {}^1T_{2g}$  transitions were found to be non-zero in general.<sup>70,71</sup> When the trigonal splitting of the degenerate octahedral  ${}^1T_{1g}$  state was considered,<sup>68,70,149,150,152</sup> the first order rotatory strengths of the component  ${}^1A_1 \rightarrow {}^1E$  and  ${}^1A_1 \rightarrow {}^1A_2$  transitions were shown to be non-vanishing and equal in magnitude with opposite signs. It was suggested<sup>70,165,166</sup> that the two bands of opposite sign under the  ${}^1A_{1g} \rightarrow {}^1T_{1g}$  envelope of the solution CD spectrum<sup>166</sup> of  $(+)\text{Co(en)}_3^{3+}$  correspond to the above trigonal components, these being identified by oriented single crystal CD spectra<sup>165,166</sup> of  $(+)\text{Co(en)}_3^{3+}$ . The magnitude of the trigonal splitting in the crystal, as determined from the plane polarized single crystal absorption

spectra of the  $[\text{Co(en)}_3]^{3+}$  ion in several different lattice environments,<sup>167-170</sup> appears to be smaller than that observed in solution<sup>70,171,172</sup> from CD and magnetic circular dichroism studies. The models of Moffitt,<sup>73</sup> Poulet<sup>150</sup> and Piper and Karipades<sup>68</sup> attributed the optical activity of the  ${}^1A_{1g} + {}^1T_{1g}$  absorption band in trigonally distorted ( $D_3$ ) six-coordinate Co(III) complexes solely to the deviation of the  $\text{CoL}_6$  chromophore from  $O_h$  symmetry, whereas that of Richardson<sup>70</sup> included the dissymmetric influences of all of the ligand atoms in the complex.

Regional or sector rules connect the relative signs and magnitudes of the rotatory strengths for particular chromophoric transitions with the configurations of the perturbing ligand groups relative to the respective chromophoric sites. The ligand perturbers must have similar electrostatic and electrodynamic properties. Thus relative optical rotatory properties may be determined for a set of dissymmetric complexes with similar chromophoric centres and ligand atoms having similar electrical properties. When the charges and electrodynamic properties of the perturbing groups differ, the sector rules must be appropriately modified in order that the correct relative contributions from the dissimilar perturbers be determined. These rules are founded on group theoretical conditions for the non-vanishing of terms in the expression for the net or component rotatory strengths of a chromophore transition, and cannot, without empirical evidence or absolute knowledge of the unperturbed chromophore transition charge distributions and dipole moments and perturber electrical properties, be used for the prediction of absolute optical rotatory properties. Regional rules have been formally

derived<sup>71,157,158,160</sup> and rationalized on an electronic basis<sup>157,158,160</sup> in terms of both the one-electron static coupling<sup>71,157,158,160</sup> and the two-electron dynamic coupling<sup>157,160</sup> mechanisms for pseudo-tetragonal and pseudo-octahedral chiral metal complexes. Richardson<sup>70,157</sup> has shown that the rules for the *net* rotatory strengths of the metal ion *d-d* transitions are identical in form for the two mechanisms, although this is not the case for the rule derived for the component trigonal transitions of trigonal pseudo-octahedral complexes.<sup>160</sup> Furthermore, both first order<sup>71,157,158,160</sup> and second order (in perturbation theory)<sup>71,157,158</sup> contributions to the *net* rotatory strength have been considered in the development of these expressions. The sector rules based on the second order terms are particularly important in the case of dissymmetric pseudo-octahedral cobalt(III) complexes. As mentioned previously, the first order contributions to the *net* rotatory strengths of the *d-d* transitions for these complexes have little significance for a crystal-field one-electron static coupling model.<sup>71,158</sup> First order rules may, however, achieve significance on a one-electron molecular orbital or charge transfer model in which the zeroth order  $CoL_6$  states allow for cobalt-ligand electron exchange and the perturbed states include mixing with ligand donor atom orbitals.<sup>160</sup> A number of analogous rules based on empirical correlations and somewhat less formal theoretical bases have also been developed<sup>21,173-176</sup> and applied to pseudo-tetragonal and pseudo-octahedral chiral transition metal complexes in recent years.

The effects of metal-donor atom electron exchange on the optical activity of transition metal complexes have been investigated in several

theoretical models<sup>69,72,153,154,156</sup> employing both metal and ligand basis orbitals in the representations of the wave functions for the spectroscopic states. A number of these studies<sup>69,72,156</sup> were concerned with the determination of rotatory strengths for the visible CD bands of six-coordinated  $D_3$  complexes in which the  $ML_6$  core ( $M$  = metal) was trigonally distorted. In the models of Karipides and Piper<sup>69</sup> and Liehr,<sup>153</sup> as well as in the calculations of Strickland and Richardson<sup>72</sup> which were based on these models, the molecular state wave functions were constructed from molecular orbitals using the LCAO approach on the metal and donor atom basis orbitals. Karipides and Piper<sup>69</sup> included the  $2s$  and  $2p\sigma$  ligand donor orbitals and the  $3d$  and  $4p$  metal orbitals in the basis set for their calculations on the rotatory strengths of the *net*  ${}^1A_{1g} \rightarrow {}^1T_{1g}$  and component  ${}^1A_1 \rightarrow {}^1E$  and  ${}^1A_1 \rightarrow {}^1A_2$  transitions of the  $Co(III)N_6$  chromophore in  $[Co(en)_3]^{3+}$ . The metal-ligand  $\sigma$  bonds were directed along the internuclear axes. Liehr<sup>153</sup> proposed a basis orbital set in which the ligand  $p\sigma$  orbitals were canted with respect to the M-L axis of an octahedral  $ML_6$  chromophore in a  $D_3$  metal complex. Thus there is an inherent dissymmetry in the molecular orbitals of the  $ML_6$  cluster for an  $O_h$  nuclear configuration, and Liehr's model<sup>153</sup> forecasts non-zero rotatory strengths for the *net* and trigonal component transitions of such a chromophore. Strickland and Richardson<sup>72</sup> have extended the molecular orbital model of Karipides and Piper<sup>69</sup> to include  $\pi$  bonding interactions between the metal and ligand donor atoms. Their atomic orbital basis set included the  $2s$  and all  $2p$  donor atom orbitals, and the  $3d$ ,  $4s$  and  $4p$  metal orbitals for calculations on the rotatory strengths

of the visible spectral bands of the  $\text{Co(III)N}_6$  core in dissymmetric  $D_3$  complexes. The model made allowance for the canting of the ligand  $p\sigma$  orbitals with respect to the Co-N axes (Liehr's model) in addition to the trigonal ( $D_3$ ) distortion of the  $\text{CoN}_6$  core from the  $O_h$  configuration (Piper's model), and so combined the essential qualities of both Liehr's and Piper's models. Schäffer<sup>156</sup> has incorporated the metal and donor atom orbitals in the angular overlap model<sup>177</sup> of bonding in metal complexes, and has considered the optical rotatory properties of tris- and *cis*-bis-bidentate complexes of Co(III) and Cr(III) in terms of this model. The optical activity in all of the above electron exchange models for the  $\text{ML}_6$  core in six-coordinate complexes derives from a similar source, *i.e.* the deviation in the configuration of the donor atom  $\sigma$  and  $\pi$  bonding orbitals from that in which the electron distribution is symmetrical about the apical directions of a regular octahedron. The effects of the non-ligating atoms on the optical activity of these complexes were included only indirectly in the above models. They were considered only in so far as they induced the appropriate distortions in the  $\sigma$  and  $\pi$  donor atom orbitals.

The detailed effects of vibronic perturbations on the electronic states of the  $\text{ML}_6$  chromophore in pseudo-octahedral complexes were not explicitly included in the above derivations of the  $d-d$  transition rotatory strengths. The coupling of triply degenerate orbital states, *e.g.*  ${}^1T_{1g}$  and  ${}^1T_{2g}$  in six-coordinate Co(III) complexes, with the  $e_g$  and  $t_{2g}$  normal vibrational modes of the  $O_h$  core has been discussed<sup>70,71,158</sup> in relation to its possible effects on the trigonal field splitting

energies in  $D_3$  pseudo-octahedral complexes. Such coupling may result in strong Jahn-Teller distortions of the orbitally degenerate states of these complexes and considerable changes in their trigonal field splitting energies, spin-orbit splittings and magnetic moments.<sup>178</sup> Thus the presence of strong  ${}^1T_{1g} - e_g$  coupling in  $D_3$  Co(III) complexes may quench<sup>70,71</sup> the effect of the trigonal perturbation on the trigonal splitting of the octahedral  ${}^1T_{1g}$  electronic state and also reduce the angular momentum of this state. There is evidence for a strong dynamic Jahn-Teller distortion<sup>168,169,170</sup> of the  ${}^1T_{1g}$  state in  $[\text{Co}(\text{en})_3]^{3+}$ , and it was thought<sup>168,169,170</sup> that the two CD bands observed in solution under the  ${}^1A_{1g} + {}^1T_{1g}$  envelope involved transitions to two separate vibronic states associated with the  ${}^1T_{1g}$  state and that this arose from Jahn-Teller vibronic coupling. As well as inducing Jahn-Teller distortions through the gerade vibrations ( $e_g$  and  $t_{2g}$ ) of the  $ML_6$  core, vibronic coupling of the electronic states with the ungerade  $t_{1u}$  and  $t_{2u}$  modes may have a measurable effect on the intensities<sup>70,71</sup> of the visible CD bands of dissymmetric pseudo-octahedral complexes. In a similar manner to the dissymmetric perturbing potential energy of the static compound, these modes induce ungerade character in the gerade electronic states of the chromophore by mixing with the ungerade states and so lead to non-zero terms in the expressions for the rotatory strengths of the  $d-d$  transitions. The effects of all vibronic coupling modes should be examined in detail if the correct signs for the rotatory strengths and the correct directions in the splitting of degenerate chromophoric transitions are to be determined for the  $d-d$  CD bands of dissymmetric



transition metal complexes.

#### 4.2 OPTICAL ACTIVITY AND ROTATORY POWER<sup>179-182</sup>

In accordance with the wave theory of electromagnetic radiation, light of any frequency  $\nu$  consists of transverse waves in which mutually orthogonal electric (E) and magnetic (H) field vectors oscillate normal to the direction of propagation of the light with frequency  $\nu$ . In polarized light the loci of the E and H vectors are completely specified in time and space. For a continuous wave train, each vector may be obtained as a function of time and distance by expression as the vector sum of two mutually orthogonal linear vibrations ( $x$  and  $y$  directions) oscillating perpendicular to the propagation direction ( $z$  direction). The nature of the polarization (elliptical, linear or circular) depends on the amplitude and phase differences between the  $x$  and  $y$  vibrations. For circularly polarized light, the  $x$  and  $y$  amplitudes are equal and the phases  $\phi_x, \phi_y$  differ by  $\pm \pi/2$  at any given time and point ( $\phi_x = \phi_y - \pi/2$  for right and  $\phi_y = \phi_x + \pi/2$  for left circularly polarized light if  $x, y, z$  form a right-handed coordinate system). The E and H vectors for plane or linearly polarized light also have a representation as the sum of these left and right circularly polarized light vectors.

Any molecule or crystal, having point group symmetry which is devoid of alternating rotary reflection ( $S_n$ ) axes,<sup>182,183</sup> can not be superimposed on its mirror image. The mirror related molecular forms are termed optical isomers or enantiomers and the molecules are described as being chiral or dissymmetric. These optical isomers interact

differently with left and right circularly polarized light, the phenomenon being termed optical activity, and a substance composed of molecules with the same chiral form is said to be optically active. Optical activity is generally observed by determination of the angle of rotation of the polarization plane of plane polarized light (optical rotation), or by the differential absorption of left and right circularly polarized light at absorption frequencies (circular dichroism), after the polarized light has traversed an optically active crystal or solution medium. The circular dichroism (CD) curve over the absorption frequency range also determines the anomalous dispersion of the optical rotation (ORD) with wavelength and the emergent ellipticity of the plane polarized light used to measure the rotation at any absorption frequency. These phenomena are manifestations of the Cotton effect.<sup>184,185</sup>

The optical rotation induced by an optically active medium is determined<sup>186</sup> as

$$\alpha = \pi l (n_l - n_r) / \lambda_{vac}$$

where  $\alpha$  is the observed rotation,  $l$  is the path length,  $n_l$  and  $n_r$  are the refractive indices for left and right circularly polarized light in the medium and  $\lambda_{vac}$  is the wavelength of the incident light in vacuo. The specific rotatory power,  $[\alpha]_{\lambda}^t$  of an optically active substance at temperature  $t$  in a given environment is defined<sup>182</sup> as

$$[\alpha]_{\lambda}^t = \alpha / l d p$$

where  $l$  is the path length in decimetres,  $d$  is the density of the medium and  $p$  is the fraction by weight of the optically active substance.  $[\alpha]_{\lambda}^t$  is constant for a fixed wavelength  $\lambda$ . The molecular rotation,  $[M]_{\lambda}^t$  is

then given as

$$[M]_{\lambda}^{\dagger} = [\alpha]_{\lambda}^{\dagger} M / 100$$

where  $M$  is the molecular weight of the optically active compound. The optical enantiomers of a given chiral compound have positive and negative values for  $\alpha$  at a particular wavelength  $\lambda$  (usually that of the  $\text{Na}_D$  line where  $\lambda = 589 \text{ nm}$ ), and these are termed  $(+)_{\lambda}$  and  $(-)_{\lambda}$  respectively. The variation of  $[M]_{\lambda}^{\dagger}$  with wavelength for an isolated absorption band essentially follows the derivative of the CD curve with respect to frequency (Figure 4.1), and is related to the anomalous dispersion of the refractive indices  $n_L$  and  $n_R$  in the region of the absorption maximum by the relations given above.

The circular dichroism of an optically active substance is measured by the difference  $(\epsilon_L - \epsilon_R)$ , where  $\epsilon_L$  and  $\epsilon_R$  are the decadic molar extinction coefficients for left and right circularly polarized light at a given wavelength. The variation of CD with wavelength and the optical rotatory dispersion (ORD) curve of  $[M]_{\lambda}^{\dagger}$  vs.  $\lambda$  are depicted in Figure 4.1 for an isolated absorption band. The curves for two mirror-related optical isomers are identical in form but opposite in sign.

After passing through an optically active absorbing medium, plane polarized light becomes elliptically polarized because of the differential absorption of the two circular components. The ratio of the minor to the major axis of the ellipse determines the tangent of the angle of ellipticity  $\psi$ . The specific ellipticity  $[\psi]_{\lambda}^{\dagger}$  and the molar ellipticity  $[\theta]_{\lambda}^{\dagger}$  are defined in a manner similar to the specific rotation  $[\alpha]_{\lambda}^{\dagger}$  and the molecular rotation  $[M]_{\lambda}^{\dagger}$  as

$$[\Psi]_{\lambda}^t = \Psi / l d p \quad (\Psi \text{ is in degrees})$$

$$[\theta]_{\lambda}^t = [\Psi]_{\lambda}^t M / 100$$

$[\theta]_{\lambda}^t$  is related to the circular dichroism by

$$[\theta]_{\lambda}^t = 3300 (\epsilon_l - \epsilon_r)$$

The amplitude  $[M]_{max} - [M]_{min}$  in the ORD curve (Figure 4.1) is related to the maximum circular dichroism as follows:

$$[M]_{max} - [M]_{min} = 4028 (\epsilon_l - \epsilon_r)_{max}$$

where  $[M]_{max}$  occurs at a higher wavelength than  $[M]_{min}$ .

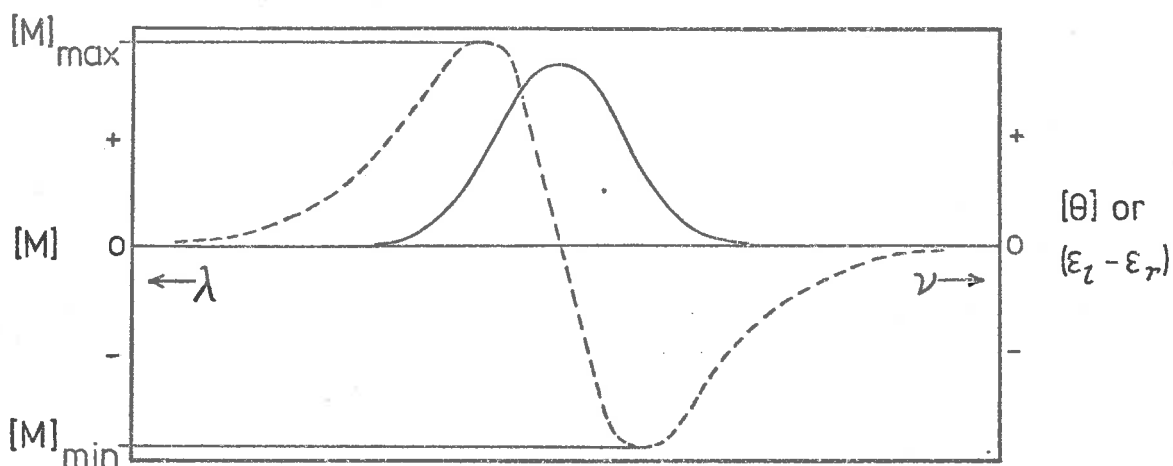


FIGURE 4.1. ORD (---) and CD (—) for a dissymmetric compound in the region of an absorption band.

The optical rotatory power of an electronic transition in a dissymmetric molecule is attributed to the helical nature of the electronic configurational changes occurring in the transition. Left and right circularly polarized radiations, impinging on the molecule normal to the axis of the helical electronic motion, induce such transitions with differing probabilities. Hence there is a preferential absorption of the left or right circularly polarized component of plane polarized incident

radiation, and a differential change in the velocities of the two components in a medium composed of the dissymmetric molecules. This gives rise to the ORD and CD associated with the optically active medium. These helical transitions have allowed electric and magnetic dipole transition moments with parallel or antiparallel components according to the general quantum-mechanical theory of optical rotatory power.<sup>187,188</sup> The rotatory power of an electronic transition  $i \rightarrow j$  between the molecular electronic states described by  $\Psi_i$  and  $\Psi_j$  is determined by the rotatory strength  $R_{ij}$ . This property is defined by<sup>188</sup>

$$R_{ij} = I_m[\langle \Psi_i | \vec{u} | \Psi_j \rangle \cdot \langle \Psi_j | \vec{m} | \Psi_i \rangle]$$

where  $I_m$  refers to the imaginary part of the scalar product, and  $\vec{u}$  and  $\vec{m}$  are the electric and magnetic dipole moment operators respectively. The rotational strength is a function of the area under the observed CD band for the optically active transition and their connection is given<sup>189</sup> by

$$R_{ij} = \frac{3hc^2303}{32\pi^3 N_0} \int (\epsilon_l - \epsilon_r) d \ln \nu \text{ in c.g.s units}$$

where  $\nu$  is the absorption frequency,  $c$  is the velocity of light in the medium,  $h$  is Planck's constant and  $N_0$  is Avogadro's number. The rotational strength may also be obtained from the observed ellipticity or the anomalous rotatory dispersion curve through the previously mentioned relations between these quantities and the observed circular dichroism.

#### 4.3 <sup>I</sup> THE PIPER-KARIPÉDES THEORY FOR $D_3$ Co(III)L<sub>6</sub> CHROMOPHORES<sup>68,69</sup>

In the introduction (Section 4.1), the crystal-field static coupling<sup>68</sup>

and molecular orbital<sup>69</sup> models of Piper and Karipides, for the optical activity of trigonally distorted ( $D_3$ ) complexes with an  $ML_6$  core, were mentioned. These have been applied to the determination of the rotatory strengths for the *net*  ${}^1A_{1g} \rightarrow {}^1T_{1g}$  and component  ${}^1A_1 + {}^1E$  and  ${}^1A_1 + {}^1A_2$  transitions of  $D_3$  symmetric Co(III) complexes. The models attributed the optical rotatory power of such transitions solely to the deviation of the ligand donor atoms, L, from a regular  $O_h$  configuration, *i.e.* the dissymmetry in the  $D_3$  Co(III) $L_6$  chromophore.

This correlation of rotational strength with trigonal distortion of the  $ML_6$  core in  $D_3$  metal complexes was originally investigated on a quantum mechanical basis by Moffitt<sup>73</sup> and subsequently amended by Sugano,<sup>148</sup> Hamer<sup>149</sup> and Poulet.<sup>150</sup> The spectroscopic  $ML_6$  states in these theories were constructed from metal atomic orbitals according to the crystal-field theory of transition metal complexes, and the rotational strengths were determined on the basis of a one-electron static coupling model<sup>70-72,160-162</sup> in which the dynamic coupling between M and L electrons was ignored.

In the above crystal-field models,<sup>68,73,148-150</sup> the  $D_3$  ligand-field potential was permitted to mix  $4p$ <sup>73,150</sup> or  $4p$  and  $4f$ <sup>68</sup> metal orbitals with the  $3d$  orbitals, and only first order perturbation theory contributions were considered in the expressions for the perturbed wave functions of the  $ML_6$  chromophore. This total first order contribution to the *net* rotatory strength for the  ${}^1A_{1g} \rightarrow {}^1T_{1g}$  transition of the Co(III) $L_6$  core was shown to be zero.<sup>70,71,148-150</sup> However, when the degenerate octahedral  ${}^1T_{1g}$  state was energetically split into  ${}^1A_2$  and  ${}^1E$  components by the  $D_3$  perturbation potential,<sup>68,149,150,152</sup> the rotatory strengths of

the separate  ${}^1A_1 \rightarrow {}^1A_2$  and  ${}^1A_1 \rightarrow {}^1E$  transitions were found<sup>68,150</sup> to be equal in magnitude and opposite in sign.

In the molecular orbital model of Karipades and Piper,<sup>69</sup> molecular orbitals for the  ${}^1A_1$ ,  ${}^1A_2$  and  ${}^1E$  state wave functions of the trigonally distorted ( $D_3$ )  $\text{Co(III)L}_6$  core were constructed from the donor atom  $2s$  and  $2p\sigma$  orbitals and the metal atom  $3d$  and  $4p$  orbitals. This model gives<sup>69</sup> a non-zero *net* rotatory strength for the  $\text{Co(III)L}_6$   ${}^1A_{1g} \rightarrow {}^1T_{1g}$  transition in  $D_3$   $\Lambda\text{-}[\text{Co(en)}_3]^{3+}$ , but the predicted absolute sign is opposite<sup>70,72</sup> the observed value in solution when the  $\text{CoN}_6$  core geometry is taken to have the configuration usually found in the crystal.<sup>15,190-196</sup>

In this configuration the  $\text{CoN}_6$  cluster has polar compression and azimuthal contraction<sup>15,38,72</sup> distortions from  $O_h$  symmetry, where the polar and azimuthal angles are determined with respect to the  $C_3$  axis of the mean  $D_3$  symmetric  $\text{CoN}_6$  core (see section 4.3.1). In some crystalline environments however,<sup>197,198</sup> the  $\text{CoN}_6$  core of  $[\text{Co(en)}_3]^{3+}$  has a slight polar elongation<sup>15</sup> along the  $C_3$  axis of the complex, which coincides with a crystallographic 3-fold axis for these structures.

The molecular orbital model then predicts<sup>72</sup> the same absolute sign for the *net*  ${}^1A_{1g} \rightarrow {}^1T_{1g}$  rotatory strength as that observed in solution<sup>199</sup> and in the solid state<sup>199</sup> KCl and KBr disc spectra of these compounds.

Despite such correlations, the structural data for many of the structures containing the  $[\text{Co(en)}_3]^{3+}$  ion are not sufficiently accurate for the polar distortions to be meaningful. Furthermore, the  $\text{CoN}_6$  core often deviates considerably from  $D_3$  symmetry in the crystal, and the validity of using structural parameters obtained from such crystals to predict their

CD on the basis of a  $D_3$  theoretical model may be questionable.

#### 4.3.1 The Crystal-Field Model<sup>68</sup>

This model relates the  $d-d$  transition rotatory strengths for  $D_3$  transition metal complexes to the static trigonal ( $D_3$ ) distortion of their  $ML_6$  cores from  $O_h$  symmetry as indicated above. Since the effects of dynamic coupling with electronic transitions in the ligands, vibronic interaction between electronic states and vibrational modes of the  $ML_6$  cluster and metal-donor atom electron exchange were ignored in this static one-electron representation, quantitative estimations of the rotatory strength are not feasible.

However, it has been suggested<sup>70,71</sup> that the fundamental symmetry-determined aspects of the optical activity of the  $d-d$  transitions can be adequately described by a static one-electron model. This is based on the assumption that the model gives a correct nodal representation for the electronic states of the trigonally distorted  $ML_6$  chromophore and also for the  $D_3$  potential energy perturbation function. The symmetry-determined or nodal properties may then be estimated from the selection rules provided by the model and the signs and relative magnitudes of the rotatory strengths of the  $d-d$  transitions determined. For this crystal-field model, the *absolute* signs and magnitudes may not be predictable because of the neglect of dynamic coupling, vibronic coupling and electron exchange contributions to the rotatory strengths. Despite these deficiencies, the nodal properties of the  $d-d$  rotatory strengths as predicted on a static crystal-field model were not expected<sup>70,71</sup> to be



altered if the effects were subsequently included in the analysis. On this basis, the crystal-field representation of Piper and Karipades<sup>68</sup> may be used to examine the effect of the  $\text{Co(III)L}_6$  core distortion in determining the observed nodal aspects of the  ${}^1A_1 \rightarrow {}^1A_2$  and  ${}^1A_1 \rightarrow {}^1E$  rotatory strengths (of  ${}^1A_{1g} \rightarrow {}^1T_{1g}$  parentage) in the visible CD bands of  $D_3$  symmetric  $\text{Co(III)}$  complexes.

In the Piper-Karipades model,<sup>68</sup> the zeroth order  ${}^1A_{1g}$  and  ${}^1T_{1g}$  electronic states of a  $D_3$   $\text{Co(III)}$  complex were described in terms of an irreducible  $O_h$  basis set of metal  $3d$  orbitals ( $t_{2g}$  and  $e_g$ ) which also form an irreducible trigonal basis set in the  $D_3$  point group. A crystal-field  $D_3$  perturbation was then imposed on these one-electron metal-localized orbital wave functions by the static charges on the donor atoms of the trigonally distorted  $\text{Co(III)L}_6$  chromophore. The  $D_3$  perturbation potential was permitted to mix  $4p$  and  $4f$  metal orbitals with the  $3d$  orbitals in the perturbed one-electron wave functions which included only zeroth and first order terms. The trigonal ( $D_3$ ) components  ${}^1A_1$ ,  ${}^1A_2$ , and  ${}^1E$  of the perturbed  ${}^1A_{1g}$  and  ${}^1T_{1g}$  states were obtained by expression as product functions of the one-electron orbitals. These perturbed state wave functions were then used to determine the rotatory strengths of the trigonal  ${}^1A_1 \rightarrow {}^1A_2$  and  ${}^1A_1 \rightarrow {}^1E$  components of the  ${}^1A_{1g} \rightarrow {}^1T_{1g}$  band in terms of the operator matrix elements with respect to the one-electron wave functions.

The  $D_3$  potential energy function was expanded about an origin defined by the  $\text{Co(III)}$  atom, in a series of spherical harmonic functions<sup>200</sup> of the metal-electron and donor atom spherical coordinates  $(r, \theta, \phi)$ . These

spherical coordinates were referred to a trigonal coordinate system  $(X, Y, Z)$  in which the  $Z$  axis was coincident with the  $C_3$  axis of the  $D_3$  symmetric  $\text{Co(III)L}_6$  core (Figure 4.2(a)). The trigonal twist or dihedral angle  $\omega$ ,<sup>15,38,72</sup> defined for tris-bidentate chelate complexes, is related to the azimuthal angles  $\phi_L$  and  $\phi_{L'}$  of the donor atoms  $L$  and  $L'$

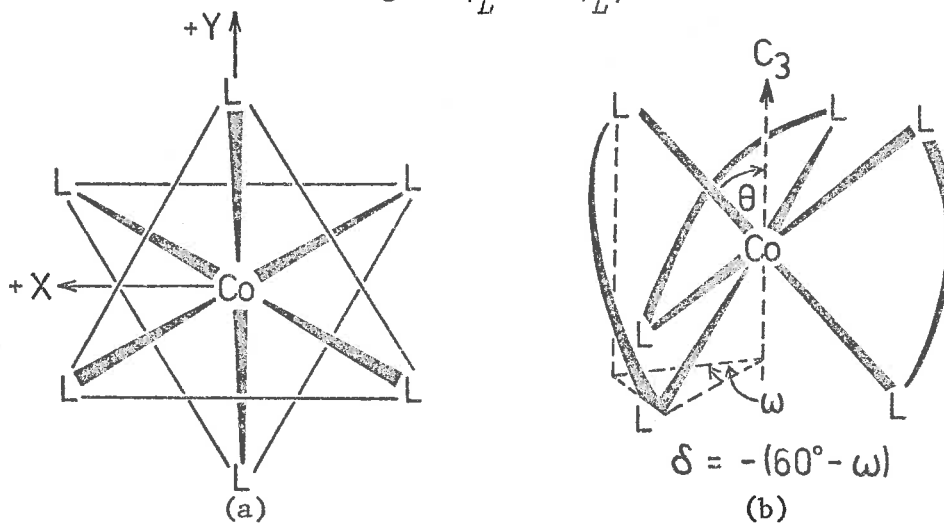


**FIGURE 4.2.** (a) Trigonal coordinate system for a  $D_3$   $\text{Co(III)L}_6$  core viewed down the  $C_3$  axis in the  $+Z$  direction. (b) The  $\omega$  and  $\delta$  angles for a  $D_3$  tris-bidentate  $\text{Co(III)}$  complex in the  $\Lambda$  configuration.  $\delta$  is the change in the azimuthal dihedral angle  $\omega$  when the  $O_h$  core distorts to the  $D_3$  configuration.

in the chelate ring by  $\omega = |\phi_L - \phi_{L'}|$ .  $\omega$  is related to the azimuthal distortion constant  $\delta$  of Piper and Karipides by  $\delta = \pm (60^\circ - \omega)$ , where the positive and negative signs refer to the  $\Delta$  and  $\Lambda$  configurations respectively. The same  $\omega$  and  $\delta$  angles may be used to describe the trigonal twist distortion of the chromophore in any  $D_3$  complex, if the positive sign in the above expression for  $\delta$  is used when the  $\omega$  angle is defined by the donor atom pairs having the same chiral sense as the chelate donor pairs of a  $\Lambda$ <sup>29</sup> tris-bidentate complex. Alternatively, if the donor

pairs defining  $\omega$  have the chiral sense of a  $\Lambda^{29}$  tris-bidentate complex, the negative sign is used in the evaluation of  $\delta$ .

On this model, the first order rotatory strengths for the  ${}^1A_1 + {}^1A_2$  and  ${}^1A_1 + {}^1E$  spectral bands of a  $D_3$  Co(III)L<sub>6</sub> core were shown<sup>68,70</sup> to be directly sign dependent on the leading component of the  $D_3$  perturbation potential energy function transforming as  $T_{2u}$  in the  $O_h$  point group of the zeroth order octahedral chromophore. The rotatory strengths are proportional to the term

$$R' = \pm ez(3/7)\sqrt{(35\pi)}. \sin^3\theta. \sin 3\delta$$

where +, - refer to the  ${}^1A_1 + {}^1E$  and  ${}^1A_1 + {}^1A_2$  bands respectively,  $e$  is the electronic charge,  $z$  is the donor atom charge (considered as a point charge),  $\theta$  is the polar coordinate of the donor atom (the angle between the Co-L bond and the  $C_3$  axis) and  $\delta$  is the azimuthal distortion angle defined above. Since  $\theta$  is less than  $180^\circ$  for all donor atoms L, the sign of  $R'$  is determined by the charge  $z$ , and the azimuthal distortion ( $\delta$ ) of the chromophore from the octahedral configuration. The trigonal splitting parameter  $K$ , defined<sup>15</sup> by  $\nu_E - \nu_A$  where  $\nu_E$ ,  $\nu_A$  are the  ${}^1E$  and  ${}^1A_2$  band transition frequencies, is dependent on the charge ( $z$ ) and the polar angle ( $\theta$ ) of the donor atom point charge in the Piper-Karipides crystal field model for a  $D_3$  Co(III)L<sub>6</sub> core. On this model, for negative  $z$ ,  $K$  is positive<sup>70,201,202</sup> for a trigonally compressed core ( $54.74^\circ < \theta < 125.26^\circ$ ). The rotatory strength  $R'$ , and trigonal splitting  $K$  have nodes at  $\delta = 0^\circ$  and  $\theta = 54.74^\circ$  (or  $125.26^\circ$ ) respectively, and change sign as  $\delta$  and  $\theta$  pass through the nodal values.

The above expression  $R'$ , for the sign dependence of the rotational

strength, indicates a negative CD for the  ${}^1A_1 \rightarrow {}^1E$ , and a positive CD for the  ${}^1A_1 \rightarrow {}^1A_2$  components of the  ${}^1A_{1g} \rightarrow {}^1T_{1g}$  transition in a  $\Lambda D_3$  Co(III) complex having negative donor atom charges and  $\omega < 60^\circ$  ( $\delta < 0^\circ$ ) *i.e.* having an azimuthal contraction distortion. However  $\Lambda-(+)_589^-$   $[\text{Co}(\text{en})_3]^{3+}$ , which exhibits an azimuthal contraction in crystalline environments<sup>15,190-198</sup> ( $\omega < 60^\circ$ ), has been found to show a positive rotatory strength for the  ${}^1A_1 \rightarrow {}^1E$  band in several single crystal CD studies.<sup>165,166,203</sup> As mentioned above, the absolute signs for the rotatory strengths are not expected to be predictable on a static crystal-field model, and the prime incentive here is the study of the nodal properties of  $R'$  with respect to  $\delta$  and of  $K$  with respect to  $\theta$ . In view of this, the signs given above for  $R'_E$  and  $R'_{A_2}$  may be reversed to conform with the observed values for the reference complex  $(+)_589^-$   $[\text{Co}(\text{en})_3]^{3+}$ . Alternatively the donor atom charges may be considered positive for this purpose. The assignment of an absolute sign to the trigonal splitting  $K$  can not be made unequivocally. The complex structures  $2[(+)_589^- \text{Co}(\text{en})_3 \text{Cl}_3] \cdot \text{NaCl} \cdot 6\text{H}_2\text{O}$ <sup>198</sup> and  $(+)_589^- [\text{Co}(\text{en})_3] \text{Br}_3 \cdot \text{H}_2\text{O}$ <sup>191</sup> respectively exhibit trigonal elongation ( $\theta < 54.74^\circ$  or  $> 125.26^\circ$ ) and trigonal compression ( $54.74^\circ < \theta < 125.26^\circ$ ) of the  $\text{Co(III)}\text{N}_6$  core. Yet the solid state KBr or KCl disc circular dichroism spectra<sup>199</sup> for both of these crystals suggest that the  ${}^1E$  component of the  ${}^1T_{1g}$  band lies at a lower frequency than the  ${}^1A_2$  component, as observed<sup>190</sup> in the solution CD spectra of these compounds. However, since the polar angles of the donor atoms in the above trigonally elongated structure are not significantly different<sup>15</sup> from the octahedral value ( $54.74^\circ$ ), and the majority of

$[\text{Co}(\text{en})_3]^{3+}$  structures,<sup>15,190-198</sup> including the more accurate ones, show a small trigonal compression of the  $\text{Co}(\text{III})\text{N}_6$  core,  $K$  may be tentatively allotted a negative sign for a trigonally compressed  $\text{Co}(\text{III})\text{N}_6$  core in a  $D_3$  complex.

#### 4.3.2 Application to $\lambda\lambda$ - $[\text{Co}(\text{tame})_2]^{3+}$

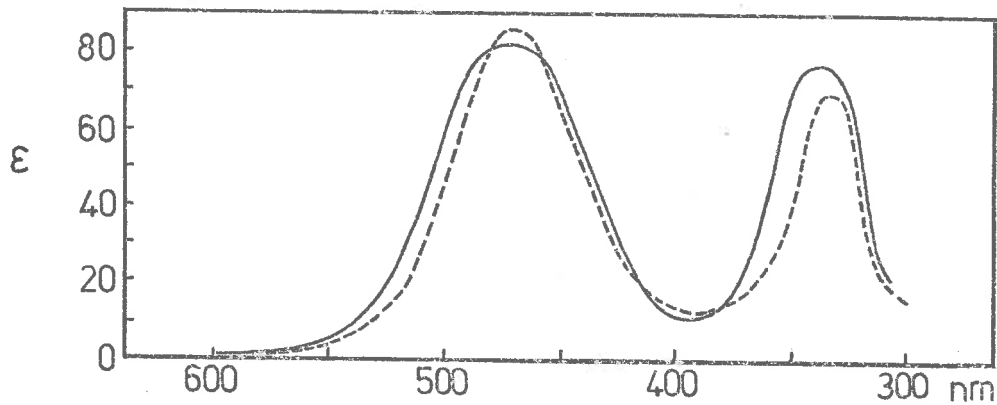
##### *Experimental Spectra*

The visible absorption spectra of  $[\text{Co}(\text{tame})_2]\text{Cl}_3$  in water and in an aqueous solution containing  $(+)\text{}_{589}$ -tartrate ion ( $[\text{tartrate}]:[\text{Co}(\text{tame})_2] = 3:2$ , for molar concentrations) were recorded for the 310-590 nm wavelength range (see Section 3.2). These were virtually identical and are depicted with the aqueous solution absorption spectrum of  $(+)\text{}_{589}$ - $[\text{Co}(\text{en})_3]\text{Cl}_3$  in Figure 4.3(a). The ORD curve for  $[\text{Co}(\text{tame})_2]^{3+}$  in aqueous  $(+)\text{}_{589}$ -tartrate solution was determined as described in Section 3.2 for the 400-600 nm visible wavelength region and is shown qualitatively with the aqueous solution ORD curve<sup>181</sup> for  $(+)\text{}_{589}$ - $[\text{Co}(\text{en})_3]^{3+}$  in Figure 4.3(b). The values for  $[M]_{\lambda}^t$  were found to increase quite steeply with increase in the tartrate to complex concentration ratio over the concentration range studied. The solid state visible circular dichroism spectra of  $(+)\text{}_{589}$ - $[\text{Co}(\text{en})_3]\text{Cl} \cdot (\text{}_{589}\text{-tartrate} \cdot x\text{H}_2\text{O})$  and  $[\text{Co}(\text{tame})_2]\text{Cl} \cdot (\text{}_{589}\text{-tartrate} \cdot 5.4\text{H}_2\text{O})$  in polished polystyrene discs were recorded over the 330-600 nm range using a Roussel-Jouan Circular Dichrograph. These were determined by Dr. M.R. Snow under the auspices of Dr. C.J. Hawkins of the Department of Chemistry, the University of Queensland, St. Lucia, Queensland. The spectra are presented in Figure 4.3(c) together with the aqueous solution CD spectrum<sup>181</sup> of

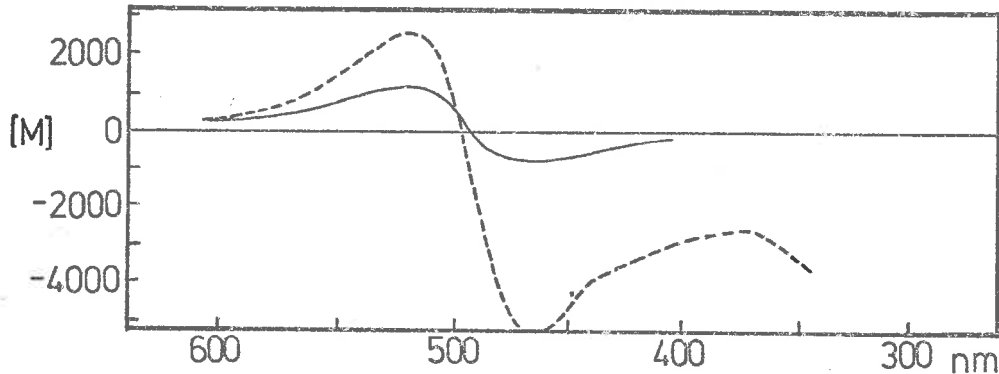
$(+)\text{}_{589}\text{-}[\text{Co}(\text{en})_3]^{3+}$  and the KBr disc CD spectrum<sup>199</sup> of  $(+)\text{}_{589}\text{-}[\text{Co}(\text{en})_3]\text{Cl}_3 \cdot 3\text{H}_2\text{O}$ .

The solid state CD spectrum of  $[\text{Co}(\text{tame})_2]\text{Cl}(\text{}_{589}\text{-tartrate} \cdot 5.4\text{H}_2\text{O})$  in a polished polystyrene disc shows a single large positive peak under the  ${}^1A_{1g} \rightarrow {}^1T_{1g}$  absorption band envelope of the  $\text{Co(III)}\text{N}_6$  chromophore (Figure 4.3(c)). As discussed in Chapter 3, the  $[\text{Co}(\text{tame})_2]^{3+}$  ion in this crystalline salt was observed to have the  $\lambda\lambda$  configuration, where  $\lambda$  describes the conformation of the Co-tame skew-boat chelate rings in the complex. The similarity between the solid state visible CD spectra of  $(+)\text{}_{589}\text{-}[\text{Co}(\text{en})_3]\text{Cl} \cdot 3\text{H}_2\text{O}$  and  $(+)\text{}_{589}\text{-}[\text{Co}(\text{en})_3]\text{Cl}(\text{}_{589}\text{-tartrate} \cdot x\text{H}_2\text{O})$  (Figure 4.3(c)) indicates that the contribution to the complex ion CD from the dissymmetric influence of the tartrate ion is considerably lower in magnitude than the intrinsic molecular effect. Hence the circular dichroism exhibited by the  $[\text{Co}(\text{tame})_2]\text{Cl}(\text{}_{589}\text{-tartrate} \cdot 5.4\text{H}_2\text{O})$  crystals in the  ${}^1A_{1g} \rightarrow {}^1T_{1g}$  absorption region should be largely representative of the  $\lambda\lambda$  configuration of the complex  $[\text{Co}(\text{tame})_2]^{3+}$  ion, as the order of magnitude observed here is similar to that found in the CD spectra of  $(+)\text{}_{589}\text{-}[\text{Co}(\text{en})_3]^{3+}$  in its aforementioned solid state compounds. Other CD studies of symmetrical  $\text{Co(III)}$  complex cations, in solid and solution media containing optically active counter anions,<sup>21,135-137</sup> have shown that the optical activity induced in these complexes by the dissymmetric environments is generally an order of magnitude less than that observed here for  $[\text{Co}(\text{tame})_2]^{3+}$  and  $(+)\text{}_{589}\text{-}[\text{Co}(\text{en})_3]^{3+}$ .

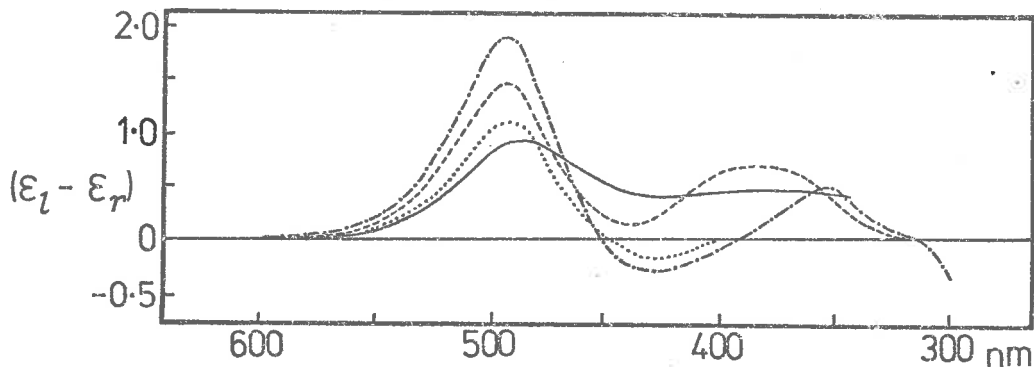
Relatively large changes induced in the visible solution CD spectra of  $[\text{Co}(\text{diamine})_3]^{3+}$  complexes by certain polarizable oxyanions (e.g.  $\text{PO}_4^{3-}$



(a) Visible absorption spectra of  $[\text{Co}(\text{tame})_2\text{Cl}_3]$  (—) and  $[\text{Co}(\text{en})_3]\text{Cl}_3$  (---) in aqueous solution.



(b) ORD curves for  $[\text{Co}(\text{tame})_2]^{3+}$  (—) in aqueous  $\text{K}_2(+)\text{}_{589}\text{-tartrate}$  solution and  $(+)\text{}_{589}\text{-}[\text{Co}(\text{en})_3]^{3+}$  (---) in aqueous solution.



(c) CD spectra of  $(+)\text{}_{589}\text{-}[\text{Co}(\text{en})_3]\text{Cl}-(+)\text{}_{589}\text{-tartrate}\cdot x\text{H}_2\text{O}$  (---) and  $[\text{Co}(\text{tame})_2]\text{Cl}-(+)\text{}_{589}\text{-tartrate}\cdot 5.4\text{H}_2\text{O}$  (—) in polystyrene discs, and  $(+)\text{}_{589}\text{-}[\text{Co}(\text{en})_3]^{3+}$  in aqueous solution (— · —) and as  $\text{Co}(\text{en})_3\text{Cl}_3\cdot 3\text{H}_2\text{O}$  in a KBr disc (· · · ·).

FIGURE 4.3. VISIBLE ABSORPTION, ORD AND CD SPECTRA.

and  $\text{SeO}_3^{2-}$ )<sup>36,204-211</sup> have sometimes been attributed<sup>1,205,207</sup> to specific ion-pair formation through hydrogen bonding between the oxyanion and preferred conformational isomers. In some cases (*e.g.*  $(+)\text{}_{589}\text{-}[\text{Co}(\text{en})_3]^{3+}$  and  $(+)\text{}_{589}\text{-}[\text{Co}((+)\text{}_{589}\text{-pn})]^{3+}$ ), the ion-pairing has been considered to modify the  $d-d$  transition rotatory strengths in the preferred complex conformer, either by mixing with a new charge-transfer transition generated by the ion-pair complex<sup>205,206</sup> or by the dissymmetry associated with new asymmetric centres at the nitrogen donors.<sup>209</sup> In others (*e.g.*  $(+)\text{}_{589}\text{-}[\text{Co}(\text{tn})_3]^{3+}$ ), it was thought that the visible solution CD spectral changes reflected a variation in conformer proportions resulting from the specific ion-pairing rather than electronic changes in the associated conformers.<sup>15,36,38</sup> In the crystalline  $[\text{Co}(\text{tame})_2]\text{-Cl}(+)\text{}_{589}\text{-tartrate}\cdot 5.4\text{H}_2\text{O}$  salt, the complex cation is elaborately hydrogen-bonded to surrounding  $(+)\text{}_{589}\text{-tartrate}$  and water molecules (see Chapter 3). However, as implied above from the studies of tartrate influence on symmetric Co(III) complexes,<sup>136,137</sup> and from the similarity between the solid state visible CD spectra of  $(+)\text{}_{589}\text{-}[\text{Co}(\text{en})_3]^{3+}$  in various halide environments<sup>199</sup> and that in a preferred  $(+)\text{}_{589}\text{-tartrate}$  environment, it is assumed here that the outer sphere  $(+)\text{}_{589}\text{-tartrate}$  perturbations on the visible CD of  $[\text{Co}(\text{tame})_2]^{3+}$  are approximately an order of magnitude lower than the observed visible CD of the  $[\text{Co}(\text{tame})_2]\text{Cl}(+)\text{}_{589}\text{-tartrate}\cdot 5.4\text{H}_2\text{O}$  compound. Consequently this spectrum should principally reflect the internal structure of  $[\text{Co}(\text{tame})_2]^{3+}$  in the crystal and be amenable to an investigation of the theoretical structure-CD correlation models of Piper, Karipides and Richardson.



The ORD curve for  $[\text{Co}(\text{tame})_2]^{3+}$  in aqueous  $(+)\text{}_{589}\text{-tartrate}$  solution (Figure 4.3(b)) indicates a substantial positive Cotton effect in the visible spectral region for the  $[\text{Co}(\text{tame})_2]^{3+}$  ion (see Section 3.2). For a high tartrate to complex concentration ratio, the effect becomes comparable in size with that observed<sup>181</sup> for  $(+)\text{}_{589}\text{-}[\text{Co}(\text{en})_3]^{3+}$  in aqueous solution (Figure 4.3(b)). It therefore appears that an optically active conformer ( $\lambda\lambda$  or  $\delta\delta$ ) of  $[\text{Co}(\text{tame})_2]^{3+}$  has been preferentially formed in aqueous solution by ion association with the  $(+)\text{}_{589}\text{-tartrate}$  ion. This is believed to have the  $\lambda\lambda$  configuration as observed in the crystal structure of  $[\text{Co}(\text{tame})_2]\text{Cl}(\text{}_{589}\text{-tartrate})\cdot 5.4\text{H}_2\text{O}$  from the following observations: the Cotton effect in the  ${}^1A_{1g} + {}^1T_{1g}$  absorption region is positive for both the crystal and solution conformers, the small differential distortions suffered by  $(+)\text{}_{589}\text{-}[\text{Co}(\text{en})_3]^{3+}$  in various crystalline environments<sup>15</sup> were observed<sup>199</sup> to induce only minor changes in its aqueous solution visible CD spectrum (Figure 4.3(c)), and the Cotton effects for  $[\text{Co}(\text{tame})_2]^{3+}$  in the crystal and in solution are comparable in magnitude.

*The Observed  $\text{Co}(\text{III})\text{N}_6$  Chromophore of  $\lambda\lambda\text{-}[\text{Co}(\text{tame})_2]^{3+}$*

The  $\text{Co}(\text{III})\text{N}_6$  chromophore of  $\lambda\lambda\text{-}[\text{Co}(\text{tame})_2]^{3+}$  observed in the crystal structure of  $[\text{Co}(\text{tame})_2]\text{Cl}(\text{}_{589}\text{-tartrate})\cdot 5.4\text{H}_2\text{O}$  (see Chapter 3) is depicted in Figure 4.4 as a projection onto the plane perpendicular to the pseudo- $C_3$  axis of the complex ion. The trigonal twist angles,  $\omega$ , were here defined by donor atom pairs having the chiral sense of a  $\Delta$  tris-bidentate complex and are shown in Figure 4.4 with the polar angles,  $\theta$ , subtended by the six Co-N bonds at the  $C_3$  axis. The pseudo- $C_3$  axis

was defined by the perpendicular (through the Co atom) to the average of the donor atom planes N(1),N(2),N(4) and N(3),N(5),N(6), and the trigonal twist angles were determined from the projections of the appropriate Co-N bonds on this mean plane. Program AZIMUTH by Butler<sup>15</sup> was used for the calculations. The mean values for  $\omega$  and  $\theta$  are  $55.83^\circ$  and  $53.97^\circ$  respectively, and the chromophore configuration is equivalent to that of a  $\Delta$ -tris-bidentate complex having an azimuthal contraction ( $\omega < 60^\circ$ ) and an insignificant polar or trigonal elongation ( $\theta < 54.74^\circ$ ) of the  $\text{Co(III)}\text{N}_6$  core. These mean values were used in the evaluation of the theoretical models of Piper, Karipades<sup>68</sup> and Richardson,<sup>70</sup> which included only  $D_3$  terms in the spherical harmonic expansion of the

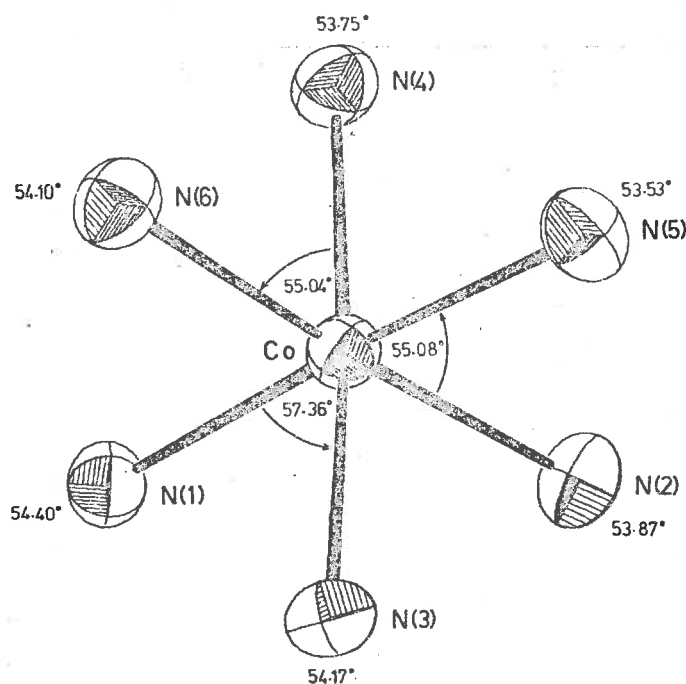


FIGURE 4.4. Observed chromophore of  $\lambda\lambda$ - $[\text{Co}(\text{tame})_2]^{3+}$  in projection down the pseudo- $C_3$  axis.

perturbation potential energy function of the chromophoric electrons. They are justified by the quasi- $D_3$  symmetry of the  $[\text{Co}(\text{tame})_2]^{3+}$  ion as observed in its crystal structure (Chapter 3).

*Correlation of Observed and Computed CD with the Chromophore Configuration*

As discussed in Section 4.3.1, the signs of the rotatory strengths for the  ${}^1A_1 \rightarrow {}^1A_2$  and  ${}^1A_1 \rightarrow {}^1E$  transitions of a  $D_3$   $\text{Co(III)N}_6$  chromophore are predicted from the first order crystal-field model of Piper and Karipides<sup>68</sup> to be determined by the term

$$R' = \pm \alpha z(3/7)\sqrt{(35\pi)}. \sin^3 \theta. \sin 3\delta$$

where +, - refer to the  ${}^1A_1 \rightarrow {}^1E$  and  ${}^1A_1 \rightarrow {}^1A_2$  bands. In the present analysis the observed CD<sup>165,166,203</sup> for the  ${}^1E$  band of  $\Lambda(+)_589^-$   $[\text{Co}(\text{en})_3]^{3+}$  is used as a reference to define the absolute sign for  $R'$ . This complex which has  $\omega < 60^\circ$  and  $\delta < 0^\circ$  in crystalline environments,<sup>15,190-198</sup> exhibits a large positive rotatory strength for the  ${}^1A_1 \rightarrow {}^1E$  chromophore transition.<sup>165,166,203</sup> The above expression for  $R'$  then gives the correct sign for the observed CD bands of  $\Lambda(+)_589^-$   $[\text{Co}(\text{en})_3]^{3+}$  if the donor atom charge  $z$  is positive as will be assumed here. Evidence for charge delocalization in complex ions<sup>93-96</sup> indicates that this situation may be physically approached, but is probably unrealistic because of the relatively large negative charges on the nitrogen atoms in uncomplexed amino groups (see Section 4.4.2). However this is unimportant when predicting the rotatory strengths of complexes with chromophores similar to that of the reference.

It was inferred above that the chromophore observed here for  $\lambda\lambda-[\text{Co}(\text{tame})_2]^{3+}$  has a trigonal twist distortion (Figure 4.4) which is

equivalent to that of a  $\Lambda$ -tris-bidentate complex having an azimuthal contraction ( $\omega < 60^\circ$ ), or alternatively a  $\Lambda$ -tris-bidentate complex having an azimuthal expansion ( $\omega > 60^\circ$ ) of the  $\text{Co(III)N}_6$  cluster. The polar distortion is not significantly different from zero and the mean polar angle ( $\theta$ ) of  $53.97^\circ$  is close to the octahedral value of  $54.74^\circ$ . The distortion constant ( $\delta$ ) for this chromophore is determined from the mean  $\omega$  value of  $55.83^\circ$  to be  $+4.17^\circ$ , and the configuration is essentially the mirror image of that for the chromophore generally observed in crystal structures of  $\Lambda\text{-[Co(en)}_3\text{]}^{3+}$  which has  $\delta < 0^\circ$ . The expression for  $R'$  then indicates a negative rotatory strength for the  ${}^1A_1 \rightarrow {}^1E$  component of the  ${}^1A_{1g} \rightarrow {}^1T_{1g}$  absorption band of the observed  $\lambda\lambda\text{-[Co(tame)}_2\text{]}^{3+}$  chromophore. Similarly a positive rotatory strength is predicted for the  ${}^1A_1 \rightarrow {}^1A_2$  transition.

If the single positive band observed in the solid state visible CD spectrum of  $\lambda\lambda\text{-[Co(tame)}_2\text{]}^{3+}$  is indeed the composite of a dominant<sup>182,212</sup>  ${}^1E$  band and a recessive  ${}^1A_2$  band, Piper's model is refuted, and the nodal properties of the rotatory strengths in  $D_3$  complexes are not trivially determined on the basis of a first order crystal-field model of the  $\text{ML}_6$  chromophore. However there is some evidence, both experimental and theoretical, to suggest that the  ${}^1A_2$  CD component of the  ${}^1A_{1g} \rightarrow {}^1T_{1g}$  octahedral transition may possibly dominate in this complex.

The effect of phosphate ion on the aqueous solution visible CD spectra of the complex ions  $(+)\text{}_{589}\text{-[Co(en)}_3\text{]}^{3+}$ ,<sup>205-208</sup>  $(+)\text{}_{589}\text{-[Co((+)pn)}_3\text{]}^{3+}$ <sup>205,207</sup> and  $\Lambda\text{-}(-)\text{}_{589}\text{-[Co((+)chxn)}_3\text{]}^{3+}$ <sup>209</sup> was described in terms of an enhancement of the  ${}^1A_1 \rightarrow {}^1A_2$  and a reduction of the  ${}^1A_1 \rightarrow {}^1E$  component rotatory

strengths under the low energy  ${}^1T_{1g}$  absorption band envelope. This was attributed<sup>1,205,207,209</sup> to the  $[\text{Co}(\text{diamine})_3]^{3+}\text{-PO}_4^{3-}$  ion pair interaction, and assignment of the CD bands was inferred from the identification<sup>166,199</sup> of the  ${}^1A_2$  and  ${}^1E$  bands observed in the visible CD spectrum of aqueous  $(+)\text{}_{589}\text{-}[\text{Co}(\text{en})_3]^{3+}$ . The visible CD spectrum of  $(+)\text{}_{589}\text{-}[\text{Co}(\text{sen})]^{3+}$ , where sen is the sexadentate ligand  $\text{CH}_3\text{C}(\text{CH}_2\text{NHCH}_2\text{-CH}_2\text{NH}_2)_3$ , was found<sup>209</sup> to be remarkably similar in form to the spectra of the above tris(diamine) complexes in phosphate ion solution. Since the  $[\text{Co}(\text{sen})]^{3+}$  complex consists of a  $[\text{Co}(\text{en})_3]^{3+}$  substrate trigonally capped by  $\text{CH}_3\text{C}(\text{CH}_2\text{-})_3$ , the assignment of the low energy trigonal CD components was again based on the  $[\text{Co}(\text{en})_3]^{3+}$  results.<sup>166,199</sup> The higher energy dominant negative CD component under the  ${}^1A_{1g} + {}^1T_{1g}$  envelope of  $(+)\text{}_{589}\text{-}[\text{Co}(\text{sen})]^{3+}$  was consequently ascribed to the  ${}^1A + {}^1A$  transition of this ideally  $C_3$  symmetric complex, and the  $[\text{Co}(\text{sen})]^{3+}$  complex was regarded as a model for the  $[\text{Co}(\text{diamine})_3]^{3+}\text{-PO}_4$  ion pair in speculation on the origin of the observed CD changes in phosphate ion solutions.<sup>209</sup> If these conjectures are correct, and the  ${}^1A$  band is dominant in the CD spectrum of the trigonally capped complex, then the single positive CD peak observed for  $[\text{Co}(\text{tame})_2]^{3+}$  under the  ${}^1A_{1g} + {}^1T_{1g}$  envelope may well be composed of a dominant  ${}^1A_2$  band and a recessive  ${}^1E$  band. Here the tame ligands simulate the  $\text{CH}_3\text{C}(\text{CH}_2\text{NH-})_3$  trigonal cap of  $[\text{Co}(\text{sen})]^{3+}$ , but the asymmetric nitrogen centres, proposed<sup>209</sup> to be the major source of differences between the visible CD spectra of  $(+)\text{}_{589}\text{-}[\text{Co}(\text{sen})]^{3+}$  and  $(+)\text{}_{589}\text{-}[\text{Co}(\text{en})_3]^{3+}$ , are absent in the  $[\text{Co}(\text{tame})_2]^{3+}$  complex. If the lower order environmental effects are disregarded (see section on

*Experimental Spectra*), the sole source of dissymmetry and optical activity in the solid state structure of  $[\text{Co}(\text{tame})_2]^{3+}$  is the conformation of the six-membered Co-tame chelate rings. The visible CD spectra of aqueous  $(+)_{589}\text{-}[\text{Co}(\text{sen})]^{3+}$ <sup>209</sup> and solid state  $\lambda\lambda\text{-}[\text{Co}(\text{tame})_2]^{3+}$  are comparable in magnitude allowing for the decrease in intensity of the disc spectrum due to depolarization of the circularly polarized light.<sup>199</sup> It then seems apparent that the spectrum observed<sup>209</sup> for  $(+)_{589}\text{-}[\text{Co}(\text{sen})]^{3+}$  and possibly those found<sup>205-209</sup> for the above  $[\text{Co}(\text{diamine})_3]^{3+}$  complexes in phosphate solution could be largely influenced (if not dominated) by the contributions arising from preferred conformations of the trigonal caps. These may be induced by the minimization of steric interactions with the Co-diamine chelate rings, although the relative energies of the possible conformers have not been estimated.

In the CD spectrum of aqueous  $(-)_{589}\text{-}[\text{Co}((+)\text{cptn})_3]\text{Cl}_3$ ,<sup>213,214</sup> the higher energy dominant negative component in the  ${}^1A_{1g} \rightarrow {}^1T_{1g}$  absorption band region was also attributed<sup>213</sup> to the  ${}^1A_1 \rightarrow {}^1A_2$  transition of the  $D_3$  complex chromophore. Although the CD of this complex may not be directly relevant to that of  $[\text{Co}(\text{tame})_2]^{3+}$ , the assignment, if correct, provides further evidence that the  ${}^1E$  CD band under the  ${}^1T_{1g}$  envelope is not always dominant in  $D_3$  Co(III)-polyamine complexes.

The one-electron crystal field model of Richardson,<sup>70</sup> (Section 4.4) which predicts the *net* rotatory strength for the  ${}^1A_{1g} \rightarrow {}^1T_{1g}$  transition of a  $D_3$  symmetric Co(III) complex to second order in perturbation theory, also offers some conjectural support for the dominance of the  ${}^1A_1 \rightarrow {}^1A_2$  trigonal component in the CD spectrum of  $[\text{Co}(\text{tame})_2]^{3+}$ . For ligand

perturbing sites having positively signed charges, the model implies a dominant  ${}^1A_2$  trigonal component in the net rotatory strength of the  ${}^1A_{1g} \rightarrow {}^1T_{1g}$  transition when the polar coordinates of the perturbers lie in the range  $\theta < 54.74^\circ$  or  $\theta > 125.26^\circ$ , as observed for the majority of the ligand atoms in the  $[\text{Co}(\text{tame})_2]^{3+}$  complex (see Section 4.4.2). This inference is based on the observation that for  $(+)\text{}_{589}\text{--}[\text{Co}(\text{en})_3]^+$ , where the corresponding atom types lie on the opposite side of the nodal polar angle ( $54.74^\circ$ ), the  ${}^1E$  band is dominant<sup>166,199</sup> (the *a priori* prediction of the model<sup>70</sup> when the perturbers with  $125.26^\circ > \theta > 54.74^\circ$  are assumed to have positive charges). The result should not be affected if the donor atom charges are negative, even when the non-ligating atoms are included (as in the Richardson model)<sup>70</sup> in the expressions for the net and component rotatory strengths. But this assumes that the relative magnitudes of the contributions from the non-ligating atoms and the donor atoms are similar for the two complexes, and that the polar dispositions of the atoms in each of these groups are on opposing sides of the nodal polar angle of  $54.74^\circ$  in  $[\text{Co}(\text{tame})_2]^{3+}$  and  $(+)\text{}_{589}\text{--}[\text{Co}(\text{en})_3]^{3+}$ . The model then predicts qualitatively that the  ${}^1A_2$  component should be dominant in the  ${}^1A_{1g} \rightarrow {}^1T_{1g}$  transition rotatory strength for  $[\text{Co}(\text{tame})_2]^{3+}$  if the  ${}^1E$  band has the dominant CD in  $(+)\text{}_{589}\text{--}[\text{Co}(\text{en})_3]^{3+}$ .

If the above evidence for the dominance of the  ${}^1A_1 \rightarrow {}^1A_2$  rotatory strength under the  ${}^1T_{1g}$  band envelope in the CD spectrum of  $[\text{Co}(\text{tame})_2]^{3+}$  is accepted, then the observed positive CD band in this region supports the model of Piper and Karipides which, as delineated above, predicts the CD for the  ${}^1A_2$  band to be positive from the observed structural geometry.

Nevertheless this first order crystal-field model remains untested by the CD of the  $[\text{Co}(\text{tame})_2]^{3+}$  complex until the symmetry of the observed band in the visible spectral region is positively identified.

#### 4.4 THE RICHARDSON THEORY FOR DISSYMMETRIC Co(III) COMPLEXES<sup>70-72,158</sup>

The crystal-field static coupling one-electron representation<sup>70,71,158</sup> of Richardson for the optical activity of chiral pseudo-octahedral transition metal complexes has been afocited in the Introduction (Section 4.1). This was formally derived on a quantum mechanical basis as were the  $D_3$  chromophoric crystal-field models of Moffitt,<sup>73</sup> Foulet,<sup>150</sup> and Piper and Karipides,<sup>68</sup> and has been applied<sup>70,71</sup> to the estimation of rotatory strengths for the *net* octahedral  ${}^1A_{1g} \rightarrow {}^1T_{1g}$  and  ${}^1A_{1g} \rightarrow {}^1T_{2g}$  transitions and their subsymmetric components in dissymmetric Co(III) complexes. The optical rotatory power of these transitions was ascribed<sup>70,71,158</sup> to the static charge dissymmetry imposed by the whole complex at the chromophoric electron localized on the cobalt atom. Sector rules,<sup>71,157,158</sup> inter-relating the relative signs and magnitudes of the *net* rotatory strengths with the Cartesian coordinates of ligand atom point charges, were derived<sup>71,158</sup> for both first and second order (in perturbation theory) contributions on this crystal-field static coupling model. The second order rules were shown<sup>71,158</sup> to be particularly important in assessing the relative *net* CD spectra of the  $d-d$  transitions in pseudo-octahedral complexes, and were applied<sup>71</sup> to the *net*  ${}^1A_{1g} \rightarrow {}^1T_{1g}$  and  ${}^1A_{1g} \rightarrow {}^1T_{2g}$  rotatory strengths in Co(III) complexes having dissymmetric point groups.



Detailed derivations of the  $d-d$  rotatory strengths in trigonal dihedral ( $D_3$ ) complexes with a pseudo-octahedral  $ML_6$  core were also made<sup>70</sup> on the basis of this model, and these were specifically determined for the *net*  ${}^1T_{1g}$  and  ${}^1T_{2g}$  bands and their respective  ${}^1A_2$ ,  ${}^1E_a$  and  ${}^1A_1$ ,  ${}^1E_b$  components in  $D_3$  Co(III) complexes. These derivations followed those of Moffitt,<sup>73</sup> Poulet,<sup>150</sup> and Piper and Karipides<sup>68</sup> in the crystal-field description of the spectroscopic states, but the mixing of metal  $3d$  orbitals with  $4p$  and  $4f$  orbitals by the  $D_3$  ligand-field perturbation potential was carried to second order in perturbation theory. Consequently first and second order contributions were included in the expressions for the rotatory strengths which were shown<sup>70,71</sup> to be non-vanishing for the *net*  ${}^1A_{1g} \rightarrow {}^1T_{1g}$  and  ${}^1A_{1g} \rightarrow {}^1T_{2g}$  transitions.

Molecular orbital calculations, based on the combined molecular orbital theories of Liehr<sup>153</sup> and Karipides and Piper,<sup>69</sup> were also applied<sup>73</sup> to the determination of rotatory strengths for the above transitions in trigonally distorted Co(III) complexes by Strickland and Richardson. As described previously, the molecular orbitals for these spectroscopic states were constructed from the  $2s$  and  $2p$  donor atom orbitals and the  $3d$ ,  $4s$  and  $4p$  metal orbitals of the  $D_3$  Co(III) $N_6$  or Co(III) $O_6$  cluster, and the effects of the non-ligating atoms were not explicitly included in the calculations. It was thought<sup>73</sup> that this may have resulted in the over-estimation of  $\pi$  bonding strength between the metal and donor atom orbitals. These molecular orbital approaches indicated the importance of metal-donor atom electron exchange in substantially contributing to the optical activity of trigonally distorted Co(III) complexes. However, they

were found<sup>73</sup> not to satisfactorily account for the *net* observed CD of the  ${}^1A_{1g} \rightarrow {}^1T_{1g}$  and  ${}^1A_{1g} \rightarrow {}^1T_{2g}$  transitions in complexes such as  $\Lambda\text{-}(+)\text{Co(en)}_3^{3+}$ ,<sup>165,166,203</sup> and it was suggested<sup>73</sup> that the effects of the non-ligating atoms need be included in the model to provide a more suitable representation of the source of *d-d* optical activity in these complexes.

#### 4.4.1 The Crystal-Field Model for $D_3$ Complexes<sup>70</sup>

As with the crystal-field model of Piper and Karipides,<sup>68</sup> the Richardson model<sup>70</sup> for the *d-d* optical activity in pseudo-octahedral  $D_3$  Co(III) complexes did not explicitly include the effects of dynamic coupling, vibronic coupling and electron exchange on the rotatory strengths of the octahedral and trigonal component transitions. Consequently, as indicated in Section 4.3.1, *absolute* signs and magnitudes may not be quantitatively determined from this crystal-field static-coupling model. However, it was asserted<sup>70</sup> that the model gave a correct representation of the nodal structure in the electronic states of the perturbed  $\text{Co(III)}N_6$  chromophore and in the  $D_3$  ligand-field perturbation potential function. The symmetry-controlled nodal properties of the *d-d* transition rotatory strengths were then considered<sup>70,71</sup> to be adequately determined. In addition to estimating the symmetry-determined aspects of the optical activity, it was implied<sup>70,71</sup> that the *absolute* signs of the *net* rotatory strengths for the octahedral *d-d* transitions are predictable on this model. This was based on the assumptions that vibronic coupling effects only weakly influence the *net* rotatory strengths,

and that it is possible to theorize on the relative importance of various ligands in inducing dynamic coupling effects between the chromophoric electrons and the electrons of the perturbing ligand groups. Electron exchange between the metal and perturbing groups was not considered in this model. The model is here used to ascertain the importance of the crystal-field imposed by all ligand perturbers in determining the absolute signs and nodal properties of the *net* octahedral CD bands for  $D_3$  symmetric Co(III) complexes.

The zeroth order (octahedral) electronic states of the complex chromophore were constructed<sup>70</sup> from a set of metal  $3d$  orbitals forming the basis of fully reduced representations in both the  $O_h$  and  $D_3$  point symmetry groups in a similar fashion to those defined by Moffitt<sup>73</sup> and Piper and Karipedes.<sup>68</sup> A static  $D_3$  ligand field potential energy function, comprising the point charges associated with all perturbing sites (atoms) in the ligands, was imposed on this trigonal basis orbital set. The perturbed orbital wave functions included  $4p$  and  $4f$  contributions to second order in perturbation theory. Wave functions for the trigonal components  ${}^1A_1$ ,  ${}^1A_2$ ,  ${}^1E_a$  and  ${}^1A_1$ ,  ${}^1E_b$  of the perturbed  ${}^1A_{1g}$ ,  ${}^1T_{1g}$  and  ${}^1T_{2g}$  chromophoric states of the  $D_3$  Co(III) complex were then expressed as products of the new one-electron orbitals. The rotatory strengths of the component transitions  ${}^1A_1 \rightarrow {}^1A_2$ ,  ${}^1A_1 \rightarrow {}^1E_a$  and  ${}^1A_1 \rightarrow {}^1A_1$ ,  ${}^1A_1 \rightarrow {}^1E_b$ , and of the *net*  ${}^1T_{1g}$  and  ${}^1T_{2g}$  transitions were subsequently evaluated in terms of the matrix elements of the unperturbed trigonal basis set of metal orbital wave functions.

In this model the  $D_3$  potential function was expressed as a series

of spherical harmonic functions<sup>200</sup> of the chromophoric electron and ligand atom point charge spherical coordinates  $(r_i, \theta_i, \phi_i)$ , which were defined with respect to a trigonal coordinate system (Figure 4.2) centred on the Co(III) atom. The potential function included contributions from all point charge sites associated with the ligands. The first order rotatory strengths for the trigonal components  ${}^1A_2$  and  ${}^1E_a$  of the  ${}^1T_{1g}$  band were shown to be proportional to the leading term in the potential expansion transforming as  $T_{2u}$  in the  $O_h$  point group of the zeroth order chromophore. The net first order  ${}^1T_{1g}$  band was shown to be zero as expected<sup>70,71,148-150</sup> for the model, which included only the leading components in the potential expansion transforming gerade and ungerade under  $O_h$  symmetry. Similar results were obtained by Piper and Karipades,<sup>68</sup> and their first order expressions for the rotatory strengths of the trigonal components of  ${}^1T_{1g}$  have nodal dependence identical with those determined by Richardson,<sup>70</sup> which, however, included the additional effects of the non-ligating atoms. The trigonal component rotatory strengths<sup>70</sup> are equal in magnitude and proportional to the functions

$$R'(E_a, A_2) = (+, -) e \left( \frac{35\pi}{14} \right)^{1/2} \sum_i q_i \sin^3 \theta_i \cos 3\phi_i / r_i^4$$

where (+, -) refer to the  ${}^1E_a$  and  ${}^1A_2$  transitions respectively,  $e$  is the electronic charge,  $q_i$  is the charge associated with atomic site  $i$ ,  $(r_i, \theta_i, \phi_i)$  are the spherical coordinates of site  $i$ , and the sum extends over all ligand atoms in the complex. These functions determine the sign dependence of the first order rotatory strengths of the trigonal components of the  ${}^1T_{1g}$  band in  $D_3$  Co(III) complexes. The first order rotatory strengths of the components  ${}^1A_1 \rightarrow {}^1A_1$  and  ${}^1A_1 \rightarrow {}^1E_b$  components of the  ${}^1T_{2g}$

band are zero<sup>70,71</sup> as expected since the  ${}^1T_{2g}$  band is magnetic dipole forbidden<sup>73,182</sup> to zeroth order in perturbation theory.

The rotatory strengths of the trigonal components  ${}^1A_2$ ,  ${}^1E_a$ ,  ${}^1A_1$ ,  ${}^1E_b$  were also computed by including both first and second order contributions,<sup>70</sup> and the  ${}^1A_1 + {}^1E_b$  component of  ${}^1A_{1g} + {}^1T_{2g}$  was found to have a non-zero rotational strength to second order. Similarly the  ${}^1T_{1g}$  and  ${}^1T_{2g}$  bands of the  $\text{Co(III)L}_6$  chromophore were shown to have non-zero *net* rotatory strengths arising from the second order contributions. As with the first order trigonal components, the second order *net* rotatory strengths on this model<sup>70</sup> have a sign dependence which is solely a function of the ligand atom point charges and spherical coordinates. It is determined by<sup>70</sup>

$$R''_{net}(T_{1g}T_{2g}) = \left(\frac{1}{28}\right)^2 \sum_{ij} \pi \Sigma \Sigma q_i q_j (3 \cos^2 \theta_i - 1) \sin^3 \theta_j \cos 3\phi_j / r_i^3 r_j^4$$

where the symbols have the same significance as those in the equation for  $R'(E_a, A_2)$  and each summation extends over all ligand atom perturbing sites. The *net* rotatory strengths for both the  ${}^1T_{1g}$  and  ${}^1T_{2g}$  transitions are proportional to this term, the proportionality constant (independent of the non-donor ligand atom parameters) being larger for the  ${}^1T_{2g}$  transition. The magnitude of this constant, however, does depend on metal-donor atom distances in the zeroth order  $O_h$  chromophore as well as on functions of pure metal atomic orbitals.<sup>70</sup>

The sign of the trigonal splitting of the  ${}^1E_a$  and  ${}^1A_2$  components of the  ${}^1T_{1g}$  band was determined to first order<sup>70</sup> on this crystal-field static coupling model as

$$K' = -\frac{1}{14} \sum_i q_i (3 \cos^2 \theta_i - 1) / r_i^3$$

where the sign of  $K'$  is the same as that of  $\nu_{E_a} - \nu_A$ , previously referred to<sup>15</sup> as the trigonal splitting parameter,  $K$  (Section 4.3.1). As in the crystal-field model for the  $D_3$  Co(III)L<sub>6</sub> chromophore (4.3.1),  $K'$  has nodes at the octahedral  $\theta_i$  values of  $54.74^\circ$  and  $125.26^\circ$  and changes sign when all  $\theta_i$  coordinates simultaneously traverse the nodal values.

In the present application of the above crystal-field model<sup>70</sup> of Richardson to the optical activity of pseudo-octahedral  $D_3$  Co(III) complexes, the nodal properties and absolute signs of the rotatory strengths for the *net*  ${}^1T_{1g}$  and  ${}^1T_{2g}$  chromophoric transitions are examined, despite the considerably larger first order effects expected<sup>70,71</sup> for the individual trigonal components. This approach is primarily necessitated by the fact that the trigonal components of the above transitions cannot<sup>71</sup> often be assigned unambiguously. Furthermore, the sign of each term in the expression  $R'(E_a, A_2)$  for the signs of the first order rotatory strengths is dependent on the absolute sign of the perturbing charge which may not be available. In the expression  $R''_{net}(T_{1g}, T_{2g})$  for the sign of the *net* rotatory strengths, the sums may be resolved in terms of the contributions from groups of symmetrically or chemically equivalent ligand atom perturbers and the interaction terms between perturbers from different groups. All atoms within a group of chemically similar atoms are assumed to bear charges of the same sign, and all individual terms contributed by such groups are thus independent of the sign of the charges. Of course the interaction terms between dissimilar groups could dominate in the expression and these depend on the relative signs of the charges

from the different groups. Finally, unless the contributions to  $R''_{net}(T_{1g}, T_{2g})$ ,  $R'(E_g, A_2)$  or  $K'(T_{1g})$  from different groups of  $D_3$  related atoms all have the same sign, the *net* signs will also depend on the relative magnitudes of the charges from these groups.

#### 4.4.2 Application to $\lambda\lambda$ -[Co(tame)<sub>2</sub>]<sup>3+</sup>

The visible circular dichroism observed for  $\lambda\lambda$ -[Co(tame)<sub>2</sub>]<sup>3+</sup> in aqueous (+)<sub>589</sub>-tartrate solution and in the [Co(tame)<sub>2</sub>]Cl(+)<sub>589</sub>-tartrate.5.4H<sub>2</sub>O solid was described, discussed and rationalized in Section 4.3.1 and will only be referenced here.

#### *The Observed Trigonal Geometry of $\lambda\lambda$ -[Co(tame)<sub>2</sub>]<sup>3+</sup>*

As discussed in Chapter 3, the  $\lambda\lambda$ -[Co(tame)<sub>2</sub>]<sup>3+</sup> ion was observed to have quasi- $D_3$  symmetry in the crystal structure of [Co(tame)<sub>2</sub>]Cl(+)<sub>589</sub>-tartrate.5.4H<sub>2</sub>O. In order to evaluate the signs predicted for the second order *net* rotatory strengths  $R''_{net}(T_{1g}, T_{2g})$  from the observed  $\lambda\lambda$ -[Co(tame)<sub>2</sub>]<sup>3+</sup> configuration, the complex ion was referred to a cobalt-centred trigonal coordinate system similar to that defined by Richardson<sup>70</sup> and depicted in Figure 4.2. The spherical coordinates ( $r_i$ ,  $\theta_i$ ,  $\phi_i$ ) for all atomic sites  $i$  observed in the structure (excluding the methyl hydrogens) were then determined with respect to this coordinate system. The Z axis here coincides with the pseudo- $C_3$  axis of the complex, and the +X direction coincides with the pseudo- $C_2$  axis relating an atom pair having the chiral sense (about  $C_3$ ) of a  $\Delta$  tris-bidentate complex (see Figure 4.2 and Sections 4.3.1 and 4.3.2).

The pseudo- $C_3$  axis was defined for each group of pseudo- $D_3$  related

atoms, in a manner similar to that described in Section 4.3.2, as the perpendicular (through the Co atom) to the average of the trigonal atom planes. An effective  $D_3$  contribution to the *net* rotatory strength  $R''_{net}$  for the observed  $\text{Co}(\text{tame})_2^{3+}$  structure may then be determined from the mean  $D_3$  spherical coordinates of the pseudo- $D_3$  symmetric sets of atoms. Hence for the purpose of this calculation, the observed quasi- $D_3$  structure was simulated by a  $D_3[\text{Co}(\text{tame})_2]^{3+}$  complex, which was constructed by referring the mean spherical coordinates of the atoms in each pseudo- $D_3$  set to the common trigonal coordinate system defined above. These  $D_3$  coordinates were obtained by averaging the radial coordinates  $r$ , the dihedral angles  $\omega$  (see Section 4.3.1), and the polar angles  $\theta$ , all of which were computed with respect to the mean  $C_3$  axis of the pseudo- $D_3$  group by means of program AZIMUTH<sup>15</sup> (Appendix I). Table 4.1 lists the spherical coordinates of the simulated  $\lambda\lambda\text{-}[\text{Co}(\text{tame})_2]^{3+}$  complex.

The spherical coordinates of this average  $D_3$  complex (Table 4.1) were used in the application of the Richardson model<sup>70</sup> for the *net* rotatory strengths of the visible absorption bands of  $D_3\text{Co(III)}$  complexes (see Section 4.4.1) from the following rationale. The model<sup>70</sup> includes only  $D_3$  terms in the expansion of the potential function. Consequently, evaluation of the signs for the rotatory strengths, in terms of the observed individual coordinates of the crystallographically symmetry independent structure, would not be complete without including the effects of other terms in the potential expansion. In view of this and the close  $D_3$  symmetry shown by the actual  $\lambda\lambda\text{-}[\text{Co}(\text{tame})_2]^{3+}$  complex, it was decided that evaluation in terms of the mean  $D_3$  related structural parameters



TABLE 4.1 MEAN  $D_3^a$  SPHERICAL COORDINATES FOR  $\lambda\lambda$ -[Co(tame) $_2$ ] $^{3+}$ 

Atom	r	$\theta$	$\phi$	Atom	r	$\theta$	$\phi$
Co	0 Å	0°	0°	H(2)	2.44Å	69.5°	41.6°
N(1) <sup>b</sup>	1.97	54.0	27.9	H(8)	2.44	69.5	161.6
N(4)	1.97	54.0	147.9	H(3)	2.44	69.5	281.6
N(2)	1.97	54.0	267.9	H(5)	2.44	110.5	-41.6
N(3)	1.97	126.0	-27.9	H(11)	2.44	110.5	-161.6
N(6)	1.97	126.0	-147.9	H(10)	2.44	110.5	-281.6
N(5)	1.97	126.0	-267.9	H(16)	3.75	34.2	25.6
C(3)	2.97	29.1	42.5	H(21)	3.75	34.2	145.6
C(5)	2.97	29.1	162.5	H(19)	3.75	34.2	265.6
C(4)	2.97	29.1	282.5	H(22)	3.75	145.8	-25.6
C(6)	2.97	150.9	-42.5	H(28)	3.75	145.8	-145.6
C(9)	2.97	150.9	-162.5	H(29)	3.75	145.8	-265.6
C(10)	2.97	150.9	-282.5	H(17)	3.39	37.3	68.9
C(2)	3.09	0.0	c	H(20)	3.39	37.3	188.9
C(7)	3.09	180.0	c	H(18)	3.39	37.3	308.9
C(1)	4.63	0.0	c	H(23)	3.39	142.7	-68.9
C(8)	4.63	180.0	c	H(27)	3.39	142.7	-188.9
H(1)	2.42	61.8	4.3	H(30)	3.39	142.7	-308.9
H(7)	2.42	61.8	124.3				
H(4)	2.42	61.8	244.3				
H(6)	2.42	118.2	-4.3				
H(12)	2.42	118.2	-124.3				
H(9)	2.42	118.2	-244.3				

<sup>a</sup> The +Z axis intersects the N(1),N(4),N(2) plane and coincides with  $C_3$ . The +X axis coincides with  $C_2$  and bisects the N(1)-Co-N(3) angle (Figure 4.4).

<sup>b</sup> The atomic spatial configuration is illustrated in Figures 3.3 and 3.4.

<sup>c</sup> These atomic sites have no  $\phi$  dependence as they lie on the Z axis.

would be equally valid, in addition to being computationally simpler. The methyl hydrogen atoms were precluded from the spherical coordinate analysis because their observed positions were at best doubtful, and they could not be meaningfully related to the same trigonal coordinate system as the other atoms of the observed complex. Furthermore, their  $r$  coordinates (5.0-5.1Å) are such that they do not contribute significantly in the expression  $R''_{net}(T_{1g}, T_{2g})$  which has an  $r$  dependence of  $r_i^{-3} r_j^{-4}$  for the term contributed by charge centres  $i$  and  $j$ .

*Correlation of the Absolute Sign for  $R''_{net}(T_{1g}, T_{2g})$  with the Observed Trigonal Geometry*

The observed trigonal geometry of  $\lambda\lambda\text{-[Co(tame)}_2\text{)]}^{3+}$  described in the previous sub-section is here employed in the evaluation of the signs of the rotatory strengths for the  $net\ ^1A_{1g} \rightarrow ^1T_{1g}$  and  $net\ ^1A_{1g} \rightarrow ^1T_{2g}$  Co(III) transitions, which are determined on the crystal-field one-electron model of Richardson<sup>70</sup> for  $D_3$  complexes by the expression  $R''_{net}(T_{1g}, T_{2g})$  (Section 4.4.1).

$R''_{net}(T_{1g}, T_{2g})$  sums the product of  $q_i(3\cos^2\theta_i - 1)/r_i^3$  and  $q_j\sin^3\theta_j\cos 3\phi_j/r_j^4$  over all ligand atom perturbing sites  $i$  and  $j$  in the complex. These two terms have the same values for all atoms in a given  $D_3$  symmetry equivalent set. Consequently they need be evaluated for only one atom of the set, and each  $D_3$  group  $L$ , of  $N_L$  atoms contributes  $N_L^2$  identical product terms of the type  $q_l(3\cos^2\theta_l - 1)/r_l^3 \times q_l\sin^3\theta_l\cos 3\phi_l/r_l^4$ , where  $l$  is any atom of the set  $L$ , to the net sum. Similarly, the terms arising from the interaction between two  $D_3$  sets of  $N_L$  and  $N_M$  atoms involve  $N_L N_M$  identical products  $q_l(3\cos^2\theta_l - 1)/r_l^3 \times q_m\sin^3\theta_m\cos 3\phi_m/r_m^4$  and  $N_L N_M$

of the type  $q_m(3\cos^2\theta_m - 1)/r_m^3 \times q_l \sin^3\theta_l \cos 3\phi_l / r_l^4$  where the atoms  $l, m$  belong to the sets  $L$  and  $M$  respectively. Thus for the purpose of computing contributions to the sum  $R_{net}^{H}(T_{1g}, T_{2g})$ , the observed  $D_3$   $\lambda\lambda$ -[Co(tame)<sub>2</sub>]<sup>3+</sup> complex was analysed in terms of the eight  $D_3$  symmetric sets of atoms listed in Table 4.1.

The calculation of the eight unique pairs  $q(3\cos^2\theta - 1)/r^3$  and  $q\sin^3\theta \cos 3\phi / r^4$  corresponding to the eight independent  $D_3$  groups is summarized in Table 4.2. These were expressed as functions of the charge  $q_l$  allotted to the independent set  $L$ . The two sets of nitrogen hydrogen atoms, being chemically identical, were assigned the same charge  $q_{NH}$ . Similarly the two  $D_3$  sets of carbon hydrogen atoms were assigned a charge of  $q_{CH}$ . The nitrogen atom and the secondary, quaternary and methyl carbon atom groups are all chemically dissimilar and these were given the charges  $q_N$ ,  $q_{C1}$ ,  $q_{C2}$  and  $q_{C3}$  respectively.

TABLE 4.2 UNIQUE  $q(3\cos^2\theta - 1)/r^3$  AND  $q\sin^3\theta \cos 3\phi / r^4$  FOR  $\lambda\lambda$ -[Co(tame)<sub>2</sub>]<sup>3+</sup>

$D_3$ Set No.	Equivalent Atoms	$q(3\cos^2\theta - 1)/r^3$	$q\sin^3\theta \cos 3\phi / r^4$
1	N(1), N(4), N(2), N(3), N(6), N(5)	4.77 <sup>a</sup> $q_N$	3.85 <sup>b</sup> $q_N$
2	C(3), C(5), C(4), C(6), C(9), C(10)	49.26 $q_{C1}$	-0.90 $q_{C1}$
3	C(2), C(7)	67.79 $q_{C2}$	0.0 $q_{C2}$
4	C(1), C(8)	20.15 $q_{C3}$	0.0 $q_{C3}$
5	H(1), H(7), H(4), H(6), H(12), H(9)	-23.29 $q_{NH}$	19.45 $q_{NH}$
6	H(2), H(8), H(3), H(5), H(11), H(10)	-43.51 $q_{NH}$	-13.23 $q_{NH}$
7	H(16), H(21), H(19), H(22), H(28), H(29)	19.95 $q_{CH}$	0.21 $q_{CH}$
8	H(17), H(20), H(18), H(23), H(27), H(30)	23.06 $q_{CH}$	-1.51 $q_{CH}$

a In Å<sup>-3</sup> ( $\times 10^3$ )

b In Å<sup>-4</sup> ( $\times 10^3$ )

The product sums  $\sum_{lm} q_l q_m (3\cos^2\theta_l - 1) \sin^3\theta_m \cos 3\phi_m / r_l^3 r_m^4$ , where  $l, m$

belong to the  $D_3$  sets  $L$  and  $M$ , were computed for  $L, M = 1 \rightarrow 8$ . As inferred above, each one,  $(L, M)$ , of the 64 sums contains  $N_L N_M$  identical products  $q_l q_m (3 \cos^2 \theta_l - 1) \sin^3 \theta_m \cos 3\phi_m / r_l^3 r_m^4$  where  $N_L$  and  $N_M$  are the numbers of atoms in the sets  $L$  and  $M$ , and  $l, m$  denote any atoms of the respective sets. These component  $D_3$  sums are given in the matrix of Table 4.3 where the row and column indices correspond to the  $D_3$  sets  $L$  and  $M$  respectively. The sum  $R''_{net}(T_{1g}, T_{2g})$  (Section 4.4.1) is then represented equivalently by  $(\frac{1}{28})^{\frac{1}{2}} \pi \sum_{L=1}^8 \sum_{M=1}^8 (L, M)$  in terms of the sums  $(L, M)$ , and was expressed as a function of the eighteen unique charge products  $q_l q_m$  by

$$R''_{net}(T_{1g}, T_{2g}) = [663q_N^2 - 14958q_{NH}^2 - 1596q_{C1}^2 - 2013q_{CH}^2] + \\ [6690q_N q_{C1} + 3140q_N q_{C2} + 933q_N q_{C3} + 12757q_{CH} q_{NH} \\ - 8214q_N q_{NH} - 3699q_{C1} q_{CH} - 1057q_{C2} q_{CH} - 314q_{C3} q_{CH}] + \\ [5753q_N q_{CH} + 12840q_{NH} q_{C1} + 5060q_{NH} q_{C2} + 1504q_{NH} q_{C3} \\ - 732q_{C2} q_{C1} - 218q_{C3} q_{C1}] 10^{-6} (\frac{1}{28})^{\frac{1}{2}} \pi \text{ \AA}^{-7}$$

Each term within the first parenthesis is independent of the charge sign of the contributing chemically identical atoms. The second and third parentheses include the interaction terms between the chemically dissimilar N, C1, C2, C3, NH and CH atom groups (Table 4.2), and the sign of each term here depends on the relative charge signs of the atoms from the different contributing groups.

Further evaluation of this expression necessarily involves some speculation on the relative charge signs and magnitudes of the non-equivalent sets. For this reason, electrostatic charges computed by Poland and Sheraga<sup>215</sup> for the atoms in saturated side chains of various amino acids

TABLE 4.3 MATRIX<sup>a</sup> OF THE SUMS (L,M) OVER THE D<sub>3</sub> SETS L AND M

	M							
	1	2	3	4	5	6	7	8
1	663q <sub>N</sub> <sup>2</sup>	-155q <sub>N</sub> <sup>2</sup> q <sub>C1</sub>	0q <sub>N</sub> <sup>2</sup> q <sub>C2</sub>	0q <sub>N</sub> <sup>2</sup> q <sub>C3</sub>	3340q <sub>N</sub> <sup>2</sup> q <sub>NH</sub>	-2272q <sub>N</sub> <sup>2</sup> q <sub>NH</sub>	369q <sub>N</sub> <sup>2</sup> q <sub>CH</sub>	-259q <sub>N</sub> <sup>2</sup> q <sub>CH</sub>
2	6845q <sub>C1</sub> <sup>2</sup> q <sub>N</sub>	-1596q <sub>C1</sub> <sup>2</sup>	0q <sub>C1</sub> <sup>2</sup> q <sub>C2</sub>	0q <sub>C1</sub> <sup>2</sup> q <sub>C3</sub>	34137q <sub>C1</sub> <sup>2</sup> q <sub>NH</sub>	-23462q <sub>C1</sub> <sup>2</sup> q <sub>NH</sub>	372q <sub>C1</sub> <sup>2</sup> q <sub>CH</sub>	-2678q <sub>C1</sub> <sup>2</sup> q <sub>CH</sub>
3	3140q <sub>C2</sub> <sup>2</sup> q <sub>N</sub>	-732q <sub>C2</sub> <sup>2</sup> q <sub>C1</sub>	0q <sub>C2</sub> <sup>2</sup>	0q <sub>C2</sub> <sup>2</sup> q <sub>C3</sub>	15822q <sub>C2</sub> <sup>2</sup> q <sub>NH</sub>	-10762q <sub>C2</sub> <sup>2</sup> q <sub>NH</sub>	171q <sub>C2</sub> <sup>2</sup> q <sub>CH</sub>	-1228q <sub>C2</sub> <sup>2</sup> q <sub>CH</sub>
4	933q <sub>C3</sub> <sup>2</sup> q <sub>N</sub>	-218q <sub>C3</sub> <sup>2</sup> q <sub>C1</sub>	0q <sub>C3</sub> <sup>2</sup> q <sub>C2</sub>	0q <sub>C3</sub> <sup>2</sup>	4703q <sub>C3</sub> <sup>2</sup> q <sub>NH</sub>	-3199q <sub>C3</sub> <sup>2</sup> q <sub>NH</sub>	51q <sub>C3</sub> <sup>2</sup> q <sub>CH</sub>	-365q <sub>C3</sub> <sup>2</sup> q <sub>CH</sub>
L 5	-3236q <sub>NH</sub> <sup>2</sup> q <sub>N</sub>	755q <sub>NH</sub> <sup>2</sup> q <sub>C1</sub>	0q <sub>NH</sub> <sup>2</sup> q <sub>C2</sub>	0q <sub>NH</sub> <sup>2</sup> q <sub>C3</sub>	-16308q <sub>NH</sub> <sup>2</sup>	11093q <sub>NH</sub> <sup>2</sup>	-176q <sub>NH</sub> <sup>2</sup> q <sub>CH</sub>	1266q <sub>NH</sub> <sup>2</sup> q <sub>CH</sub>
6	-6046q <sub>NH</sub> <sup>2</sup> q <sub>N</sub>	1410q <sub>NH</sub> <sup>2</sup> q <sub>C1</sub>	0q <sub>NH</sub> <sup>2</sup> q <sub>C2</sub>	0q <sub>NH</sub> <sup>2</sup> q <sub>C3</sub>	-30466q <sub>NH</sub> <sup>2</sup>	20723q <sub>NH</sub> <sup>2</sup>	-329q <sub>NH</sub> <sup>2</sup> q <sub>CH</sub>	2365q <sub>NH</sub> <sup>2</sup> q <sub>CH</sub>
7	2772q <sub>CH</sub> <sup>2</sup> q <sub>N</sub>	-646q <sub>CH</sub> <sup>2</sup> q <sub>C1</sub>	0q <sub>CH</sub> <sup>2</sup> q <sub>C2</sub>	0q <sub>CH</sub> <sup>2</sup> q <sub>C3</sub>	13969q <sub>CH</sub> <sup>2</sup> q <sub>NH</sub>	-9502q <sub>CH</sub> <sup>2</sup> q <sub>NH</sub>	151q <sub>CH</sub> <sup>2</sup>	-1084q <sub>CH</sub> <sup>2</sup>
8	3204q <sub>CH</sub> <sup>2</sup> q <sub>N</sub>	-747q <sub>CH</sub> <sup>2</sup> q <sub>C1</sub>	0q <sub>CH</sub> <sup>2</sup> q <sub>C2</sub>	0q <sub>CH</sub> <sup>2</sup> q <sub>C3</sub>	16147q <sub>CH</sub> <sup>2</sup> q <sub>NH</sub>	-10983q <sub>CH</sub> <sup>2</sup> q <sub>NH</sub>	174q <sub>CH</sub> <sup>2</sup>	-1254q <sub>CH</sub> <sup>2</sup>

<sup>a</sup> All terms in this matrix are  $\times 10^6$  (Å<sup>-7</sup>).

were assigned to the relevant chemically equivalent atoms of the tame ligands in  $\lambda\lambda\text{-[Co(tame)}_2\text{]}^{3+}$ . The accumulation of charge on atoms in partially unsaturated amino acid systems was considered<sup>215</sup> by these workers to be caused by  $\sigma$  and  $\pi$  bonding effects, and they used the molecular orbital-linear combination of atomic orbital (MO-LCAO) method of Del Re<sup>216-218</sup> to evaluate the net  $\sigma$  induced atomic charges in the saturated side chains. This method was found<sup>215-218</sup> to suitably reproduce the observed dipole moments and inductive effects in small saturated molecules, and its extension to partially unsaturated systems by Berthod and Pullman<sup>219</sup> was successfully used<sup>215,220-222</sup> in determining the electrostatic contribution to the conformational potential energy in computations on polypeptide conformations.

Although delocalization of charge over the complex sphere may occur to some extent in  $\lambda\lambda\text{-[Co(tame)}_2\text{]}^{3+}$ , the immediate aim here was to assess the worth of the pure crystal-field model of Richardson.<sup>70</sup> Consequently the charges assigned were those expected for the isolated tame ligands rather than the cobalt-bonded entities. The assignments were made from reference atoms in the compounds whose charge distributions were determined and listed by Poland and Scheraga.<sup>215</sup> These reference atoms were chosen to have neighbouring structural environments as closely similar as possible, if not effectively identical, to those of the corresponding atom types in the tame ligands. This procedure is justified by the observation<sup>215</sup> that the backbone charges calculated for polypeptide chains were approximately independent of the nature of the side chains, despite the entire intramolecular connectivity<sup>215-218</sup>

of the procedure. The charges used here for the nitrogen (-0.505), the amino hydrogen (0.207), the methylene carbon (-0.013), and the methylene hydrogen (0.046) atom groups were those computed<sup>215</sup> for the saturated side chain (NH<sub>2</sub>-CH<sub>2</sub>-CH<sub>2</sub>-CH<sub>2</sub>-CH<sub>2</sub>-) of the lysine molecule. The methyl carbon charge (-0.116) was that calculated<sup>215</sup> for the methyl groups of leucine which has the side chain ((CH<sub>3</sub>)<sub>2</sub>-CH-CH<sub>2</sub>-), and the quaternary carbon atom charge (0.00) was estimated by inference from the values determined<sup>215</sup> for the carbon and hydrogen atoms of the tertiary carbon in leucine. All of these charges are expressed in units of the electron charge magnitude  $|e|$ .

When the charge products in the expression for  $R''_{net}(T_{1g}, T_{2g})$  are evaluated from the atomic charges obtained as described above, we have

$$\begin{aligned}
 R''_{net}(T_{1g}, T_{2g}) = & [169.1 - 640.9 - 0.3 - 4.3] + \\
 & [43.9 + (-)0.0 + 54.7 + 121.5 \\
 & + 858.7 + 2.2 + (-)0.0 + 1.7] + \\
 & [-133.6 - 34.6 - (-)0.0 - 36.1 \\
 & - (-)0.0 - 0.3] 10^{-8} \left(\frac{1}{28}\right)^{\frac{1}{2}} \pi \text{ \AA}^{-7} e^2
 \end{aligned}$$

The order of the numerical terms in this equation is the same as the order of the symbolic charge product terms ( $q_l q_m$ ) in the previous representation. It is apparent, from a direct comparison of these two expressions, that the dominant terms in the sum arise from the nitrogen (169.1) and amino hydrogen atom groups (-640.9) and their interaction product sums (858.7), the major contributing factors to their high weight being the relatively large charges associated with the groups and their close proximity to the cobalt atom. Significant contributions

are also made by the  $N \leftrightarrow Cl$ ,  $N \leftrightarrow C3$ ,  $N \leftrightarrow CH$ ,  $NH \leftrightarrow CH$ ,  $NH \leftrightarrow Cl$  and  $NH \leftrightarrow C3$  interaction products, owing to a combination of the above factors with the large polar distortions from  $O_h$  geometry ( $\theta = 54.74^\circ$  or  $125.26^\circ$ ) provided by the  $Cl$ ,  $C3$  and  $CH$  groups, and the large azimuthal twist distortions of the  $NH$  groups from the octahedral nodal geometry where  $\phi = \pm(2n + 1)\pi/6$  ( $n = 0, 1, 2, \dots$ ).

The *net* sign for the rotatory strengths of the  ${}^1A_{1g} \rightarrow {}^1T_{1g}$  and  ${}^1A_{1g} \rightarrow {}^1T_{2g}$  absorption bands of the observed  $\lambda\lambda$ - $[Co(tame)_2]^{3+}$  complex is then determined on the second order crystal-field static-coupling model of Richardson,<sup>70</sup> by the above expression, as

$$R''_{net}(T_{1g}, T_{2g}) = +[401.7]10^{-6} \left(\frac{1}{2\theta}\right)^2 \pi A^{-7} e^2$$

Although as mentioned in Section 4.4.1, accurate quantitative calculations of the rotatory strengths are not possible for this model,<sup>70</sup> the magnitude of each term in the expression  $R''_{net}(T_{1g}, T_{2g})$  is indicative of the relative magnitude of the crystal-field contribution made by the appropriate atomic groups to the *net* rotatory strengths. Consequently the *net* crystal-field contribution (+401.7), which has the same order of magnitude as the large component terms from the  $N$  and  $NH$  atom groups, is predicted to be large and positive. Similarly the *net*  $T_{1g}$  and  $T_{2g}$  band rotatory strengths for  $\lambda\lambda$ - $[Co(tame)_2]^{3+}$  are predicted to be relatively large and positive from this model. The large positive circular dichroism observed in the region of the  ${}^1A_{1g} \rightarrow {}^1T_{1g}$  absorption band of the crystalline  $[Co(tame)_2]Cl(+)_589$ -tartrate.5.4H<sub>2</sub>O compound (Section 4.3.1) then verifies the *net* CD predictions made on the basis of the Richardson crystal-field model<sup>70</sup> for  $D_3$  complexes.



*Discussion of the Observed and Predicted Nodal Properties*

In this section the nodal properties of the *net* rotatory strength of the  ${}^1A_{1g} \rightarrow {}^1T_{1g}$  Co(III) transition are qualitatively discussed, with reference to  $\lambda\lambda$ -[Co(tame) $_2$ ] $^{3+}$  in [Co(tame) $_2$ ]Cl(+) $_{589}$ -tartrate.5.4H $_2$ O and  $\Lambda$ -(+) $_{589}$ -[Co(en) $_3$ ] $^{3+}$  in (+) $_{589}$ -[Co(en) $_3$ ]Br $_3$ .H $_2$ O and (+) $_{589}$ -[Co(en) $_3$ ]Cl $_3$ .3H $_2$ O, for which the solid state structural geometry (Chapter 3 and reference 191,197) and disc CD spectra (Section 4.3.2 and reference 199) of the complex ions are known.

It was previously observed that the major contributions to  $R''_{net}(T_{1g}, T_{2g})$  for  $\lambda\lambda$ -[Co(tame) $_2$ ] $^{3+}$  (in the crystal-field model<sup>70</sup>) were made by the nitrogen and amino hydrogen atom groups because of their relatively high charges and low distances from the cobalt atom, despite the large polar and azimuthal distortions of the carbon and methylene hydrogen atoms from  $O_h$  geometry. Consequently the visible CD of (+) $_{589}$ -[Co(en) $_3$ ] $^{3+}$ , for which the nitrogen, methylene carbon, amino hydrogen and methylene hydrogen atoms have structural environments and radial coordinates similar to those of  $\lambda\lambda$ -[Co(tame) $_2$ ] $^{3+}$ , is expected to be largely determined by the nitrogen and amino hydrogen atom configurations on a crystal-field basis. The terms in  $R''_{net}(T_{1g}, T_{2g})$  arising from N  $\leftrightarrow$  C, N  $\leftrightarrow$  CH, NH  $\leftrightarrow$  C and NH  $\leftrightarrow$  CH interaction pairs may make a significant total contribution if all are of the same sign. However the large nitrogen, amino hydrogen and N  $\leftrightarrow$  NH interaction terms are expected to have the same signs for the  $\Lambda(\delta\delta\delta)$  twist contracted (see Section 4.3) conformer of (+) $_{589}$ -[Co(en) $_3$ ] $^{3+}$  observed in the structures considered here.<sup>15,191,197</sup> This may be seen qualitatively

by referring a Dreiding model of the  $\Lambda(\delta\delta\delta)$  conformer to the trigonal coordinate system of Figure 4.2, which defines the spherical atomic coordinates in  $R''_{net}(T_{1g}, T_{2g})$  (see the previous sub-section), and allows the following crude qualitative evaluation of the terms  $q(3\cos^2\theta - 1)/r^3$  and  $q\sin^3\theta\cos 3\phi/r^4$  for  $(+)_589-[Co(en)_3]^{3+}$  in the  $\Lambda(\delta\delta\delta)$  configuration of the above structures.<sup>15,191,197</sup>

$D_3$ sets in $\Lambda(\delta\delta\delta)-[Co(en)_3]^{3+}$	$q(3\cos^2\theta-1)/r^3$	$q\sin^3\theta\cos 3\phi/r^4$
Nitrogen	large <sup>a</sup> (+ve or 0)	large (+ve)
Amino hydrogen set 1	small	v. large (+ve)
Amino hydrogen set 2	v. large (+ve)	small

<sup>a</sup> This assumes  $\theta_N$  is not significantly  $< 54.74^\circ$  or  $> 125.26^\circ$ .

Thus the total nitrogen and amino hydrogen contribution to the *net* sum  $R''_{net}(T_{1g}, T_{2g})$  should be large and positive, and probably an order of magnitude larger than the total expected contribution from the carbon and methyl hydrogens and their interaction products with the nitrogen and amino hydrogen atoms. The crystal-field<sup>70</sup> contribution ( $\alpha R''_{net}(T_{1g}, T_{2g})$ ) to the *net* rotatory strength of the  ${}^1A_{1g} \rightarrow {}^1T_{1g}$  transition of  $(+)_589-[Co(en)_3]^{3+}$  in its above solid state environments<sup>191,197</sup> is then expected to be large and positive. The *net* solid state visible CD spectra of these and other compounds containing  $(+)_589-[Co(en)_3]^{3+}$  was observed<sup>199</sup> to be relatively large and positive under the  ${}^1A_{1g} \rightarrow {}^1T_{1g}$  band envelope, and the qualitative crystal-field theoretical predictions for the *net* CD of this complex are verified.

For the purpose of this analysis, the complexes  $(+)_589-[Co(en)_3]^{3+}$  and  $\lambda\lambda-[Co(tame)_2]^{3+}$  differ in a fundamental aspect of their trigonal

geometry. All sets of chemically equivalent atoms (N, NH, C, CH) having significant polar distortions lie on opposite sides of the nodal polar angle of  $54.74^\circ$  (or  $125.26^\circ$ ) for the two complexes. Thus for  $\lambda\lambda\text{-[Co(tame)}_2\text{]}^{3+}$ , the nitrogen, carbon and methylene hydrogen atoms all have  $\theta < 54.74^\circ$  or  $> 125.26^\circ$  and the amino hydrogens have  $54.74^\circ < \theta < 125.26^\circ$ . In  $(+)\text{}_{589}\text{-[Co(en)}_3\text{]}^{3+}$  however, for the carbon, methylene hydrogen and usually<sup>15</sup> the nitrogen atoms,  $54.74^\circ < \theta < 125^\circ$ , whereas the amino hydrogen atoms have  $\theta < 54.74^\circ$  or  $> 125.26^\circ$  ( $\theta = 54.74^\circ$  for one  $D_3$  set in the  $\Lambda(\delta\delta\delta)$  conformer). Yet in both complexes the carbon and major methylene hydrogen contributors to  $R_{net}^n (T_{1g}, T_{2g})$  have  $30^\circ < \phi < 90^\circ$ , and the sums  $\sum_{lm} q_l q_m (3\cos^2\theta_l - 1) \sin^3\theta_m \cos\phi_m / r_l^3 r_m^4$ , where both  $l, m$  are carbon or methylene hydrogen atoms, differ in sign for  $\lambda\lambda\text{-[Co(tame)}_2\text{]}^{3+}$  and  $(+)\text{}_{589}\text{-[Co(en)}_3\text{]}^{3+}$ . Despite the differences in polar geometry and signs for the carbon, methylene hydrogen and  $C \leftrightarrow CH$  interaction terms, the *net* sums of the nitrogen, amino hydrogen and  $N \leftrightarrow NH$  products have the same sign for each complex and these, in conjunction with the sums of lower weight interaction products of the type  $N \leftrightarrow C$ ,  $N \leftrightarrow CH$ ,  $NH \leftrightarrow C$  and  $NH \leftrightarrow CH$ , lead to the prediction of the same sign for the *net* visible CD of  $\lambda\lambda\text{-[Co(tame)}_2\text{]}^{3+}$  and  $(+)\text{}_{589}\text{-[Co(en)}_3\text{]}^{3+}$ .

In essence then, the predictions of the second order crystal-field model of Richardson<sup>70</sup> for the absolute sign and nodal properties of the *net* visible CD for these two complexes appear to be supported by their observed solid state trigonal geometry and CD disc spectra. Furthermore, the crystal-field contribution to the visible circular dichroism of  $D_3$  cobalt(III)-polyamine complexes is largely determined by the configuration

of the nitrogen and hydrogen atoms of the amino groups, and is primarily dependent on chelate conformation in so far as this influences the relative spatial orientation of these atoms with respect to the cobalt atom.

CHAPTER 5. CONFORMATIONAL ANALYSIS OF METAL COMPLEXES5.1 INTRODUCTION

The classical mechanical relationship between relative internal potential energy and intramolecular configuration was first applied to the conformational analysis of organic molecules with energetically preferred conformations by Westheimer and Mayer.<sup>223,224</sup> This initial approach, which involved the calculation of energies corresponding to rigid molecular conformations, was employed by Corey and Bailar<sup>4</sup> in their analysis of the non-bonded potential energies associated with various fixed ring conformations in metal chelate complexes. Potential energy calculations based on the *molecular mechanics* rationale were subsequently introduced in studies of the conformations and relative energies of polypeptides<sup>225-229</sup> and other polymeric molecules.<sup>230-232</sup> The procedure has also been extended to the study of molecular packing<sup>233-236</sup> and detailed intramolecular configuration<sup>237</sup> in crystals by minimization of the potential energy of the crystal lattice. Minimization techniques<sup>53-55,58,59,237,238</sup> and force field parameterization technology<sup>237-244</sup> have advanced considerably since the pioneering work,<sup>2,3,52,220</sup> and the theoretical determination of individual molecular geometries, thermodynamic functions<sup>54,226,227</sup> and vibrational spectra,<sup>54,238</sup> as well as the intramolecular geometries,<sup>237,245</sup> packing arrangements<sup>246,247</sup> and dynamic effects<sup>245</sup> in crystal lattices, has approached predictive reliability.

The molecular energy minimization mode in the conformational analysis of metal chelate complexes has recently been considerably

refined, through the implementation of potential surface mapping<sup>50</sup> and efficient energy search<sup>51</sup> and mathematical minimization schemes.<sup>48,49</sup> This has resulted in the relatively successful prediction of detailed molecular geometries<sup>48-51,56,57,74-76,248-251</sup> and the relative thermodynamic stabilities<sup>48-50,57,60-62,76,248,251</sup> of solution stereoisomers for metal chelate complex systems.

Owing to the large number of independent atomic coordinates normally associated with these systems (*e.g.*  $[\text{Co}(\text{en})_3]^{3+}$  has 37 atoms and 105 independent internal coordinates), the potential energy surface mapping procedure<sup>50,60-62</sup> was computationally restricted to the discontinuous variance of a few selected independent variables defining the backbone conformation of each chelate ring. Hydrogen atoms were fixed with respect to the ring atoms and bond length variance was generally restricted in these studies.<sup>50,60-62</sup>

An energy search technique, based on the method of steepest-descent<sup>252</sup> employed by Wiberg,<sup>55</sup> and used successfully in the energy minimization of organic molecules,<sup>52,55,253-255</sup> has also been applied<sup>51,250</sup> to studies of the energy minimized geometry of metal chelate complexes. However, several problems are known<sup>52,58,59,252</sup> to be associated with the steepest-descent procedure when the potential energy surface is a function of many variables, as in the case where the independent coordinates of a metal complex are simultaneously adjusted to determine the minimum energy for a given conformer. In this scheme<sup>52,55,252</sup> the coordinates are arbitrarily and iteratively varied by an amount proportional to the components of the potential energy gradient vector

at the current geometry, and no functional dependence of these components on the coordinate geometry is considered. Consequently the minimum energy configuration can not be directly determined and convergence may be very slow in this region.<sup>52,59,252</sup> Another disadvantage, which is coupled with the assumption that the coordinate shifts in the minimum energy direction depend solely on first order partial derivatives at the trial geometry, lies with the consistency of the method in detecting different minimum geometries (*local* or *false* minima)<sup>52,254,255</sup> for different starting configurations of the same conformer. For example, in the application to the conformational analysis of the complex molecules  $[\text{Co}(\text{tn})_3]^{3+}$ ,  $[\text{Co}(\text{ptn})_3]^{2+}$  and  $[\text{Co}(\text{bn})_3]^{3+}$ , the energy minimized configuration for a given conformer was found to be highly dependent on the initial trial geometry.<sup>51,250</sup>

The most reliable, powerful and general iterative minimization techniques,<sup>52</sup> for molecules with large numbers of independent variables, have been those based on the direct solution of the inter-coordinate relationships which exist at the minimum of a quadratic function fitted to the potential energy surface.<sup>53,54,237,238</sup> These equations of condition may normally be obtained from a Newton-Raphson approximation,<sup>54,237,238</sup> whereby the gradient vector of the general quadratic Taylor series expansion about the trial geometry is equated to zero. The coordinate shifts then obtained from the solution of these equations are those required to minimize the value of the general quadratic energy expansion, and depend on both first and second order partial derivatives of the potential energy at the trial configuration. The reliability and

power of these techniques have been adequately demonstrated in organic<sup>52,53,54,237,238</sup> and metal chelate complex<sup>2,48,49,56,57,74-76,248,249</sup> systems, and the *final* minimized geometry has been found to be generally independent of the trial coordinates<sup>48,49,52,256</sup> or the energy minimization route<sup>56,256</sup> for a particular conformational isomer. Convergence to *local* minima within the potential energy well associated with the specified conformer (*i.e.* having torsion angles with a given sign) is thus rarely encountered,<sup>48,49,52,57</sup> and may sometimes be detected intuitively from an examination of the symmetry of the starting model (Section 5.4). Because of the close correspondence usually found between the quadratic expansion and the potential energy surface near the equilibrium geometry, the Newton-Raphson minimization in this region converges more rapidly than that of the steepest-descent method<sup>54,59,238</sup> and provides a further real advantage in the conformational analysis of the many dimensional metal complex molecules.

One of these mathematical minimization procedures, which was developed by Boyd<sup>54</sup> and has proven remarkably successful in the prediction of detailed metal complex geometries,<sup>2,48,49,56,57,74-76,248,249,251</sup> was used here to determine the equilibrium molecular geometries and relative potential energies of some conformational isomers of the molecules  $[\text{Co}(\text{tame})_2]^{3+}$ ,  $[\text{Co}(\text{tn})_3]^{3+}$ <sup>76</sup> and  $[\text{Co}(\text{tn})_2\text{CO}_3]^+$ .<sup>76</sup> The scheme was extended to include a very fast iterative refinement technique for molecules having symmetric configurations at their energy minima,<sup>56</sup> and a procedure for avoiding convergence to the saddle-point equilibrium geometries associated with some symmetric molecules.<sup>56</sup>



## 5.2 ENERGY REPRESENTATION AND FORCE FIELD

In accord with the strain energy concept,<sup>52,257</sup> the potential strain energy of a metal complex molecule was simulated by the non-interactive summation<sup>48,49,56,76</sup>

$$U_{TOTAL} = \sum_{ij} U_B(r_{ij}) + \sum_{ijk} U_\theta(\theta_{ijk}) + \sum_{ijkl} U_\phi(\phi_{ijkl}) + \sum_{ij} U_{NB}(r_{ij})$$

where  $U_B(r_{ij})$  is the potential energy of deformation of the bond length  $r_{ij}$  between bonded atoms  $i$  and  $j$ ,  $U_\theta(\theta_{ijk})$  is the potential energy of distortion of the valence angle  $\theta_{ijk}$  between the bonded pairs  $i-j$  and  $j-k$ ,  $U_\phi(\phi_{ijkl})$  is the energy associated with torsional strain in the dihedral angle  $\phi_{ijkl}$  of the bonded sequence  $i-j-k-l$ , and  $U_{NB}(r_{ij})$  is the potential energy of the non-bonded interaction (short-range repulsion and London dispersion attraction) between atoms  $i$  and  $j$  separated by the interatomic distance  $r_{ij}$ . In this representation,  $U_{TOTAL}$  is the potential energy difference between the real molecule and a hypothetical atomic configuration in which there are no non-bonded interactions ( $U_{NB}(r_{ij}) = 0$  for all  $r_{ij}$ ), and the equilibrium geometry is defined by the zero strain energy values of the bond length, bond angle and torsion angle coordinates. For two molecules having different connective structures, these hypothetical configurations generally have different absolute energies, and consequently  $\Delta U_{TOTAL}$  represents a potential energy difference only for two stereoisomeric configurations of a given molecular structure. In order to determine enthalpies of formation or potential energy differences between structural isomers, the bond energies for the hypothetical configurations must be acquired or extrapolated from the thermochemical data for a group

of compounds which are also ideally strainless.<sup>52,255,258</sup>

### *The General Force Field*

In the subsequent analysis of the  $[\text{Co}(\text{tame})_2]^{3+}$ ,  $[\text{Co}(\text{tn})_3]^{3+}$  and  $[\text{Co}(\text{tn})_2\text{CO}_3]^+$  conformers (Section 5.5), all interactions to be included in the sum  $U_{TOTAL}$  were located and assigned the appropriate potential functions prior to each cycle of minimization. The computational search procedure was essentially that adopted by Snow<sup>48</sup> in which the interaction potential energies were generated from the trial atomic coordinates (general crystal systems allowed), a bonded atom matrix and a set of unique potential function parameters. However, the routine was modified<sup>256</sup> here to include the systematic detection and processing of the torsional strain contributions  $U_{\phi}(\phi_{ijkl})$  associated with the dihedral angles  $\phi_{ijkl}$  about the bonds  $j-k$ .

All potential energy terms arising from non-interaction bond length ( $U_B(r_{ij})$ ) and valence angle ( $U_{\theta}(\theta_{ijk})$ ) deformations were included in the total energy expressions for the above metal complex molecules, except for those related to linear  $\theta_{iCok}$  angles. Torsional energies ( $U_{\phi}(\phi_{ijkl})$ ) were included for all dihedral angles of the type  $\phi_{iCNl}$  and  $\phi_{iCCl}$  where C and N are carbon and nitrogen atoms.

A number of interaction terms of the non-bonded type ( $U_{NB}(r_{ij})$ ) were precluded from the analysis for several reasons, the principal justifications being that the *final* minimized geometries are relatively insensitive to these terms,<sup>48,52,251,256</sup> and their contributions to *final* strain energy differences are not of sufficient weight to override the quantitative functional deficiencies in the summation  $U_{TOTAL}$ .<sup>52</sup>

Weakly attractive dispersion interactions satisfying the inter-atomic distance condition  $r_{ij} > 1.16(w_i + w_j)$ , where  $w_i$  is the van der Waals radius<sup>102</sup> of atom  $i$ , were omitted from the non-bonded energy terms.<sup>48</sup> These terms have not been observed to effect significant changes in the equilibrium geometry,<sup>251,256</sup> and although their *net* contribution may change the relative stereoisomeric energies,<sup>251</sup> any improvement in the accuracy of  $U_{TOTAL}$  or  $\Delta U_{TOTAL}$  is questionable for the following reasons. The overall weight of the dispersion energies is generally low ( $\sim 0 \rightarrow 1 \text{ kcal mol}^{-1}$ )<sup>251</sup> and probably less than the *net* error introduced by inaccuracies in the functional form and parameterization of  $U_{TOTAL}$ . Verification of the intramolecular pairwise additivity of these low weight terms is not well established<sup>52</sup> and non-additivity effects may alter the relative magnitudes of their contributions to  $U_{TOTAL}$  for different stereoisomers. Furthermore, many of the dispersion interactions in metal complex molecules are *trans*-atom and *trans*-bond, and there is no simple and reliable treatment to correct for the intervening charge distributions.<sup>52</sup>

The geminal 1,3 non-bonded interactions between atoms  $i$  and  $k$  of the angle  $\theta_{ijk}$  were generally precluded from the non-bonded energy summation. However their relative contributions are incorporated to some extent in the angular deformation force constants defining the terms  $U_9(\theta_{ijk})$ . The force constants used here are *diagonal* or non-interaction *valence*<sup>259</sup> force field values, which were determined (*e.g.* ref. 260) by fitting the observed vibrational frequencies of relatively strain-free compounds (except for 1,3 non-bonded strain) to those calculated by the

FG matrix method of Wilson *et al.*<sup>259</sup> assuming a *reduced harmonic* force field (*valence, interaction valence, Urey-Bradley*<sup>259</sup> or *interaction Urey-Bradley*). Hence the hypothetical strain-free configuration previously described has bond lengths and angles similar to those employed in the vibrational frequency fitting analysis (not always the true equilibrium values of the ideally strain-free compounds analysed), and includes the absolute 1,3 non-bonded repulsive strain associated with these parameters. Although the *harmonic* force field approximation may not adequately account for the geminal repulsions occurring with moderately large angular deformations,<sup>48,52</sup> the *net* 1,3 non-bonded energies about tetrahedral and octahedral centres remain relatively static in these cases,<sup>52,48,256</sup> and the approximation has been found satisfactory for metal complexes of the type studied here. However, the *harmonic* stretch-bend interaction force constants are often quite large,<sup>260</sup> and for molecules with large angular strain it may be necessary to include these to suitably represent the 1,3 van der Waals repulsion strain.<sup>258</sup> Alternatively the *Urey-Bradley* force field description<sup>259</sup> may be used to include these repulsions as discrete interactions,<sup>258</sup> but the *diagonal valence* force field constants used here have been found adequate for the moderate angular strain encountered in other metal complex molecular analyses.<sup>48-51,56,57,60-62,74-76,248-251</sup>

Finally, the non-bonded interactions with the cobalt atom were excluded owing to the deficiency of appropriate potential function parameters. However very few of the non-geminal repulsions are normally significant,<sup>256</sup> and these (when over-estimated) did not affect

the final geometries or stereoisomeric strain energy differences in other studies.<sup>251</sup>

*Potential Energy Functions and Parameterization*

*Bond Stretching and Bending Potential Energies*

As indicated above, these were represented by the *diagonal valence* force field terms in the general *harmonic* expansion of the potential energy about the equilibrium geometry of the hypothetical strain-free configuration. Force constant transferability was assumed,<sup>260</sup> and the force constants and strain-free internal coordinates were ideally acquired from the vibrational analyses (sometimes employing arbitrary strain-free coordinates) of compounds incorporating the component bond lengths and angles of the complex molecule, and having no significant non-geminal repulsive interactions. The stretching and bending energies had the functional forms

$$U_B(r_{ij}) = \frac{1}{2}k_{ij}^x (r_{ij} - R_{ij})^2$$

$$U_\theta(\theta_{ijk}) = \frac{1}{2}k_{ijk}^\theta (\theta_{ijk} - \Theta_{ijk})^2$$

respectively, where  $k_{ij}^x$  and  $k_{ijk}^\theta$  are the *diagonal valence* force constants for bond length and angle deformations, and  $R_{ij}$  and  $\Theta_{ijk}$  are the corresponding internal coordinates of the zero strain energy configuration.

The constant parameters used in the conformational calculations here are contained in Table 5.1, and most of these have been used successfully<sup>48,49,51,56,57,-</sup> in previous conformational computations on metal complex molecules.

74-76,248-251 In practice some of the strain-free bond lengths were chosen<sup>48</sup> to reproduce the observed X-ray structural bond lengths in the same molecule. This was done for the Co-N and Co-O bonds of the

chromophoric clusters.<sup>48,76</sup> Others, in particular those with large force constants (e.g. C-N, C-C, N-H, C-H, C-O, C=O), were obtained from average interatomic or internuclear crystal distances<sup>98</sup> or the values employed in the force constant determinations. The strain-free valence angles assigned here were generally those used in the vibrational analyses.

### *Torsional Potential Energies*

In accord with previously established methods for representing bond twisting potential energy functions,<sup>48,49,52,228</sup> the internal rotational barrier about C-C and C-N bonds was regarded as the sum of an intrinsic component of quantum mechanical origin,<sup>52</sup> (independent of  $i$  and  $l$  in the dihedral angles  $\phi_{iCCl}$  and  $\phi_{iCNl}$ ) and the total vicinal 1,4 non-bonded interaction energy of the carbon and nitrogen substituents. The latter contribution was included in the non-bonded energy terms ( $U_{NB}(r_{ij})$ ), and the intrinsic torsional strain ( $U_{\phi}(\phi_{ijkl})$ ) was<sup>261,262</sup> represented by a three-fold periodic Fourier cosine series expansion to account for the three-fold periodicity of the observed barriers<sup>263</sup> in ethane and methylamine. The functional form is

$$U_{\phi}(\phi_{ijkl}) = \frac{1}{2}V_{jk}(1 + \cos 3\phi_{ijkl})$$

where higher order terms were assumed insignificant<sup>261-264</sup> and  $\theta V_{jk}$  is the intrinsic component of the experimental barrier to rotation about the bond  $j-k$ . The angle  $\phi_{ijkl}$  is zero when the bonds  $i-j$  and  $k-l$  are eclipsed, and the individual energy functions associated with all nine dihedral angles were normally included in the energy representation for the net torsional strain<sup>55</sup> about  $j-k$ . The net intrinsic barriers about

C-C and C-N bonds were determined as  $2.40 \text{ kcal mol}^{-1}$  and  $1.54 \text{ kcal mol}^{-1}$  <sup>49</sup> from the experimental barriers <sup>263</sup> in ethane ( $2.88 \text{ kcal mol}^{-1}$ ) and methylamine ( $1.98 \text{ kcal mol}^{-1}$ ). Intrinsic torsional strain about the Co-N and Co-O bonds was expected to be negligible <sup>48,49,251</sup> and their torsional energies were suitably represented by the non-bonded energy contributions alone.

#### *Non-bonded Potential Energies*

These were represented here by potential energy functions of the Buckingham type <sup>265,266</sup>

$$U_{NB}(r_{ij}) = a_{ij} \exp(-b_{ij} r_{ij}) - c_{ij} / r_{ij}^6$$

where the first and second terms correspond to the short-range repulsive and the London dispersion attractive energies respectively. The questions of functional form and parameterization of these energies have been considered at length in various contexts. <sup>52,220,237-244</sup> Here they were selected <sup>48,49</sup> on an empirical basis <sup>52,243</sup> rather than a least-squares observational fit, <sup>237-242</sup> and the selection criteria included the correct relative balancing of the various non-bonded energy types <sup>52</sup> and the positions of their minima in relation to the observed van der Waals contact radii <sup>102</sup> in crystals. <sup>48,227</sup> The Buckingham parameters employed here have been used with considerable <sup>48,49,56,74-76,248,249,251</sup> success in metal complex conformational analysis, and these are tabulated in Table 5.1 in conjunction with the parameters for the other potential energy functions defining the force field.

TABLE 5.1 POTENTIAL ENERGY FUNCTION PARAMETERS

*Bond Stretching Parameters*

<i>i-j</i>	$k_{ij}^r$	$R_{ij}$	Reference
Co-N	$1.75 \cdot 10^5 \text{ dyn cm}^{-1} \text{ molecule}^{-1}$	$1.925 \text{ \AA}$	267
Co-O	2.00	1.85	268
N-C	6.0	1.49	a
N-H	5.64	0.99	267
C-O	4.10	1.32	268
C=O	9.00	1.24	269
C-C	5.0	1.50	224,260
C-H	5.0	1.06	224,260

*Bond Angle Distortion Parameters*

<i>i-j-k</i>	$k_{ijk}^\theta$	$\theta_{ijk}$	Reference
Co-N-C	$0.40 \cdot 10^5 \text{ erg molecule}^{-1}$	$1.911 \text{ radians}$	a
Co-N-H	0.20	1.911	267
Co-O-C	0.05	1.484	268
N-Co-N	0.68	1.571	267
N-Co-O	0.05	1.571	a
N-C-C	1.00	1.911	a
N-C-H	0.65	1.911	a
C-N-H	0.65	1.911	a
C-C-C	1.0	1.911	260
C-C-H	0.65	1.911	260
H-N-H	0.53	1.911	267
H-C-H	0.52	1.911	260
O-Co-O	0.05	1.222	268
O-C-O	0.15	2.094	268
O-C=O	1.0	2.094	a

(contd.)



TABLE 5.1 (contd.)*Non-bonded Interaction Parameters*

<i>i...j</i>	$a_{ij}$	$b_{ij}$	$\sigma_{ij}$	Reference
N...O	1295 $10^{-11}$ erg $\text{molecule}^{-1}$	4.55 $\text{\AA}^{-1}$	1.39 $10^{-11}$ erg $\text{\AA}^6$	270
N...N	1295 $\text{molecule}^{-1}$	4.55	1.39 $\text{molecule}^{-1}$	270
N...C	1472	4.44	1.695	270
N...H	195	4.32	0.69	270
C...C	1640	4.32	2.07	271
C...H	218	4.20	0.84	271
C...O	1472	4.44	1.695	270
H...O	195	4.32	0.69	270
H...H	45.8	4.08	0.342	271

<sup>a</sup> These parameters were estimated<sup>48,49</sup> and have given acceptable agreement with observed structural data.

### 5.3 THE MOLECULAR ENERGY MINIMIZATION PROCEDURE

The mathematical scheme employed here for the minimization of the molecular energy function  $U_{TOTAL}$  was originally programmed and applied to the conformational analysis of organic molecules by Boyd,<sup>54</sup> and subsequently introduced in the study of metal chelate complexes by Snow<sup>48</sup> and Buckingham *et al.*<sup>49</sup>

The technique involves the determination, by the Newton-Raphson approximation, of the roots to the equations of condition necessary for a minimum in  $U_{TOTAL}$ .

$$\nabla_{\underline{X}} U_{TOTAL}(\underline{X}) = 0$$

where  $\nabla_{\underline{X}} U_{TOTAL}(\underline{X})$  is the potential energy gradient vector, which is a function of the independent molecular Cartesian geometry  $\underline{X}$ . Here  $\underline{X} = (X_i)$  is a  $3N$  dimensional vector defined by the Cartesian coordinates ( $i = 1 \dots 3N$ ) of the  $N$  atoms in the molecule.  $\nabla_{\underline{X}} U_{TOTAL}(\underline{X})$  is then given by the vector  $(\partial U_{TOTAL} / \partial X_i)$  of first order partial derivatives. In the Newton-Raphson approximation, this is represented by a linear Taylor series expansion about an initial or trial Cartesian geometry  $\underline{X}^0$

$$\nabla_{\underline{X}} U_{TOTAL}^0(\underline{X}) = \nabla_{\underline{X}} U_{TOTAL}(\underline{X}^0) + \underline{F}(\underline{X}^0) \Delta \underline{X}$$

where

$$\underline{F}(\underline{X}^0) = (\partial^2 U_{TOTAL} / \partial X_i \partial X_j) \text{ at } \underline{X}^0$$

is the matrix of second order partial derivatives evaluated at the trial configuration  $\underline{X}^0$ , and

$$\Delta \underline{X} = \underline{X} - \underline{X}^0$$

is the vector  $(\Delta X_i)$  of coordinate increments from the trial values.

Application of the equations of condition to the approximate

$\nabla_{\underline{X}} U_{TOTAL}(\underline{X})$  then results in

$$\underline{\Delta X} = -\underline{F}^{-1}(\underline{X}^{\circ}) \nabla_{\underline{X}} U_{TOTAL}(\underline{X}^{\circ})$$

where  $\underline{F}^{-1}$  is the inverse of  $\underline{F}$ . The coordinate changes  $\underline{\Delta X}$  are precisely those required to minimize the value of  $U_{TOTAL}^{\rho}$ , the general quadratic expansion for  $U_{TOTAL}$  about the  $3N$  independent components of the trial Cartesian coordinate vector  $\underline{X}^{\circ} = (X_i^{\circ})$ . In practice the  $\underline{\Delta X}$  were obtained<sup>54</sup> by using a modified Gauss elimination procedure to solve the system of linear equations

$$\underline{F}(\underline{X}^{\circ}) \underline{\Delta X} = -\nabla_{\underline{X}} U_{TOTAL}(\underline{X}^{\circ})$$

However, in our computational scheme,<sup>256</sup> the solution algorithm required only the upper triangle of second derivative coefficients in the symmetric matrix  $\underline{F}(\underline{X}^{\circ})$ .

Since the potential energy function  $U_{TOTAL}$  is not quadratic in the Cartesian coordinates  $(X_i)$ , the true gradient vector  $\nabla_{\underline{X}} U_{TOTAL}(\underline{X})$  is not linear, and the new coordinates,  $\underline{X} = \underline{\Delta X} + \underline{X}^{\circ}$ , obtained from the above Newton-Raphson minimization cycle do not exactly solve the equations

$$\nabla_{\underline{X}} U_{TOTAL}(\underline{X}) = 0$$

In general however,  $\underline{X}$  describes a molecular configuration closer to the minimum energy one than does the trial geometry  $\underline{X}^{\circ}$ , and the new  $(X_i)$  are then employed as the trial coordinates in a repetition of the Newton-Raphson cycle. This iterative sequence is continued until the coordinate changes  $(\Delta X_i)$  and intercycle energy changes  $\Delta U_{TOTAL}$  become insignificant, and the molecular geometry which minimizes  $U_{TOTAL}$  for a

given conformational isomer is attained. The convergence criterion  $\Delta X_i < 0.002 \text{ \AA}$  ( $i = 1 \dots 3N$ ) was imposed here.

For molecules with many independent Cartesian coordinates, such as the metal chelate complexes encountered here, the general quadratic expansion  $U_{TOTAL}^Q$  is not often a suitable representation of  $U_{TOTAL}$  away from the region of the fit, particularly when the initial trial geometry is well removed from the *final* minimum energy configuration. Consequently, the molecular geometry at the minimum of  $U_{TOTAL}^Q$  may not lie within the region of positive curvature associated with the potential energy minimum of the conformational isomer under analysis (where  $\partial^2 U_{TOTAL} / \partial X_i^2 > 0$ , for  $i = 1 \dots 3N$  near the trial geometry). This usually occurs when the components of the potential energy gradient vector at the trial configuration are large ( $(\partial U_{TOTAL} / \partial X_i)$  at  $\underline{x}^0$  large) and relatively independent of the Cartesian geometry ( $(\partial^2 U_{TOTAL} / \partial X_i \partial X_j)$  at  $\underline{x}^0$  small), and very large coordinate changes ( $\Delta X_i$ ) are required to minimize the value of  $U_{TOTAL}^Q$ . In order to avoid the problems sometimes accompanying this effect (e.g. inter minima transitions and saddle-point convergence where  $\partial^2 U_{TOTAL} / \partial X_i^2 < 0$  for some  $i$  near the equilibrium geometry), and other related problems (e.g. divergent oscillation and libration), the calculated components of the translation vector  $\Delta \underline{X}$  for a given cycle were reduced by the factor  $\lambda$ , which is an inverse function of the sum of the squares of the calculated shifts  $(\Delta X_i)$ .<sup>56,248</sup> The new vector  $\Delta \underline{X}'$  was given by

$$\Delta \underline{X}' = \lambda \Delta \underline{X}$$

where

$$\lambda = 1 / (1 + \eta \sum_{i=1}^{3N} \Delta X_i^2)$$

as defined by Dwyer<sup>56,248</sup> and the new coordinates were subsequently obtained as

$$\underline{X}' = \Delta \underline{X}' + \underline{X}^0$$

The procedure was completely successful in eliminating the above problems and promoting rapid convergence in the Gauss-Newton-Raphson iterative refinement.<sup>256</sup> This mode of damping enables the energy surface to be followed closely along the geometrical path of the refinement for molecules in which  $U_{TOTAL}$  is poorly represented by the quadratic function  $U_{TOTAL}^R$  away from the trial geometry. The optimal value for the constant  $\eta$  should give the maximum convergence rate in a given refinement although in practice the value must be arbitrarily preset. However, some idea of the relative magnitude of  $\eta$  may be obtained from the complexity of the energy function (number of independent variables) and the quality of the initial trial coordinates for the molecule. In this analysis, the starting Cartesian trial coordinates for the complex molecules were normally acquired by transformations from the standard crystal bond lengths and valence angles, and the torsion angles obtained by visual examination of Dreiding models. The number of Cartesian coordinates for these molecules (Section 5.5) ranged from 102 to 141, and a value of 0.5 for  $\eta$  was used to achieve fast and efficient convergence in all cases.

The internal potential strain energy  $U_{TOTAL}$  was considered above to be a function of  $3N$  independent Cartesian coordinates for an  $N$  atom

molecule. However, by definition (Section 5.2)  $U_{TOTAL}$  depends solely on the intramolecular arrangement (interatomic distances, valence angles and torsion angles) and is independent of molecular translational and rotational motion. It is then sufficient to describe the intramolecular energy as a function of  $3N - 6$  independent coordinates, by imposing six redundancy conditions (corresponding to no translation of, or rotation about, the molecular centre of mass<sup>259</sup>) on the  $3N$  Cartesian coordinates. In the algorithm used here<sup>256</sup> for the solution of the equations ( $\partial U_{TOTAL}^Q / \partial X_i = 0; i = 1 \dots 3N$ ), this is also a necessary description from the following. Although these equations in the  $3N$  Cartesian coordinates hold true at the minimum  $U_{TOTAL}^Q$  configuration,<sup>259</sup> they are not uniquely soluble since the  $3N \times 3N$  matrix  $F(\underline{X}^0)$  has a rank of  $3N - 6$ . In principle six coordinates must be arbitrarily determined and these should be chosen to satisfy the six redundancy conditions. In this event the solution would preclude translational or rotational components, the true internal atomic motivation would be simulated (according to the internal energy function  $U_{TOTAL}$ ), and the internal coordinates would have their correct variance with no constraints on their magnitudes. However the solution scheme employed here requires that the matrix  $F(\underline{X}^0)$  be non-singular and hence that  $U_{TOTAL}^Q$  be a function of  $3N - 6$  independent Cartesian coordinates. This was most efficiently accomplished by constraining six of the  $X_i$  at their trial values  $X_i^0$ ,<sup>48,49,56</sup> rather than using the true redundancy conditions to eliminate them from the  $3N$  coordinate quadratic expansion for  $U_{TOTAL}$ . Thus  $U_{TOTAL}$  was here regarded as a function of the  $3N - 6$

variable  $X_i$ 's in deriving the expansions  $\nabla_{\underline{X}} U_{TOTAL}^Q(\underline{X})$  and  $U_{TOTAL}^Q$ , and the dimensions of the vectors  $\nabla_{\underline{X}} U_{TOTAL}(\underline{X}^0)$  and  $\Delta \underline{X}$  were then reduced to  $3N - 6$  and that of the matrix  $\underline{F}(\underline{X}^0)$  to  $3N - 6 \times 3N - 6$ . Although the individual atoms of the molecule are not adjusted strictly in accord with the internal force field (defined by  $U_{TOTAL}$ ) when these constraints are applied, the *final* minimized internal geometry is not affected provided the internal coordinates involving the fixed  $X_i$  can assume their equilibrium values. Occasionally this anomalous intracyclic atomic variance effect may be exploited (Section 5.4.3). The six Cartesian coordinates to be constrained must be chosen so that the *independent* internal coordinates containing them can have some *independent* variance, in order to assume chemically reasonable values. Gross translational and rotational motion of the molecule is then eliminated during the refinement and the true equilibrium internal geometry is attained at convergence. In the present energy minimizations, involving the simultaneous and coordinated refinement of  $3N - 6$  independent Cartesian coordinates (termed independent refinements), the optimal choice for the fixed  $X_i$  was dependent to some extent on the orientation of the molecule with respect to the coordinate system. Generally, however, the X,Y,Z coordinates of the Co atom were fixed, together with three coordinates of the ligand donor atoms chosen in accord with the above conditions for internal coordinate variance.

Both the matrix of second order derivatives  $(\partial^2 U_{TOTAL} / \partial X_i \partial X_j)$  at  $\underline{X}^0$  and the first order derivative vector  $(\partial U_{TOTAL} / \partial X_i)$  at  $\underline{X}^0$  were calculated prior to each minimization cycle, in the manner delineated

and programmed by Boyd.<sup>54</sup> These derivatives are given by

$$\partial U_{TOTAL} / \partial X_i = \sum_{\alpha} (\partial U_{TOTAL} / \partial I_{\alpha}) (\partial I_{\alpha} / \partial X_i)$$

and

$$\begin{aligned} \partial^2 U_{TOTAL} / \partial X_i \partial X_j &= \sum_{\alpha} (\partial U_{TOTAL} / \partial I_{\alpha}) (\partial^2 I_{\alpha} / \partial X_i \partial X_j) \\ &+ \sum_{\alpha} (\partial^2 U_{TOTAL} / \partial I_{\alpha}^2) (\partial I_{\alpha} / \partial X_i) (\partial I_{\alpha} / \partial X_j) \end{aligned}$$

where  $i, j = 1 \dots 3N - 6$ ,  $I_{\alpha}$  is an internal coordinate ( $r, \theta$ , or  $\phi$ ) defining the interaction  $\alpha$  and the sums are over all interactions included in the expression for  $U_{TOTAL}$  (Section 5.2). In this scheme all derivatives are evaluated analytically at the trial configuration  $\underline{X}^{\circ}$ , except those of the type  $\partial^2 I_{\alpha} / \partial X_i \partial X_j$  where  $I_{\alpha}$  is a valence bond angle ( $\theta$ ) or dihedral angle ( $\phi$ ), which are calculated by numerical differentiation.<sup>54</sup>

Although the computation of the components of the matrices  $\underline{F}(\underline{X}^{\circ})$  and  $\nabla_{\underline{X}} U_{TOTAL}(\underline{X}^{\circ})$  was executed according to Boyd's scheme<sup>54</sup> for the  $3N - 6$  variable or independent minimization, the entire program structure has been altered<sup>56,256</sup> from that used in the initial applications to the conformational analysis of metal complexes.<sup>48,49,75,248</sup> The fundamental sequential structure of the present program and the major modifications implemented here<sup>56,256</sup> are described in Appendix II. The main computational changes included the introduction of a routine to solve the Newton-Raphson system of linear equations from the upper triangle of the symmetric matrix  $\underline{F}(\underline{X}^{\circ})$ , and the accommodation of the scheme for the fast energy minimization of symmetric molecules<sup>56,256</sup> which is developed in the following section. In addition the overlay structure<sup>75</sup> and the interaction search, storage and manipulation routines were considerably modified<sup>75,256</sup> to find and process all of the



correct interactions required, while maintaining maximum efficiency and minimum computer core storage requirements. With these developments a molecular energy minimization involving 140 refining coordinates and an unlimited number of interactions required only 23 K (decimal) words of core storage on a CDC 6400 computer. For interaction sets of the type considered here (Section 5.2), a problem of this magnitude had a typical minimization cycle time of 32 sec on the CDC 6400 which included a complete precycle interaction search. These cycle times were dramatically reduced for the energy minimizations of symmetric molecules in the manner described in the next section.

#### 5.4 THE REFINEMENT OF SYMMETRIC MOLECULES

The scheme described above, for the potential strain energy minimization of the  $3N - 6$  independent Cartesian coordinates of an  $N$  atom metal complex molecule, has been modified to utilize the intrinsic molecular symmetry operations present in molecules having apparently non-trivial (*i.e.* symmetric or non-trivial dissymmetric) symmetry point groups.

This extension was developed for several reasons, the most obvious being associated with the reduction in the number of refining variables by a factor of at least  $1/2$  for a molecule with one or more symmetry elements. Since a maximum of about 115 atoms (345 variables) could be refined simultaneously (utilizing present maximum core storage on the CDC 6400), the coordinated refinement of very large symmetric molecules with 230 or more atoms is feasible despite the computational size

restrictions. Although the procedure is not completely rigorous for an individual cycle, since the matrices  $\underline{F}(\underline{X}^{\circ})$  and  $\nabla_{\underline{X}} U_{TOTAL}(\underline{X}^{\circ})$  do not include the symmetry information (see Section 5.4.2), the converged geometry correctly minimizes  $U_{TOTAL}$  for the symmetric molecule and the overall minimization is very fast by this method.

In some molecules, the minimized symmetric configuration for a particular conformational isomer may not be equivalent to the *true* minimum  $U_{TOTAL}$  configuration (where  $\partial^2 U_{TOTAL} / \partial X_i^2 > 0$  for  $i = 1 \dots 3N - 6$ , e.g. see Section 5.4.1). Such an isomer may first be rapidly refined to the minimum energy symmetric configuration and then independently refined to the *true* minimum energy geometry (see Section 5.4.3). This enables the equilibrium geometries of both the symmetric and independently minimized configurations of the same conformer to be studied, while inducing maximum efficiency in the search for the *true* minimum  $U_{TOTAL}$  configuration.

#### 5.4.1 Energy Minima and Saddle-points of Symmetric Configurations

The internal force field of a symmetric metal complex molecule has by necessity the same symmetry properties as the atomic configuration and the potential strain energy function  $U_{TOTAL}$ . The force field for a given symmetric trial configuration  $\underline{X}^{\circ}$  is mathematically represented by the negative of the potential energy gradient vector  $\nabla_{\underline{X}} U_{TOTAL}(\underline{X}^{\circ})$ , the components of which define the Cartesian base components of the forces on the individual atoms at  $\underline{X}^{\circ}$ . The vector  $-\nabla_{\underline{X}} U_{TOTAL}(\underline{X}^{\circ})$  then has the same symmetry as the internal force field at  $\underline{X}^{\circ}$ . The differential

translation vector  $d\underline{X} = (dX_i)$  which is proportional to  $-\nabla_{\underline{X}} U_{TOTAL}(\underline{X}^{\circ})$  is that required to effect the greatest decrease in  $U_{TOTAL}$  at  $\underline{X}^{\circ}$ , and is symmetric in the same sense as the configuration and the force field at  $\underline{X}^{\circ}$ . Hence the molecular symmetry is maintained in the direction of  $d\underline{X}$ . In any translation vector direction orthogonal to  $\nabla_{\underline{X}} U_{TOTAL}(\underline{X}^{\circ})$ , *i.e.* for any  $d\underline{X}'$  such that  $\sum_i (\partial U_{TOTAL} / \partial X_i(\underline{X}_i^{\circ})) dX_i' = 0$ ,  $U_{TOTAL}(\underline{X}^{\circ})$  is at a maximum or minimum since  $dU_{TOTAL} = \sum_i (\partial U_{TOTAL} / \partial X_i) dX_i$ .  $U_{TOTAL}$  is considered to be expressed rigorously in terms of the  $3N - 6$  independent Cartesian coordinates for this discussion. If the energy of the symmetric molecule is now minimized, either by repetitively shifting the configuration in the direction of  $d\underline{X}$  or by a rigorous  $3N - 6$  coordinate Newton-Raphson minimization, the symmetry of the initial trial configuration  $\underline{X}^{\circ}$  is preserved until convergence is achieved, and the minimum energy symmetric configuration is acquired. At this point  $\partial U_{TOTAL} / \partial X_i = 0$  for  $i = 1 \dots 3N - 6$ . Consequently, the minimized symmetric configuration always corresponds to a *true* minimum ( $\partial^2 U_{TOTAL} / \partial X_i^2 > 0$  at equilibrium for  $i = 1 \dots 3N - 6$ ) or saddle-point ( $\partial^2 U_{TOTAL} / \partial X_i^2 < 0$  at equilibrium for some  $i$  from  $1 \rightarrow 3N - 6$ ) configuration in the  $3N - 6$  dimensional energy function  $U_{TOTAL}$ .

It is usually possible to make an intuitive inference on the minimum or saddle-point alternatives for the minimized symmetric arrangement of a particular conformational isomer, from the examination of a Dreiding model for the conformer. Hence if any of the strain-causing interactions between symmetry equivalent sub-units of the isomer are relieved more effectively (*e.g.* by changes in torsion angles

rather than valence angles) by a finite translation vector  $\Delta\underline{X}$  with asymmetric components, than by the symmetric one, the minimum energy symmetric configuration will probably be at a saddle-point in the function  $U_{TOTAL}$ .

In general, if there are no strain-causing interactions between structurally equivalent sub-units of a given metal complex conformer with a possible symmetric configuration, there will always be a minimum in  $U_{TOTAL}$  with the symmetric arrangement, although it may not be the only one. This is true in a trivial sense because the structurally similar parts can each be independently minimized to the same sub-configuration, and the symmetric arrangement of these is then consistent with a minimum in  $U_{TOTAL}$ . It is not generally the case when strain-causing interactions exist between the possible asymmetric units of the conformer, as is true for most metal complex molecules, especially those of the sterically hindered chelate type discussed here (Section 5.5).

However, when these equivalent sub-units can interlock while maintaining the molecular symmetry, a minimum in  $U_{TOTAL}$  will occur at  $\underline{X}^0$  in all directions  $d\underline{X}'$  orthogonal to the symmetry direction  $d\underline{X}$ , and the minimized symmetric configuration corresponds to a *true* minimum energy configuration. Conformer configurations having dissymmetric point groups (*i.e.* having only rotational axes of symmetry) can normally achieve this symmetric interlocking and refine to a *true* minimum in  $U_{TOTAL}$  with the point group symmetry. But if the molecular symmetry includes a mirror plane ( $\sigma$ ), the symmetry related parts can not interlock

arbitrarily while preserving the mirror, and  $U_{TOTAL}$  may be at a maximum with respect to translation vectors  $d\underline{X}'$  having components orthogonal to the vector  $d\underline{X}$  which maintains the mirror symmetry. The minimized mirror configuration may then correspond to a saddle-point in  $U_{TOTAL}$  if a maximum in an antisymmetric direction persists at convergence. As implied above, the presence of a *true* minimum or saddle-point at such a configuration can often be detected intuitively by the visual examination of a structural model of the conformational isomer in question.

The existence of a saddle-point configuration at the symmetric minimum in many cases suggests the presence of well-defined *local* minima within the potential energy well associated with a given conformer. This is especially true when the structural connectivity between certain parts of the molecule is weak (e.g. between separate ligands), and each part may minimize relatively independently in either of the absolute antisymmetric vector directions  $\pm d\underline{X}'$ . For example if the conformer has the point group symmetry  $C_{2h}$  and a saddle-point due to the mirror ( $\sigma_h$ ) at the minimum of the  $C_{2h}$  configuration, minimization of  $U_{TOTAL}$  could result in the location of *true* minima at both the  $C_1$  and  $C_2$  configurations. Once again the possible occurrence of such *local* minima can usually be inferred from the careful examination of a structural model of the isomer.

#### 5.4.2 Symmetry-dependent Refinement

In this procedure, the Gauss-Newton-Raphson iterative molecular

energy minimization scheme (Section 5.3) is made very efficient for a symmetric metal chelate conformer, by utilizing the linear transformations relating the asymmetric units to refine the molecule in the symmetric configuration.

The computational scheme requires the atomic coordinates of the asymmetric unit at the initial trial configuration, as well as the linear transformation matrices necessary to generate the coordinates of the symmetry equivalent atoms. A symmetry-dependent refinement cycle then involves the following operations. The atomic coordinates of the symmetry equivalent units are first generated from the trial asymmetric coordinates. The force field defining  $U_{TOTAL}$  is then determined by including all interactions involving the asymmetric unit atoms in the computational search procedure. Finally a Gauss-Newton-Raphson minimization cycle is executed by allowing the asymmetric atom coordinates to vary in this force field, while constraining the coordinates of the symmetry equivalent atoms at the trial values. This is accomplished by precluding from the matrices  $\underline{F}(\underline{X}^*)$  and  $\nabla_{\underline{X}} U_{TOTAL}(\underline{X}^*)$  all terms of the type  $\partial^2 U_{TOTAL} / \partial X_i \partial X_j$  and  $\partial U_{TOTAL} / \partial X_i$  when  $X_i$  or  $X_j$  are symmetry-generated atomic coordinates. When  $X_i$  and  $X_j$  belong to the asymmetric input unit the above terms are computed as normal, and the overall computational load for the construction of  $\underline{F}(\underline{X}^*)$  and  $\nabla_{\underline{X}} U_{TOTAL}(\underline{X}^*)$  is considerably reduced in the symmetry-dependent refinement cycle. The Newton-Raphson equations

$$\underline{F}(\underline{X}^*) \Delta \underline{X} = -\nabla_{\underline{X}} U_{TOTAL}(\underline{X}^*)$$

where  $\Delta \underline{X}$  are the refining asymmetric atom coordinate shifts, are then

solved as before (Section 5.3), and the refined coordinates are given by

$$\underline{X}' = \lambda \underline{\Delta X} + \underline{X}^0$$

where  $\lambda$  is the damping function defined in Section 5.3. The  $(X_i')$  are then employed as the new trial coordinates for the asymmetric unit in the ensuing symmetry-dependent refinement cycle, and the process is repeated until the convergence criterion for the  $(\Delta X_i)$  is satisfied.

In the above minimization cycle,  $U_{TOTAL}$  is considered to be a variable function only of the asymmetric atom coordinates, the symmetry-related coordinates being constants generated from the trial asymmetric unit. The procedure then locates the minimum of the quadratic expansion ( $U_{TOTAL}^Q$ ) of  $U_{TOTAL}$  about the trial values of the variable asymmetric coordinates, by solving the Newton-Raphson equations for the coordinate shifts  $(\Delta X_i)$ . Since the symmetry-related coordinates are not considered as symmetry transformation functions of the variable  $X_i$  and  $X_j$  in the determination of the derivatives  $\partial^2 U_{TOTAL} / \partial X_i \partial X_j$  and  $\partial U_{TOTAL} / \partial X_i$ , the atoms of the refining asymmetric unit are not adjusted rigorously according to the internal force field. Thus, although the molecular symmetry is preserved in the minimization by regeneration of the symmetry-related coordinates prior to each cycle (and before the final strain energy and internal coordinate computations), that part of  $\underline{\Delta X}$  resulting from interasymmetric unit interaction is over-estimated in the regenerated symmetric molecule, by the partially constrained pseudo-force field assumed for  $U_{TOTAL}$ . However, the correct minimum  $U_{TOTAL}$  symmetric configuration is obtained at convergence (as illustrated in Section 5.5),

and the method normally requires less cycles to converge than the independent  $3N - 6$  coordinate minimization for the same symmetric conformational isomer.

The individual cycle times for this symmetry-dependent refinement technique are dramatically faster than those for the independent minimization, because of the reduced interaction search, the reduced derivative computations for the components of  $\underline{F}(\underline{X}^*)$  and  $\nabla_{\underline{X}} U_{TOTAL}(\underline{X}^*)$ , and the reduced solution time of the Newton-Raphson equations for the refining asymmetric atom coordinates. For example, in the energy minimization of the  $[\text{Co}(\text{tame})_2\delta\delta]^{3+}$  conformer, which has a *true* minimum in  $U_{TOTAL}$  with  $D_3$  symmetry, the cycle times for the  $D_3$  symmetry-dependent, the  $C_3$  symmetry-dependent, and the independent minimizations were 3, 8 and 27 sec respectively. The independent refinement required 18 cycles to converge compared with 15 for the symmetry-dependent refinements, the final converged  $D_3$  configurations being identical (see Section 5.5:1).

The symmetry elements of the molecule, defined indirectly by the linear transformation matrices, are fixed with respect to the Cartesian coordinate system in the symmetry-dependent refinement cycle. Hence any atoms which reside on these symmetry elements must be constrained to remain on them in order to preserve the molecular symmetry and prevent oscillation or libration during the course of the refinement. This does not restrain the magnitudes or orientations of the internal coordinates for the asymmetric unit in any way, and a routine to accommodate these constraints was included in the minimization scheme.



In general, translational and rotational components are eliminated from the solution  $\Delta \underline{X}$  by the constraints on the symmetry-generated atomic coordinates. However the technique may sometimes introduce oscillation effects, unless specific constraints are introduced to impede motion of the asymmetric unit along or about the symmetry elements, and once again the equilibrium magnitudes and orientations of the asymmetric internal coordinates must not be affected. The introduction of the above restrictions enhances the efficiency of the minimization cycle, by reducing the number of asymmetric variables and hence the dimensions of the matrices  $\underline{F}(\underline{X}^0)$  and  $\nabla_{\underline{X}} U_{TOTAL}(\underline{X}^0)$  in the Newton-Raphson equations.

#### 5.4.3 Evasion of Saddle-point Convergence

If the energy of a symmetric conformational isomer is minimized by a rigorous  $3N - 6$  coordinate refinement (in which the six redundancy conditions for non-translation and rotation are used to express  $U_{TOTAL}^0$  in terms of  $3N - 6$  independent coordinates), the minimum energy for the symmetric configuration is generally obtained at convergence and the symmetry is preserved during the refinement. This occurs because  $U_{TOTAL}$  at the symmetry conformation is always at a minimum or maximum in translation vector directions  $d\underline{X}'$  orthogonal to the symmetric vector  $d\underline{X}$  (Section 5.4.1). Hence the rigorous Newton-Raphson  $3N - 6$  coordinate minimization will not locate the *true* minimum energy configuration of a symmetric trial conformer if there is a saddle-point at the symmetric minimum conformation. However the present independent minimization

procedure (Section 5.3) may be used to locate this *true* minimum energy configuration or the symmetry-defined *local* minima (see Section 5.4.1) of such a symmetric trial molecule, in the manner described in the following paragraphs.

As indicated in Section 5.4.1, it is usually possible to decide whether the minimized symmetric conformation corresponds to a *true* minimum or saddle-point in  $U_{TOTAL}$ , from an examination of the symmetry and structural connectivity in a Dreiding model of the symmetric conformer. In any case the equilibrium geometry and energy of the symmetric conformation may first be obtained by the fast symmetry-dependent refinement procedure described in Section 5.4.2. A check on the diagonal elements of  $\underline{F}(\underline{X}^{\circ})$  from the final cycle then determines the possibility of a saddle-point ( $\partial^2 U_{TOTAL} / \partial X_i^2 (X_i^{eq}) < 0$  for some  $i$ ). If the presence of a saddle-point is confirmed, the molecule may be independently refined to a *true*  $U_{TOTAL}$  minimum as follows.

As explained in Section 5.3, the individual atoms of the molecule are not adjusted rigorously in accord with the true internal force field for the independent  $3N - 6$  coordinate minimization cycle procedure used here. This is due to the fixed constraints placed on six of the Cartesian coordinates ( $X_i$ ). When a symmetric trial molecule is subjected to such an independent minimization cycle, and the fixed  $X_i$  are chosen to be *inconsistent* with the molecular symmetry, the effective force field at the trial geometry  $\underline{X}^{\circ}$  defined by  $-\nabla_{\underline{X}} U_{TOTAL}(\underline{X}^{\circ})$  is no longer symmetric, and hence the direction  $d\underline{X}$  of greatest decrease in  $U_{TOTAL}$  is not symmetric. Similarly,  $U_{TOTAL}(\underline{X}^{\circ})$  is no longer at a maximum or minimum in translation

vector directions orthogonal to the symmetric vector. Thus the quadratic expansion  $U_{TOTAL}^Q$  about  $\underline{X}^\circ$ , defined by  $\nabla_{\underline{X}} U_{TOTAL}(\underline{X}^\circ)$  and  $\underline{F}(\underline{X}^\circ)$ , does not reflect the symmetry of the internal force field when these six coordinates are fixed asymmetrically. The internal molecular symmetry at  $\underline{X}^\circ$  is then not necessarily or generally retained at the minimum of  $U_{TOTAL}^Q$ , or in the direction of  $\Delta\underline{X}$ , when the asymmetric solution  $\Delta\underline{X}$  for the coordinate shifts is applied to the symmetric trial geometry  $\underline{X}^\circ$ . This is especially true when  $\underline{X}^\circ$  is the starting trial model, *i.e.* not normally close to the minimum symmetric conformation. However in practice, unless the shifts  $\Delta\underline{X}$  are zero, the actual shifts  $\lambda\Delta\underline{X}$  applied to the refining coordinates can usually be made sufficiently large to break away from the saddle-point region ( $\partial^2 U_{TOTAL} / \partial X_i^2 (X_i^\circ) < 0$  for some  $i$ ) associated with the symmetric conformation in the initial independent minimization cycle. The molecule is then independently refined to an equilibrium conformation which corresponds to a *true* minimum in  $U_{TOTAL}$  and is devoid of those symmetry elements associated with the saddle-point.

When using this procedure, the six constrained Cartesian coordinates should be chosen to provide as much asymmetry in the shifts ( $\Delta X_i$ ) as possible for the saddle-point symmetry elements, and so are normally selected from atoms within strongly interacting parts of the appropriate asymmetric units. The internal structural connectivity then usually ensures a break-away from the saddle-point region for the whole molecule and convergence to a *true* minimum energy configuration. However, if the independent minimization is initiated from the minimized symmetric

conformation (Section 5.4.2) rather than the symmetric trial molecule, the shifts ( $\Delta X_i$ ) are very small ( $< 0.002 \text{ \AA}$ ) and  $\lambda$  should be made accordingly large for the initial independent cycle. For conformational isomers with more than one *true* minimum energy configuration (see Section 5.4.1), the choice for the coordinate constraints also determines which of these will be obtained on convergence. Finally it must be ensured, as in a normal independent refinement procedure (Section 5.3), that the independent internal coordinates can assume their equilibrium values, at least in the final minimization cycles.

### 5.5 ENERGY MINIMIZATION RESULTS AND DISCUSSION

In the following conformational analyses of  $[\text{Co}(\text{tame})_2]^{3+}$ ,  $[\text{Co}(\text{tn})_3]^{3+}$  and  $[\text{Co}(\text{tn})_2\text{CO}_3]^+$  conformers, the energy minimization schemes described in Sections 5.3 and 5.4 were applied to the determination of the minimum  $U_{TOTAL}$  configuration and energy for each conformer, where  $U_{TOTAL}$  was defined by the general interaction force field and potential energy functions specified in Section 5.2. All calculations were executed on a CDC 6400 computer using the molecular energy minimization program developed here<sup>56,75,248,256</sup> to accommodate the features of Sections 5.3 and 5.4 (Appendix II), and derived from the original scheme<sup>54</sup> used in the initial applications to metal complex conformational analysis.<sup>48,49</sup>

The perspective ellipsoid plots were drawn from the *final* equilibrium Cartesian coordinates using the program ORTEPB by Johnson (Appendix I), and the bond lengths and angles involving hydrogen atoms are normally precluded from the tables of refined internal geometries presented here.

The general convergence criterion,  $\Delta X_i < 0.002 \text{ \AA}$  for all variable  $X_i$ , was adopted here as the condition for the attainment of the equilibrium configuration and associated minimum value of  $U_{TOTAL}$  for a given conformational isomer. The damping function  $\lambda$ , defined by Dwyer<sup>56,248</sup> and described in Section 5.3, was applied to the calculated shifts ( $\Delta X_i$ ) after each minimization cycle, and a value of 0.5 for the parameter  $\eta$  was normally used in the function  $\lambda$  to give a relatively fast convergence rate for the metal complex molecules investigated here.

### 5.5.1 Conformers of $[\text{Co}(\text{tame})_2]^{3+}$

#### *The $[\text{Co}(\text{tame})_2\delta\delta, \lambda\lambda]^{3+}$ Isomers*

The three possible conformational isomers of the  $[\text{Co}(\text{tame})_2]^{3+}$  ion were designated  $\delta\delta$ ,  $\lambda\delta$  and  $\lambda\lambda$  in Chapter 3, where  $\delta, \lambda$  refer to the conformation<sup>29</sup> of the three six-membered asymmetric skew-boat rings in the Co-tame connection. These are in fact the only stereochemically reasonable configurational isomers possible for this complex ion. The  $\delta\delta$  and  $\lambda\lambda$  forms analysed here are dissymmetric mirror image isomers (optical antipodes) whose maximum symmetry configurations belong to the  $D_3$  point group. From the analysis of Section 5.4.1 and the visual examination of a Dreiding model of the isomers, symmetry saddle-points are absent and the energy minimized configuration would also be expected to have  $D_3$  symmetry. This anticipation is supported by the fact that local minima within the potential well for a particular conformer are, in general, undetected by the present method,<sup>48,49,52,57,256</sup> unless

symmetry saddle-points are present (Section 5.4.1). The potential strain energy  $U_{TOTAL}$  is identical in value and functional form for the mirror image  $\delta\delta$  and  $\lambda\lambda$  conformers and only the  $\delta\delta$  form is considered here (Figures 5.1 and 5.2).

The Cartesian coordinates for the initial trial model of  $[\text{Co}(\text{tame})_2\delta\delta]^{3+}$  were routinely determined by transformation from standard crystal bond lengths and angles, and torsion angles visually estimated from a Dreiding model. This was done using program CART (Appendix I) according to the procedure of Hilderbrandt<sup>272</sup> which was here found perfectly adequate for the generation of chemically reasonable trial coordinates. The trial model was constructed with  $D_3$  symmetry, and the Cartesian coordinates were referenced to a trigonal coordinate system in which the  $Z$  axis was coincident with the  $C_3$  molecular axis and the  $X$  axis coincided with a  $C_2$  symmetry axis (*i.e.* similar to that depicted in Figure 4.2).

Three distinct energy minimizations were initiated from the above trial coordinates for  $[\text{Co}(\text{tame})_2\delta\delta]^{3+}$ , with the exclusion of the methyl hydrogen atom coordinates, in order to examine and test the developments of Section 5.4. These comprised an independent  $3N - 6$  coordinate refinement and two symmetry-dependent refinements, one utilizing the  $D_3$  point group operations and the other using only the  $C_3$  sub-group operations. A total of 392 potential interactions were generated for the starting trial molecule in accord with the general force field described in Section 5.2, and this decreased to 380 as the equilibrium geometry was approached (*i.e.* as the number of repulsive non-bonded terms decreased)

in the final minimization cycles. In the independent energy minimization the coordinates  $X, Y, Z$  of Co,  $Y, Z$  of N(1) and  $Z$  of N(1<sup>1</sup>) (see Figure 5.2 for atomic notation) were constrained as discussed in Sections 5.3 and 5.4.3. This refinement (117 variable coordinates) converged in 18 cycles (27 sec/cycle) to a *true* minimum energy geometry ( $\partial^2 U_{TOTAL} / \partial X_i^2 > 0$  for  $i = 1 \dots 117$ ) having precise  $D_3$  symmetry. For the  $C_3$  symmetry-dependent refinement, the coordinates  $X, Y, Z$  of Co and  $X, Y$  of C(2), C(3), C(2<sup>1</sup>) and C(3<sup>1</sup>) (see Figure 5.2) were allowedly fixed to maintain  $C_3$  symmetry and prevent oscillation (Section 5.4.2), and 277 interactions were generated for the force field connected with the variable asymmetric unit (40 refining coordinates). The minimized configuration was obtained in 15 cycles (8 sec/cycle) and was also  $D_3$  symmetric. The  $D_3$  symmetry-dependent minimization involved the refining atoms Co, N(1), C(1), C(2), C(3) and their associated hydrogens, and 171 interactions were initially required (decreasing to 167) to define the force field for these atoms. The coordinates  $X, Y, Z$  of Co and  $X, Y$  of C(2), C(3) were appropriately fixed for this refinement which then included only 20 variable coordinates and converged in 15 cycles (3 sec/cycle) of minimization. The *final* equilibrium internal coordinates, close contacts and total energies from these minimizations were identical to within the converged coordinate shifts (all  $< 0.002 \text{ \AA}$ ) and are listed in Tables 5.3 and 5.6 which are self-explanatory. The minimized  $[\text{Co}(\text{tame})_2\delta\delta, \lambda\lambda]^{3+}$  geometry is discussed in conjunction with the observed crystal geometry for  $[\text{Co}(\text{tame})_2\lambda\lambda]^{3+}$  (Chapter 3) in Chapter 6. The three minimizations illustrate the utility and efficiency of the symmetry-dependent refinement procedure (Section

5.4.2) in the Newton-Raphson molecular energy minimization of metal complexes having symmetric configurations at their true energy minima. They also provide an excellent example of the reliability and power of the energy minimization method (Section 5.3), and the effectiveness of the technique (Section 5.4.3) for introducing asymmetry into the symmetric trial molecule in the course of the refinement. Thus, although the  $C_3$  and  $D_3$  symmetry constrained refinements necessarily maintained  $D_3$  symmetry throughout the minimization, the independently refined molecule initially departed markedly from the symmetry of the trial model owing to the asymmetrically constrained coordinates, and yet converged to an identical  $D_3$  symmetric configuration. To further illustrate this power and consistency, several other independent minimizations of this same  $[\text{Co}(\text{tame})_2\delta\delta]^{3+}$  molecule were conducted from vastly distorted asymmetric trial models, some with Cartesian coordinates up to 2 Å from their equilibrium values, and all converged with precisely the same  $D_3$  geometry.

Although the methyl hydrogen coordinates were not required for the purposes of the above refinements, a final independent minimization of the  $[\text{Co}(\text{tame})_2\delta\delta]^{3+}$  conformer with these included was carried out for completeness and the comparison with crystal data (Chapter 6). This was done under the same conditions as the  $3N - 6$  coordinate minimization above. However the refinement (135 variables) was based on 440 interactions (near convergence) and required 20 cycles (30 sec/cycle) to converge. The final minimum geometry is also exactly  $D_3$  symmetric and not significantly different from that for the above minimizations (except for the C(2)-C(3) distance). The final Cartesian coordinates of



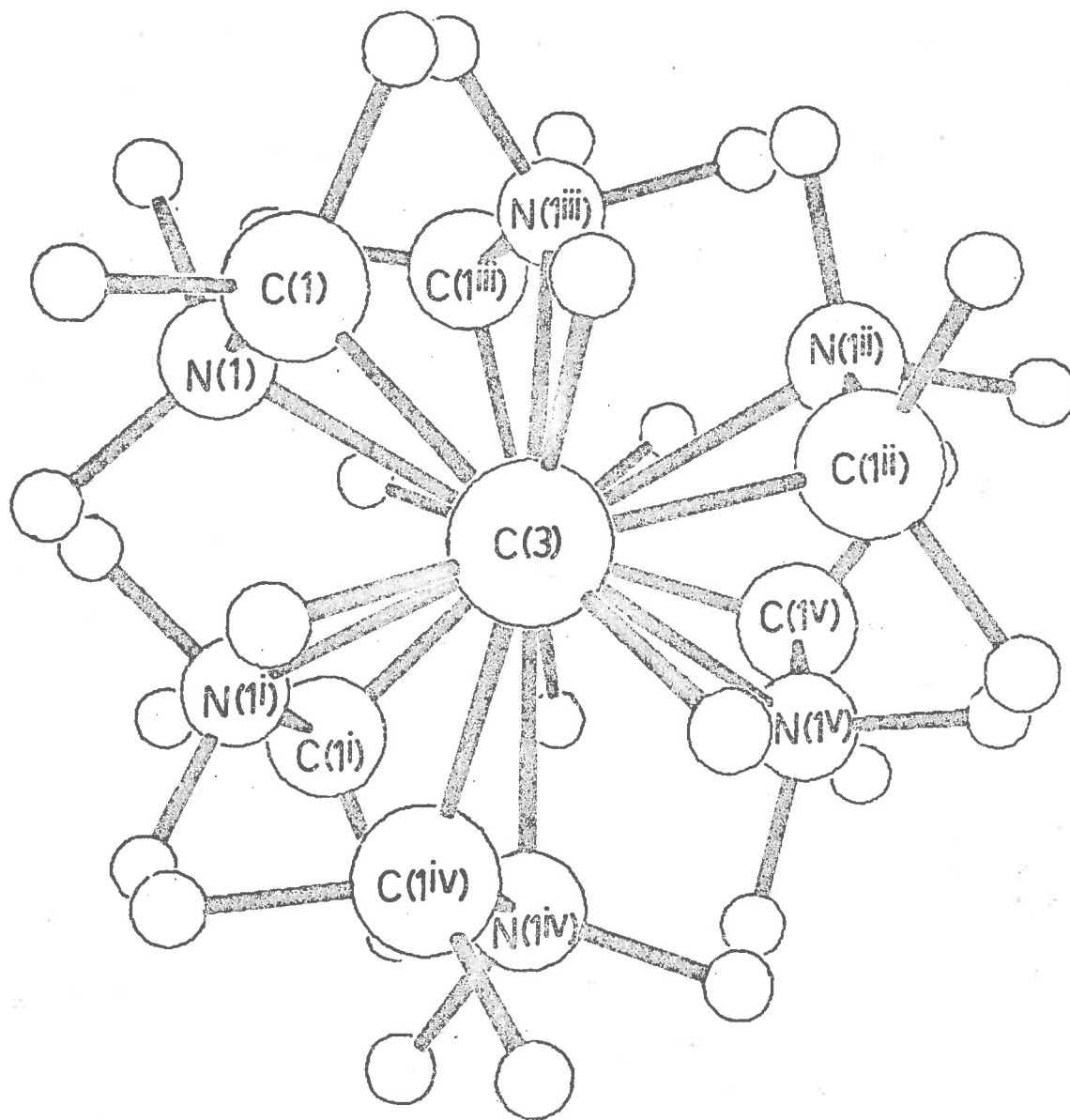


FIGURE 5.1.  $[\text{Co}(\text{tame})_2]^{3+}$  VIEWED DOWN THE  $C_3$  AXIS.

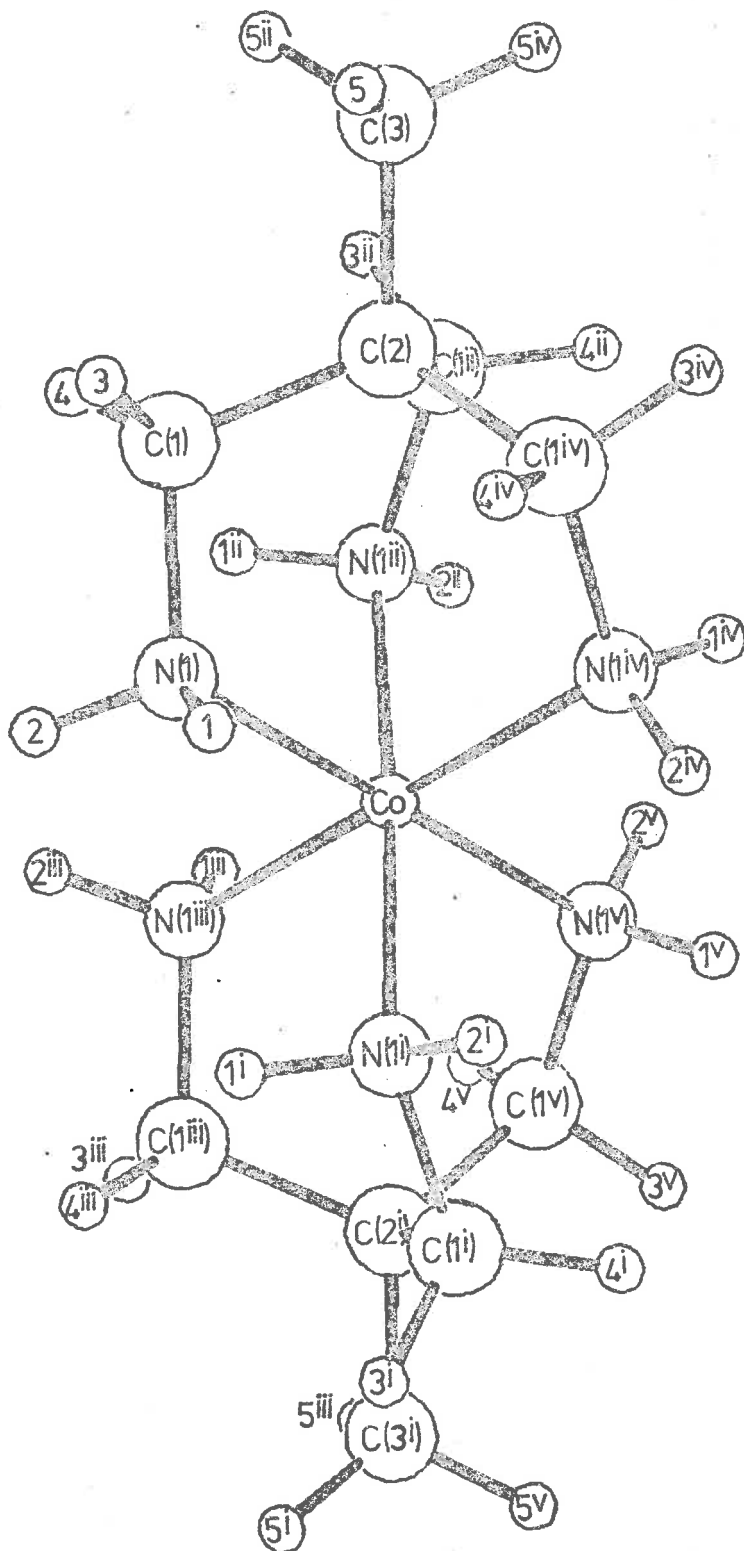


FIGURE 5.2. VIEW OF  $[\text{Co}(\text{tame})_2]^{3+}$  TO THE  $C_3$  AXIS.

TABLE 5.2. FINAL ORTHOGONAL COORDINATES FOR THE  $[\text{Co}(\text{tame})_2\delta\delta]^{3+}$  MOLECULE.<sup>a</sup>

Atom	X	Y	Z	Atom	X	Y	Z
Co	0.000	0.000	0.000	H(3 <sup>i</sup> )	1.938	0.774	-3.183
N(1)	1.362	-0.817	1.154	H(4 <sup>i</sup> )	0.730	1.887	-2.704
N(1 <sup>i</sup> )	1.451	0.645	-1.154	H(5 <sup>i</sup> )	0.912	-0.506	-4.920
N(1 <sup>ii</sup> )	-1.411	-0.726	1.156	H(1 <sup>ii</sup> )	-1.258	-1.704	1.181
N(1 <sup>iii</sup> )	-0.145	-1.624	-1.094	H(2 <sup>ii</sup> )	-2.312	-0.588	0.771
N(1 <sup>iv</sup> )	0.055	1.630	1.094	H(3 <sup>ii</sup> )	-1.848	-0.956	3.188
N(1 <sup>v</sup> )	-1.312	0.892	-1.156	H(4 <sup>ii</sup> )	-1.999	0.658	2.641
C(1)	0.953	-1.012	2.582	H(5 <sup>ii</sup> )	-0.242	-0.837	4.954
C(2)	0.005	0.078	3.044	H(1 <sup>iii</sup> )	-1.105	-1.865	-1.086
C(3)	0.007	0.116	4.560	H(2 <sup>iii</sup> )	0.343	-2.386	-0.692
C(1 <sup>i</sup> )	1.069	0.888	-2.582	H(3 <sup>iii</sup> )	-0.236	-2.190	-3.104
C(2 <sup>i</sup> )	-0.005	-0.078	-3.044	H(4 <sup>iii</sup> )	1.322	-1.680	-2.614
C(3 <sup>i</sup> )	-0.007	-0.116	-4.560	H(5 <sup>iii</sup> )	-0.797	-0.731	-4.912
C(1 <sup>ii</sup> )	-1.403	-0.218	2.566	H(1 <sup>iv</sup> )	-0.870	1.986	1.086
C(1 <sup>iii</sup> )	0.285	-1.471	-2.521	H(2 <sup>iv</sup> )	0.632	2.326	0.692
C(1 <sup>iv</sup> )	0.462	1.425	2.521	H(3 <sup>iv</sup> )	0.033	2.203	3.104
C(1 <sup>v</sup> )	-1.366	0.387	-2.566	H(4 <sup>iv</sup> )	1.517	1.506	2.614
H(1)	2.133	-0.195	1.137	H(5 <sup>iv</sup> )	-0.702	0.823	4.912
H(2)	1.684	-1.680	0.792	H(1 <sup>v</sup> )	-1.041	1.845	-1.181
H(3)	1.829	-1.005	3.183	H(2 <sup>v</sup> )	-2.223	0.866	-0.771
H(4)	0.494	-1.961	2.704	H(3 <sup>v</sup> )	-1.717	1.174	-3.188
H(5)	0.967	0.391	4.920	H(4 <sup>v</sup> )	-2.064	-0.410	-2.641
H(1 <sup>i</sup> )	2.141	-0.067	-1.137	H(5 <sup>v</sup> )	-0.138	0.860	-4.954
H(2 <sup>i</sup> )	1.877	1.462	-0.792				

Symmetry operations<sup>b</sup> described by the superscripts in Tables 5.2 and 5.3

1	$C_2$	iv	$C_3$
ii	$C_3^2$	v	$C_3C_2$ or $C_2''$
iii	$C_3^2C_2$ or $C_2'$		

<sup>a</sup> These are in Å, and are the coordinates from the independent refinement of the entire molecule. Hence, although the molecule has  $D_3$  symmetry, the symmetry elements have migrated marginally from their initial positions with respect to the coordinate axes.

<sup>b</sup> These operations are applied to the asymmetric unit (with no superscript) to generate the appropriate atoms. The positive direction of the  $C_3$  axis is taken as that of  $\text{Co} \rightarrow \text{C}(2)$ .

TABLE 5.3. REFINED INTERNAL COORDINATES OF THE  $[\text{Co}(\text{tame})_2\delta\delta]^{3+}$  MOLECULE.<sup>a</sup>

<i>Bond lengths</i>				
Atoms	Independent 1	Independent 2 <sup>b</sup>	$C_3$ constrained <sup>b</sup>	$D_3$ constrained <sup>b</sup>
Co-N(1)	1.963Å	1.965Å	1.965Å	1.965Å
N(1)-C(1)	1.498	1.498	1.498	1.498
C(1)-C(2)	1.516	1.513	1.513	1.513
C(2)-C(3)	1.517	1.506	1.506	1.506
<i>Bond angles</i>				
N(1)-Co-N(1 <sup>11</sup> ) <sup>c</sup>	89.92°	90.01°	90.02°	90.03°
Co-N(1)-C(1)	115.15	115.06	115.00	115.00
N(1)-C(1)-C(2)	111.57	111.28	111.26	111.26
C(1)-C(2)-C(3)	108.76	108.31	108.31	108.31
C(1)-C(2)-C(1 <sup>11</sup> )	110.17	110.61	110.61	110.61
N(1)-Co-N(1 <sup>1</sup> )	88.25	88.18	88.24	88.22
N(1)-Co-N(1 <sup>111</sup> )	91.97	91.87	91.77	91.78
N(1)-Co-N(1 <sup>v</sup> )	177.07	177.27	177.40	177.40
<i>Close contacts</i>				
N(1)...C(1 <sup>iv</sup> )	2.776Å	2.780Å	2.779Å	2.779Å
H(1)...H(4 <sup>iv</sup> )	2.335	2.346	2.342	2.342
H(1)...H(3)	2.221	2.222	2.223	2.223
H(2)...H(4)	2.269	2.270	2.271	2.271
H(2)...H(2 <sup>111</sup> )	2.121	2.121	2.119	2.119
H(1)...H(1 <sup>i</sup> )	2.278	2.275	2.277	2.276
<i>Torsion angles</i>				
Co-N(1)-C(1)-C(2)	-32.49°	-32.06°	-32.21°	-32.20°
N(1)-C(1)-C(2)-C(3)	-160.66	-160.83	-160.74	-160.74
N(1)-C(1)-C(2)-C(1 <sup>11</sup> )	+80.21	+80.61	+80.71	+80.70
N(1)-C(1)-C(2)-C(1 <sup>iv</sup> )	-41.54	-42.28	-42.18	-42.19
C(1)-C(2)-C(3)-H(5)	+64.12	b	b	b
C(1)-C(2)-C(3)-H(5 <sup>11</sup> )	-55.88			

<sup>a</sup> The independent refinements converged with precise  $D_3$  symmetry. Only asymmetric geometry is presented here. All parameters involving hydrogen atoms conformed to the precise  $D_3$  symmetry of the independent convergence point.

<sup>b</sup> In these refinements the methyl hydrogens were not included.

<sup>c</sup> See Table 5.2 for the definitions of symmetry operations associated with the superscripts.

this complete molecule are given in Table 5.2, and the internal equilibrium geometry, close contacts and total energies are listed in Tables 5.3 and 5.6 in comparison with those for the reduced molecule refinements. Figures 5.1 and 5.2 display the complete molecule in its equilibrium conformation.

*The  $[\text{Co}(\text{tame})_2\lambda\delta]^{3+}$  Isomer*

The maximum symmetry configuration of this conformer (see Figures 5.3 and 5.4) has the point group  $C_{3i}$  (or  $S_6$ ), and because of the apparent absence of symmetry saddle-points (Section 5.4.1) the isomer is expected to have a *trus* minimum energy configuration with  $C_{3i}$  symmetry. Cartesian trial coordinates for the initial model were determined using program CART (Appendix I)<sup>272</sup> as before and the molecule was constructed with  $C_{3i}$  symmetry. These coordinates were again referenced to a trigonal coordinate system with the  $Z$  axis coincident to the molecular  $C_3$  axis and the origin lying at the centre of symmetry.

As with  $[\text{Co}(\text{tame})_2\delta\delta]^{3+}$ , several energy minimizations (independent and symmetry-dependent) were initiated from the above and other asymmetric trial coordinates with the methyl hydrogen atoms excluded. All of these converged with identical *trus* minimum energy configurations which were rigorously  $C_{3i}$  symmetric as anticipated. However, the features of Section 5.4 were demonstrated in much the same fashion as previously discussed for the  $[\text{Co}(\text{tame})_2\delta\delta]^{3+}$  conformer, and only the independent  $3N - 6$  coordinate refinement is considered here. For this, the coordinates  $X, Y, Z$  of Co,  $Y, Z$  of N(1) and  $Z$  of N(1<sup>1</sup>) (see Figure 5.4 for atomic notation) were constrained according to the method outlined

in Sections 5.3 and 5.4.3. This 117 variable minimization required 7 cycles (27 sec/cycle) to converge to the *true* minimum energy configuration which had exact  $C_{31}$  symmetry. Initially 386 interactions were generated and this decreased to 374 near convergence. The *final* equilibrium internal coordinates, close contacts and total energies from the minimization of the  $[\text{Co}(\text{tame})_2\lambda\delta]^{3+}$  isomer (methyl hydrogens excluded) are given in Tables 5.5 and 5.6.

An independent energy minimization of the complete  $[\text{Co}(\text{tame})_2\lambda\delta]^{3+}$  conformer including the methyl hydrogens was also carried out under the same conditions as that above. The total strain energy included 434 interactions (near convergence) and the refinement of the 135 variables converged in 27 cycles (30 sec/cycle) to a *true* minimum with precise  $C_{31}$  symmetry as expected. Again the *final* internal geometry is not significantly different from that of the non-methyl hydrogen refinements above except for the C(2)-C(3) distance (see Table 5.5). *Final* Cartesian coordinates of the complete  $[\text{Co}(\text{tame})_2\lambda\delta]^{3+}$  conformer are listed in Table 5.4, and the *final* internal geometry, close contacts and total energies are compared with those for the reduced molecule in Tables 5.5 and 5.6. Perspective diagrams of the final complete molecule are shown in Figures 5.3 and 5.4.

#### *Comparison of the $\delta\delta$ , $\lambda\lambda$ and $\lambda\delta$ Isomers*

The equilibrium internal geometries and intra-ligand close contacts of the Co-tame connections are essentially similar for the  $[\text{Co}(\text{tame})_2\delta\delta, \lambda\lambda]^{3+}$  and  $[\text{Co}(\text{tame})_2\lambda\delta]^{3+}$  conformers, (Tables 5.3 and 5.5) except for the signs of the torsion angles (as defined in Table 1.6) describing

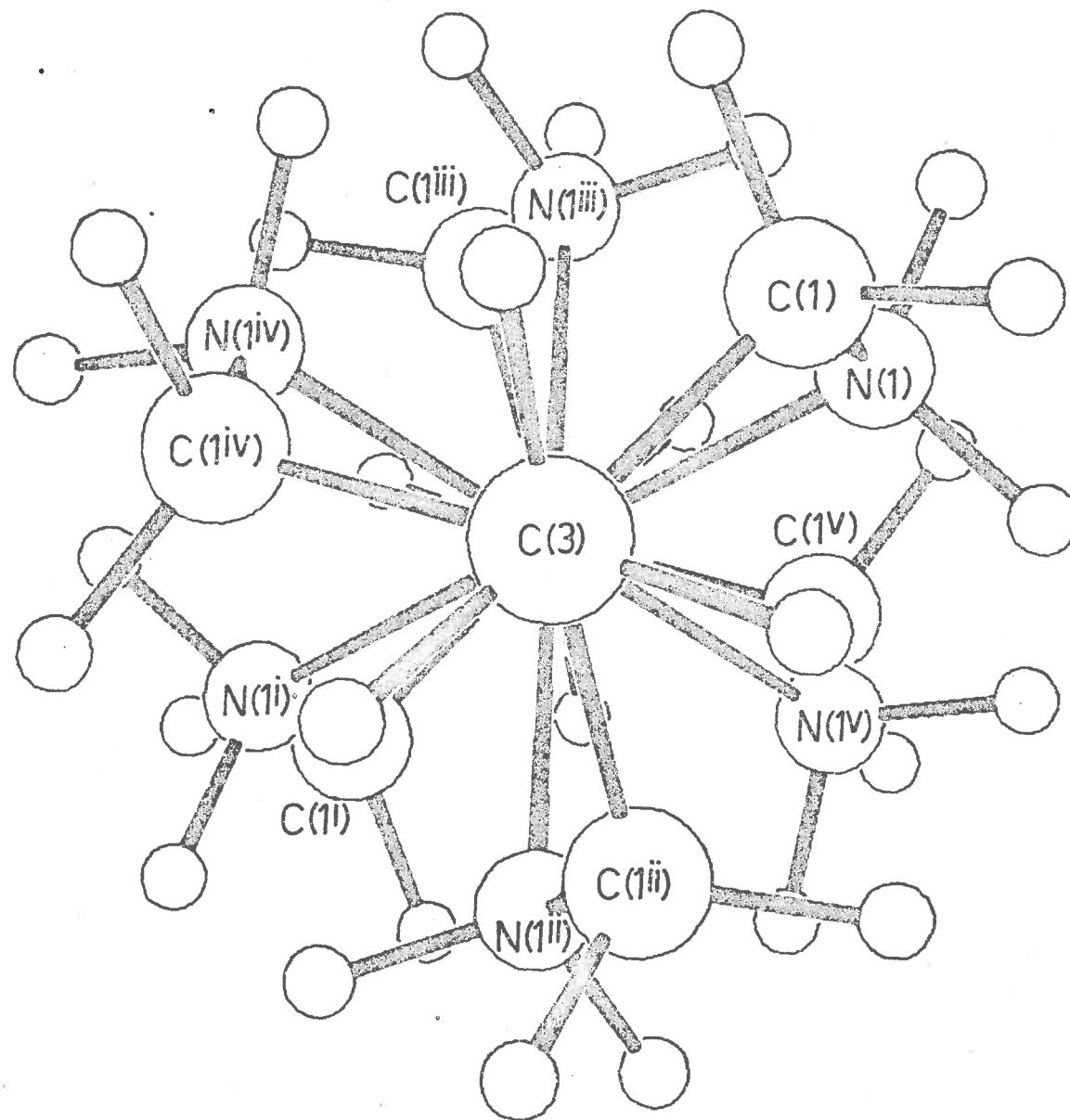


FIGURE 5.3. PERSPECTIVE VIEW OF  $[\text{Co}(\text{tamc})_2]^{3+}$  DOWN THE  $C_3$  AXIS.

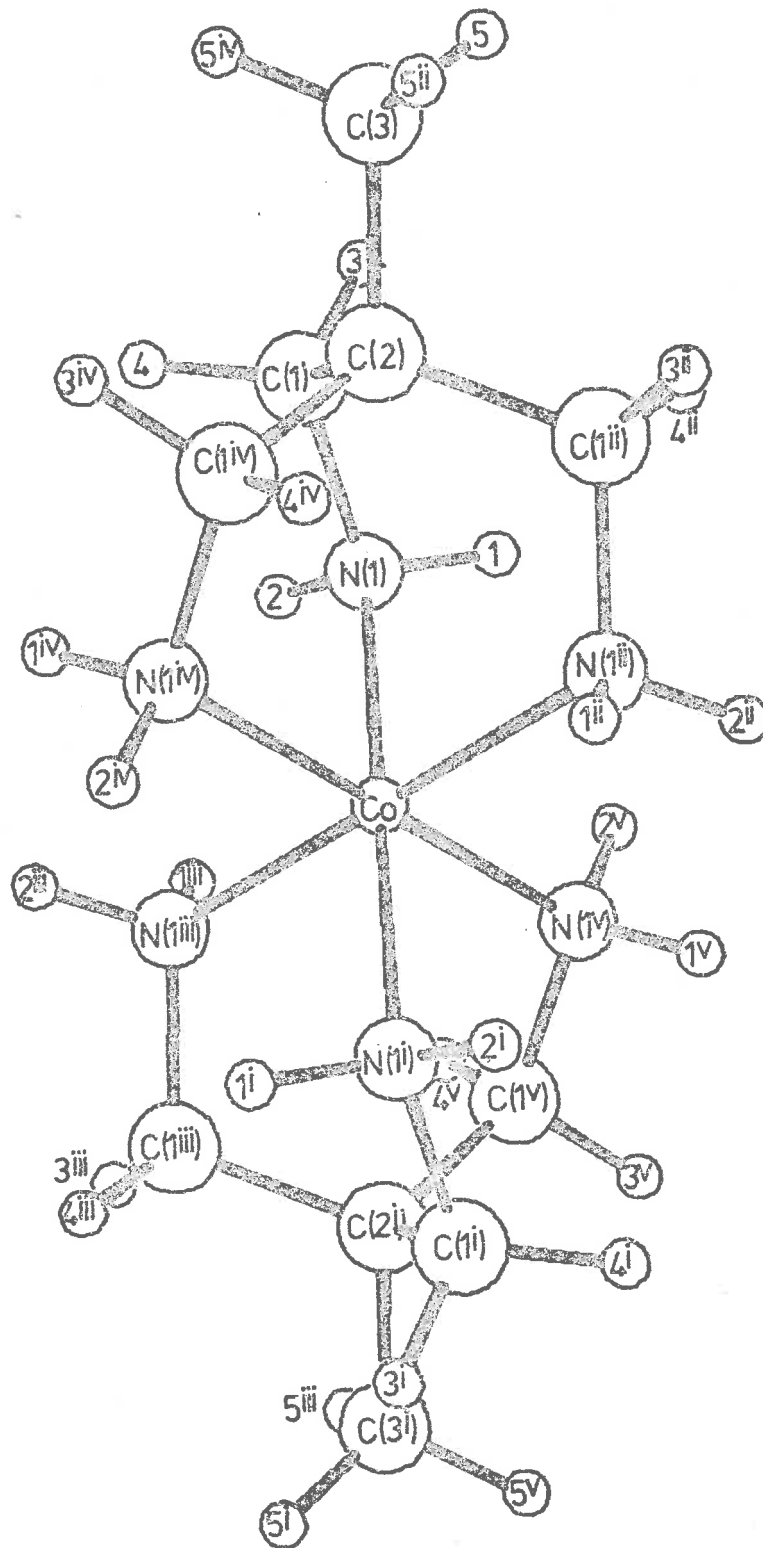


FIGURE 5.4.  $[\text{Co}(\text{tame})_2\lambda\delta]^{3+}$  VIEWED  $\perp^r$  TO THE  $C_3$  AXIS.



TABLE 5.4. FINAL ORTHOGONAL COORDINATES FOR THE  $[\text{Co}(\text{tame})_2\lambda\delta]^{3+}$  MOLECULE.<sup>a</sup>

Atom	X	Y	Z	Atom	X	Y	Z
Co	0.000	0.000	0.000	H(3 <sup>i</sup> )	1.734	1.208	-3.176
N(1)	-1.370	-0.817	1.154	H(4 <sup>i</sup> )	0.527	2.213	-2.499
N(1 <sup>i</sup> )	1.370	0.817	-1.154	H(5 <sup>i</sup> )	0.648	0.104	-4.996
N(1 <sup>ii</sup> )	0.171	1.487	1.279	H(1 <sup>ii</sup> )	1.119	1.770	1.262
N(1 <sup>iii</sup> )	-0.171	-1.487	-1.279	H(2 <sup>ii</sup> )	-0.366	2.270	1.001
N(1 <sup>iv</sup> )	1.394	-0.985	0.981	H(3 <sup>ii</sup> )	0.350	1.816	3.336
N(1 <sup>v</sup> )	-1.394	0.985	-0.981	H(4 <sup>ii</sup> )	-1.217	1.316	2.865
C(1)	-0.899	-1.219	2.519	H(5 <sup>ii</sup> )	1.052	0.174	4.924
C(2)	0.173	-0.281	3.036	H(1 <sup>iii</sup> )	-1.119	-1.770	-1.262
C(3)	0.259	-0.420	4.544	H(2 <sup>iii</sup> )	0.366	-2.270	-1.001
C(1 <sup>i</sup> )	0.899	1.219	-2.519	H(3 <sup>iii</sup> )	-0.350	-1.816	-3.336
C(2 <sup>i</sup> )	-0.173	0.281	-3.036	H(4 <sup>iii</sup> )	1.217	-1.316	-2.865
C(3 <sup>i</sup> )	-0.259	0.420	-4.544	H(5 <sup>iii</sup> )	-1.052	-0.174	-4.924
C(1 <sup>ii</sup> )	-0.181	1.153	2.697	H(1 <sup>iv</sup> )	1.163	-1.945	0.916
C(1 <sup>iii</sup> )	0.181	-1.153	-2.697	H(2 <sup>iv</sup> )	2.282	-0.876	0.559
C(1 <sup>iv</sup> )	1.516	-0.642	2.434	H(3 <sup>iv</sup> )	1.924	-1.482	2.942
C(1 <sup>v</sup> )	-1.516	0.642	-2.434	H(4 <sup>iv</sup> )	2.196	0.164	2.563
H(1)	-2.085	-0.143	1.268	H(5 <sup>iv</sup> )	0.436	-1.432	4.811
H(2)	-1.785	-1.605	0.724	H(1 <sup>v</sup> )	-1.163	1.945	-0.916
H(3)	-1.734	-1.208	3.176	H(2 <sup>v</sup> )	-2.282	0.876	-0.559
H(4)	-0.527	-2.213	2.499	H(3 <sup>v</sup> )	-1.924	1.482	-2.942
H(5)	-0.648	-0.104	4.996	H(4 <sup>v</sup> )	-2.196	-0.164	-2.563
H(1 <sup>i</sup> )	2.085	0.143	-1.268	H(5 <sup>v</sup> )	-0.436	1.432	-4.811
H(2 <sup>i</sup> )	1.785	1.605	-0.724				

Symmetry operations<sup>b</sup> described by the superscripts in Tables 5.4 and 5.5

i	i	iv	$C_3$
ii	$C_3^2$	v	$C_3^i$ or $S_6^5$
iii	$C_3^i$ or $S_6$		

<sup>a</sup> In Å. These are the converged coordinates from the independent refinement of the complete molecule. The total coordinate list is presented because the  $C_3$  axis has migrated from its initial position and the new transformation matrices were not computed.

<sup>b</sup> The transformations associated with these operations generate the superscripted atoms from the asymmetric set (no superscript). The positive direction of the  $C_3$  is that of Co  $\rightarrow$  C(2).

TABLE 5.5. REFINED INTERNAL COORDINATES OF THE  $[\text{Co}(\text{tame})_2\lambda\delta]^{3+}$  MOLECULE.<sup>a</sup>

<i>Bond lengths</i>					
Atoms	Independent 1	Independent 2 <sup>b</sup>	Atoms	Independent 1	Independent 2 <sup>b</sup>
Co-N(1)	1.969Å	1.971Å	C(1)-C(2)	1.516Å	1.512Å
N(1)-C(1)	1.498	1.498	C(2)-C(3)	1.517	1.506
<i>Bond angles</i>					
N(1)-Co-N(1 <sup>1i</sup> )	89.58°	89.68°	C(1)-C(2)-C(1 <sup>1ii</sup> )	110.12°	110.56°
Co-N(1)-C(1)	115.24	115.15	N(1)-Co-N(1 <sup>1j</sup> )	180.00	180.00
N(1)-C(1)-C(2)	111.55	111.27	N(1)-Co-N(1 <sup>1ii</sup> )	90.42	90.32
C(1)-C(2)-C(3)	108.82	108.36			
<i>Close contacts</i>					
N(1)...C(1 <sup>1ii</sup> )	2.771Å	2.775Å	H(2)...H(4)	2.260Å	2.261Å
H(1)...N(4 <sup>1ii</sup> )	2.331	2.342	H(1)...H(2 <sup>v</sup> )	2.101	2.100
H(1)...H(3)	2.213	2.214	H(2)...H(1 <sup>1ii</sup> )	2.101	2.100
<i>Torsion angles</i>					
Co-N(1)-C(1)-C(2)	+32.99°	+32.55°	N(1)-C(1)-C(2)-C(1 <sup>1iv</sup> )	-80.41°	-80.80°
N(1)-C(1)-C(2)-C(3)	+160.40	+160.58	C(1)-C(2)-C(3)-H(5)	-64.14	b
N(1)-C(1)-C(2)-C(1 <sup>1ii</sup> )	+41.21	+41.96	C(1)-C(2)-C(3)-H(5 <sup>1v</sup> )	+55.86	b

<sup>a</sup> The independent refinements converged with precise  $S_6$  symmetry. Only asymmetric geometry is tabulated. All parameters involving hydrogen atoms were consistent with the precise  $S_6$  symmetry.

<sup>b</sup> Methyl hydrogens were not included in this refinement.

<sup>c</sup> See Table 5.4 for the definitions of symmetry operations associated with the superscripts.

**TABLE 5.6.** FINAL STRAIN ENERGIES<sup>a</sup> OF THE [Co(tame)<sub>2</sub>]<sup>3+</sup> MOLECULES.

<i>Conformer</i>	<i>Refinement</i>	$\Sigma U_B$	$\Sigma U_{NB}$	$\Sigma U_\theta$	$\Sigma U_\phi$	$U_{TOTAL}$
$\delta\delta$	Independent 1	2.07	13.57	4.61	6.64	26.90
$\delta\delta$	Independent 2	1.76	11.83	4.43	6.64	24.66
$\delta\delta$	$C_3$ constrained	1.77	11.89	4.37	6.63	24.67
$\delta\delta$	$D_3$ constrained	1.77	11.89	4.37	6.64	24.67
$\delta\delta$	Independent 3 <sup>b</sup>	1.81	12.00	4.18	7.15	25.14
$\lambda\delta$	Independent 1	2.37	15.09	4.26	6.77	28.49
$\lambda\delta$	Independent 2	2.09	13.34	4.07	6.77	26.27
$\lambda\delta$	Independent 3 <sup>b</sup>	2.13	13.53	3.78	7.12	26.56

<sup>a</sup> All energies in kcal mol<sup>-1</sup>.

<sup>b</sup> In these refinements, the intrinsic torsion energies about the bonds were defined as functions of only 1 of the 9 torsion angles.

the  $\lambda$  and  $\delta$  conformations of the six-membered rings.

The main geometrical and energy differences between the conformers are associated with the inter-ligand close contacts and angular geometries at the Co atoms. Thus for the  $[\text{Co}(\text{tame})_2\delta\delta]^{3+}$  isomer (Figure 5.2 and Table 5.3), the repulsive  $\text{H}(2)\dots\text{H}(2^{\text{iii}})$  and symmetry-related contacts induce a small compression of the  $\text{N}(1)\text{-Co-N}(1^{\text{i}})$  and related angles and a small expansion of the  $\text{N}(1)\text{-Co-N}(1^{\text{iii}})$  angles, by means of a relative trigonal twist of the two tame ligands. This results in the dihedral or trigonal twist angle  $\omega$  (see Sections 4.3.1 and 4.3.2) being significantly different from the  $O_h$  or  $C_{3i}$  value of  $60^\circ$ , and for the  $\delta\delta$  isomer (Figures 5.1 and 5.2), the  $\text{CoN}_6$  core of the minimized molecule has the same absolute configuration as that for the energy minimized and observed  $\Lambda\text{-}(+)\text{589-}[\text{Co}(\text{en})_3]^{3+}$  molecules (see Section 4.3.2 and ref. 15). The *final* inter-ligand repulsive contact distances  $\text{H}(2)\dots\text{H}(2^{\text{iii}})$  and  $\text{H}(1)\dots\text{H}(1^{\text{i}})$  have the respective values  $2.12 \text{ \AA}$  ( $0.6 \text{ kcal mol}^{-1}$ ) and  $2.28 \text{ \AA}$  ( $0.3 \text{ kcal mol}^{-1}$ ), while the compressed  $\text{N}(1)\text{-Co-N}(1^{\text{i}})$  and expanded  $\text{N}(1)\text{-Co-N}(1^{\text{iii}})$  angles converged with the values  $88.3^\circ$  ( $0.05 \text{ kcal mol}^{-1}$ ) and  $92.0^\circ$  ( $0.06 \text{ kcal mol}^{-1}$ ). For the  $[\text{Co}(\text{tame})_2\lambda\delta]^{3+}$  isomer (Figure 5.4 and Table 5.5), the minimized configuration has  $C_{3i}$  symmetry and the  $\omega$  angles of the  $\text{CoN}_6$  core necessarily have the value  $60^\circ$ . The  $\text{N-H}\dots\text{N-H}$  inter-ligand contacts in this case merely serve to maintain the inter-ligand angles  $\text{N}(1)\text{-Co-N}(1^{\text{iii}})$  near their octahedral values of  $90^\circ$ . All inter-ligand  $\text{N-Co-N}$  angles, except the linear ones (which are necessarily  $180.0^\circ$ ), are symmetry-related and have the *final* value  $90.4^\circ$ , and the *final*  $\text{CoN}_6$  core for this conformer

is essentially octahedral. The repulsive inter-ligand contacts  $H(1)\dots H(2^V)$  and  $H(2)\dots H(1^{III})$  are related by the  $C_{3i}$  symmetry and have a converged distance of 2.10 Å (0.7 kcal mol<sup>-1</sup>).

The final strain energies of the  $[Co(tame)_2\delta\delta,\lambda\lambda]^{3+}$  and  $[Co(tame)_2\lambda\delta]^{3+}$  isomers are 26.9 and 28.5 kcal mol<sup>-1</sup> (Table 5.6) for the complete molecules. From the sub-division in terms of the net  $U_B$ ,  $U_{NB}$ ,  $U_\theta$  and  $U_\phi$  energies given in Table 5.6 and the above discussion, it is apparent that the major part of the total energy difference of 1.6 kcal mol<sup>-1</sup> resides in the inter-ligand N-H...N-H non-bonded interaction terms. Thus in  $[Co(tame)_2\lambda\delta]^{3+}$  the  $H(1)\dots H(2^V)$  interactions contribute six terms of 0.7 kcal mol<sup>-1</sup> (total 4.2 kcal mol<sup>-1</sup>), whereas in  $[Co(tame)_2\delta\delta,\lambda\lambda]^{3+}$  the  $H(2)\dots H(2^{III})$  and  $H(1)\dots H(1^I)$  contacts contribute three terms each of 0.6 and 0.3 kcal mol<sup>-1</sup> (total 2.7 kcal mol<sup>-1</sup>). It is also evident from Table 5.6 that the isomeric energy differences are similar for the complete and reduced molecules, although for comparative refinements in which the torsion energies were defined as functions of only one of the nine torsion angles the energy difference is only 1.4 kcal mol<sup>-1</sup>.

### 5.5.2 Symmetric Conformers of $[Co(tn)_3]^{3+}$

In this section the equilibrium geometries and energies of the apparently symmetric tris-chair, tris-lel-skew-boat and tris-ob-skew-boat conformational isomers of  $[Co(tn)_3]^{3+}$  are determined by the molecular energy minimization procedure described in Section 5.3 (see ref. 76). Here lel and ob refer to the parallel and oblique orientations of the

C-C-C sections of the skew-boat Co-tn rings with respect to the apparent (or pseudo)  $C_3$  symmetry axis relating these rings in the  $[\text{Co}(\text{tn})_3]^{3+}$  molecule. Isomers having true boat ring conformations were considered unimportant in contributing to solution equilibrium isomer populations and normal crystal conformations, because of the excessive number of repulsive inter- and intra-ring interactions and the high torsional energies<sup>76,181,256</sup> associated with these isomers. In addition the asymmetric and lower symmetry conformers with mixed ring conformations were not considered here. Some of these have been shown to have energies comparable with the high symmetry forms by the unreliable steepest-descent energy search procedure<sup>51,250</sup> and may be statistically preferred in solution. However the prime purpose here was the investigation of the supposedly symmetric forms in relation to the developments of Sections 5.3 and 5.4, and the comparison with the observed pseudo- $C_3$   $[\text{Co}(\text{tn})_3\text{chair}_3]^{3+}$ <sup>43,273</sup> and pseudo- $D_3$   $\Delta[\text{Co}(\text{R,R-ptn})_3]^{3+}$ - $(\text{lel}_3)^{17}$  and  $\Lambda-[\text{Co}(\text{R,R-ptn})_3]^{3+}(\text{ob}_3)^{16}$  crystal conformers (see Chapter 6).

*The Symmetric  $\Delta-[\text{Co}(\text{tn})_3\text{chair}_3]^{3+}$  Isomer*

Both the analysis of Section 5.4.1 and the visual examination of a Dreiding model for this isomer indicate that there are no energy saddle-points associated with the apparent  $C_3$  molecular symmetry, and the true energy minimized configuration is then expected to have exact  $C_3$  symmetry. In addition, the energy minimization<sup>256</sup> and visual interpretation of an individual Co-tn (chair) ring indicate that the minimum energy chair configuration has mirror symmetry, and there is no symmetry saddle-point associated with this mirror plane for an individual chair

ring. This is because strain-causing interactions between the mirror-related sub-units of the minimized symmetric ring are not relieved by configurational shifts  $\Delta X$  which do not maintain the mirror plane. Of course these intra-ring mirror planes do not persist in the complex molecule, and the individual chair rings will not be mirror symmetric in the minimized molecular conformation which is supposedly  $C_3$  symmetric.

The initial trial Cartesian coordinates for the  $\Delta$ -[Co(tn)<sub>3</sub>chair<sub>3</sub>]<sup>3+</sup> conformer were derived from the orthogonalized crystal coordinates for the *B* chair Co-tn ring in the structure of *cis*-[Co(tn)<sub>2</sub>CO<sub>3</sub>]ClO<sub>4</sub> (ref. 76), by rotation about a  $C_3$  axis at approximately 54.5° and 125.5° to the Co-N bonds of the crystal Co-tn ring. The skew-lines formed by the nitrogen donors of the observed ring and the  $C_3$  axis, defined a left-handed helix and the generated trial complex had the  $\Delta$  absolute ring configuration.<sup>29</sup> The trial model then had  $C_3$  symmetry, and the Cartesian coordinates referred to a trigonal coordinate system with the *Y* axis coinciding with the  $C_3$  axis and the *X* axis residing on a pseudo- $C_2$  axis. This starting structure was well removed from that of the crystal [Co(tn)<sub>3</sub>chair<sub>3</sub>]<sup>3+</sup> complex<sup>43,273</sup> and the *final* energy minimized configuration discussed here.

An independent  $3N - 6$  coordinate minimization involving 132 variable coordinates was conducted from the above trial model with the force field generally described in Section 5.2. The coordinates *X*, *Y*, *Z* of Co, *Y*, *Z* of N(1) and *Z* of C(1) (see Figure 5.5 for atomic notation) were fixed as described in Sections 5.3 and 5.4.3, and the refinement (based on 405 interactions near equilibrium) converged in 30 cycles

(29-30 sec/cycle) to a *true* minimum energy configuration with exact  $C_3$  symmetry as expected. The *final* internal geometry is considerably different to that of the starting model but similar to the mean observed pseudo- $C_3$  structure<sup>43,273</sup> (see Chapter 6), and the molecule departed markedly from  $C_3$  symmetry during the refinement owing to the asymmetrically fixed coordinates. Several other distorted trial configurations were also minimized and all converged with precisely the same  $C_3$  configuration as above, again illustrating the ability of the Newton-Raphson minimization to determine a unique *true* minimum configuration despite the nature of the trial model for a given conformer. *Final* Cartesian coordinates from the minimization are shown in Table 5.7 and the refined internal geometry, close contacts and total energies are presented in Tables 5.8 and 5.13. The equilibrium  $\Delta$ -[Co(tn)<sub>3</sub>chair<sub>3</sub>]<sup>3+</sup> molecule is shown in Figure 5.5. Observed and calculated geometries are compared in Chapter 6.

An additional independent minimization with N...N 1,3 non-bonded interactions explicitly included was also conducted from the above starting coordinates and under the above conditions. The *final* geometry and total energies for this are also presented in Tables 5.8 and 5.13. As expected the difference in geometries using these two force fields is insignificant, with the only slight variations arising from the slightly longer Co-N bonds (by 0.01 Å) when the N...N interactions are included. This verifies the use of the harmonic bending functions about an octahedral centre which were employed here (Section 5.2) to include the 1,3 non-bonded strain.



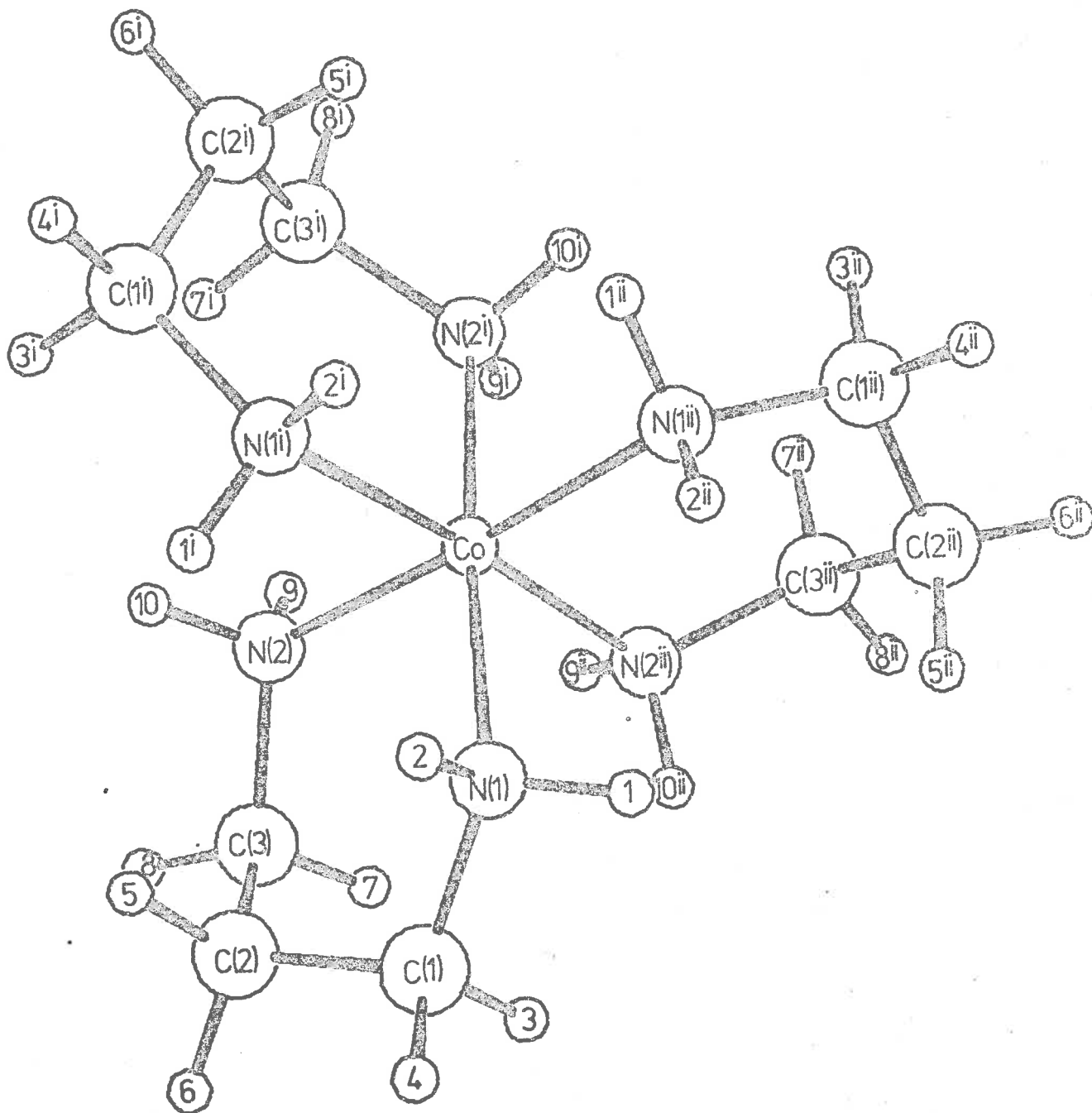


FIGURE 5.5.  $\Delta$ -[Co(tn)<sub>3</sub>chair<sub>3</sub>]<sup>3+</sup> - VIEW APPROX. DOWN THE  $C_3$  AXIS.



**TABLE 5.8.** REFINED INTERNAL GEOMETRY OF THE  $\Delta$ -[Co(tn)<sub>3</sub>chair<sub>3</sub>]<sup>3+</sup> MOLECULE.<sup>a</sup>*Bond lengths*

<i>Atoms</i>	<i>1<sup>b</sup></i>	<i>2<sup>c</sup></i>	<i>Atoms</i>	<i>1</i>	<i>2</i>
Co-N(1)	1.995Å	2.007Å	N(2)-C(3)	1.496Å	1.496Å
Co-N(2)	1.978	1.990	C(1)-C(2)	1.503	1.503
N(1)-C(1)	1.499	1.499	C(2)-C(3)	1.504	1.504

*Bond angles*

N(1)-Co-N(2)	94.33°	93.86°	Co-N(2)-C(3)	119.25°	119.19°
Co-N(1)-C(1)	121.90	121.77	N(1)-Co-N(1 <sup>1</sup> ) <sup>d</sup>	87.97	88.17
N(1)-C(1)-C(2)	112.20	112.18	N(1)-Co-N(2 <sup>11</sup> )	88.63	88.74
C(1)-C(2)-C(3)	110.31	110.37	N(1)-Co-N(2 <sup>1</sup> )	175.83	175.93
C(2)-C(3)-N(2)	111.07	111.08	N(2)-Co-N(2 <sup>1</sup> )	89.20	89.35

*Close contacts*

H(1)...H(3)	2.276Å	2.280Å	H(8)...H(10)	2.297Å	2.301Å
H(2)...H(4)	2.248	2.254	H(1)...H(2 <sup>11</sup> )	2.121	2.122
H(4)...H(6)	2.347	2.345	H(3)...H(10 <sup>11</sup> )	2.176	2.178
H(6)...H(8)	2.320	2.320	H(7)...H(9 <sup>11</sup> )	2.340	2.337
H(7)...H(9)	2.346	2.348			

*Torsion angles*

Co-N(1)-C(1)-C(2)	-46.39°	-47.14°	N(1)-C(1)-C(2)-C(3)	+69.94°	+70.26°
Co-N(2)-C(3)-C(2)	+56.53	+56.94	C(1)-C(2)-C(3)-N(2)	-76.04	-76.17

<sup>a</sup> These independent refinements converged with precise  $C_3$  symmetry. Only asymmetric geometry is presented.

<sup>b</sup> No H...N interactions specifically included.

<sup>c</sup> N...N interactions included.

<sup>d</sup> See Table 5.7 for definitions of symmetry operations.

The  $\Lambda$ -[Co(tn)<sub>3</sub> δ skew-boat<sub>3</sub>]<sup>3+</sup> Isomer

In this conformer the skew-boat rings have the 1el arrangement and the maximum symmetry configuration has the point group  $D_3$ . Again no symmetry saddle-points are present and the *true* minimum energy configuration is expected to have  $D_3$  symmetry. *i.e.* the *true*  $U_{TOTAL}$  minimum may be determined by the fast symmetry-dependent refinement procedure of Section 5.4.2.

The Cartesian trial coordinates for the starting model were obtained by transformation from standard internal coordinates using program CART (Appendix I) and were constructed with  $D_3$  symmetry. The coordinates were referred to a tetragonal coordinate system in which the  $X, Y, Z$  axes were coincident with the  $C_3$ -related coordinate bonds and the chelate rings were in the  $\Lambda$  absolute configuration.

An independent minimization, again involving 132 variable coordinates, was initiated from this trial model of the  $\Lambda$ -[Co(tn)<sub>3</sub> δ skew-boat<sub>3</sub>]<sup>3+</sup> isomer using the general force field of Section 5.2. For this the coordinates  $X, Y, Z$  of Co,  $X, Z$  of N(1) and  $X$  of N(1<sup>1</sup>) (see Figure 5.6 for atomic notation) were fixed and the refinement, based on 423 interactions near equilibrium, converged to a *true* minimum energy configuration with exact  $D_3$  symmetry in 10 cycles (29-30 sec/cycle). The *final* Cartesian coordinates are listed in Table 5.9 and the internal geometry, close contacts and total energies for the minimized configuration are given in Tables 5.10 and 5.13. Figure 5.6 displays the molecule in its equilibrium conformation.

A supplementary independent minimization involving the explicit

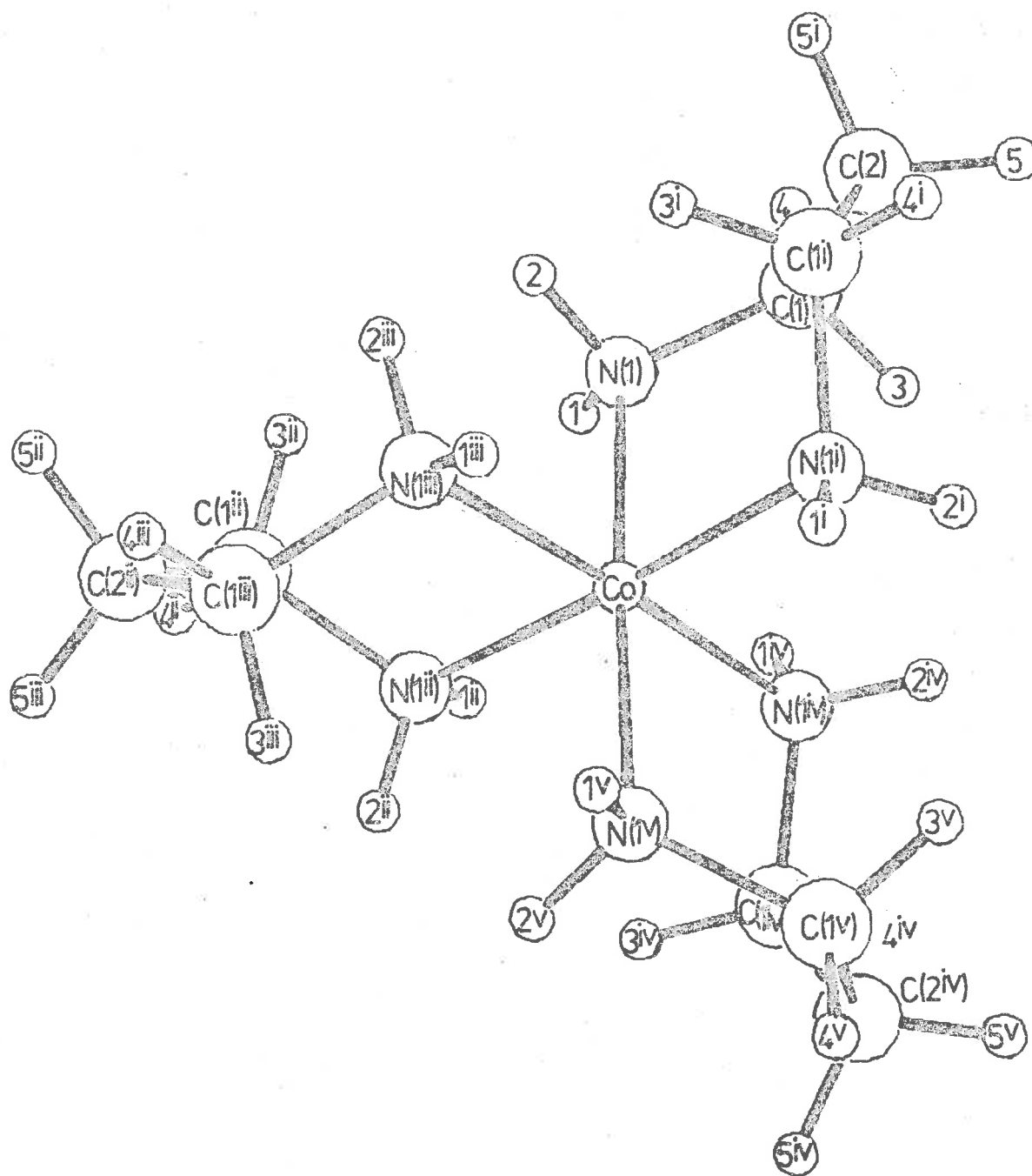


FIGURE 5.6.  $\Lambda$ -[Co(tn)<sub>3</sub>δskew boat<sub>3</sub>]<sup>3+</sup> - VIEW APPROX. DOWN THE C<sub>3</sub> AXIS.

TABLE 5.9. FINAL ORTHOGONAL COORDINATES FOR THE  $\Lambda$ -[Co(tn)<sub>3</sub>skew boat<sub>3</sub>]<sup>3+</sup> MOLECULE.<sup>a</sup>

Atom	X	Y	Z	Atom	X	Y	Z
Co	0.000	0.000	0.000	H(3 <sup>i</sup> )	1.698	-1.317	2.099
N(1)	-0.006	-1.984	0.000	H(4 <sup>i</sup> )	0.938	-1.038	3.603
N(1 <sup>i</sup> )	0.005	-0.065	1.983	H(5 <sup>i</sup> )	0.688	-3.324	2.505
N(1 <sup>ii</sup> )	0.076	-0.013	-1.983	H(1 <sup>iii</sup> )	-0.736	-0.485	-2.298
N(1 <sup>iii</sup> )	1.982	0.087	0.010	H(2 <sup>iii</sup> )	0.045	0.902	-2.358
N(1 <sup>iv</sup> )	-1.982	-0.006	-0.088	H(3 <sup>iii</sup> )	1.396	-1.654	-2.083
N(1 <sup>v</sup> )	-0.075	1.981	0.078	H(4 <sup>iii</sup> )	1.094	-0.914	-3.593
C(1)	-0.758	-2.611	1.135	H(5 <sup>iii</sup> )	3.363	-0.565	-2.484
C(2)	-0.001	-2.519	2.438	H(1 <sup>iiii</sup> )	2.245	0.540	0.851
C(1 <sup>i</sup> )	0.756	-1.221	2.573	H(2 <sup>iiii</sup> )	2.390	-0.814	0.024
C(1 <sup>ii</sup> )	1.264	-0.719	-2.562	H(3 <sup>iiii</sup> )	2.076	1.779	-1.245
C(2 <sup>ii</sup> )	2.530	0.091	-2.425	H(4 <sup>iiii</sup> )	3.599	1.083	-0.905
C(1 <sup>iii</sup> )	2.584	0.858	-1.126	H(5 <sup>iiii</sup> )	2.599	0.780	-3.230
C(1 <sup>iv</sup> )	-2.583	1.155	-0.822	H(1 <sup>v</sup> )	-2.245	-0.832	-0.568
C(2 <sup>iv</sup> )	-2.529	2.428	-0.013	H(2 <sup>v</sup> )	-2.391	-0.049	0.812
C(1 <sup>v</sup> )	-1.263	2.538	0.802	H(3 <sup>v</sup> )	-2.075	1.303	-1.738
H(1)	-0.443	-2.270	-0.842	H(4 <sup>v</sup> )	-3.598	0.942	-1.054
H(2)	0.911	-2.355	-0.007	H(5 <sup>v</sup> )	-2.597	3.255	-0.675
H(3)	-1.700	-2.141	1.247	H(1 <sup>v</sup> )	0.736	2.280	0.561
H(4)	-0.940	-3.635	0.919	H(2 <sup>v</sup> )	-0.044	2.387	-0.824
H(5)	-0.691	-2.612	3.240	H(3 <sup>v</sup> )	-1.396	2.029	1.721
H(1 <sup>i</sup> )	0.443	0.767	2.296	H(4 <sup>v</sup> )	-1.093	3.562	1.030
H(2 <sup>i</sup> )	-0.912	-0.070	2.354	H(5 <sup>v</sup> )	-3.362	2.466	0.645

Symmetry operations<sup>b</sup> described by the superscripts in Tables 5.9 and 5.10

i C<sub>2</sub>  
 ii C<sub>3</sub><sup>2</sup>  
 iii C<sub>3</sub><sup>2</sup> C<sub>2</sub> or C<sub>2</sub>'

iv C<sub>3</sub>  
 v C<sub>3</sub>C<sub>2</sub> or C<sub>2</sub>'

<sup>a</sup> In Å. The transformation matrices for the D<sub>3</sub> symmetry operations of the converged molecule must be determined from the coordinate list if necessary.

<sup>b</sup> The positive direction of the C<sub>3</sub> axis is taken as that of (N(1), N(1<sup>iv</sup>)) × (N(1), N(1<sup>iii</sup>)) where N(1), N(1<sup>iv</sup>) is an interatom vector in the direction N(1) → N(1<sup>iv</sup>) etc.

**TABLE 5.10.** REFINED INTERNAL GEOMETRY OF THE  $\Lambda$ -[Co(tn)<sub>3</sub>δskew boat<sub>3</sub>]<sup>3+</sup> MOLECULE.<sup>a</sup>

<i>Bond lengths</i>					
<i>Atoms</i>	<i>1<sup>b</sup></i>	<i>2<sup>b</sup></i>	<i>Atoms</i>	<i>1</i>	<i>2</i>
Co-N(1)	1.984Å	1.997Å	C(1)-C(2)	1.509Å	1.509Å
N(1)-C(1)	1.499	1.499			
<i>Bond angles</i>					
N(1)-Co-N(1 <sup>i</sup> ) <sup>c</sup>	88.12°	88.16°	N(1)-Co-N(1 <sup>ii</sup> )	89.64°	89.74°
Co-N(1)-C(1)	114.80	114.43	N(1)-Co-N(1 <sup>iii</sup> )	92.69	92.43
N(1)-C(1)-C(2)	112.12	112.18	N(1)-Co-N(1 <sup>v</sup> )	176.58	177.18
C(1)-C(2)-C(1 <sup>i</sup> )	112.41	112.53			
<i>Close contacts</i>					
N(1)...C(1 <sup>i</sup> )	2.790Å	2.797Å	H(1)...H(3 <sup>ii</sup> )	2.304Å	2.304Å
H(1)...H(4)	2.283	2.285	H(1)...H(1 <sup>ii</sup> )	2.321	2.341
H(3)...H(5)	2.283	2.284	H(2)...H(2 <sup>iii</sup> )	2.136	2.148
H(4)...H(5 <sup>i</sup> )	2.295	2.296	H(2)...H(3 <sup>ii</sup> )	2.245	2.252
<i>Torsion angles</i>					
Co-N(1)-C(1)-C(2)	-74.81°	-74.90°	N(1)-C(1)-C(2)-C(1 <sup>i</sup> )	+36.64°	+36.97°

<sup>a</sup> These independent refinements converged with precise  $D_3$  symmetry. Hence only asymmetric geometry is presented. The C-C-C chain in this molecule is approximately parallel to the  $C_3$  axis.

<sup>b</sup> *1* has no specific N...N interactions. These are included in *2*.

<sup>c</sup> See Table 5.9 for definitions of symmetry operations identified by the superscripts.

N...N 1,3 non-bonded energies was also executed for this isomer under the above conditions. The results from this are presented in comparison with those above in Tables 5.10 and 5.13. As for the tris-chair isomer, the geometrical differences are insignificant, further justifying the non-inclusion of the 1...3 repulsion interactions about the octahedral centres as explicit terms.

*The  $\Lambda$ -[Co(tn)<sub>3</sub>  $\lambda$  skew-boat<sub>3</sub>]<sup>3+</sup> Isomer*

The skew-boat rings are in the ob arrangement with respect to the apparent  $C_3$  axis of this conformer, for which the maximum symmetry configuration has the point group  $D_3$ . This conformer is also expected to have a *true* minimum energy configuration with  $D_3$  symmetry.

The initial Cartesian trial coordinates were again determined using program CART and the trial model had  $D_3$  symmetry. As for the tris-lal-skew-boat isomer, the coordinates were referenced to a tetragonal coordinate system with the  $C_3$ -related coordinate bonds lying along the X, Y, Z axes. The chelate rings were in the  $\Lambda$  absolute configuration.

An independent minimization (132 variables), initiated from this trial model and employing the general force field (Section 5.2), converged in 15 cycles (29-30 sec/cycle) to a *true* minimum energy structure having exact  $D_3$  symmetry. The coordinates X, Y, Z of Co, X, Z of N(1) and X of N(1<sup>1</sup>) (see Figure 5.7 for atomic notation) were fixed for the refinement which was based on 414 interactions near convergence. The *final* Cartesian coordinates for the minimized  $\Lambda$ -[Co(tn)<sub>3</sub>  $\lambda$  skew-boat<sub>3</sub>]<sup>3+</sup> conformer are given in Table 5.11, and the equilibrium internal geometry, close contacts and total energies are listed in Tables 5.12



and 5.13. A perspective drawing of the molecule in its equilibrium conformation is given in Figure 5.7.

In accord with the other symmetric isomers of  $[\text{Co}(\text{tn})_3]^{3+}$ , an independent minimization of the above model with 1,3 N...N interactions included resulted in only trivial differences in the final internal molecular structure, these being associated with the expected slight increase (0.01 Å) in the Co-N bond lengths. The results of this minimization are compared with those above in Tables 5.12 and 5.13.

*Comparison of the Minimized Symmetric Conformers*

The final strain energies of the tris-lel-skew-boat, tris-chair and tris-ob-skew-boat conformers of  $[\text{Co}(\text{tn})_3]^{3+}$  have the values 26.4, 27.6 and 33.3 kcal mol<sup>-1</sup> respectively, for the refinements based on the general force field of Section 5.2 (see Table 5.13).

The relatively high strain energy of the tris-ob-skew-boat form compared to that of the tris-lel isomer stems from the inter-ring N-H...N-H and N-H...C-H contacts. The close contacts of this type are generally considerably higher in energy for the tris-ob form (Tables 5.10, 5.12 and Figures 5.6, 5.7), and these are not relieved any more effectively through angular or torsional deformation than those of the tris-lel isomer. Consequently the *net* bonded, non-bonded, angular and, to a lesser extent, the torsional strain energies listed in Table 5.13, are generally larger for the minimized tris-ob conformer of  $[\text{Co}(\text{tn})_3]^{3+}$ , but the intra-ring internal geometry is only slightly more strained (see Tables 5.10 and 5.12). In the tris-ob structure the major N-H...N-H contacts are the six symmetry-related contacts H(1)...H(2<sup>ii</sup>)

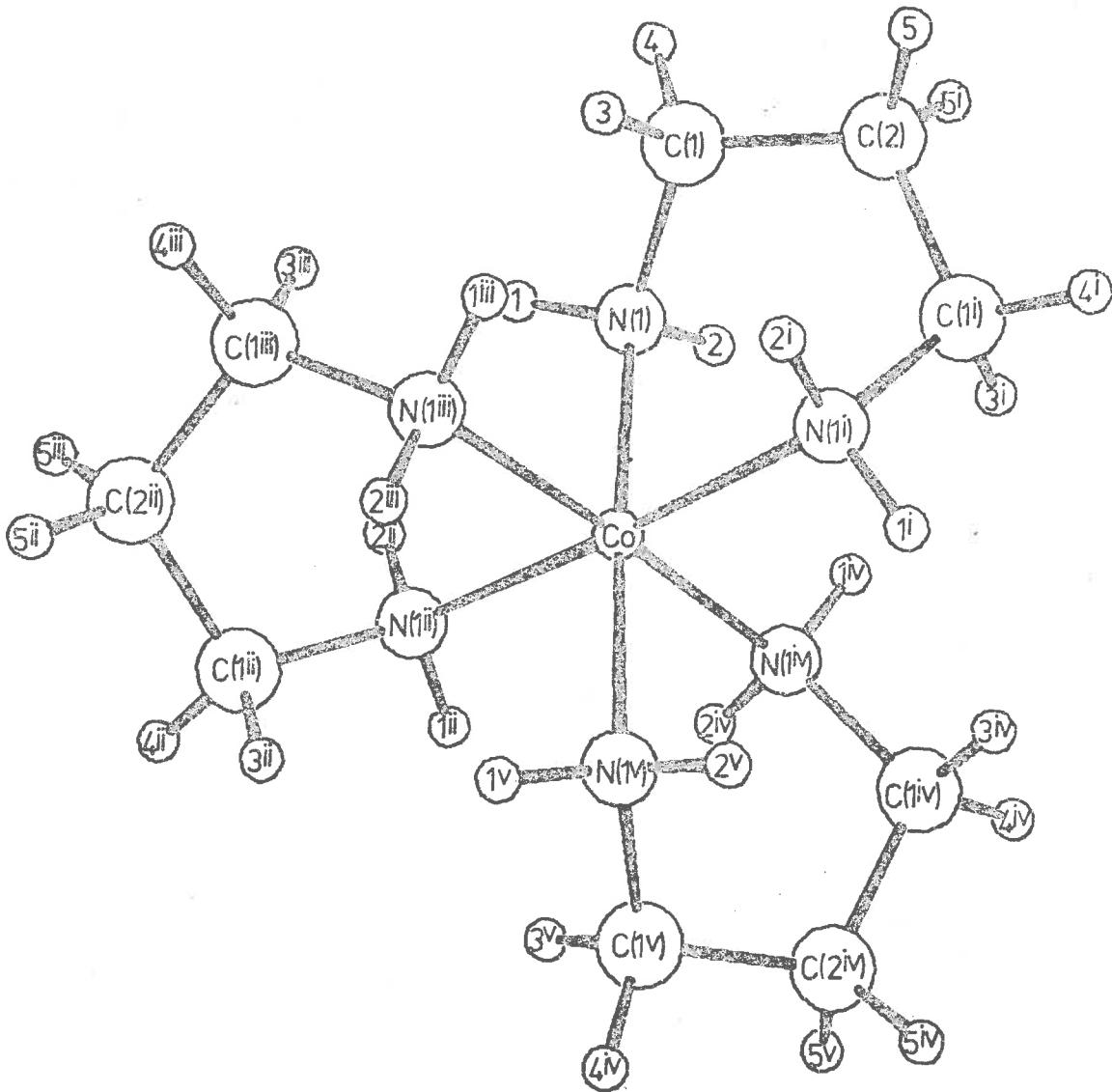


FIGURE 5.7.  $\Lambda$ -[Co(tn)<sub>3</sub>skew boat<sub>3</sub>]<sup>3+</sup> - VIEW APPROX. DOWN THE C<sub>3</sub> AXIS.

**TABLE 5.11.** FINAL ORTHOGONAL COORDINATES FOR THE  $\Lambda$ -[Co(tn)<sub>3</sub>skew boat<sub>3</sub>]<sup>3+</sup> MOLECULE.<sup>a</sup>

Atom	X	Y	Z	Atom	X	Y	Z
Co	0.000	0.000	0.000	H(3 <sup>i</sup> )	-2.275	-0.903	1.809
N(1)	-0.373	-1.960	0.000	H(4 <sup>i</sup> )	-1.712	-0.742	3.409
N(1 <sup>i</sup> )	-0.373	-0.005	1.960	H(5 <sup>i</sup> )	-1.751	-3.058	2.347
N(1 <sup>ii</sup> )	0.446	-0.098	-1.942	H(1 <sup>iii</sup> )	-0.236	0.389	-2.463
N(1 <sup>iii</sup> )	1.941	-0.263	0.382	H(2 <sup>iii</sup> )	0.400	-1.032	-2.263
N(1 <sup>iv</sup> )	-1.907	0.350	-0.469	H(3 <sup>iii</sup> )	1.914	1.414	-1.897
N(1 <sup>v</sup> )	0.267	1.976	0.069	H(4 <sup>iii</sup> )	1.823	0.584	-3.381
C(1)	0.018	-2.692	1.247	H(5 <sup>iii</sup> )	3.808	0.142	-1.846
C(2)	-0.914	-2.407	2.400	H(1 <sup>iiii</sup> )	2.050	-0.663	1.278
C(1 <sup>i</sup> )	-1.414	-0.982	2.417	H(2 <sup>iiii</sup> )	2.407	0.608	0.428
C(1 <sup>ii</sup> )	1.784	0.457	-2.327	H(3 <sup>iiii</sup> )	2.141	-2.027	-0.754
C(2 <sup>ii</sup> )	2.923	-0.442	-1.911	H(4 <sup>iiii</sup> )	3.618	-1.406	-0.175
C(1 <sup>iii</sup> )	2.679	-1.132	-0.590	H(5 <sup>iiii</sup> )	3.078	-1.183	-2.656
C(1 <sup>iv</sup> )	-2.510	1.575	0.148	H(1 <sup>iv</sup> )	-2.462	-0.420	-0.197
C(2 <sup>iv</sup> )	-2.009	2.849	-0.490	H(2 <sup>iv</sup> )	-2.018	0.416	-1.450
C(1 <sup>v</sup> )	-0.556	2.774	-0.896	H(3 <sup>iv</sup> )	-2.305	1.595	1.185
H(1)	0.101	-2.387	-0.753	H(4 <sup>iv</sup> )	-3.567	1.540	0.042
H(2)	-1.333	-2.131	-0.166	H(5 <sup>iv</sup> )	-2.142	3.646	0.199
H(3)	1.007	-2.436	1.521	H(1 <sup>v</sup> )	1.215	2.188	-0.107
H(4)	0.010	-3.738	1.060	H(2 <sup>v</sup> )	0.089	2.319	0.979
H(5)	-0.402	-2.612	3.308	H(3 <sup>v</sup> )	-0.482	2.356	-1.864
H(1 <sup>i</sup> )	-0.668	0.894	2.243	H(4 <sup>v</sup> )	-0.172	3.763	-0.954
H(2 <sup>i</sup> )	0.455	-0.180	2.471	H(5 <sup>v</sup> )	-2.590	3.064	-1.352

Symmetry operations<sup>b</sup> described by the superscripts in Tables 5.11 and 5.12

i	$C_2$	iv	$C_3$
ii	$C_3^2$	v	$C_3C_2$ or $C_2'$
iii	$C_3^2C_2$ or $C_2'$		

<sup>a</sup> In  $\Lambda$ . The converged molecule has  $D_3$  symmetry. Transformation matrices associated with the symmetry operations may be computed from the coordinate list.

<sup>b</sup> The positive direction of the  $C_3$  axis is that of  $(N(1), N(1^{iv})) \times (N(1), N(1^{ii}))$  where  $(N(1), N(1^{iv}))$  is an interatom vector in the direction  $N(1) \rightarrow N(1^{iv})$  etc.

**TABLE 5.12.** REFINED INTERNAL GEOMETRY OF THE  $\Lambda$ - $[\text{Co}(\text{tn})_3]^{3+}$  MOLECULE.<sup>a</sup>

<i>Bond lengths</i>					
Atoms	1 <sup>b</sup>	2 <sup>b</sup>	Atoms	1	2
Co-N(1)	1.995Å	2.006Å	C(1)-C(2)	1.510Å	1.510Å
N(1)-C(1)	1.499	1.498			
<i>Bond angles</i>					
N(1)-Co-N(1 <sup>i</sup> ) <sup>c</sup>	87.85°	87.88°	N(1)-Co-N(1 <sup>ii</sup> )	89.63°	89.63°
Co-N(1)-C(1)	115.55	115.24	N(1)-Co-N(1 <sup>iii</sup> )	93.02	92.98
N(1)-C(1)-C(2)	112.46	112.52	N(1)-Co-N(1 <sup>v</sup> )	176.32	176.82
C(1)-C(2)-C(1 <sup>i</sup> )	113.02	113.15			
<i>Close contacts</i>					
N(1)...C(1 <sup>i</sup> )	2.808Å	2.814Å	H(4)...H(5 <sup>i</sup> )	2.286Å	2.287Å
H(1)...H(4)	2.263	2.265	H(1)...H(3 <sup>iii</sup> )	2.072	2.074
H(3)...H(5)	2.282	2.283	H(1)...H(2 <sup>ii</sup> )	2.050	2.064
<i>Torsion angles</i>					
Co-N(1)-C(1)-C(2)	+73.63°	+73.69°	N(1)-C(1)-C(2)-C(1 <sup>i</sup> )	-36.04°	-36.31°

<sup>a</sup> Only asymmetric geometry is presented since the refinements converged with precise  $D_3$  symmetry. The C-C-C chain is oblique to the  $C_3$  axis.

<sup>b</sup> 1 has no specific N...N interactions. These are included in 2.

<sup>c</sup> See Table 5.11 for definitions of symmetry operations associated with the superscripts.

**TABLE 5.13.** FINAL STRAIN ENERGIES<sup>a</sup> OF THE  $[\text{Co}(\text{tn})_3]^{3+}$  MOLECULES.

Conformer	Refinement	$\Sigma U_B$	$\Sigma U_{NB}$	$\Sigma U_\theta$	$\Sigma U_\phi$	$U_{TOTAL}$
chair <sub>3</sub>	1	3.08	11.31	11.07	2.08	27.55
lel skew boat <sub>3</sub> <sup>b</sup>	1	3.08	12.41	5.15	5.75	26.38
ob skew boat <sub>3</sub> <sup>b</sup>	1	4.20	15.91	7.14	6.10	33.34
chair <sub>3</sub>	2	4.37	11.90	10.63	2.04	28.94
lel skew boat <sub>3</sub>	2	4.31	13.31	4.89	5.63	28.14
ob skew boat <sub>3</sub>	2	5.45	16.17	6.85	6.01	34.49

<sup>a</sup> All energies in kcal mol<sup>-1</sup>.

<sup>b</sup> These definitions refer to the conformers in which the C-C-C chain is parallel (lel) or oblique (ob) with respect to the  $C_3$  axis.

(Figure 5.7) ( $2.05 \text{ \AA}$ ,  $0.9 \text{ kcal mol}^{-1}$ ), whereas the tris-lel isomer has only three close N-H...N-H interactions of the type H(2)...H(2<sup>iii</sup>) (which occur across a  $C_2$  axis as shown in Figure 5.6) and these are of lower energy ( $2.14 \text{ \AA}$ ,  $0.6 \text{ kcal mol}^{-1}$ ). The six weaker interactions H(1)...H(1<sup>ii</sup>) also contribute to the N-H...N-H strain in tris-lel-skew-boat  $[\text{Co}(\text{tn})_3]^{3+}$  ( $2.32 \text{ \AA}$ ,  $0.2 \text{ kcal mol}^{-1}$ ). Similarly there are six close N-H...C-H contacts of the type H(1)...H(3<sup>iii</sup>) ( $2.07 \text{ \AA}$ ,  $0.8 \text{ kcal mol}^{-1}$ ) in the tris-ob, and twelve weaker ones of the types H(1)...H(3<sup>ii</sup>) ( $2.30 \text{ \AA}$ ,  $0.2 \text{ kcal mol}^{-1}$ ) and H(2)...H(3<sup>ii</sup>) ( $2.25 \text{ \AA}$ ,  $0.3 \text{ kcal mol}^{-1}$ ) in the tris-lel molecule. The above interactions thus account for the major non-bonded strain energy differences between the tris-lel and tris-ob skew-boat conformers, and the generally higher instability of the tris-ob form. They also effect the compression of the chelate angles N(1)-Co-N(1<sup>i</sup>) to  $87.9^\circ$  (tris-ob) and  $88.1^\circ$  (tris-lel) and the general expansion of the other ligand angles (Tables 5.10 and 5.12).

In the  $[\text{Co}(\text{tn})_3\text{chair}_3]^{3+}$  isomer, the net torsional strain about the N-C and C-C bonds is considerably lower than that in the tris-lel and tris-ob forms (Table 5.13) owing to the greater staggering of the terminal groups. This is exemplified by the torsion angles in Tables 5.8, 5.10 and 5.12, in particular those about the C-C bonds. The inter-ring N-H...N-H and N-H...C-H contact strain is also relatively low compared with that of tris-ob and slightly lower than that of tris-lel. Thus for the tris-chair conformer there are three close N-H...N-H contacts of the type H(1)...H(2<sup>ii</sup>) ( $2.12 \text{ \AA}$ ,  $0.6 \text{ kcal mol}^{-1}$ ), three close N-H...C-H contacts, H(3)...H(10<sup>ii</sup>) ( $2.18 \text{ \AA}$ ,  $0.5 \text{ kcal mol}^{-1}$ ),

and three weaker ones of the type H(7)...H(9<sup>11</sup>) (2.34 Å, 0.2 kcal mol<sup>-1</sup>). These N-H...C-H contacts (see Figure 5.5), which are much shorter when the rings have their unstrained geometries (*e.g.* in a Dreiding model), are effectively relieved in the tris-chair conformer through expansion of the chelate angle N(1)-Co-N(2) to 94.3° (0.3 kcal mol<sup>-1</sup>) and the ligand angles Co-N(1)-C(2), Co-N(2)-C(3) to 121.9° (1.4 kcal mol<sup>-1</sup>) and 119.3° (0.8 kcal mol<sup>-1</sup>), and the relative flattening of the dihedral angles about the bonds N(1)-C(1) to -46.4°. As a result the angular strain in the minimized tris-chair isomer is considerably larger than that in the tris-lel and tris-ob-skew-boat conformers, as indicated in Table 5.13.

### 5.5.3 Chair Conformers of [Co(tn)<sub>2</sub>CO<sub>3</sub>]<sup>+</sup>

The energy minimized geometries of the conformational isomers of *cis*-[Co(tn)<sub>2</sub>CO<sub>3</sub>]<sup>+</sup> with the tn rings in the chair configuration are described in this section. Three of these isomers are possible and are denoted by the symbols AB, AA and BB for the purpose of this discussion (ref. 76). Figures 5.8, 5.9 and 5.10 display the conformers in their equilibrium conformations.

#### *The AB-Δ-[Co(tn)<sub>2</sub>CO<sub>3</sub>chair<sub>2</sub>]<sup>+</sup> Isomer*

This conformer is asymmetric (Figure 5.8) and as such must necessarily be minimized by the independent 3N - 6 coordinate refinement procedure of Section 5.3. This has been done previously,<sup>76</sup> and the minimization was conducted from the initial Cartesian trial coordinates obtained by a linear transformation from the crystal coordinates in the structure

of  $[\text{Co}(\text{tn})_2\text{CO}_3]\text{ClO}_4$ .<sup>76</sup> This refinement was based on the general force field of Section 5.2, with the N...N and N...O 1,3 interactions included explicitly because of the large angular distortion of the Co-O bonds from the octahedral positions. Furthermore, the torsional energies about N-C and C-C bonds were described as functions of only the single torsion angle defined by the chelate ring bonds. With this force field, 224 interactions defined the total strain energy  $U_{\text{TOTAL}}$  near the equilibrium configuration of the isomer, and the refinement of 96 variables (the carbonyl oxygen of  $\text{CO}_3$  was deleted because of its non-interaction with the Co-tn chair rings) converged to a *true* minimum energy configuration in 28 cycles.<sup>76</sup> A fixed damping factor  $\lambda$  was used here and the convergence criterion  $(\sum \Delta X_i^2 / (3N - \theta))^{1/2} < 0.005 \text{ \AA}$  was employed. The *final* Cartesian coordinates, internal geometry and total strain energies are listed in Tables 5.14, 5.15 and 5.20, and the equilibrium conformation of the  $AB-\Delta-[\text{Co}(\text{tn})_2\text{CO}_3\text{chair}_2]^+$  isomer is shown in Figure 5.8.

*The AA- $\Delta$ - $[\text{Co}(\text{tn})_2\text{CO}_3\text{chair}_2]^+$  Isomer*

In this conformer the maximum symmetry configuration belongs to the point group  $C_2$  (Figure 5.9 and ref. 76) and the *true* minimum energy arrangement is also expected to be  $C_2$  symmetric (Section 5.4).

The starting Cartesian coordinates for the trial model were in this case derived from the orthogonalized crystal coordinates for the A chair Co-tn ring and the Co- $\text{CO}_3$  ring in the structure of *cis*- $[\text{Co}(\text{tn})_2\text{CO}_3]\text{ClO}_4$  (ref. 76). The coordinates for the remaining A ring were then generated by rotation about a  $C_2$  axis approximately coincident

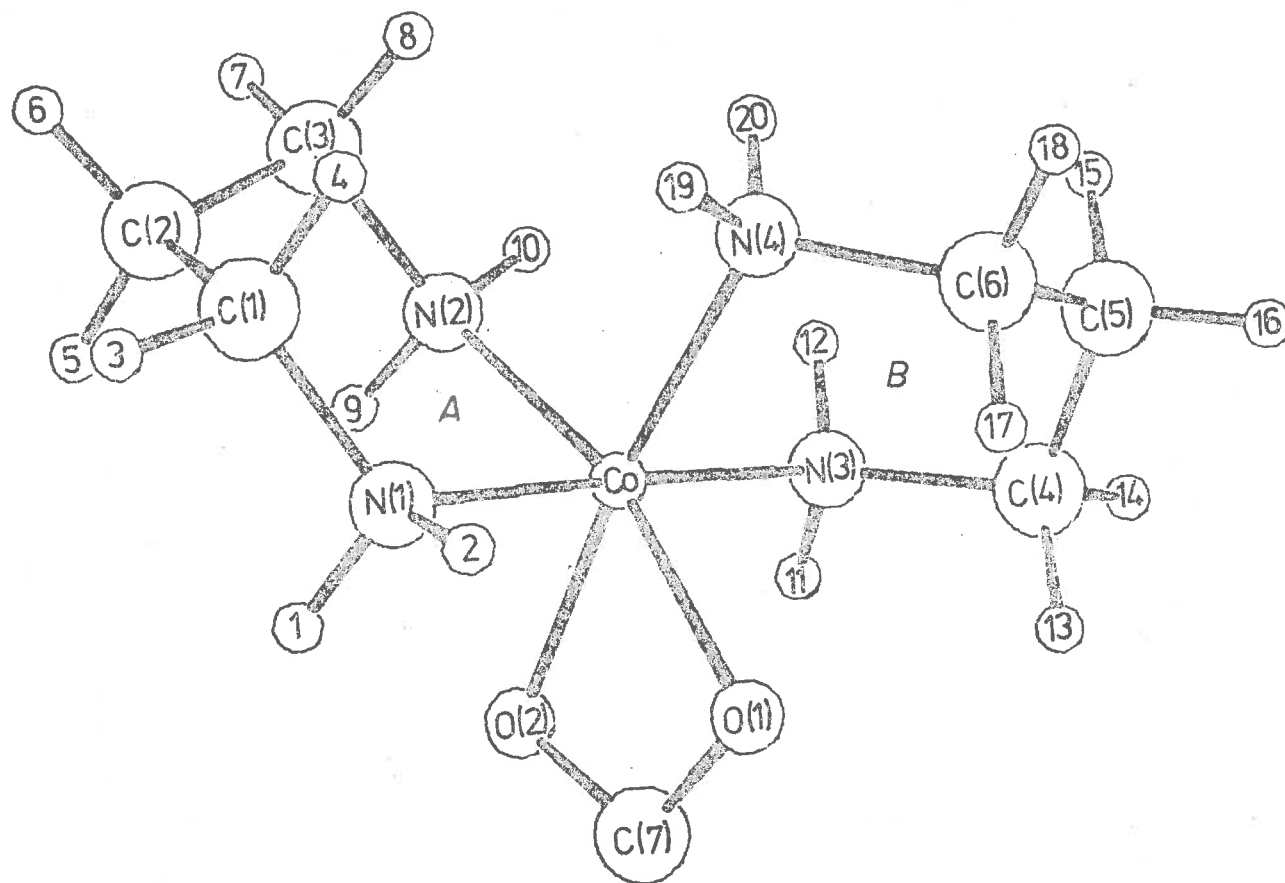


FIGURE 5.8. PERSPECTIVE VIEW OF  $\Delta$ -[Co(tn)<sub>2</sub>CO<sub>3</sub>chair<sub>2</sub>]<sup>+</sup>: AB FORM.  
The carbonyl oxygen was deleted.



TABLE 5.14 FINAL ORTHOGONAL COORDINATES FOR  $\Delta$ -[Co(tn)<sub>2</sub>CO<sub>3</sub>chair<sub>2</sub>]<sup>+</sup>:

AB FORM <sup>a</sup>							
Atom	X	Y	Z	Atom	X	Y	Z
Co	4.122	2.452	0.827	H(4)	1.283	0.806	1.203
N(1)	2.796	1.356	-0.175	H(5)	0.885	3.192	-0.548
N(2)	2.794	3.882	1.143	H(6)	-0.280	2.587	0.562
N(3)	5.505	3.499	1.790	H(7)	0.813	4.344	1.658
N(4)	3.752	1.518	2.510	H(8)	1.392	2.902	2.380
O(1)	5.428	1.356	0.036	H(9)	2.773	4.422	0.313
O(2)	4.690	3.232	-0.789	H(10)	3.120	4.473	1.866
C(1)	1.367	1.305	0.271	H(11)	5.933	4.115	1.143
C(2)	0.761	2.679	0.373	H(12)	5.083	4.053	2.493
C(3)	1.395	3.473	1.485	H(13)	7.025	2.033	1.708
C(4)	6.564	2.657	2.432	H(14)	7.315	3.292	2.833
C(5)	5.998	1.812	3.547	H(15)	5.561	2.443	4.281
C(6)	4.966	0.827	3.052	H(16)	6.790	1.277	4.009
C(7)	5.548	2.244	-0.928	H(17)	5.391	0.214	2.298
H(1)	2.817	1.670	-1.115	H(18)	4.677	0.198	3.858
H(2)	3.153	0.431	-0.166	H(19)	3.046	0.839	2.377
H(3)	0.809	0.742	-0.437	H(20)	3.428	2.176	3.175

<sup>a</sup> In Å. The torsion energy about a single bond was described as a function of one torsion angle only.

The carbonyl oxygen was not included in the refinement.

TABLE 5.15 REFINED INTERNAL GEOMETRY OF THE  $\Delta$ -[Co(tn)<sub>2</sub>CO<sub>3</sub>chair<sub>2</sub>]<sup>+</sup>MOLECULE: AB FORM<sup>a</sup>*Bond lengths*

Co-N(1)	1.992 <sup>o</sup> Å	N(3)-C(4)	1.498 <sup>o</sup> Å
Co-N(2)	1.977	C(4)-C(5)	1.510
Co-N(3)	1.984	C(5)-C(6)	1.510
Co-N(4)	1.960	C(6)-N(4)	1.498
N(1)-C(1)	1.498	Co-O(1)	1.879
C(1)-C(2)	1.506	Co-O(2)	1.882
C(2)-C(3)	1.506	O(1)-C(7)	1.316
C(3)-N(2)	1.497	C(7)-O(2)	1.316

(contd.)

TABLE 5.15 (contd.)

*Bond angles*

N(1)-Co-N(2)	91.80°	O(1)-C(7)-O(2)	111.65°
Co-N(1)-C(1)	120.23	Co-O(2)-C(7)	88.67
N(1)-C(1)-C(2)	111.91	N(1)-Co-O(1)	85.94
C(1)-C(2)-C(3)	111.18	N(1)-Co-O(2)	89.82
C(2)-C(3)-N(2)	111.62	N(1)-Co-N(3)	177.45
Co-N(2)-C(3)	117.82	N(1)-Co-N(4)	92.53
N(3)-Co-N(4)	88.09	N(2)-Co-O(1)	162.93
Co-N(3)-C(4)	113.86	N(2)-Co-O(2)	92.32
N(3)-C(4)-C(5)	111.47	N(2)-Co-N(3)	90.55
C(4)-C(5)-C(6)	112.26	N(2)-Co-N(4)	94.64
C(5)-C(6)-N(4)	111.82	N(3)-Co-O(1)	91.57
Co-N(4)-C(6)	112.20	N(3)-Co-O(2)	89.28
O(1)-Co-O(2)	70.75	N(4)-Co-O(1)	102.39
Co-O(1)-C(7)	38.80	N(4)-Co-O(2)	172.61

*Close contacts*

H(1)...H(3)	2.314 <sup>a</sup>	H(8)...H(20)	2.303 <sup>a</sup>
H(2)...H(4)	2.348	H(10)...H(12)	2.103
H(6)...H(7)	2.342	H(2)...O(1)	2.464
H(7)...H(10)	2.321	H(1)...O(2)	2.461
H(11)...H(14)	2.333	H(13)...O(1)	2.410
H(18)...H(19)	2.295	H(11)...O(2)	2.461
H(4)...H(19)	2.119		

*Torsion angles*

Co-N(1)-C(1)-C(2)	+55.26°	Co-N(3)-C(4)-C(5)	-65.97°
N(1)-C(1)-C(2)-C(3)	-67.30	N(3)-C(4)-C(5)-C(6)	+62.64
C(1)-C(2)-C(3)-N(2)	+71.51	C(4)-C(5)-C(6)-N(4)	-65.08
C(2)-C(3)-N(2)-Co	-61.84	C(5)-C(6)-N(4)-Co	+69.67

<sup>a</sup> The carbonyl oxygen was not included in the refinement and the torsion energy about a single bond was described as a function of one torsion angle only.

with Co...C(4) (atomic notation is shown in Figure 5.9), and were referenced to a coordinate system in which the Z axis was collinear with this  $C_2$  and Y lay approximately along the Co-N(1) bond. The chelate rings for this trial structure were in the  $\Delta$  configuration.<sup>29</sup>

The independent energy minimization of the above model was executed using the same general force field and conditions described for the  $AB-\Delta-[Co(tn)_2CO_3chair_2]^+$  conformer and was dependent on 225 interactions. The coordinates X,Y,Z of Co, X,Z of N(1) and Z of C(1) were constrained during the refinement which converged (within an RMS shift of 0.005 Å) to a *true* minimum energy geometry having  $C_2$  symmetry in 25 cycles (.14 sec/cycle). The equilibrium Cartesian coordinates, internal geometry, and total strain energies are given in Tables 5.16, 5.17 and 5.20, and the final molecule is illustrated in Figure 5.9.

*The  $BB-\Delta-[Co(tn)_2CO_3chair_2]^+$  Isomer*

This molecule is also expected to have a *true* minimum energy arrangement with  $C_2$  symmetry (Figure 5.10). The Cartesian coordinates for the initial trial molecule were generated in a manner similar to those for the AA isomer above. For this isomer however, three independent minimizations were performed, in order to compare results obtained using the reduced force field above (*i.e.* with the incomplete torsion energy description and the carbonyl oxygen deleted) with those found for the complete molecule using the more rigorous torsion energy description of the previous analyses (Sections 5.5.1 and 5.5.2). For the first refinement the carbonyl oxygen was deleted and the single angle torsion

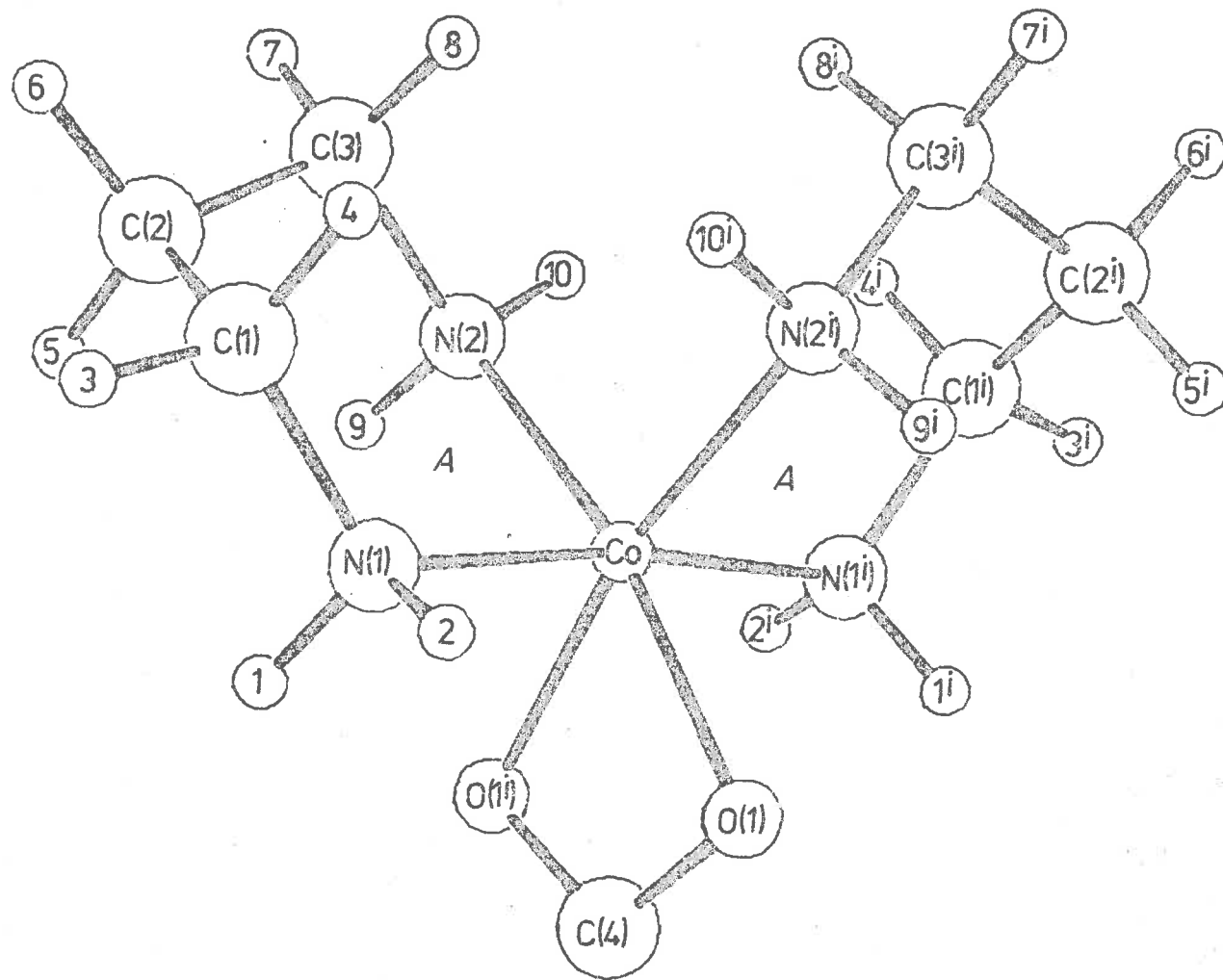


FIGURE 5.9. PERSPECTIVE VIEW OF  $\Delta$ -[Co(tn)<sub>2</sub>CO<sub>3</sub>chair<sub>2</sub>]<sup>+</sup>: AA FORM  $\perp^r$  TO THE C<sub>2</sub> AXIS.  
The carbonyl oxygen was deleted.

TABLE 5.16. FINAL ORTHOGONAL COORDINATES FOR  $\Delta$ -[Co(tn)<sub>2</sub>CO<sub>3</sub>chair<sub>2</sub>]<sup>+</sup>:AA FORM.<sup>a</sup>

Atom	X	Y	Z	Atom	X	Y	Z
Co	0.000	0.000	0.000	H(4)	-0.468	2.720	1.818
N(1)	0.337	1.970	0.000	H(5)	2.432	2.018	1.666
N(2)	1.155	-0.287	1.565	H(6)	1.667	2.714	3.040
N(1 <sup>1</sup> )	-0.289	-1.961	-0.235	H(7)	1.754	0.412	3.450
N(2 <sup>1</sup> )	-1.695	0.207	0.975	H(8)	0.120	0.764	3.073
O(1)	-0.735	0.245	-1.717	H(9)	2.076	-0.310	1.201
O(1 <sup>1</sup> )	1.371	-0.161	-1.281	H(10)	0.975	-1.179	1.948
C(1)	0.462	2.695	1.311	H(1 <sup>1</sup> )	-0.821	-2.080	-1.062
C(2)	1.515	2.085	2.197	H(2 <sup>1</sup> )	0.611	-2.341	-0.406
C(3)	1.100	0.718	2.672	H(3 <sup>1</sup> )	-1.093	-3.757	0.487
C(4)	0.470	0.062	-2.217	H(4 <sup>1</sup> )	-0.290	-2.850	1.689
C(1 <sup>1</sup> )	-0.931	-2.771	0.849	H(5 <sup>1</sup> )	-2.882	-2.083	0.418
C(2 <sup>1</sup> )	-2.258	-2.195	1.269	H(6 <sup>1</sup> )	-2.732	-2.868	1.940
C(3 <sup>1</sup> )	-2.080	-0.863	1.949	H(7 <sup>1</sup> )	-2.996	-0.592	2.415
H(1)	1.162	2.132	-0.524	H(8 <sup>1</sup> )	-1.344	-0.946	2.707
H(2)	-0.417	2.373	-0.502	H(9 <sup>1</sup> )	-2.389	0.260	0.269
H(3)	0.734	3.703	1.114	H(10 <sup>1</sup> )	-1.703	1.073	1.449

Symmetry operation<sup>b</sup> described by the superscripts in Tables 5.16 and 5.17i C<sub>2</sub>

<sup>a</sup> In Å. Transformation matrices associated with the C<sub>2</sub> operation may be computed from the coordinates. The torsion energy of a bond in this refinement was described as a function of one torsion angle only. The carbonyl oxygen was not included in the refinement.

<sup>b</sup> The C<sub>2</sub> element in this refinement is not present rigorously since the convergence limit was set to a relatively high value (R.M.S. coordinate shift of 0.005) compared with subsequent refinements. However, the limit is sufficiently accurate for comparison of internal geometries and energies with experimental results.

**TABLE 5.17.** REFINED INTERNAL GEOMETRY OF THE  $\Delta$ -[Co(tn)<sub>2</sub>CO<sub>3</sub>chair<sub>2</sub>]<sup>+</sup>  
MOLECULE: AA FORM.<sup>a</sup>

*Bond lengths*

Co-N(1)	1.997Å	C(1)-C(2)	1.505Å
Co-N(2)	1.966	C(2)-C(3)	1.506
Co-O(1)	1.883	C(3)-N(2)	1.497
N(1)-C(1)	1.501	O(1)-C(4)	1.318

*Bond angles*

N(1)-Co-N(2)	92.36°	N(1)-Co-O(1)	86.52°
Co-N(1)-C(1)	119.92	N(1)-Co-O(1 <sup>1</sup> )	87.88
N(1)-C(1)-C(2)	112.00	N(1)-Co-N(1 <sup>1</sup> )	173.10
C(1)-C(2)-C(3)	111.11	N(1)-Co-N(2 <sup>1</sup> )	92.37
C(2)-C(3)-N(2)	111.58	N(2)-Co-O(1)	166.91
Co-N(2)-C(3)	117.97	N(2)-Co-O(1 <sup>1</sup> )	95.83
O(1)-Co-O(1 <sup>1</sup> ) <sup>b</sup>	71.04	N(2)-Co-N(1 <sup>1</sup> )	92.01
Co-O(1)-C(4)	88.36	N(2)-Co-N(2 <sup>1</sup> )	97.30
O(1)-C(4)-O(1 <sup>1</sup> )	112.25		

*Close contacts*

H(1)...H(3)	2.304Å	H(1)...O(1 <sup>1</sup> )	2.421Å
H(2)...H(4)	2.342	H(2)...O(1)	2.469
H(3)...H(6)	2.361	H(8)...H(8 <sup>1</sup> )	2.281
H(6)...H(7)	2.340	H(10)...H(4 <sup>1</sup> )	2.101
H(7)...H(10)	2.321		

*Torsion angles*

Co-N(1)-C(1)-C(2)	+54.36°	C(1)-C(2)-C(3)-N(2)	+71.97°
N(1)-C(1)-C(2)-C(3)	-67.63	C(2)-C(3)-N(2)-Co	-61.59

<sup>a</sup> The average of  $C_2$  related geometry is presented. The carbonyl oxygen was not included in the refinement and the torsion energy about a single bond was described as a function of one torsion angle only.

<sup>b</sup> See Table 5.16 for the definition of the symmetry operation.

description was used (as for AA and AB); for the second the carbonyl oxygen was included, and for the third the carbonyl oxygen was included with a full torsion angle field. The remainder of the force field was of the same general nature as that used for the AA and AB isomers. These force fields then comprised 224, 227 and 288 interactions respectively near convergence and the coordinates  $X, Y, Z$  of Co,  $X, Z$  of N(1) and  $Z$  of C(1) were fixed for the refinements which converged in 8, 10 and 11 cycles to *true* minimum energy geometries with  $C_2$  symmetry (within the convergence limits of  $(\sum \Delta X_i^2 / (3N - 6))^{1/2} < 0.005 \text{ \AA}$  for the first and  $\Delta X_i < 0.002 \text{ \AA}$ ;  $i = 1 \dots 3N - 6$  for the others). The *final* Cartesian coordinates, internal geometries and total strain energies of these independent minimizations are listed in Tables 5.18, 5.19 and 5.20, and the equilibrium conformation of the  $BB-A-[Co(tn)_2-CO_3\text{chair}_2]^+$  isomer is shown in Figure 5.10. It is apparent that the equilibrium geometries are only trivially different for the three refinements except for the Co-CO<sub>3</sub> ring angles, which are significantly altered when the carbonyl oxygen (O(2)) in the form of the O(1)-C(4)=O(2) bending interaction is included in the force field. The force constant for this interaction is probably over-estimated with respect to the other angular force constants for the Co-CO<sub>3</sub> ring (Table 5.1).

An additional energy minimization of the  $BB-A-[Co(tn)_2CO_3\text{chair}_2]^+$  conformer was conducted according to the symmetry-dependent refinement procedure of Section 5.4.2 in which the  $C_2$  symmetry constraint was imposed. For this the variable asymmetric unit comprised 50 refining coordinates and was defined by a force field of 141 interactions. The

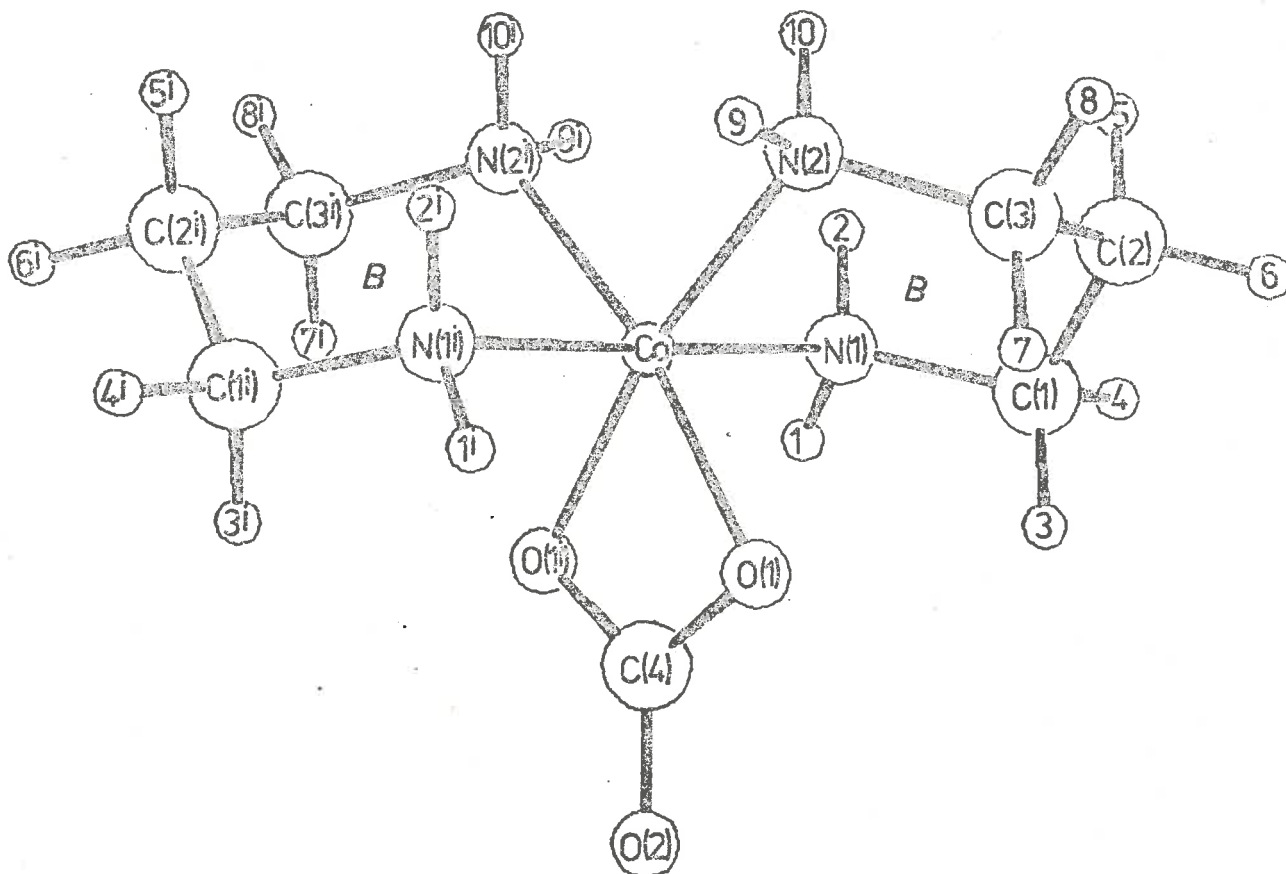


FIGURE 5.10.  $\Delta$ -[Co(tn)<sub>2</sub>CO<sub>3</sub>chair<sub>2</sub>]<sup>+</sup>: BB FORM, VIEWED  $\perp^F$  TO THE  $C_2$  AXIS.



TABLE 5.18. FINAL ORTHOGONAL COORDINATES FOR  $\Delta$ -[Co(tn)<sub>2</sub>CO<sub>3</sub>chair<sub>2</sub>]<sup>+</sup>:BB FORM.<sup>a</sup>

Atom	X	Y	Z	Atom	X	Y	Z
Co	0.000	0.000	0.000	N(4)	1.166	3.661	-0.350
N(1)	-0.043	1.983	0.000	H(5)	1.801	2.750	1.815
N(2)	1.315	0.114	1.467	H(6)	3.138	2.886	0.745
N(1 <sup>1</sup> )	0.036	-1.981	0.092	H(7)	2.967	0.507	0.214
N(2 <sup>1</sup> )	-1.521	-0.055	1.255	H(8)	3.254	0.797	1.879
O(1)	1.228	-0.116	-1.421	H(9)	1.599	-0.796	1.729
O(2)	0.260	-0.074	-3.427	H(10)	0.883	0.534	2.254
O(1 <sup>1</sup> )	-0.999	0.050	-1.594	H(1 <sup>1</sup> )	0.760	-2.306	-0.502
C(1)	1.295	2.612	-0.237	H(2 <sup>1</sup> )	0.252	-2.275	1.013
C(2)	2.229	2.365	0.923	H(3 <sup>1</sup> )	-1.538	-2.293	-1.283
C(3)	2.538	0.898	1.101	H(4 <sup>1</sup> )	-1.112	-3.676	-0.364
C(4)	0.166	-0.048	-2.191	H(5 <sup>1</sup> )	-2.063	-2.675	1.639
C(1 <sup>1</sup> )	-1.253	-2.624	-0.317	H(6 <sup>1</sup> )	-3.224	-2.861	0.386
C(2 <sup>1</sup> )	-2.350	-2.330	0.677	H(7 <sup>1</sup> )	-2.967	-0.507	-0.215
C(3 <sup>1</sup> )	-2.678	-0.858	0.743	H(8 <sup>1</sup> )	-3.503	-0.726	1.399
H(1)	-0.668	2.280	-0.710	H(9 <sup>1</sup> )	-1.839	0.865	1.431
H(2)	-0.395	2.315	0.864	H(10 <sup>1</sup> )	-1.215	-0.439	2.116
H(3)	1.722	2.241	-1.134				

Symmetry operation described by the superscripts in Tables 5.18 and 5.19

1 C<sub>2</sub>

<sup>a</sup> In Å. Transformation matrices associated with the C<sub>2</sub> operation may be computed from the coordinate list. These are the coordinates from the independent refinement in which the torsion energy of a bond was described as a function of all torsion angles about the bond (nine for bonds between tetrahedral atoms).

TABLE 5.19. REFINED INTERNAL GEOMETRY OF THE  $\Delta$ -[Co(tn)<sub>2</sub>CO<sub>3</sub>chair<sub>2</sub>]<sup>+</sup>MOLECULE: BB FORM.<sup>a</sup>*Bond lengths*

Atoms	Independent 1 <sup>b</sup>	Independent 2 <sup>c</sup>	C <sub>2</sub> constrained <sup>c</sup>	Independent 3 <sup>c,d</sup>
Co-N(1)	1.984Å	1.983Å	1.983Å	1.983Å
Co-N(2)	1.973	1.972	1.972	1.970
Co-O(1)	1.882	1.882	1.882	1.878
N(1)-C(1)	1.497	1.497	1.497	1.498
C(1)-C(2)	1.510	1.510	1.510	1.510
C(2)-C(3)	1.510	1.510	1.510	1.510
C(3)-N(2)	1.498	1.498	1.498	1.498
O(1)-C(4)	1.313	1.313	1.313	1.315
C(4)-O(2)	1.240	1.240	1.240	d

*Bond angles*

N(1)-Co-N(2)	87.51°	87.52°	87.53°	87.65°
Co-N(1)-C(1)	113.60	113.69	113.70	113.63
N(1)-C(1)-C(2)	111.27	111.44	111.44	111.47
C(1)-C(2)-C(3)	112.11	112.33	112.33	112.33
C(2)-C(3)-N(2)	111.72	111.87	111.87	111.85
Co-N(2)-C(3)	113.15	113.22	113.22	112.92
O(1)-Co-O(1 <sup>1</sup> ) <sup>e</sup>	73.05	73.04	73.04	70.59
Co-O(1)-C(4)	84.94	84.95	84.95	89.08
O(1)-C(4)-O(1 <sup>1</sup> )	117.07	117.06	117.06	111.25
O(1)-C(4)-O(2)	121.47	121.47	121.47	d
N(1)-Co-O(1)	94.35	94.38	94.39	94.02
N(1)-Co-O(1 <sup>1</sup> )	87.81	87.71	87.69	87.83
N(1)-Co-N(1 <sup>1</sup> )	177.08	177.40	177.00	177.38
N(1)-Co-N(2 <sup>1</sup> )	90.64	90.65	90.68	90.75
N(2)-Co-O(1)	97.48	97.47	97.47	98.66
N(2)-Co-O(1 <sup>1</sup> )	169.20	169.08	168.98	168.08
N(2)-Co-N(1 <sup>1</sup> )	90.64	90.66	90.68	90.78
N(2)-Co-N(2 <sup>1</sup> )	92.44	92.47	92.48	92.51

(contd.)

TABLE 5.19. (contd.)

## Close contacts

Atoms	Independent 1 <sup>b</sup>	Independent 2 <sup>c</sup>	$C_2$ constrained <sup>c</sup>	Independent 3 <sup>c,d</sup>
H(1)...H(4)	2.324Å	2.323Å	2.323Å	2.325Å
H(4)...H(6)	2.385	2.389	2.389	2.390
H(6)...H(8)	2.380	2.383	2.383	2.382
H(8)...H(9)	2.302	2.301	2.301	2.300
H(1)...O(1 <sup>1</sup> )	2.421	2.427	2.425	2.430
H(2)...H(9 <sup>1</sup> )	2.125	2.128	2.129	2.130
H(3)...O(1)	2.425	2.426	2.426	2.426
H(7)...O(1)	2.466	2.463	2.463	2.480
H(10)...H(10 <sup>1</sup> )	2.317	2.314	2.315	2.323
<i>Torsion angles</i>				
Co-N(1)-C(1)-C(2)	-67.83°	-67.49°	-67.51°	-67.23°
N(1)-C(1)-C(2)-C(3)	+63.86	+63.24	+63.23	+63.11
C(1)-C(2)-C(3)-N(2)	-64.42	-63.86	-63.84	-64.10
C(2)-C(3)-N(2)-Co	+68.49	+68.27	+68.25	+68.60

<sup>a</sup> The independent refinements converged with  $C_2$  symmetry. Only asymmetric geometry is presented.

<sup>b</sup> Torsion energy about a single bond was described as a function of nine torsion angles.

<sup>c</sup> Torsion energy about a single bond was described as a function of one torsion angle only.

<sup>d</sup> In this refinement the carbonyl oxygen was not included.

<sup>e</sup> See Table 5.18 for the definition of the symmetry operation.

TABLE 5.20. FINAL STRAIN ENERGIES<sup>a</sup> OF THE  $[\text{Co}(\text{tn})_2\text{CO}_3\text{chair}_2]^+$  MOLECULES.

Conformer	Refinement	$\Sigma U_B$	$\Sigma U_{NB}$	$\Sigma U_\theta$	$\Sigma U_\phi$	$U_{TOTAL}$
AB	Independent 3	1.98	7.12	4.36	0.51	13.97
AA	Independent 3	2.28	7.32	6.43	0.72	16.74
BB	Independent 3	1.87	7.09	2.63	0.35	11.94
BB	Independent 1	2.02	7.56	2.42	0.28	12.27
BB	Independent 2	2.00	7.48	2.52	0.34	12.34
BB	$C_2$ constrained	1.99	7.49	2.52	0.34	12.34

<sup>a</sup> All energies in kcal mol<sup>-1</sup>.

<sup>b</sup> The conditions under which independent refinements 1, 2, 3 and the  $C_2$  refinement were done are described in Table 5.19.

force field was of the same general form as that used for the independent refinement of the complete molecule above (*i.e.* with the carbonyl oxygen included) with the single dihedral angle torsion energy description. The coordinates  $X, Y, Z$  of Co,  $X, Y$  of C(4) and  $X, Y$  of O(2) were constrained for the reasons outlined in Section 5.4.2. However motion of the asymmetric unit around the  $C_2$  axis was not constrained, and the refinement required 32 cycles (3 sec/cycle) to achieve equilibrium, due to a convergent oscillation of the molecule around the symmetry axis. This was probably caused by the deficiency of strong connective interactions between the Co-tn rings, and the consequent low curvature and gradient dependence of the function  $U_{TOTAL}$  with respect to motion of the asymmetric unit in this direction. Nevertheless the efficiency of the procedure compared with the equivalent independent refinement (10 cycles at 16 sec/cycle) is still evident, and would be considerably enhanced by imposing the correct constraints on the above oscillatory motion. The *final* geometries and energies for this refinement are also given in Tables 5.19 and 5.20, and, as expected, the equilibrium configuration is essentially identical to that obtained for the equivalent independent minimization (*i.e.* *Independent 2* in Tables 5.19 and 5.20).

#### *Comparison of the Minimized Chair Conformers*

In this discussion, the *final* geometries and energies of the AB, AA and BB isomers refined under the equivalently defined force fields (*i.e.* with the carbonyl oxygen deleted and single torsion angle description) are compared for consistency. In any case it is apparent from the above considerations that the *final* geometry of the BB isomer refined under the

more complete force field is only trivially different except for the Co-CO<sub>3</sub> ring angles.

The major energy differences (Table 5.20) and variations in the internal Co-tn ring geometries (Tables 5.15, 5.17 and 5.19) for these conformers are induced by the N-H...N-H and N-H...C-H inter-ring interactions. In addition some C-H...O(carboxyl) and N-H...O(carboxyl) repulsions may be of some importance in determining the final conformational differences between the A and B rings, but these are similar in magnitude and number, and do not largely affect the *final* energy differences between the AB, AA and BB isomers.

It is obvious, from a comparison of the internal geometries in Tables 5.15, 5.17 and 5.19, that the rings designated A in the AB and AA isomers (Figures 5.8 and 5.9) have very similar internal coordinates and conformations despite their different environments. This is due to the fact that the inter-ring H...H repulsions inducing distortion in these rings act on the same atoms and are relieved (in the A rings) by similar conformational and geometrical changes in both the AB and AA complexes. Thus in the AB isomer the atoms H(4), H(8) and H(10) of ring A (Figure 5.8) are involved in the close contacts H(4)...H(19) (2.12 Å, 0.6 kcal mol<sup>-1</sup>), H(8)...H(20) (2.30 Å, 0.2 kcal mol<sup>-1</sup>) and H(10)...H(12) (2.10 Å, 0.7 kcal mol<sup>-1</sup>). These are largely relieved in the energy minimized configuration by the expansion of the Co-N(1)-C(1) (120.2°, 1.0 kcal mol<sup>-1</sup>) and Co-N(2)-C(3) (117.8°, 0.6 kcal mol<sup>-1</sup>) ligand angles, and by the decrease in the Co-N(1)-C(1)-C(2) and Co-N(2)-C(3)-C(2) torsion angles to 55° and 62° (-68° in the free Co-tn

ring<sup>256</sup>). This same form of N-H...N-H and C-H...N-H interaction is observed between the chair rings of the symmetric  $[\text{Co}(\text{tn})_3\text{chair}_3]^{3+}$  isomer (Section 5.5.2), and the distortions found in the *A* ring here are similar but not as great as those found in the chelate rings of the tris-chair complex. In the *AA* isomer of  $[\text{Co}(\text{tn})_2\text{CO}_3]^+$  the atoms H(4), H(8) and H(10) of the *A* rings (similar to those in the *AB* isomer as seen from Figures 5.8 and 5.9) are involved in the close contacts H(4)...H(10<sup>1</sup>) (2.10 Å, 0.7 kcal mol<sup>-1</sup>), H(8)...H(8<sup>1</sup>) (2.28 Å, 0.3 kcal mol<sup>-1</sup>) and H(10)...H(4<sup>1</sup>) (symmetry-related to H(4)...H(10<sup>1</sup>)). These are relieved in a similar manner to those above through the expansion of the Co-N(1)-C(1) (119.9°, 0.9 kcal mol<sup>-1</sup>) and Co-N(2)-C(3) (118.0°, 0.6 kcal mol<sup>-1</sup>) ligand angles of each *A* ring, and through the decrease in the Co-N(1)-C(1)-C(2) and Co-N(2)-C(3)-C(2) torsion angles to 54° and 62°. These and the distortions induced in the angular geometry of the hydrogen atoms largely account for the net strain energy differences between the *AB* (14.0 kcal mol<sup>-1</sup>) and *AA* (16.7 kcal mol<sup>-1</sup>) isomers (Table 5.20).

By comparing the internal geometries of the *B* rings for the *AB* and *BB* conformers (Tables 5.15 and 5.19), it is evident that they also have similar geometries and conformations in each isomer and are relatively less distorted than the *A* rings. Again the same *B* ring atoms are involved in repulsive H...H inter-ring interactions for both the *AB* and *BB* complexes. The directions of the forces on these atoms are also similar in both conformers, and this leads to the equivalent minimized geometries for the *B* rings. The close contacts most important in determining the final

*B* ring geometry in the *AB* isomer are the H(4)...H(19), H(8)...H(20) and H(10)...H(12) repulsions mentioned previously (Figure 5.8). However these are not very effectively relieved through angular distortions or torsional twists in the *B* ring, which then remains relatively undistorted in the final conformation. In the *BB* isomer (Figure 5.10), the atoms H(2), H(9) and H(10) (similar to the above atoms H(12), H(19), H(20) of the *B* ring in *AB*) are involved in the close contacts H(2)...H(9<sup>1</sup>) (2.13 Å, 0.6 kcal mol<sup>-1</sup>), H(10)...H(10<sup>1</sup>) (2.32 Å, 0.2 kcal mol<sup>-1</sup>) and H(9)...H(2<sup>1</sup>) (symmetry-related to H(2)...H(9<sup>1</sup>)). These interactions are not initially as strongly repulsive as those in the *AB* isomer, which are relieved through distortion of the *A* ring. Hence the *B* rings of *BB* also remain relatively undistorted, since these close contacts are not as effectively relieved through angular or torsional distortion in the *BB* conformer. At the same time the non-bonded inter-ring strain for the final *AB* and *BB* conformations is similar because of the initially weaker repulsions in *BB*. These, and the above considerations of the *AB* and *AA* differences, then lead to the conclusion that the *final* net strain energy differences between the three chair conformers of [Co(tn)<sub>2</sub>CO<sub>3</sub>]<sup>+</sup> are largely determined by differences in the angular strain of the final *A* and *B* rings. This is supported by the results presented in Table 5.20, which lists the final strain energies for the *AA*, *AB* and *BB* conformers as 16.7, 14.0 and 11.9 kcal mol<sup>-1</sup>.

#### 5.5.4 Discussion of the Geometric Isomers of [Co(dien)<sub>2</sub>]<sup>3+</sup>

The preparation, characterization and configurational aspects of

the symmetric facial (*s-facial*), the unsymmetric facial (*u-facial*) and the meridional (*mer*) geometric isomers of the  $[\text{Co}(\text{dien})_2]^{3+}$  complex ion have recently been described in considerable detail.<sup>274-276</sup> In addition the X-ray crystal structures of some conformers of these geometric isomers have been determined,<sup>277,278</sup> and several Newton-Raphson molecular energy minimizations have also been conducted on these and other conformers using the procedures outlined in Sections 5.3 and 5.4.<sup>56,74,75</sup>

#### *The s-facial- $[\text{Co}(\text{dien})_2]^{3+}$ Conformers*

In the *s-facial- $[\text{Co}(\text{dien})_2]^{3+}$*  isomer,<sup>56,274-277</sup> (Figure 5.11(a)) the secondary nitrogen donors of the two dien ligands are *trans* to each other (through Co) while the primary nitrogens within each ligand occupy *cis* positions in the coordination sphere. If the  $\lambda$  and  $\delta$  conformations for each of the four chelate rings are considered, it is evident from a Dreiding model of the *s-facial* isomer that there are ten configurationally distinct conformational isomers possible. However, six of these are dissymmetric optical isomers (including the mirror image pairs), and as a result there are only seven geometrically and energetically distinct conformers. These may be designated  $(\lambda\delta, \lambda\delta)$ ,  $(\delta\lambda, \delta\lambda)$ ,  $(\lambda\delta, \delta\lambda)$ ,  $(\lambda\lambda, \delta\delta)$ ,  $(\delta\lambda, \lambda\lambda)$ ,  $(\lambda\delta, \lambda\lambda)$  and  $(\delta\lambda, \lambda\lambda)$  where  $\lambda$  and  $\delta$  refer to the conformations of the chelate rings 1,2,3 and 4 in Figure 5.11(a) in the order (1 2, 3 4). The  $(\lambda\delta, \lambda\delta)$  and  $(\delta\lambda, \delta\lambda)$  conformers have maximum symmetry configurations belonging to the point group  $C_{2h}$ , and from the considerations of Section 5.4.1 are expected to have saddle-points in  $U_{TOTAL}$  associated with the mirror plane at their energy minimized  $C_{2h}$  configurations. Consequently true minimum energy



configurations with both  $C_2$  and  $C_i$  symmetry are expected for each of these conformers (the symmetry-defined *local* minima of Section 5.4.1),

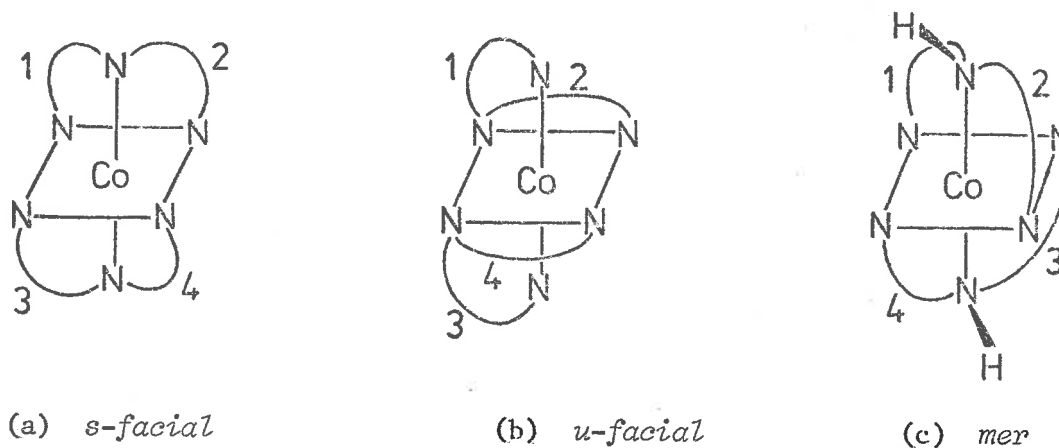


FIGURE 5.11. GEOMETRIC ISOMERS OF  $[\text{Co}(\text{dien})_2]^{3+}$ .

and fast symmetry-dependent refinement procedures (Section 5.4.2) utilizing the  $C_2$  and  $C_i$  symmetry elements may be used to locate these *true* minima when conducted under the conditions of Section 5.4.3. Alternatively, independent  $3N - 6$  coordinate minimizations performed under these conditions will converge to the same  $C_2$  and  $C_i$  *true* minimum energy configurations with much lower efficiency. The  $(\lambda\delta, \delta\lambda)$  conformer, which has a maximum symmetry configuration of  $C_s$  (one mirror plane) is also anticipated to have a saddle-point at the energy minimized  $C_s$  arrangement. Because of the relative independence of the dien ligands, two distinct *true* minimum energy geometries with asymmetric configurations are expected when this conformer is independently minimized (Section 5.4.1). The conformers  $(\lambda\lambda, \delta\delta)$ ,  $(\lambda\lambda, \lambda\lambda)$  and the pair  $(\lambda\delta, \lambda\lambda)$ ,  $(\delta\lambda, \lambda\lambda)$  have  $C_i$ ,  $C_2$  and  $C_1$  maximum symmetries respectively, and are expected to

have *true* minimum energy geometries with these point groups because of the absence of symmetry-defined energy saddle-points. The above energy minimized geometries need not all necessarily be distinct however, *e.g.* the  $C_2$  *true* minimum configuration of the starting conformer  $(\lambda\delta, \lambda\delta)$  could possibly be identical (in geometry and energy) to the  $(\lambda\lambda, \lambda\lambda)$  minimum energy configuration which also has  $C_2$  symmetry, if no minimum exists in the  $(\lambda\delta, \lambda\delta)$  conformation. The number and type of distinct *true* minimum energy geometries must then be determined by minimizing the energies of all of the above conformers.

The  $(\lambda\delta, \lambda\delta)$  conformer described above has been refined by Dwyer<sup>56,75</sup> using the Newton-Raphson energy minimization schemes described in Sections 5.3 and 5.4. An independent refinement of this conformer (maximum symmetry  $C_{2h}$ ) using the method of Section 5.4.3 converged to a *true* minimum energy geometry with exact  $C_1$  symmetry<sup>56</sup> as expected. To obtain the *local* minimum geometry with  $C_2$  symmetry from the same starting model would require the appropriate adjustment of coordinate constraints, as indicated in Section 5.4.3. Fast symmetry-dependent refinements (Section 5.4.2) constraining the conformer to  $C_1$  and  $C_{2h}$  symmetry were also effected<sup>56,75</sup> in order to further test the developments of Section 5.4. The converged geometry and energy of the  $C_1$ -dependent minimization was identical to that of the independent refinement<sup>56,75</sup> (within the convergence uncertainties). The minimized  $C_{2h}$  configuration however, was at a saddle-point with respect to anti-mirror symmetric translation vectors as expected, and converged to exactly the same  $C_1$  configuration as above when independently refined under similar constraint conditions.<sup>56,75</sup>

Finally this ( $\lambda\delta, \lambda\delta$ ) conformer with the  $C_1$  symmetric configuration has been observed in the crystal structure of *s-facial*-[Co(dien)<sub>2</sub>]Br<sub>3</sub>.<sup>277</sup> The observed geometry (determined to some extent by intermolecular hydrogen bonding and close crystal contacts) is closer to the minimized  $C_{2h}$  configuration than the *true* minimum energy  $C_1$  geometry,<sup>56</sup> but these differ only nominally in strain energy and internal geometry.<sup>56,75</sup>

*The u-facial*-[Co(dien)<sub>2</sub>]<sup>3+</sup> Conformers

In this isomer<sup>274-276,278</sup> (Figure 5.11(b)) the secondary nitrogen donors of the two dien ligands, as well as the primary nitrogens within each ligand, occupy *cis* positions in the coordination sphere. The absolute chelate ring configuration about Co is dissymmetric, and for a given absolute configuration ( $\Lambda$  or  $\Delta$ )<sup>29</sup> there are ten possible combinations of ring conformations which are geometrically and energetically distinct. These correspond to the ten configurationally (but not energetically) distinct conformational possibilities for the *s-facial* isomer above, and are designated ( $\lambda\delta, \lambda\delta$ ), ( $\delta\lambda, \delta\lambda$ ), ( $\lambda\lambda, \lambda\lambda$ ), ( $\delta\delta, \delta\delta$ ), ( $\lambda\delta, \lambda\lambda$ ), ( $\lambda\delta, \delta\delta$ ), ( $\delta\lambda, \lambda\lambda$ ), ( $\delta\lambda, \delta\delta$ ), ( $\lambda\delta, \delta\lambda$ ) and ( $\lambda\lambda, \delta\delta$ ). Here  $\delta$  and  $\lambda$  refer to the conformations of the chelate rings 1, 2, 3 and 4 in Figure 5.11(b) in the order (1 2, 3 4). The conformers ( $\lambda\delta, \lambda\delta$ ), ( $\delta\lambda, \delta\lambda$ ), ( $\lambda\lambda, \lambda\lambda$ ) and ( $\delta\delta, \delta\delta$ ) are expected to refine to *true* minimum energy configurations with  $C_2$  symmetry whereas the remainder are asymmetric. Again the *true* minimum energy configurations for these conformers may not all be distinct, and hence in some cases a refinement may converge with a conformation different from that of the starting conformer (but still one of the ten above).

Two of these  $C_2$  symmetric conformers, the  $\Delta(\lambda\delta, \lambda\delta)$  and the  $\Delta(\lambda\lambda, \lambda\lambda)$  were observed in the crystal structure of  $\Delta(-)_{589}$ -*u-facial*- $[\text{Co}(\text{dien})_2][\text{Co}(\text{CN})_6] \cdot 2\text{H}_2\text{O}$ .<sup>278</sup> The  $(\lambda\delta, \lambda\delta)$  conformer has also been independently energy minimized by Dwyer,<sup>75</sup> and this converged to a *true* minimum energy configuration having  $C_2$  symmetry and similar internal geometry to that found in the crystal.<sup>278</sup>

#### *The mer- $[\text{Co}(\text{dien})_2]^{3+}$ Conformers*

Both the secondary nitrogen donors of the two ligands and the primary nitrogens within each ligand assume *trans* positions in the  $\text{CoN}_6$  chromophore of this geometric isomer<sup>274-276</sup> (Figure 5.11(c)). The *mer* isomer is dissymmetric despite the chelate ring conformation, because of the dissymmetry imposed by the relative orientations of the two secondary nitrogen bonding frameworks with respect to each other.<sup>275,276</sup> Consequently for a given absolute configuration of this type there are ten possible geometrically and energetically distinct conformers. These are designated  $(\lambda\delta, \lambda\delta)$ ,  $(\delta\lambda, \delta\lambda)$ ,  $(\lambda\lambda, \lambda\lambda)$ ,  $(\delta\delta, \delta\delta)$ ,  $(\lambda\delta, \lambda\lambda)$ ,  $(\lambda\delta, \delta\delta)$ ,  $(\delta\lambda, \lambda\lambda)$ ,  $(\delta\lambda, \delta\delta)$ ,  $(\lambda\delta, \delta\lambda)$  and  $(\lambda\lambda, \delta\delta)$  where the ring conformations are in the order (1 2, 3 4) for the rings numbered 1, 2, 3 and 4 in Figure 5.11(c). The first four of the above conformers can have  $C_2$  symmetric conformations and the remainder are asymmetric. The existence of *true* minimum energy configurations for some of these conformers is not likely, because of the large internal ring strain generated when dien is coordinated in this fashion, and some very close N-H...C-H repulsive contacts. However, as before, the number of distinct *true* minimum energy conformations must be determined by minimizing the

energies of all of the above ten conformers. One of these, the  $(\lambda\delta, \lambda\delta)$ , has been minimized by the independent refinement methods of Sections 5.3 and 5.4.1<sup>75</sup> and converged to a *true* minimum energy geometry with  $C_2$  symmetry within the uncertainties imposed by the convergence criterion.

CHAPTER 6. ENERGY MINIMIZED CONFIGURATIONS AND THEIR SIGNED ROTATORY STRENGTHS

6.1 INTRODUCTION

If quantum theoretical models (or regional rules derived therefrom) correlating stereochemical configuration with the signs and/or relative magnitudes of the observed circular dichroism for the  $d-d$  transitions of transition metal complexes are reliably established, either generally or for particular complex classes, the detailed internal geometry of the complex must be accurately known in order to make reliable predictions of the absolute configuration. This is especially true if the optical activity is highly dependent on small dissymmetric distortions of the ligand donor atoms and the positions of atoms immediately connected with these, as indicated by the crystal-field static coupling<sup>68,70,73,150</sup> and molecular orbital<sup>69,72,153,156</sup> models for pseudo-octahedral  $D_3$  Co(III) complexes which were discussed in Chapter 4. For such predictions of absolute configuration from the observed visible CD, this knowledge of the detailed internal geometry must normally be obtained by some means other than that of X-ray or neutron solid state structural analysis.

Similarly, in order to accurately assess the validity of these theoretical correlation models when the absolute chirality about the metal atom is known, the detailed internal structure of the complex is required. If the absolute configuration was directly determined by the X-ray anomalous dispersion method<sup>18,19</sup> the solid state structural knowledge is generally incidental, and the relation between the complex stereochemistry and the observed microcrystalline visible CD<sup>199</sup> spectrum

of the same crystalline compound may be directly observed. However, if the chirality of the optical isomer was obtained by some relative means, *e.g.* chemical correlation (retention of configuration during synthesis), the method of active racemates,<sup>279,280</sup> the least soluble diastereoisomer approach,<sup>281,282</sup> X-ray powder diffraction correlations based on these<sup>15</sup> or the stereospecific coordination of optically active ligands,<sup>1-10</sup> the detailed intramolecular structural information is still generally unavailable and again must be indirectly obtained by comparison with similar known structures or from theoretical sources.

In addition it is usually important to have some knowledge of the particular conformational isomer present (for correlation with solid state CD spectra), or the possible conformer types and their relative proportions (for correlation with solution CD spectra) in a crystal or solution of the dissymmetric complex molecule. This information is often *necessary* for the determination of absolute configuration from the stereospecificity of optically active ligands of known configuration, which for metal chelate complexes usually depends on the known presence of a particular ring conformer from steric considerations.<sup>1-10,20-24</sup> For these reasons some idea of the standard free energy differences between conformers (ideally in their solid state or solution environments) is often required, to accurately assess or make predictions from the theoretical correlations between absolute stereochemical configuration and observed circular dichroism.

For metal chelate complexes which are inherently dissymmetric, *e.g.* tris-bidentate conformers, *cis*-bis-bidentate conformers, polydentate

conformers with helical ring structures or complexes which are dissymmetric solely because of conformational and/or vicinal asymmetric group (*i.e.* chromophoric or ligand group) effects, the required internal structural information is in principle obtainable from the energy minimized molecular conformations (Chapter 5), provided the minimization procedure is reliable and produces results in agreement with observed structural data. This should be true for both solution and solid state CD-absolute structure correlations, if environmentally induced distortions of these complexes are relatively small and not sufficient to traverse the nodes of the theoretical CD models. However when a dissymmetric complex suffers large lattice induced distortions, or an intrinsically symmetric complex is dissymmetrically perturbed in solution (*e.g.* by association with chiral solvent or counterion molecules)<sup>135-137</sup> or in the crystal (*e.g.* by crystallization in a dissymmetric space group),<sup>135,283,284</sup> energy minimized molecular configurations are not adequate for reproducing the complex dissymmetry, and do not give any account of the environmental configuration which in some instances may contribute significantly in the theoretical CD model. In these cases, theoretical solid state CD-structure correlations may still be possible if the energy minimized configuration is determined by a more elaborate procedure, in which the potential energy of the crystal lattice containing the complex compound is minimized with respect to all atomic coordinates in the asymmetric unit.<sup>237,245,256</sup> The most favourable molecular packing arrangement in the crystal (if unknown) must first be determined by a similar procedure<sup>58,59,237,243,245</sup> if this



approach is adopted however, and this may not be reliable for strongly hydrogen-bonded and/or ionic crystals of the type often formed by the complex compounds considered here.

The molecular energy minimization procedure may also be used to provide information on the possible conformers present in solution and their relative proportions, from a consideration of their *final* strain energy differences and calculated entropy (including statistical terms) differences,<sup>1-3,48-50,60-62</sup> provided this is not available from experimental sources (*e.g.* NMR studies<sup>25-28</sup> or solution equilibrium isomer separation studies<sup>5-8</sup>). However, in the solid state, energetically unfavourable conformers<sup>45,46,76</sup> may be stabilized by crystal packing forces (*e.g.* electrostatic, non-bonded and hydrogen-bonding interactions), and any theoretical information on the most likely conformer (or conformers) present in a crystal of the relevant complex may have to be obtained by molecular packing analysis.<sup>58,59,237,243,245</sup>

The Newton-Raphson energy minimization scheme<sup>54</sup> used here (Sections 5.3 and 5.4) has proven extremely efficient and reliable<sup>48,49,57,256</sup> (Section 5.5) in the determination of the minimum relative energies and equilibrium conformations of metal chelate complex molecules. Hence the detailed molecular structures of intrinsically dissymmetric chelate complexes obtained by this scheme should be adequate to establish both the solution and solid state CD-absolute structure correlations discussed above, if the environmentally induced distortions of the complex are not sufficient to reverse the theoretically predicted CD signs, and the contribution to the CD from the environmental configuration

(*e.g.* through hydrogen-bonding, crystal-field, dispersion, orbital interaction effects *etc.*) is relatively less than the intrinsic molecular contribution. This latter environmental contribution was discussed in Section 4.3.2, and in definitive cases (*i.e.* for known dissymmetric complex structures and conformations, *e.g.* ref. 199), is generally of relatively low magnitude unless there are very strong specific interactions<sup>204-211</sup> between the complex and the surrounding molecules. The magnitudes of lattice induced distortions commonly found in Co(III) chelate complexes of the type studied here are discussed in the following section, by comparison of observed solid state structural data with the energy minimized internal geometries of some of the Co(III) chelate conformers analysed in the previous Chapter.

## 6.2 COMPARISON OF OBSERVED AND CALCULATED DATA

The molecular energy minimization scheme described in Section 5.3 has previously been found to yield detailed equilibrium geometries for sterically hindered metal chelate complexes which are in close agreement with observed solid state structural data,<sup>2,48,49,56,75,76,248,249,251,256</sup> except for very flexible relatively unhindered chelate rings,<sup>251</sup> and in regions of strong specific repulsive lattice interactions.<sup>48</sup> In these latter cases however, it is usually the ring conformation which is grossly distorted, the bond length and angular geometries of the distorted rings often being closely similar to the energy minimized values. For the pseudo- $C_3$  and  $D_3$  Co(III) polyamine complexes and the  $[\text{Co}(\text{tn})_2\text{CO}_3]^+$  complex discussed here, the flexible six-membered Co-tn rings have

relatively rigid conformations determined by inter-ring steric and intra-ring torsional and steric interactions. The observed solid state and computed internal geometries of the  $[\text{Co}(\text{tame})_2\lambda\lambda]^{3+}$ ,  $[\text{Co}(\text{tn})_3\text{chair}_3]^{3+}$ ,  $\Delta\text{-}[\text{Co}(\text{R,R-ptn})_3]^{3+}$ ,  $\Lambda\text{-}[\text{Co}(\text{R,R-ptn})_3]^{3+}$  and  $\text{AB-}[\text{Co}(\text{tn})_2\text{CO}_3\text{chair}_2]^+$  complex isomers are respectively presented in Tables 6.1 to 6.5 which are self-explanatory.

*The  $[\text{Co}(\text{tame})_2\lambda\lambda]^{3+}$  Isomer*

The detailed intramolecular geometry of this isomer, observed in the crystal structure analysis of  $[\text{Co}(\text{tame})_2]\text{Cl}(+)_{589}\text{-tartrate}\cdot 5.4\text{H}_2\text{O}$ , was discussed in Chapter 3 and is illustrated in Figures 3.3 to 3.5. The computed equilibrium geometry was presented and discussed in Section 5.5.1 (Figures 5.1 and 5.2), and the internal coordinates for both structures are here compared in Table 6.1 with reference to the atomic notation scheme shown in Figures 5.1 and 5.2. Since the computed complex was exactly  $D_3$  symmetric and the observed structure was closely  $D_3$  (Chapter 3), only the mean values of the observed pseudo- $D_3$  related parameters are presented.

The observed and calculated bond lengths do not differ significantly except for the C(2)-C(3) distance where C(3) is the methyl carbon atom. However the observed thermal motion of C(3) is considerable, and the slightly longer observed value (1.543(3) Å *cf.* 1.517 Å) may be a function of the uncertainties introduced in the refinement as a result of this.

The observed angular geometry of the complex (including hydrogen atoms) is accurately reproduced by the energy minimized values (Table

6.1), despite the high accuracy of the structural analysis and the extensive hydrogen-bonding of the N-H hydrogen atoms in the crystal (Chapter 3). In particular the small observed relative trigonal twist of the two tame ligands, exemplified here by the expansion of the N(1)-Co-N(1<sup>iii</sup>) angles (93.5(1)° crystal, 92.0° minimized) and the compression of the N(1)-Co-N(1<sup>i</sup>) angles (88.8(1)° crystal, 88.3° computed), is similarly predicted by the molecular energy minimization. In addition the intra- and inter-ligand close contacts are essentially identical in the observed and computed molecules, allowing for the slight reduction in the X-ray N-H (0.91(2) Å) and C-H (0.99(2) Å) bond lengths from the minimized values (0.99 and 1.06 Å). The torsion angles about the N-C and C-C bonds defining the chelate ring conformations are slightly more eclipsed in the observed structure (28.8(2)° and 163.2(2)° *cf.* 32.5° and 160.7° calculated), but this is not sufficient to significantly alter the positional contributions to the *net* CD in the theoretical models discussed in Chapter 4. It is of interest to note that even the observed relative staggering of the methyl groups about the C(2)-C(3) bonds is predicted in the computed molecule (as shown by the torsion angles about C(2)-C(3) in Table 6.1), although this may be fortuitous because of the inaccuracies introduced by thermal motion effects in the observed methyl groups.

From the above discussion (and those in Sections 3.5 and 5.5.1) it appears that the observed solid state and computed geometries of  $[\text{Co}(\text{tame})_2\lambda\lambda]^{3+}$  are almost identical except for a very slight flattening of the chelate rings in the observed structure, which is probably caused

by the elaborate hydrogen-bonding network found here, since there are no obvious highly repulsive inter-ionic or inter-molecular close contacts in the crystal of  $[\text{Co}(\text{tame})_2]\text{Cl}(\text{+})_{589}\text{-tartrate}\cdot 5.4\text{H}_2\text{O}$  (Chapter 3). Consequently, despite the extensive hydrogen bonding of the complex cation in the solid, the intramolecular CD contributions in the crystal-field model<sup>70,71</sup> of Chapter 4 based on the non-donor atom positional coordinates are essentially similar for the observed and computed  $[\text{Co}(\text{tame})_2\lambda\lambda]^{3+}$  molecules. The very small differences in the  $\text{CoN}_6$  core geometries (Section 6.3) do result in significantly different contributions (in magnitude) to the *net* visible CD, due to the relatively large charges on the nitrogens and their close proximity to the Co atom, but the overall contribution is large and positive for both observed and calculated complexes in terms of the Richardson model<sup>70,71</sup> discussed in Section 4.4.2. Similarly the contributions of the  $\text{CoN}_6$  core to the CD of the trigonal components of the  ${}^1A_{1g} + {}^1T_{1g}$   $\text{Co}(\text{III})$  transition are similar in sign and magnitude for the two configurations according to the models of Piper and Karipades.<sup>68,69</sup>

#### The $[\text{Co}(\text{tn})_3\text{chair}_3]^{3+}$ Isomer

The observed geometries of the pseudo- $C_3$  symmetric conformer found in the crystal structures of  $(-)\text{589-}[\text{Co}(\text{tn})_3]\text{Cl}_3\cdot\text{H}_2\text{O}$ <sup>43</sup> and  $(-)\text{589-}[\text{Co}(\text{tn})_3]\text{Br}_3\cdot\text{H}_2\text{O}$ <sup>273</sup> are compared in Table 6.2 with the equilibrium geometry of the calculated complex ion, which was discussed in Section 5.5.2 (Figure 5.5). The computed complex was exactly  $C_3$  symmetric and the mean values for the pseudo- $C_3$  related internal coordinates of the observed structures are given here. In the structure of  $(-)\text{589-}$

$[\text{Co}(\text{tn})_3]\text{Cl}_3 \cdot \text{H}_2\text{O}$ <sup>43</sup> only the *B* and *C* rings were averaged because of errors in *A* caused by large thermal motion effects.

The intramolecular bond length geometry is identical for the three structures (Table 6.2) within the limits of accuracy imposed by the experimental determinations.<sup>43,273</sup> The angular geometry and the distortions induced by the inter-ring N-H...N-H and N-H...C-H contacts (Sections 5.5.2 and 5.5.3) are also closely similar, and only the N(1)-Co-N(2) chelate angles ( $91.0(1)^\circ$ ) and the C(1)-C(2)-C(3) ligand angles ( $113.6(2)^\circ$ ) of the more accurately determined  $(-)_589-[\text{Co}(\text{tn})_3]-\text{Cl}_3 \cdot \text{H}_2\text{O}$ <sup>43</sup> structure differ significantly from the corresponding calculated values ( $94.3^\circ$  and  $110.3^\circ$ ). However errors in the positional parameters were probably under-estimated in this structure because of the excessive thermal motion in part of the complex ion. Furthermore, the outer (C-C-C) sections of the chelate rings in this complex are not rigidly constrained by inter-ring steric interactions, and are readily susceptible to deformation by intermolecular lattice repulsions. The trends in the mean observed values for the Co-N-C-C and N-C-C-C torsion angles (especially those of the *C* ring in the trichloride structure<sup>43</sup>) are also reproduced by the energy minimized values.

Here again the lattice induced deformation of the  $[\text{Co}(\text{tn})_3\text{chair}_3]^{3+}$  isomer in crystal environments with few repulsive intermolecular close contacts<sup>43,273</sup> appears relatively small, despite the numerous hydrogen bonds formed with the complex ion. Both the observed distortions within the chelate rings, and to a lesser extent, the observed configurational deviation of the  $\text{CoN}_6$  core from  $O_h$  geometry (Section 6.3) are predicted

**TABLE 6.1** COMPARISON OF OBSERVED AND COMPUTED INTERNAL GEOMETRY OF  
 $[\text{Co}(\text{tame})_2\lambda\lambda]^{3+}$ .

<i>Bond lengths</i>					
<i>Atoms</i>	<i>Observed<sup>a</sup></i>	<i>Computed</i>	<i>Atoms</i>	<i>Observed</i>	<i>Computed</i>
Co-N(1) <sup>b</sup>	1.972(2)Å	1.963Å	C(1)-C(2)	1.527(2)Å	1.516Å
N(1)-C(1)	1.495(2)	1.498	C(2)-C(3)	1.543(3)	1.517
<i>Bond angles</i>					
N(1)-Co-N(1 <sup>ii</sup> ) <sup>c</sup>	88.92(6)°	89.92°	Co-N(1)-H(2)	111(1)°	112°
Co-N(1)-C(1)	117.37(10)	115.15	C(1)-N(1)-H(1)	107(1)	108
N(1)-C(1)-C(2)	111.66(13)	111.57	N(1)-C(1)-H(3)	107(1)	108
C(1)-C(2)-C(3)	108.68(15)	108.76	C(1)-N(1)-H(2)	106(1)	109
C(1)-C(2)-C(1 <sup>ii</sup> )	110.25(14)	110.17	N(1)-C(1)-H(4)	109(1)	110
N(1)-Co-N(1 <sup>i</sup> )	88.77(8)	88.25	C(2)-C(1)-H(3)	113(1)	110
N(1)-Co-N(1 <sup>iii</sup> )	93.51(8)	91.97	C(2)-C(1)-H(4)	110(1)	110
N(1)-Co-N(1 <sup>v</sup> )	176.56(8)	177.07	C(2)-C(3)-H(5)	110(1)	110
Co-N(1)-H(1)	107(1)	106			
<i>Close contacts</i>					
N(1)...C(1 <sup>iv</sup> )	2.816(2)Å	2.776Å	H(2)...H(4)	2.13(3)Å	2.27Å
H(1)...H(4 <sup>iv</sup> )	2.49(3)	2.34	H(2)...H(2 <sup>iii</sup> )	2.24(4)	2.12
H(1)...H(3)	2.12(3)	2.22	H(1)...H(1 <sup>i</sup> )	2.31(4)	2.28
<i>Torsion angles</i>					
<i>Atoms</i>	<i>Observed</i>	<i>Computed</i>			
Co-N(1)-C(1)-C(2)	+28.8(2)°	+32.49°			
N(1)-C(1)-C(2)-C(3)	+163.2(2)	+160.66			
C(1)-C(2)-C(3)-H(5)	-63 (1)	-64.12			
C(1)-C(2)-C(3)-H(5 <sup>ii</sup> )	+57 (1)	+55.88			

<sup>a</sup> The observed molecule has only approximate  $D_3$  symmetry. The mean of the  $D_3$  related parameters was computed and is here compared with the asymmetric parameter of the computed  $D_3$  molecule. The parentheses enclose e.s.d.'s in the mean observed parameters (see Appendix III).

<sup>b</sup> The atom numbering scheme is that used for the computed molecule as in Figures 5.1 and 5.2.

<sup>c</sup> See Table 5.2 for the definitions of symmetry operations associated with the superscripts.

TABLE 6.2. COMPARISON OF OBSERVED AND COMPUTED INTERNAL GEOMETRY OF

*Bond lengths*

Atoms	Observed 1 <sup>a</sup>	Observed 2 <sup>b</sup>	Computed
Co-N(1) <sup>c</sup>	1.992(2)Å	2.00(2)Å	1.995Å
Co-N(2)	1.971(2)	2.00(2)	1.978
N(1)-C(1)	1.487(4)	1.47(3)	1.499
N(2)-C(3)	1.488(4)	1.46(3)	1.496
C(1)-C(2)	1.497(5)	1.54(3)	1.503
C(2)-C(3)	1.499(5)	1.54(3)	1.504

*Bond angles*

N(1)-Co-N(2)	91.0(1)°	94.3(6)°	94.33°
Co-N(1)-C(1)	122.1(2)	117.0(14)	121.90
N(1)-C(1)-C(2)	112.5(2)	113.7(17)	112.20
C(1)-C(2)-C(3)	113.6(2)	114.0(17)	110.31
C(2)-C(3)-N(2)	112.2(2)	111.0(17)	111.07
Co-N(2)-C(3)	121.9(2)	118.0(12)	119.25

*Torsion angles*

Co-N-C-C	51.9° (ring C)	56.7°	51.46°
	56.1 (ring B)		
N-C-C-C	67.6 (ring C)	67.1	72.99
	63.5 (ring B)		

<sup>a</sup> This data was transcribed from reference 43 on the crystal structure of (-)<sub>589</sub>-[Co(tn)<sub>3</sub>]Cl<sub>3</sub>·H<sub>2</sub>O. The mean of the pseudo-C<sub>3</sub> related parameters was computed and is here tabulated.

The parentheses enclose e.s.d's in the mean values (Appendix III).

<sup>b</sup> The data here was extracted from reference 273 on the crystal structure of (-)<sub>589</sub>-[Co(tn)<sub>3</sub>]Br<sub>3</sub>·H<sub>2</sub>O. As in 1 the mean of the pseudo-C<sub>3</sub> related parameters was computed.

<sup>c</sup> The atom numbering scheme is that used for the computed molecule as in Figure 5.5.



**TABLE 6.3.** COMPARISON OF OBSERVED AND COMPUTED INTERNAL GEOMETRY OF*Bond lengths*

Atoms	Observed <sup>a</sup>	Computed	Atoms	Observed <sup>a</sup>	Computed
Co-N(1) <sup>b</sup>	1.985(5)Å	1.984Å	C(1)-C(2)	1.516(10)Å	1.509Å
N(1)-C(1)	1.489(9)	1.499			

*Bond angles*

N(1)-Co-N(1 <sup>1</sup> ) <sup>c</sup>	89.0(3)°	88.12°	N(1)-C(1)-C(2)	112.0(6)°	112.12°
Co-N(1)-C(1)	118.0(4)	114.80	C(1)-C(2)-C(1 <sup>1</sup> )	117.2(7)	112.41

*Torsion angles*

Co-N(1)-C(1)-C(2)	+67.7°	+74.81°	N(1)-C(1)-C(2)-C(1 <sup>1</sup> )	-33.0°	-36.64°
-------------------	--------	---------	-----------------------------------	--------	---------

<sup>a</sup> This data is from reference 17 on the crystal structure of  $\Delta$ -[Co(R,R-ptn)<sub>3</sub>]-Cl<sub>3</sub>·2H<sub>2</sub>O. The mean of pseudo-*D*<sub>3</sub> related parameters is tabulated. E.s.d's in the mean parameters are enclosed in parentheses (see Appendix III).

<sup>b</sup> The atom numbering scheme is that shown in Figure 5.6 for the computed molecule which converged with precise *D*<sub>3</sub> symmetry.

<sup>c</sup> See Table 5.9 for definitions of symmetry operations.

**TABLE 6.4.** COMPARISON OF OBSERVED AND COMPUTED INTERNAL GEOMETRY OF*Bond lengths*

Atoms	Observed <sup>a</sup>	Computed	Atoms	Observed	Computed
Co-N(1) <sup>b</sup>	1.99(2)Å	1.995Å	C(1)-C(2)	1.53(3)Å	1.510Å
N(1)-C(1)	1.50(3)	1.499			

*Bond angles*

N(1)-Co-N(1 <sup>1</sup> ) <sup>c</sup>	88.3(6)°	87.85°	N(1)-C(1)-C(2)	109.0(16)°	112.46°
Co-N(1)-C(1)	115.7(10)	115.55	C(1)-C(2)-C(1 <sup>1</sup> )	116.7(25)	113.02

*Torsion angles*

Co-N(1)-C(1)-C(2)		+73.69°	N(1)-C(1)-C(2)-C(1 <sup>1</sup> )		-36.04°
-------------------	--	---------	-----------------------------------	--	---------

<sup>a</sup> This data is from reference 16 on the crystal structure of  $\Lambda$ -[Co(R,R-ptn)<sub>3</sub>]-Cl<sub>3</sub>·H<sub>2</sub>O. As above the mean of pseudo-*D*<sub>3</sub> related parameters is tabulated.

<sup>b</sup> The atom numbering scheme is that shown in Figure 5.7 for the computed molecule which converged with *D*<sub>3</sub> symmetry.

<sup>c</sup> See Table 5.11 for definitions of symmetry operations.

TABLE 6.5. COMPARISON OF OBSERVED AND COMPUTED INTERNAL GEOMETRY OF

*Bond lengths*

<i>Atoms</i>	<i>Observed<sup>a</sup></i>	<i>Computed</i>	<i>Atoms</i>	<i>Observed<sup>a</sup></i>	<i>Computed</i>
Co-N(1)	1.97(2)Å	1.992Å	N(3)-C(4)	1.49(3)Å	1.498Å
Co-N(2)	1.97(2)	1.977	C(4)-C(5)	1.51(3)	1.510
Co-N(3)	1.95(2)	1.984	C(5)-C(6)	1.47(3)	1.510
Co-N(4)	1.94(2)	1.960	C(6)-N(4)	1.49(3)	1.498
N(1)-C(1)	1.53(3)	1.498	Co-O(1)	1.89(1)	1.879
C(1)-C(2)	1.56(3)	1.506	Co-O(2)	1.94(1)	1.882
C(2)-C(3)	1.46(3)	1.506	O(1)-C(7)	1.32(2)	1.316
C(3)-N(2)	1.44(3)	1.497	C(7)-O(2)	1.32(2)	1.316

*Bond angles*

N(1)-Co-N(2)	91.9(7)°	91.80°	O(1)-C(7)-O(2)	110.4(17)°	111.65°
Co-N(1)-C(1)	121.2(13)	120.23	Co-O(2)-C(7)	89.2(11)	88.67
N(1)-C(1)-C(2)	107.6(18)	111.91	N(1)-Co-O(1)	86.4(6)	85.94
C(1)-C(2)-C(3)	113.8(19)	111.18	N(1)-Co-O(2)	85.9(6)	89.82
C(2)-C(3)-N(2)	112.5(19)	111.62	N(1)-Co-N(3)	175.3(7)	177.45
Co-N(2)-C(3)	120.2(13)	117.82	N(1)-Co-N(4)	93.5(7)	92.53
N(3)-Co-N(4)	89.7(7)	88.09	N(2)-Co-O(1)	166.5(6)	162.93
Co-N(3)-C(4)	117.5(13)	113.86	N(2)-Co-O(2)	97.7(6)	92.32
N(3)-C(4)-C(5)	110.3(18)	111.47	N(2)-Co-N(3)	91.4(7)	90.55
C(4)-C(5)-C(6)	112.7(19)	112.26	N(2)-Co-N(4)	94.8(7)	94.64
C(5)-C(6)-N(4)	111.9(18)	111.82	N(3)-Co-O(1)	89.6(6)	91.57
Co-N(4)-C(6)	115.8(13)	112.20	N(3)-Co-O(2)	90.2(6)	89.28
O(1)-Co-O(2)	68.8(5)	70.75	N(4)-Co-O(1)	98.7(6)	102.39
Co-O(1)-C(7)	91.1(11)	88.80	N(4)-Co-O(2)	167.5(6)	172.62

*Close contacts*

H(4)...H(19)	2.18Å	2.119Å	H(10)...H(12)	2.04Å	2.103Å
H(8)...H(20)	2.31	2.303			

(contd.)

TABLE 6.5. (contd.)*Torsion angles*

<i>Atoms</i>	<i>Observed<sup>a</sup></i>	<i>Computed</i>	<i>Atoms</i>	<i>Observed<sup>a</sup></i>	<i>Computed</i>
Co-N(1)-C(1)-C(2)	54.9°	55.26°	Co-N(3)-C(4)-C(5)	62.5°	65.97°
N(1)-C(1)-C(2)-C(3)	66.7	67.30	N(3)-C(4)-C(5)-C(6)	64.6	62.64
C(1)-C(2)-C(3)-N(2)	70.6	71.51	C(4)-C(5)-C(6)-N(4)	66.6	65.08
C(2)-C(3)-N(2)-Co	58.5	61.84	C(5)-C(6)-N(4)-Co	64.8	69.67

<sup>a</sup> This data was extracted from reference 76. The atom numbering scheme is depicted in Figure 5.8.

by the molecular energy minimization, and the computed equilibrium geometry should then provide a reasonable coordinate basis in the evaluation of the theoretical intramolecular CD models (Chapter 4).

*The  $\Delta$ - and  $\Lambda$ -[Co(*R,R*-ptn)<sub>3</sub>]<sup>3+</sup> Isomers*

In the energy minimized [Co(tame)<sub>2</sub>]<sup>3+</sup> complexes (Section 5.5.1), the inclusion of the methyl hydrogens in the general force field (Section 5.2) had no significant effect on the equilibrium geometry of the chelate rings or the CoN<sub>6</sub> core (Tables 5.3 and 5.5). Similarly for the [Co(*R,R*-ptn)<sub>3</sub>]<sup>3+</sup> isomers, which have equatorially disposed methyl groups not involved in any direct interaction between chelate rings, the deletion of the methyl hydrogens from the minimizations should not significantly change the [Co(tn)<sub>3</sub>]<sup>3+</sup> substrate equilibrium geometry,<sup>256</sup> which is required for the evaluation of the intramolecular theoretical CD models discussed above. Consequently the observed pseudo-*D*<sub>3</sub> geometries for the [Co(tn)<sub>3</sub>skew-boat<sub>3</sub>]<sup>3+</sup> substrates of these isomers, in the crystal structures of  $\Delta$ -[Co(*R,R*-ptn)<sub>3</sub>]Cl<sub>3</sub>·2H<sub>2</sub>O(1el<sub>3</sub>)<sup>17</sup> and  $\Lambda$ -[Co(*R,R*-ptn)<sub>3</sub>]Cl<sub>3</sub>·H<sub>2</sub>O(ob<sub>3</sub>),<sup>16</sup> are compared in Tables 6.3 and 6.4 with the computed equilibrium *D*<sub>3</sub> geometries of the  $\Delta$ -[Co(tn)<sub>3</sub>  $\lambda$  skew-boat<sub>3</sub>]<sup>3+</sup> (or equivalently the  $\Lambda$ -( $\delta$  skew-boat<sub>3</sub>)) and the  $\Lambda$ -[Co(tn)<sub>3</sub>  $\lambda$  skew-boat<sub>3</sub>]<sup>3+</sup> conformers discussed in Section 5.5.2. Figures 5.6 and 5.7, depicting the equilibrium conformations of these conformers, also give the atom labelling scheme used for the comparisons.

The observed and calculated bond lengths are essentially identical for the two isomers of [Co(*R,R*-ptn)<sub>3</sub>]<sup>3+</sup>, as indicated in Tables 6.3 and 6.4. The only significant differences between observed and computed

angular geometry occur in the Co-N(1)-C(1) angles (118.0(4)° observed, 114.8° computed) and C(1)-C(2)-C(1<sup>1</sup>) angles (117.2(7)° observed, 112.4° computed) of the  $\Delta$ -[Co(R,R-ptn)<sub>3</sub>]<sup>3+</sup> isomer<sup>17</sup> (Table 6.3). These disparities, however, may readily be effected by weak crystal packing induced repulsive contacts acting on the protruding methyl groups of the observed complex.<sup>17</sup> The small angular variance is accompanied by a slight decrease in the magnitude of the observed Co-N-C-C and N-C-C-C torsion angles from the computed values (68(1)° and 33(1)° *cf.* 75° and 37°), but the trigonal geometry (Section 4.3.2) of the non-donor ligand atoms is not largely affected by these small differences. In addition the observed and computed CoN<sub>6</sub> core geometries are closely similar for both complexes, and the computed trigonal geometry should be adequate for a good estimation of the intramolecular induced CD expected on the basis of the theoretical correlation models for these isomers.

*The AB-[Co(tn)<sub>2</sub>CO<sub>3</sub>chair<sub>2</sub>]<sup>+</sup> Isomer*

The observed geometry of this isomer in the crystal structure of [Co(tn)<sub>2</sub>CO<sub>3</sub>]<sub>2</sub>ClO<sub>4</sub><sup>76</sup> is presented in Table 6.5 in comparison with the calculated equilibrium geometry described in Section 5.5.3 (Figure 5.8).

From an analysis of Table 6.5 it is apparent that the interatomic distances, valence angles and torsion angles are virtually identical (within three estimated standard deviations of the observed coordinates) for the observed and computed molecules, with the exception of the Co-O(2) bond length and the N-Co-O(2) angles. However, these disagreements are not large and were attributed<sup>76</sup> to lattice distortions induced by hydrogen bonding or to systematic errors in the data or structural

model (the perchlorate group in the observed structure is thermally or statistically disordered over a considerable region).

This analysis provides yet another example of the close correlation between the observed solid state and computed molecular geometries (using the molecular energy minimization procedure<sup>54</sup> described in Chapter 5) of metal chelate complexes having six-membered metal-diamine rings. The complex ions in all of the above observed structures are extensively hydrogen-bonded through the N-H hydrogens to surrounding counter-ions, water molecules or other complex ions ( $\text{Co}(\text{tn})_2\text{CO}_3^+$ ), the specific repulsive lattice contacts being relatively weak and few in number. It thus seems evident that the observed complex geometries of this type are generally well reproduced by the molecular minimization process<sup>54</sup> (Chapter 5) when there are no strong specific repulsive interactions with the complex molecule in the crystal lattice.

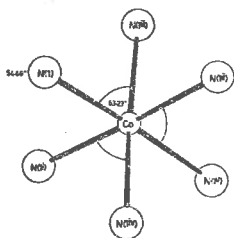
### 6.3 CONCLUDING DISCUSSION

From the close agreement between observed crystal and calculated molecular conformations which is exemplified in the Co(III)-diamine six-membered ring chelate complexes (Section 6.2), and in many other Co(III)-polyamine chelates using similar Newton-Raphson energy minimization procedures,<sup>2,48,49,56,57,75,76,248,249,251,256</sup> it appears that the molecular energy minimization scheme described in Chapter 5<sup>48,49,54</sup> should be generally adequate to provide a reasonable estimation of the intramolecular configurational information required in an evaluation of the visible CD models<sup>68-70,72,73,150,153,156</sup> (Chapter 4)

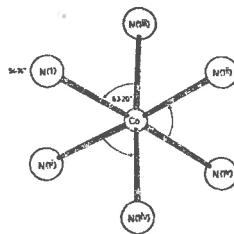
for intrinsically dissymmetric chelate complexes of this type. Of course, as mentioned above (Section 6.1), in view of the general sensitivity of these models to the conformations of the chelate rings (especially with regard to their effect on the configurations of the donor atoms and the contiguous extra-chromophoric atoms), it is normally necessary to have information on the conformer or conformers present in the observed CD medium when correlating stereochemistry with solid state or solution visible CD spectra. Furthermore, if environmentally induced distortions of the dissymmetric complex become important (*e.g.* in crystal lattices with strongly repulsive non-bonded contacts<sup>48</sup>), or if the environmental configuration is required for a plausible evaluation of the CD model (*e.g.* for an intrinsically symmetric complex in a dissymmetric environment<sup>135-137,283,284</sup> or when the lattice contributes significantly in the theoretical CD model for the chromophoric transition), the molecular energy minimization scheme becomes inadequate for theoretical CD-stereochemistry correlations. In this case the appropriate knowledge of the environmental configuration must be obtained by experimental or other theoretical means as indicated previously (Section 6.1). In conclusion, owing to the importance of the  $\text{CoL}_6$  core configuration in the theoretical CD models<sup>68-70,72,73,150,153,156</sup> described for  $D_3$  Co(III) complexes in Chapter 4, some further remarks on the agreement between the observed and calculated  $\text{CoN}_6$  geometries of the trigonal complexes discussed in Section 6.2 are warranted if energy minimized configurations are to be used in the evaluation of these models.

For the computed  $[\text{Co}(\text{tame})_2\delta\delta]^{3+}$  molecule, the *final* trigonal twist ( $\omega$ ) and polar ( $\theta$ ) angles of the  $\text{CoN}_6$  core (Section 4.3.1) are shown in Figures 6.1(a), (b) and (c), as calculated under the various force fields described in Section 5.5.1. The  $\omega$  angles of the  $[\text{Co}(\text{tame})_2\lambda\lambda]^{3+}$  isomer are the  $120^\circ$  complements of the angles shown when defined by the same  $\Delta$ -disposed donor atom pairs (Section 4.3.2). Thus for the complete  $[\text{Co}(\text{tame})_2\lambda\lambda]^{3+}$  computation, the  $\omega$  and  $\theta$  angles are  $56.8^\circ$  and  $54.7^\circ$ ; compared with the corresponding mean  $D_3$  observed values of  $55.8^\circ$  and  $54.0^\circ$  (Section 4.3.2). Although these differences are insignificant (e.s.d.'s in the observed values are  $-0.5^\circ$ ), and the two configurations lead to similar predictions in the first-order crystal-field models for the visible CD of the trigonal components of the  ${}^1A_{1g} \rightarrow {}^1T_{1g}$  and  ${}^1A_{1g} \rightarrow {}^1T_{2g}$  transitions (Chapter 4), they do result in considerably different contributions (in magnitude since the  $\omega$  and  $\theta O_h$  nodal values of  $60^\circ$  and  $54.74^\circ$  are not traversed) in the second-order crystal-field model<sup>70,71</sup> for the *net* CD of these transitions (Section 4.4). This occurs because of the large weight of the nitrogen donor atom terms in the dominant  $N \leftrightarrow N$  and  $N \leftrightarrow NH$  interaction products of the expression  $R''_{net}(T_{1g}, T_{2g})$  for the *net* visible CD (Section 4.4.2). However, the *net* effect in this model<sup>70,71</sup> for the whole computed molecule includes a smaller positive contribution to the  $N \leftrightarrow N$  product sums and a larger positive contribution (of about the same order of magnitude) to the  $N \leftrightarrow NH$  product sums, and the predicted resultant *net* CD's from the observed and calculated molecular configurations are similar in sign and of the same order of magnitude.

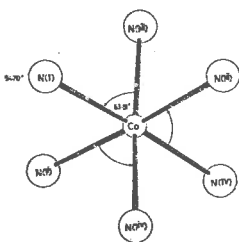




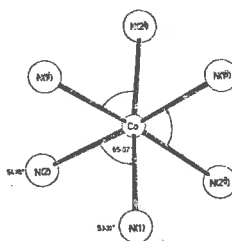
(a)  $[\text{Co}(\text{tame})_2\delta\delta]^{3+}$   
Complete molecule with  
complete torsion angle  
description.



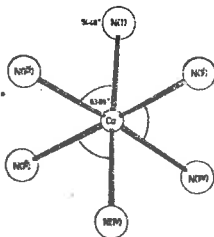
(b)  $[\text{Co}(\text{tame})_2\delta\delta]^{3+}$   
Methyl hydrogens deleted.  
Complete torsion angle  
description



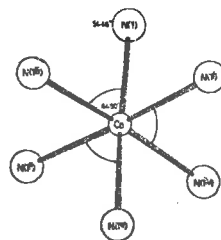
(c)  $[\text{Co}(\text{tame})_2\delta\delta]^{3+}$   
Methyl hydrogens deleted.  
Single torsion angle  
description.



(d)  $\Delta\text{-}[\text{Co}(\text{tn})_3\text{chair}_3]^{3+}$



(e)  $\Lambda\text{-}[\text{Co}(\text{tn})_3\delta\text{skew-boat}_3]^{3+}$



(f)  $\Lambda\text{-}[\text{Co}(\text{tn})_3\lambda\text{skew-boat}_3]^{3+}$

FIGURE 6.1. COMPUTED CHROMOPHORES IN PROJECTION DOWN THEIR PSEUDO- $C_3$   
AXES.

In the crystal structures of the  $[\text{Co}(\text{tn})_3\text{chair}_3]^{3+}$  isomer<sup>43,273</sup> discussed in Section 6.2, the lattice distortion of the  $\text{CoN}_6$  core is slightly greater than that of the observed  $[\text{Co}(\text{tame})_2\lambda\lambda]^{3+}$  complex. Yet the resultant configurations are probably not significantly different from that for the computed molecule (Tables 5.8 and 6.2 and Figure 6.1(d)) owing to inaccuracies in the structure determinations. The large thermal motion of the atoms in ring A of the  $(-)_589^-$   $[\text{Co}(\text{tn})_3]\text{Cl}_3\cdot\text{H}_2\text{O}$  structure<sup>43</sup> prevented the computation of a reliable mean  $C_3$  axis for the chromophore. The observed mean  $\theta$  and  $\omega$  values for the  $\text{CoN}_6$  core in  $(-)_589^-[\text{Co}(\text{tn})_3]\text{Br}_3\cdot\text{H}_2\text{O}$ <sup>273</sup> are  $52.6^\circ$  and  $62.5^\circ$ <sup>15</sup> (e.s.d.'s  $\sim 3-4^\circ$ ) whereas the values for the computed complex (Section 5.5.2) are  $53.7^\circ$  and  $65.1^\circ$ . Consequently the theoretical relative CD contribution from the calculated chromophore may not be a good indication of the relative contribution from the solid state chromophore, if these absolute configurations are used to evaluate crystal-field CD models of the type discussed in Chapter 4 for  $C_3$  complexes. Once again this is due to the high sensitivity of the donor atom terms in the theoretical CD expressions to small changes in their trigonal geometry near the  $\theta_h$  configuration. However, the final assessment of the validity of using the computed molecule in solid state CD-structure correlations must come from a consideration of the relative weights of other dominant terms in these expressions, such as those contributed by the amino hydrogens in this case for the crystal-field models,<sup>70,71</sup> or the effect of the non-donor atoms in determining the molecular orbital characteristics of the chromophore in the molecular orbital models.<sup>69,72,153,156</sup>

The mean  $D_3$  observed  $\omega$  and  $\theta$  angles of the  $\text{CoN}_6$  cores in  $\Delta\text{-}[\text{Co}(\text{R,R-ptn})_3]\text{Cl}_3 \cdot 2\text{H}_2\text{O}$ <sup>17</sup> and  $\Lambda\text{-}[\text{Co}(\text{R,R-ptn})_3]\text{Cl}_3 \cdot \text{H}_2\text{O}$ <sup>16</sup> have the values  $57.0^\circ$  and  $54.2^\circ$ <sup>285</sup> (e.s.d.'s  $-1^\circ$ ), and  $55.9^\circ$  and  $54.4^\circ$ <sup>15</sup> (e.s.d.'s  $-3-4^\circ$ ) respectively. These compare well with the corresponding computed values of  $56.0^\circ$  and  $54.5^\circ$ , and  $55.5^\circ$  and  $54.5^\circ$ , where the  $\omega$  angles are here defined by the chelate ring donor atom pairs and are the  $120^\circ$  complements of the angles shown in Figures 6.1(e) and 6.1(f). Hence the calculated crystal-field contribution to the net visible CD<sup>70,71</sup> from the computed  $\text{CoN}_6$  chromophore should be a good indication of that from the observed chromophore in these complexes within the accuracy of the structure analyses, although again the small differences between the observed and computed core geometries may result in quite large differences in the relative magnitudes of the corresponding crystal-field CD contributions.

In the final analysis then, it appears that the minimized molecular geometries of these and similar trigonal  $\text{Co}(\text{III})$  complexes should be suitable for use as configurational models in the intramolecular evaluation of the crystal-field visible CD representations described in Chapter 4, within the current uncertainty ranges of observed geometrical parameters, and when there are no strongly distorting repulsive lattice contacts with the metal complex ion. However, because of the sensitivity of the high weight donor atom terms in the CD expressions to insignificant differences in observed and calculated  $\text{CoL}_6$  core geometries, this practice should be treated with caution, especially when the extra-chromophoric terms in these expressions are of relatively low weight.

APPENDICESAPPENDIX I CATALOGUE OF COMPUTER PROGRAMS<sup>a</sup>

<u>PROGRAM</u>	<u>OPERATION(S)</u>	<u>AUTHOR(S)</u>	<u>LOCAL MOD(S)</u>
AUFAC	Least-squares determination of inter-film scale factors; Lorentz-polarization corrections for densitometer data; weighting analysis.	G.L. Paul (1966) School of Chemistry, University of Sydney.	M.R. Snow, Physical & Inorganic Chem. Dept., University of Adelaide.
AULAC	Least-squares determination of inter-layer scale factors; Data packing, sorting and editing.	G.L. Paul (1966)	M.R. Snow
AUPTP	Reading and processing of STOE diffractometer paper tape output data.	R.J. Hill (1973) Geology Dept., University of Adelaide.	M.R. Snow
AZIMUTH	Calculation of mean $C_3$ axes and geometrical parameters for pseudo-trigonal chromophores.	K.R. Butler (1972) P. & I. Chemistry Dept., University of Adelaide.	K.R. Butler
BLANDA	Calculation of inter-atomic distances and angles.	J.F. Blount (1966) School of Chemistry, University of Sydney.	M.R. Snow
CART	Calculation of Cartesian coordinates from internal molecular coordinates.	R.L. Hilderbrandt (1969) Chemistry Dept., Cornell University, Ithaca, New York.	M.R. Snow & R.J. Geue
CUPICK	Coordination of reduced Picker diffractometer O/P data with AULAC I/P.	M.R. Snow (1971)	R.J. Geue
DATA	Reading, sorting and editing of densitometer paper tape reflection data.	M.R. Snow & R.J. Geue (1970)	R.J. Geue

(contd.)

APPENDIX I (contd.)

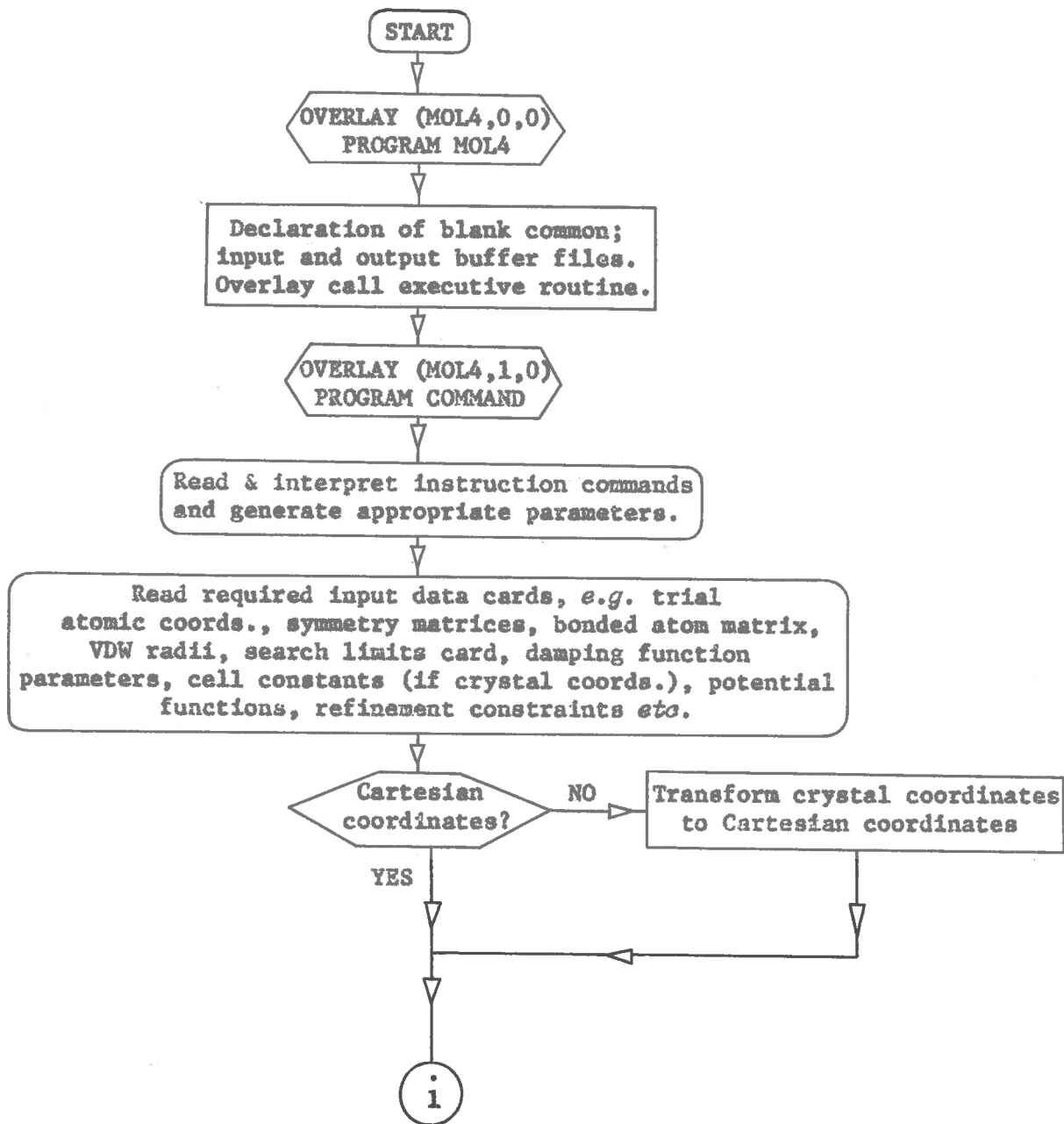
<u>PROGRAM</u>	<u>OPERATION(S)</u>	<u>AUTHOR(S)</u>	<u>LOCAL MOD(S)</u>
FORDAPB	Computation of Fourier summations; peak height and position inter-polations.	A. Zalkin (1968) mod. by J.A. Ibers, Chemistry Dept., Northwestern University, Evanston, Illinois.	M.R. Snow
FUORFLS	Least-squares refinement and calculation of unit cell structure factors.	W.R. Busing, K.O. Martin, H.A. Levy (1962) Oak Ridge National Lab., Oak Ridge, Tennessee.	M.R. Taylor, School of Physical Sciences, Flinders University of South Australia.
MOL4	Gauss-Newton-Raphson molecular energy minimization; includes full interaction search, symmetry-dependent refinement and constraint options (Chapter 5).	R.H. Boyd (1966) Chemistry Dept., Utah State University, Logan, Utah; extensively modified and extended locally (Appendix II).	M.R. Snow (1968); M. Dwyer (1970), Research School of Chemistry, A.N.U., Canberra; R.J. Geue & M. Dwyer (1971-1973).
ORFFE	Calculation of functions of crystallographic coordinates and their errors.	W.R. Busing, K.O. Martin, H.A. Levy (1964).	M.R. Taylor
ORTEPA	Perspective thermal atomic ellipsoid plotting.	C.K. Johnson (1965) Oak Ridge National Lab., Oak Ridge, Tennessee.	M.R. Taylor
ORTEPB	Thermal ellipsoid plotting with elimination of bond and atom underlapping.	C.K. Johnson (1973)	M.R. Taylor
PLANEH	Computation of least-squares planes equations, inter-planar dihedral angles and hydrogen atom coordinates.	D.L. Smith (1964) University of Wisconsin; mod. by J.F. Blount (1966).	M.R. Snow

(contd.)

APPENDIX I (contd.)

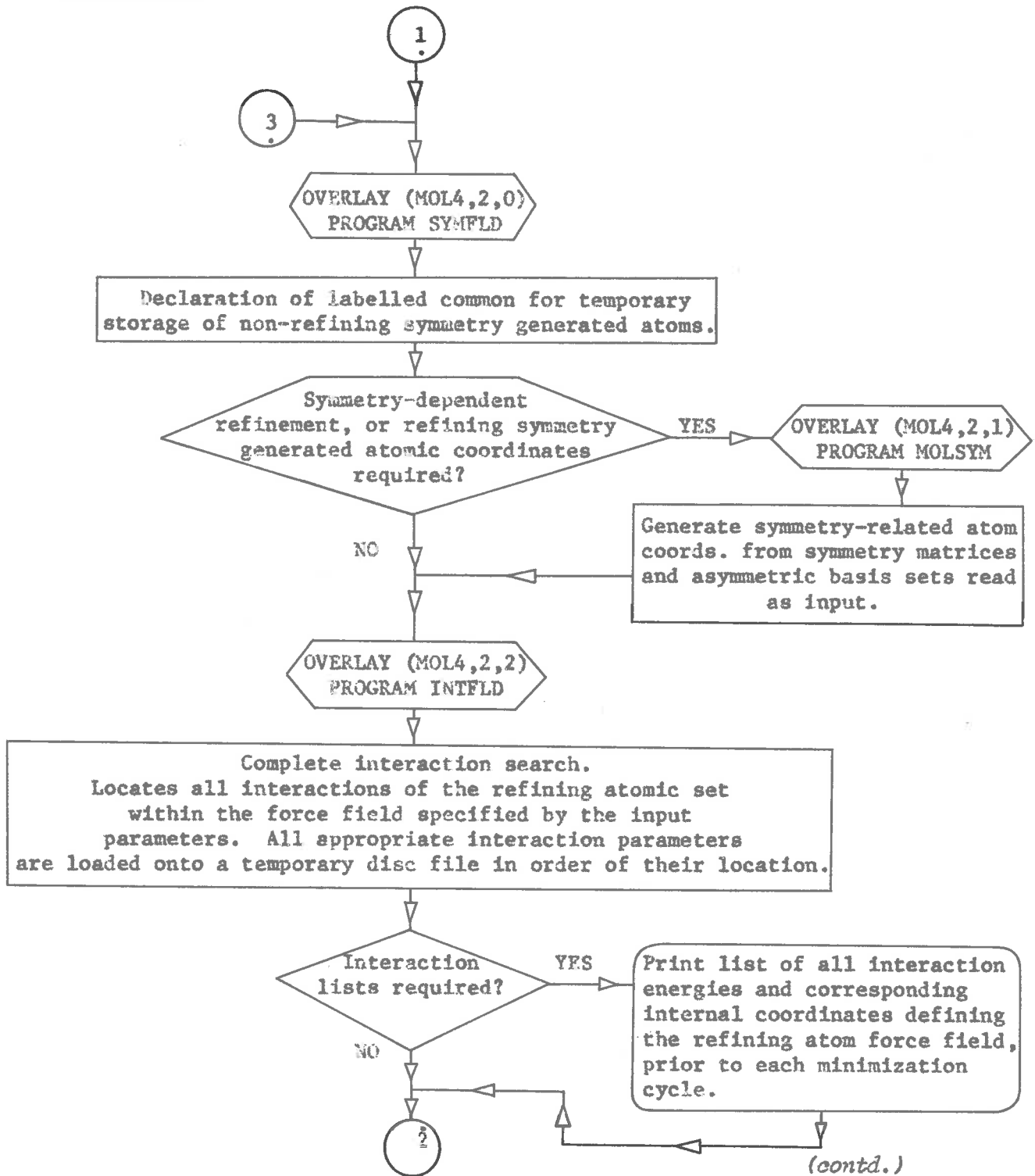
<u>PROGRAM</u>	<u>OPERATION(S)</u>	<u>AUTHOR(S)</u>	<u>LOCAL MOD(S)</u>
PRELIM	Calculation of crystal density, linear absorption coefficients and unit cell data.	M.R. Snow (1972)	M.R. Snow & R.J. Geue
PUTAB	Tabulation of observed and calculated structure factors for publication.	R.C. Elder; mod. by B. Foxman (1968) A.N.U., Canberra.	M.R. Snow
SETUP	Reading and processing of Picker diffractometer output intensities.	B. Foxman, P.O. Whimp (1970) A.N.U., Canberra.	
SUUCLS	Least-squares refinement of unit cell constants.	M.T. Barnet (1966) School of Chemistry, University of Sydney.	M.R. Snow

<sup>a</sup> All programs listed here were written in FORTRAN.<sup>286</sup>  
 With the exceptions of DATA (CDC 3200) and SETUP (CDC 3600) all  
 were written for the CDC 6400 computer system operating under  
 SCOPE Version 3.4.<sup>287</sup>

APPENDIX II MODIFICATIONS TO BOYD'S<sup>54</sup> ENERGY MINIMIZATION PROGRAM(1) SEQUENTIAL STRUCTURE OF THE MODIFIED MOLECULAR ENERGY MINIMIZATION PROGRAM MOL4

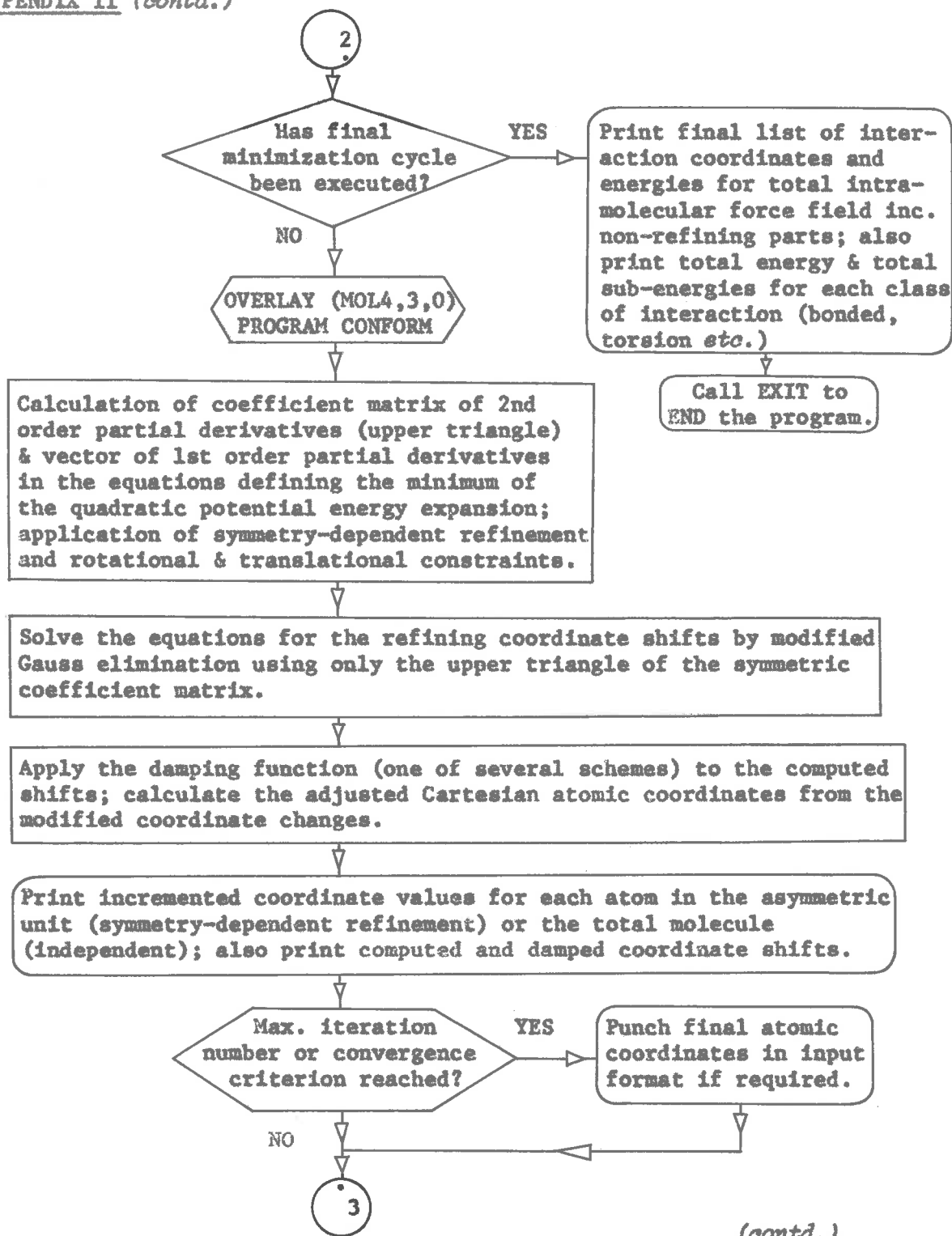
(contd.)

## APPENDIX II (contd.)





## APPENDIX II (contd.)



## APPENDIX II (contd.)

(11) LOCAL MODIFICATIONS (R.J. Geue<sup>256</sup> & M. Dwyer<sup>248,256</sup>) OF THE PROGRAM  
ORIGINALLY APPLIED TO THE CONFORMATIONAL ANALYSIS OF METAL CHELATE  
COMPLEXES (M.R. Snow<sup>48</sup> & D.A. Buckingham *et al.*<sup>49</sup>)

1. Segmentation of the program into overlay<sup>286-288</sup> modules which are individually executed according to the sequence given in (i). This procedure considerably reduces the net instantaneous core storage requirements of the program instruction coding and transient variable arrays (*e.g.* those for the non-refining symmetry-generated atomic parameters and the matrix of coordinate shift coefficients).
2. Complete modification of the instruction and data input routines and the corresponding parameter storage procedures (OVERLAY(MOL4,1,0)). This was designed to facilitate preparation of the input data decks, to reduce core storage requirements, and to incorporate the input required by the symmetry-dependent refinement procedure (*e.g.* symmetry matrices, symmetry basis atom sets), the refinement constraint routine and the damping scheme (Sections 5.3 and 5.4).
3. Generation of symmetry-related atomic coordinates from the symmetry transformation matrices and the correlated asymmetric basis atom sets read as input (OVERLAY(MOL4,2,1)). This routine may be used for either the symmetry-dependent refinement technique (symmetry-generated coordinates are constrained for a given minimization cycle), or an independent (or semi-independent) minimization (Sections 5.3 and 5.4) in which all (or some) of the symmetry-generated coordinates are refined.
4. The interaction<sup>48,285</sup> search routine, originally developed and implemented by Snow, has been considerably modified and extended (OVERLAY-(MOL4,2,2)) to include several innovations. These comprise the triangularization of the bonded atom connection matrix,<sup>48,285</sup> the location of all dihedral angles of the type *i-j-k-l* where *i,j,k* and *l* are bond connected, the location of intra- and intermolecular and intra- and interionic non-bonded, hydrogen bonded and electrostatic interactions if required (by the force field definition parameters), and the loading of all interactions onto a temporary disc file. This file, generated prior to each minimization cycle, is then processed sequentially by program CONFORM (OVERLAY(MOL4,3,0)) in logical binary record buffers of 30 interactions. In addition, for a minimization involving non-refining atoms, the search procedure normally locates only those interactions required by the minimization

(contd.)

APPENDIX II (contd.)(11) LOCAL MODIFICATIONS (contd.)

*i.e.* all interactions involving a refining atom. However, after the final cycle a complete interaction search (within the defined force field limits) is always made (over all molecules if more than one present), and this complete set is listed with the corresponding interaction energies.

5. Modification of the first and second order partial derivative computational procedures (OVERLAY(MOL4,3,0)) for each interaction class (bonded, non-bonded, torsion *etc.*) to accommodate all possible permutations of refining and non-refining atoms in the interaction atoms lists. These routines were also altered to effect the computation (and storage) of only the upper triangle of the symmetric second derivative matrix of coordinate shift coefficients.
6. Introduction of a routine to apply symmetry-dependent refinement (Section 5.4) or other constraints to selected atoms (or coordinates) (OVERLAY(MOL4,3,0)). A new sub-routine<sup>289</sup> was also incorporated (OVERLAY(MOL4,3,0)) to solve the equations for the refining coordinate shifts using the stored upper triangle of the symmetric coefficient matrix.
7. Incorporation of the damping function  $\lambda^{248}$  (Section 5.3) which is a continuous function of the calculated coordinate shifts. This proved to be very useful in expediting convergence, and could alternatively be used to closely follow the potential strain energy surface throughout the refinement if so desired.

With the above modifications implemented, a problem involving up to 140 refining coordinates and 4500 symmetry-generated (non-refining) coordinates required only 23000 central memory words (decimal) of computer core storage on the CDC 6400 computer system. For larger problems, the appropriate storage array dimensions in the program could be simply increased up to a current maximum core storage size of about 74000 (decimal) computer words. In addition the program has, in principle, the capacity to process an unlimited number of interactions for a problem of any size, and there is no dependence of computer core requirements on the interaction number.

APPENDIX III SUPPLEMENTARY INFORMATION ON THE STRUCTURE ANALYSES

The derived structural information and theoretical parameter sources (*e.g.* atomic scattering factor curves, anomalous scattering factor components) for the three crystal structure analyses presented here have normally been adequately presented in Chapters 1, 2 and 3. Some additional notes of general relevance in these areas are presented here.

*Linear Absorption Coefficients*

Values for the atomic mass attenuation coefficients ( $\mu/\rho \text{ cm}^2 \text{ g}^{-1}$ ) used in the derivations of  $\mu_{\text{MoK}\alpha}$  and  $\mu_{\text{CuK}\alpha}$  were obtained from the recently revised tables presented in International Tables for X-ray Crystallography, Volume IV.<sup>290</sup>

*Errors in the Derived Structural Parameters*

In determining the individual estimated standard deviations ( $\sigma$ ) of the parameters listed in the Tables of Sections 1.6, 2.5 and 3.4, the covariances of the unit cell parameters were assumed to be zero. The unit cell variances however, were included in the e.s.d. determinations. Furthermore the structural parameters and their e.s.d.'s were not generally corrected for thermal motion anomalies except as where mentioned in the text.

*Mean Observed Parameters and Their Standard Deviations*

The mean parameter values quoted in the text were computed from the designated chemically equivalent internal coordinates as

$$\bar{x} = \frac{\sum_i x_i}{i}$$

where  $\bar{x}$  is the mean observed value,  $x_i$  is an individual observation, and

the sum is taken over all observed values included in the mean. Here  $p_i$  is  $1/n$ ,  $n$  being the total number of observations. Since  $n$  was not normally large enough to give a reliable estimate of the variance  $\bar{\sigma}^2$  from the expression<sup>85,86</sup>

$$\bar{\sigma}^2 = 1/(n(n-1)) \sum_i (x_i - \bar{x})^2,$$

the standard deviation  $\bar{\sigma}$  in the mean observed value  $\bar{x}$  was here determined as

$$\bar{\sigma} = \sigma/n^{1/2}$$

where  $\sigma$  is the maximum e.s.d. found for the individual observations. This was computed (program ORFFE - Appendix I) from the e.s.d.'s in the atomic positional coordinates, which were determined through the least-squares refinement procedure (Section 1.4). The ranges of observed values used in the evaluation of the means  $\bar{x}$  may be obtained from the Tables of Sections 1.6, 2.5 and 3.4.

#### *Torsion Angles and Interplanar Dihedral Angles*

The torsion angles described here as the angles between the planes 1,j,k and j,k,l in the bonded atom chain i-j-k-l were generally assigned positive values if the skew lines  $i \leftrightarrow l$  and  $j \leftrightarrow k$  defined a right-handed helix.<sup>29</sup> For a left-handed helix they were given negative signs.

Finally, the dihedral angles between least-squares planes of four or more atoms listed in Tables 1.5 and 2.5 were computed using the program PLANEH (Appendix I), and the e.s.d.'s for these were not evaluated here.

BIBLIOGRAPHY

1. Sargeson, A.M., *Transition Metal Chem.*, **3**, 303 (1966).
2. Buckingham, D.A. and Sargeson, A.M., *Topics in Stereochem.*, **6**, 219 (1971).
3. Hawkins, C.J., "Absolute Configuration of Metal Complexes", Wiley-Interscience, New York, N.Y., 1971.
4. Corey, E.J. and Bailar, J.C. Jr., *J. Amer. Chem. Soc.*, **81**, 2620 (1959).
5. Dwyer, F.P., Garvan, F.L. and Shulman, A., *J. Amer. Chem. Soc.*, **81**, 290 (1959).
6. Dwyer, F.P., MacDermott, T.E. and Sargeson, A.M., *J. Amer. Chem. Soc.*, **85**, 2913 (1963).
7. Dwyer, F.P., Sargeson, A.M. and James, L.B., *J. Amer. Chem. Soc.*, **86**, 590 (1964).
8. Sargeson, A.M. in "Chelating Agents and Metal Chelates", Chapt. 5, Ed. F.P. Dwyer and D.P. Mellor, Academic Press, New York, N.Y., 1964.
9. Cahn, R.S., Ingold, C.K. and Prelog, V., *Angew Chem., Int. Ed. Engl.*, **5**, 385 (1966).
10. Mizukami, F., Ito, H., Fujita, J. and Saito, K., *Bull. Chem. Soc. Japan*, **45**, 2129 (1972).
11. McCaffery, A.J., Mason, S.F. and Ballard, R.E., *J. Chem. Soc. (A)*, 2883 (1965).
12. McCaffery, A.J., Mason, S.F., Norman, B.J. and Sargeson, A.M., *J. Chem. Soc. (A)*, 1304 (1968).
13. Iwasaki, H. and Saito, Y., *Bull. Chem. Soc. Japan*, **39**, 92 (1966).
14. Butler, K.R. and Snow, M.R., *Chem. Comm.*, 550 (1971).

15. Butler, K.R., Ph.D. Thesis, University of Adelaide (1973).
16. Kobayashi, A., Marumo, F. and Saito, Y., *Acta Cryst.*, *B28*, 3591 (1972).
17. Kobayashi, A., Marumo, F. and Saito, Y., *Acta Cryst.*, *B29*, 2443 (1973).
18. Bijvoet, J.M., Peerdeman, A.F. and Van Bommel, A.J., *Nature*, *168*, 271 (1951).
19. James, R.W., "The Optical Principles of the Diffraction of X-rays", Chapt. 7, Cornell University Press, Ithaca, N.Y., 1965.
20. Buckingham, D.A., Mason, S.F., Sargeson, A.M. and Turnbull, K.R., *Inorg. Chem.*, *5*, 1649 (1966).
21. Bosnich, B. and Harrowfield, J. MacB., *J. Amer. Chem. Soc.*, *94*, 3425 (1972).
22. Denning, R.G. and Piper, T.S., *Inorg. Chem.*, *5*, 1056 (1966).
23. Gillard, R.D., *Inorg. Chim. Acta*, *1*, 69 (1967).
24. Mizukami, F., Ito, H., Fujita, J. and Saito, K., *Bull. Chem. Soc. Japan*, *44*, 3051 (1971).
25. Beattie, J.K., *Accounts Chem. Res.*, *4*, 253 (1971).
26. Sudmeier, J.L. and Blackmer, G.L., *Inorg. Chem.*, *10*, 2010 (1971).
27. Sudmeier, J.L., Blackmer, G.L., Bradley, C.H. and Anet, F.A.L., *J. Amer. Chem. Soc.*, *94*, 757 (1972).
28. Gollogly, J.R., Hawkins, C.J. and Beattie, J.K., *Inorg. Chem.*, *10*, 317 (1971).
29. Commission on Nomenclature of Inorganic Chemistry, *Inorg. Chem.*, *9*, 1 (1970): *IUPAC Information Bulletin*, *33*, 68 (1968).
30. Ho, F.F.-L. and Reilley, C.N., *Anal. Chem.*, *42*, 600 (1970).

31. Appleton, T.G. and Hall, J.R., *Inorg. Chem.*, *9*, 1807 (1970);  
*ibid.*, *10*, 1717 (1971); *ibid.*, *11*, 117 (1972).
32. Jonasson, I.R., Lincoln, S.F. and Stranks, D.R., *Aust. J. Chem.*,  
*23*, 2267 (1970).
33. Buckingham, D.A., Durham, L. and Sargeson, A.M., *Aust. J. Chem.*,  
*20*, 257 (1967).
34. McCaffery, A.J., Mason, S.F. and Norman, B.J., *Chem. Comm.*, 49 (1965).
35. Larsson, R., Searle, G.H., Mason, S.F. and Sargeson, A.M., *J. Chem.*  
*Soc. (A)*, 1310 (1968).
36. Beddoe, P.G., Harding, M.J., Mason, S.F. and Peart, B.J., *Chem.*  
*Comm.*, 1283 (1971).
37. Bosnich, B. and Harrowfield, J. MacB., *J. Amer. Chem. Soc.*, *94*,  
989 (1972).
38. Butler, K.R. and Snow, M.R., *Inorg. Chem.*, *10*, 1838 (1971).
39. Judkins, R.R. and Royer, D.J., *Inorg. Nuclear Chem. Letters*, *6*,  
305 (1970).
40. Iwata, M., Nakatsu, K. and Saito, Y., *Acta Cryst.*, *B25*, 2562 (1969).
41. Raymond, K.N., Corfield, P.W.R. and Ibers, J.A., *Inorg. Chem.*, *7*,  
842 (1968).
42. Lethbridge, J.W., Deut Glasser, L.S. and Taylor, H.F.W., *J. Chem.*  
*Soc (A)*, 1862 (1970).
43. Nagao, R., Marumo, F. and Saito, Y., *Acta Cryst.*, *B29*, 2438 (1973).
44. Freeman, H.C., *Adv. Protein Chem.*, *22*, 257 (1967).
45. Raymond, K.N., Corfield, P.W.R. and Ibers, J.A., *Inorg. Chem.*, *7*,  
1362 (1968).



46. Raymond, K.N. and Ibers, J.A., *Inorg. Chem.*, **7**, 2333 (1968).
47. Pratt Brock, C. and Ibers, J.A., *Acta Cryst.*, **B29**, 2426 (1973).
48. Snow, M.R., *J. Amer. Chem. Soc.*, **92**, 3610 (1970).
49. Buckingham, D.A., Maxwell, I.E., Sargeson, A.M. and Snow, M.R., *J. Amer. Chem. Soc.*, **92**, 3617 (1970).
50. Gollogly, J.R. and Hawkins, C.J., *Inorg. Chem.*, **8**, 1168 (1969).
51. Niketić, S.R. and Woldbye, F., *Acta Chem. Scand.*, **27**, 621 (1973).
52. Williams, J.E., Stang, P.J. and Schleyer, P. von R., *Ann. Rev. Phys. Chem.*, **19**, 531 (1968).
53. Jacob, E.J., Thompson, H.B. and Bartell, L.S., *J. Chem. Phys.*, **47**, 3736 (1967).
54. Boyd, R.H., *J. Chem. Phys.*, **49**, 2574 (1968).
55. Wiberg, K.B., *J. Amer. Chem. Soc.*, **87**, 1070 (1965).
56. Dwyer, M., Geue, R.J. and Snow, M.R., *Inorg. Chem.*, **12**, 2057 (1973).
57. Brubaker, G.R. and Euler, R.A., *Inorg. Chem.*, **11**, 2357 (1972).
58. Williams, D.E., *Acta Cryst.*, **A25**, 464 (1969).
59. Williams, D.E., *Acta Cryst.*, **A28**, 629 (1972).
60. Gollogly, J.R. and Hawkins, C.J., *Inorg. Chem.*, **9**, 576 (1970).
61. Gollogly, J.R. and Hawkins, C.J., *Inorg. Chem.*, **11**, 157 (1972).
62. Gollogly, J.R., Hawkins, C.J. and Beattie, J.K., *Inorg. Chem.*, **10**, 317 (1971).
63. Weakliem, H.A. and Hoard, J.L., *J. Amer. Chem. Soc.*, **81**, 549 (1959).
64. Lee, B., *Inorg. Chem.*, **11**, 1072 (1972).
65. Mazurek, W., Phillip, A.T., Geue, R.J. and Snow, M.R., *Technical Note 286, Defence Standards Labs., Dept. of Supply, Brunswick, Victoria, 1973.*

66. M.J. O'Connor, private communication.
67. Brush, J.R., Magee, R.J., O'Connor, M.J., Teo, S.B., Geue, R.J. and Snow, M.R., *J. Amer. Chem. Soc.*, *95*, 2034 (1973).
68. Piper, T.S. and Karipades, A., *Mol. Phys.*, *5*, 475 (1962).
69. Karipades, A. and Piper, T.S., *J. Chem. Phys.*, *40*, 674 (1964).
70. Richardson, F.S., *J. Phys. Chem.*, *75*, 692 (1971).
71. Richardson, F.S., *Inorg. Chem.*, *11*, 2366 (1972).
72. Strickland, R.W. and Richardson, F.S., *Inorg. Chem.*, *12*, 1025 (1973).
73. Moffitt, W., *J. Chem. Phys.*, *25*, 1189 (1956).
74. Dwyer, M. and Searle, G.H., *Chem. Comm.*, 726 (1972).
75. Dwyer, M., personal communication.
76. Geue, R.J. and Snow, M.R., *J. Chem. Soc. (A)*, 2981 (1971).
77. Magee, R.J., Mazurek, W., O'Connor, M.J. and Phillip, A.T., *Aust. J. Chem.*, *27*, 1629 (1974).
78. Majer, J., Springer, V.S. and Kopecka, B., *Chem. Zvesti.*, *20*, 414 (1966).
79. Neal, J.A. and Rose, N.J., *Inorg. Chem.*, *7*, 2405 (1968).
80. Nagao, R., Marumo, F. and Saito, Y., *Acta Cryst.*, *B28*, 1852 (1972).
81. Neal, J.A. and Rose, N.J., *Inorg. Chem.*, *12*, 1226 (1973).
82. Freeman, H.C. and Colomb, M.L., *Chem. Comm.*, 1523 (1970).
83. Rae, A.D., *Acta Cryst.*, *19*, 683 (1965).
84. Hamilton, W.C., *Acta Cryst.*, *8*, 185 (1955).
85. Hamilton, W.C., "Statistics in Physical Science", Ronald Press, New York, N.Y., 1964.
86. Stout, G.H. and Jensen, L.H., "X-ray Structure Determination", Macmillan, London, 1969.

87. "Computing Methods in Crystallography", Ed. J.S. Rollett,  
Pergamon Press, Oxford, 1965.
88. "International Tables for X-ray Crystallography", Vol. II, Ed.  
J.S. Kasper and K. Lonsdale, Kynoch Press, Birmingham, England,  
1972.
89. "Computing Methods and the Phase Problem in X-ray Crystal Analysis",  
Ed. R. Pepinsky, J.M. Robertson and J.C. Speakman, Pergamon  
Press, Oxford, 1961.
90. Hamilton, W.C. and Abrahams, S.C., *Acta Cryst.*, *A26*, 18 (1970).
91. Hamilton, W.C., *Acta Cryst.*, *18*, 502 (1965).
92. "International Tables for X-ray Crystallography", Vol. I, Ed.  
N.F.M. Henry and K. Lonsdale, Kynoch Press, Birmingham, England,  
1969.
93. Pauling, L., "The Nature of the Chemical Bond", 3rd Edtn., Cornell  
Univ. Press, N.Y., 1960.
94. Raymond, K.N., Meek, D.W. and Ibers, J.A., *Inorg. Chem.*, *7*, 1111  
(1968).
95. Kobayashi, A., Marumo, F. and Saito, Y., *Acta Cryst.*, *B28*, 2709  
(1972).
96. Iwata, M. and Saito, Y., *Acta Cryst.*, *B29*, 822 (1973).
97. Doyle, P.A. and Turner, P.S., *Acta Cryst.*, *A24*, 390 (1968).
98. "International Tables for X-ray Crystallography", Vol. III, Ed.  
C.H. Macgillivray, G.D. Rieck and K. Lonsdale, Kynoch Press,  
Birmingham, England, 1968.
99. Stewart, R.F., Davidson, E.R. and Simpson, W.T., *J. Chem. Phys.*,  
*42*, 3175 (1965).

100. Levy, H.A., *Acta Cryst.*, *9*, 679 (1956).
101. Hamilton, W.C. and Ibers, J.A., "Hydrogen Bonding in Solids",  
W.A. Benjamin, Inc., New York, N.Y., 1968.
102. Bondi, A., *J. Phys. Chem.*, *68*, 441 (1964).
103. "CRC Handbook of Chemistry and Physics", Ed. in Chief, R.C.  
Weast, The Chemical Rubber Company, Cleveland, Ohio, 52nd Edn.,  
1971-1972.
104. Merlino, S., *Acta Cryst.*, *B24*, 1441 (1968).
105. Brennan, T. and Bernal, I., *J. Phys. Chem.*, *73*, 443 (1969).
106. Ting-i, L. and Lippard, S.J., *Inorg. Chem.*, *13*, 1791 (1974).
107. Merlino, S., *Acta Cryst.*, *B25*, 2270 (1969).
108. McConnell, J.F. and Schwarz, A., *Acta Cryst.*, *B28*, 1546 (1972).
109. Khare, G.P. and Eisenberg, R., *Inorg. Chem.*, *9*, 2211 (1970).
110. Pierpont, C.G. and Eisenberg, R., *Inorg. Chem.*, *9*, 2218 (1970).
111. Butler, K.R. and Snow, M.R., *Inorg. Nucl. Chem. Letters*, *8*, 541  
(1972).
112. Oonishi, I., Shibata, M., Marumo, F. and Saito, Y., *Acta Cryst.*,  
*B29*, 2448 (1973).
113. Basolo, F. and Pearson, R.G., "Mechanisms of Inorganic Reactions",  
Wiley, New York, N.Y., 1967, p. 633.
114. Akabori, S., Otani, T.T., Marshall, R., Winitz, M. and Greenstein,  
J.P., *Arch. Biochem. Biophys.*, *83*, 1 (1959).
115. Williams, D.H. and Busch, D.H., *J. Amer. Chem. Soc.*, *87*, 4644 (1965).
116. Buckingham, D.A., Marzilli, L.G. and Sargeson, A.M., *J. Amer. Chem.  
Soc.*, *89*, 5133 (1967).

117. Aune, J.P., Maldonado, P., Larcheres, G. and Pierrot, M., *Chem. Comm.*, 1351 (1970).
118. Larcheres, G. and Pierrot, M., *Acta Cryst.*, B27, 442 (1971).
119. Churchill, M.R., *Inorg. Chem.*, 12, 1213 (1973).
120. Gillard, R.D., Mason, R., Payne, N.C. and Robertson, G.B., *J. Chem. Soc. (A)*, 1864 (1969).
121. Van der Helm, D. and Tatsch, C.E., *Acta Cryst.*, B28, 2307 (1972).
122. Cameron, T.S., Prout, K., Rossotti, F.J.C. and Steele, D., *J. Chem. Soc. (Dalton)*, 2626 (1973).
123. Freeman, H.C., Snow, M.R., Nitta, I. and Tomita, K., *Acta Cryst.*, 17, 1463 (1964).
124. Freeman, H.C., *Adv. Protein Chem.*, 22, 257 (1967).
125. Hall, D. and Waters, T.N., *J. Chem. Soc.*, 2644 (1960).
126. Baker, E.N., Hall, D. and Waters, T.N., *J. Chem. Soc. (A)*, 400 (1970).
127. Baker, E.N., Hall, D. and Waters, T.N., *J. Chem. Soc. (A)*, 406 (1970).
128. Ramachandran, G.N. in "Symmetry and Function of Biological Systems at the Macromolecular Level", Nobel Symposium 11 (1968).
129. Mathieson, A.A. and Welsh, H.K., *Acta Cryst.*, 5, 599 (1952).
130. Muir, K.W. in "Molecular Structure by Diffraction Methods", Vol. 1, The Chemical Society, Burlington House, Piccadilly, London, 1973.
131. Barclay, G.A. and Stephens, F.S., *J. Chem. Soc.*, 2027 (1963).
132. Freeman, H.C., "The Biochemistry of Copper", Ed. J. Peisach, P. Aisen and W.E. Blumberg, Academic Press, New York, N.Y., 1966, p. 105.

133. Muto, A., Marumo, F. and Saito, Y., *Acta Cryst.*, *B26*, 226 (1970).
134. Stetter, H. and Böckmann, W., *Chem. Ber.*, *84*, 834 (1951).
135. Bosnich, B. and Harrowfield, J. MacB., *J. Amer. Chem. Soc.*, *93*, 4086 (1971).
136. Mason, S.F. and Norman, B.J., *Chem. Comm.*, 335 (1965).
137. Norden, B., *Acta Chem. Scand.*, *28*, 111 (1972).
138. Vogel, A.I., "Macro and Semimicro Qualitative Analysis", 4th Edtn., Longmans, Green and Co., London, England, 1954, p. 353, 404.
139. "Operational Instructions for the STOE on line automatic 2-circle diffractometer STADI 2", Wissenschaftliche Instrumente, Darmstadt, Germany, 1972.
140. Freeman, H.C., Guss, J.M., Nockolds, C.E., Page, R. and Webster, A., *Acta Cryst.*, *A26*, 149 (1970).
141. Phillips, D.C., *Acta Cryst.*, *7*, 746 (1954).
142. Whittaker, E.J., *Acta Cryst.*, *6*, 222 (1953).
143. Finar, I.L., "Organic Chemistry, Volume I, The Fundamental Principles", Longmans, Green and Co., London, England, 4th Edtn., 1963, p. 402.
144. Cromer, D.T. and Liberman, D., *J. Chem. Phys.*, *53*, 1891 (1970).
145. Yadara, V.S. and Padmanabhan, V.M., *Acta Cryst.*, *B29*, 493 (1973).
146. Okaya, Y., Stemple, N.R. and Kay, M.I., *Acta Cryst.*, *21*, 237 (1966).
147. Ambady, G.K. and Kartha, G., *Acta Cryst.*, *B24*, 1540 (1968).
148. Sugano, S., *J. Chem. Phys.*, *33*, 1883 (1960).
149. Hamer, N.K., *Mol. Phys.*, *5*, 339 (1962).
150. Poulet, H., *J. Chim. Phys.*, *59*, 584 (1962).

151. McCaffery, A.J. and Mason, S.F., *Mol. Phys.*, *6*, 359 (1963).
152. Břrer, T., *Mol. Phys.*, *6*, 541 (1963).
153. Liehr, A.D., *J. Phys. Chem.*, *68*, 665 (1964).
154. Liehr, A.D., *J. Phys. Chem.*, *68*, 3629 (1964).
155. Shinada, M., *J. Phys. Soc. Jap.*, *19*, 1607 (1964).
156. Schřffer, C.E., *Proc. Roy. Soc. (A)*, *297*, 96 (1968).
157. Richardson, F.S., *J. Chem. Phys.*, *54*, 2453 (1971).
158. Richardson, F.S., *Inorg. Chem.*, *10*, 2121 (1971).
159. Strickland, R. and Richardson, F.S., *J. Chem. Phys.*, *57*, 589 (1972).
160. Mason, S.F., *J. Chem. Soc. (A)*, 667 (1971).
161. Schellman, J.A., *J. Chem. Phys.*, *44*, 55 (1966).
162. Condon, E.U., Altar, W. and Eyring, H., *J. Chem. Phys.*, *5*, 753 (1937).
163. Tinoco, I., *Adv. Chem. Phys.*, *4*, 113 (1962).
164. Hřhn, E.G. and Weigang, O.E., *J. Chem. Phys.*, *48*, 1127 (1968).
165. Ballard, R., McCaffery, A. and Mason, S.F., *Proc. Chem. Soc.*, 331 (1962).
166. McCaffery, A.J. and Mason, S.F., *Mol. Phys.*, *6*, 359 (1963).
167. Yamada, S. and Tsuchida, R., *Bull. Chem. Soc. Jap.*, *33*, 98 (1960).
168. Dingle, R., *Chem. Comm.*, 304 (1965).
169. Dingle, R. and Ballhausen, C.J., *Mat. Fys. Medd. Dan. Vid. Selsk.*, *35*, No. 12 (1967).
170. Denning, R.G., *Chem. Comm.*, 120 (1967).
171. Russel, R.L. and Douglas, B.E., *Inorg. Chim. Acta*, *3*, 426 (1969).
172. Judkins, R.R. and Royer, D.J., *Inorg. Chem.*, *13*, 945 (1974).
173. Hawkins, C.J. and Larsen, E., *Acta Chem. Scand.*, *19*, 185, 1969 (1965).

174. Wellman, K.M., Mungall, W., Mecca, T.G. and Hare, C.R., *J. Amer. Chem. Soc.*, *89*, 3647 (1967).
175. Martin, R.B., Tsangaris, J.M. and Chang, J.W., *J. Amer. Chem. Soc.*, *90*, 821 (1968).
176. Mason, S.F., *Chem. Comm.*, 856 (1969).
177. Schäffer, C.E., *Structure and Bonding*, *5*, 68 (1968).
178. Ham, F.S., *Phys. Rev. (A)*, *138*, 1727 (1965).
179. Gillard, R.D., *Progr. Inorg. Chem.*, *7*, 215 (1966).
180. Kirschner, S., *Coord. Chem. Rev.*, *2*, 461 (1967).
181. Woldbye, F., "Studier Over Optisk Aktivitet", Polyteknisk Forlag, Copenhagen, Denmark, 1969.
182. Mason, S.F., *Quart. Rev.*, *17*, 20 (1963).
183. Voigt, W., *Ann. Phys.*, *18*, 649 (1905).
184. Mathieu, J.P., *Ann. Phys., Series 11*, *3*, 371 (1935).
185. Mathieu, J.P., *J. Chim. Phys.*, *33*, 78 (1936).
186. Fresnel, A., *Ann. Chim. Phys.*, *28*, 147 (1825).
187. Rosenfeld, L., *Z. Physik*, *52*, 161 (1928).
188. Condon, E.U., *Rev. Mod. Phys.*, *9*, 432 (1937).
189. Moffitt, W. and Moscovitz, A., *J. Chem. Phys.*, *30*, 648 (1959).
190. Iwata, M., Nakatsu, K. and Saito, Y., *Acta Cryst.*, *B25*, 2562 (1969).
191. Nakatsu, K., *Bull. Chem. Soc. Japan*, *35*, 832 (1962).
192. Hodgson, D.J., Hale, P.K. and Hatfield, W.E., *Inorg. Chem.*, *10*, 1061 (1971).
193. Deusler, E.N. and Raymond, K.N., *Inorg. Chem.*, *10*, 1486 (1971).
194. Enemark, J.H., Quinby, M.S., Reed, L.L., Steuck, M.J. and Walthers, K.K., *Inorg. Chem.*, *9*, 2397 (1970).



195. Veal, J.T. and Hodgson, D.J., *Inorg. Chem.*, *11*, 597 (1972).
196. Witiak, D., Clardy, J.C. and Martin, D.S. Jr., *Acta Cryst.*, *B28*, 2694 (1972).
197. Nakatsu, K., Saito, Y. and Kuroya, H., *Bull. Chem. Soc. Japan*, *29*, 428 (1956).
198. Nakatsu, K., Shiro, M., Saito, Y. and Kuroya, H., *Bull. Chem. Soc. Japan*, *30*, 158 (1957).
199. McCaffery, A.J., Mason, S.F. and Norman, B.J., *Chem. Comm.*, 661 (1966).
200. Condon, E.U. and Shortley, G.H., "The Theory of Atomic Spectra", Cambridge University Press, New York, N.Y., 1951.
201. Palmer, R.A. and Piper, T.S., *Inorg. Chem.*, *5*, 864 (1966).
202. Orgel, L.E., *J. Chem. Soc.*, *8*, 3683 (1961).
203. Drouard, E. and Mathieu, J.P., *Compt. rend.*, *236*, 2395 (1953).
204. Smith, H.L. and Douglas, B.E., *J. Amer. Chem. Soc.*, *86*, 3885 (1964).
205. Mason, S.F. and Norman, B.J., *Proc. Chem. Soc.*, 339 (1964).
206. Larsson, R., Mason, S.F. and Norman, B.J., *J. Chem. Soc. (A)*, 301 (1966).
207. Mason, S.F. and Norman, B.J., *J. Chem. Soc. (A)*, 307 (1966).
208. Smith, H.L. and Douglas, B.E., *Inorg. Chem.*, *5*, 784 (1966).
209. Sarneski, J.E. and Urbach, F.L., *J. Amer. Chem. Soc.*, *93*, 884 (1971).
210. Beddoe, P.G. and Mason, S.F., *Inorg. Nucl. Chem. Lett.*, *4*, 433 (1968).
211. Gollogly, J.R. and Hawkins, C.J., *Chem. Comm.*, 689 (1968).
212. Bürer, T., *Helv. Chim. Acta*, *46*, 2388 (1963).
213. Ito, M., Marumo, F. and Saito, Y., *Inorg. Nucl. Chem. Lett.*, *6*, 519 (1970).

214. Ito, M., Marumo, F. and Saito, Y., *Acta Cryst.*, *B27*, 2187 (1971).
215. Poland, D. and Scheraga, H.A., *Biochemistry*, *6*, 3791 (1967).
216. Del Re, G., *J. Chem. Soc.* 4031 (1958).
217. Del Re, G., *Theoret. Chim. Acta*, *1*, 188 (1963).
218. Del Re, G., "Electronic Aspects of Biochemistry", Academic Press, New York, N.Y., 1963.
219. Berthod, H. and Pullman, A., *J. Chim. Phys.*, *62*, 942 (1965).
220. Scheraga, H.A., *Advan. Phys. Org. Chem.*, *6*, 103 (1968).
221. Gibson, K.D. and Scheraga, H.A., *Proc. Natl. Acad. Sci., U.S.*, *58*, 420 (1967).
222. Gibson, K.D. and Scheraga, H.A., *Proc. Natl. Acad. Sci., U.S.*, *58*, 1317 (1967).
223. Westheimer, F.H. and Mayer, J.E., *J. Chem. Phys.*, *14*, 733 (1946).
224. Westheimer, F.H., "Steric Effects in Organic Chemistry", Chapt. 12, M.S. Newman, Wiley, New York, N.Y., 1956.
225. Ramachandran, G.N., Ramakrishnan, C. and Sasisekharan, V., *J. Mol. Biol.*, *7*, 95 (1963).
226. Brant, D.A. and Flory, P.J., *J. Amer. Chem. Soc.*, *87*, 2791 (1965).
227. Brant, D.A., Miller, W.G. and Flory, P.J., *J. Mol. Biol.*, *23*, 47 (1967).
228. Scott, R.A. and Scheraga, H.A., *J. Chem. Phys.*, *42*, 2209 (1965).
229. Scott, R.A. and Scheraga, H.A., *J. Chem. Phys.*, *44*, 3054 (1966).
230. De Santis, P., Giglio, E., Liquori, A.M. and Ripamonti, A., *J. Polymer Sci., A*, *1*, 1383 (1963).

231. Sasisekharan, V., Lakshminarayanan, A.V. and Ramachandran, G.N. in "Conformation of Biopolymers", p. 641, Ed. G.N. Ramachandran, Academic Press, London, 1967.
232. Rao, V.S.R., Sundararajan, P.R., Ramakrishnan, C. and Ramachandran, G.N., *ibid.*, p. 721.
233. Williams, D.E., *Science*, *147*, 605 (1965).
234. Williams, D.E., *Acta Cryst.*, *21*, 340 (1966).
235. Giglio, E. and Liquori, A.M., *Acta Cryst.*, *22*, 437 (1967).
236. Damiani, A., Giglio, E., Liquori, A.M. and Mazzarella, L., *Nature*, *215*, 1161 (1967).
237. Warshel, A. and Lifson, S., *J. Chem. Phys.*, *53*, 582 (1970).
238. Lifson, S. and Warshel, A., *J. Chem. Phys.*, *49*, 5116 (1968).
239. Hagler, A.T. and Lifson, S., *Acta Cryst.*, *B30*, 1336 (1974).
240. Williams, D.E., *J. Chem. Phys.*, *45*, 3770 (1967).
241. Williams, D.E., *Trans. Amer. Cryst. Assoc.*, *6*, 21 (1970).
242. Williams, D.E., *Acta Cryst.*, *A30*, 71 (1974).
243. Coiro, V.M., Giglio, E. and Quagliata, C., *Acta Cryst.*, *B28*, 3601 (1972).
244. Brant, D.A., *Ann. Rev. Biophys. Bioeng.*, *1*, 369 (1972).
245. Huler, E. and Warshel, A., *Acta Cryst.*, *B30*, 1822 (1974).
246. Kitaigorodskii, A.I., *Advan. Struc. Res. Diff. Methods*, *3*, 173 (1970).
247. Mason, R. in "Perspectives in Structural Chemistry", Vol. III, p. 59, Ed. J. Dunitz and J.A. Ibers, Wiley, New York, N.Y., 1970.
248. Dwyer, M., Ph.D. Thesis, Australian National University (1971).

249. Snow, M.R., *J. Chem. Soc. (Dalton)*, 1627 (1972).
250. Niketić, S.R. and Woldbye, F., *Acta Chem. Scand.*, 27, 3811 (1973).
251. Buckingham, D.A., Cresswell, P.J., Dellacchi, R.J., Dwyer, M., Gainsford, G.J., Marzilli, L.G., Maxwell, I.E., Robinson, W.T., Sargeson, A.M. and Turnbull, K.R., *J. Amer. Chem. Soc.*, 86, 1713 (1974).
252. Wilde, D.J., "Optimum Seeking Methods", Prentice-Hall, Englewood Cliffs, N.J., 1964.
253. Bixon, M. and Lifson, S., *Tetrahedron*, 23, 769 (1967).
254. Allinger, N.L., Miller, M.A., Van-Catledge, F.A. and Hirsch, J.A., *J. Amer. Chem. Soc.*, 89, 4345 (1967).
255. Allinger, N.L., Hirsch, J.A., Miller, M.A., Tyminski, I.J. and Van-Catledge, F.A., *J. Amer. Chem. Soc.*, 90, 1199 (1968).
256. Geue, R.J., Dwyer, M. and Snow, M.R., unpublished results.
257. Eliel, E.L., Allinger, N.L., Angyal, S.J. and Morrison, G.A., "Conformational Analysis", Chapt. 1, Interscience, New York, N.Y., 1965.
258. Allinger, N.L., Tribble, M.T., Miller, M.A. and Wertz, D.H., *J. Amer. Chem. Soc.*, 93, 1637 (1971).
259. Wilson, E.B., Jr., Decius, J.C. and Cross, P.C., "Molecular Vibrations", McGraw-Hill, New York, N.Y., 1955.
260. Schachtschneider, J.H. and Snyder, R.G., *Spectrochim. Acta*, 19, 117 (1963).
261. Millen, D.J., *Progr. Stereochem.*, 3, 138 (1962).
262. Pitzer, K.S. and Hollenberg, J.L., *J. Amer. Chem. Soc.*, 75, 2219 (1953).

263. Lowe, J.P., *Progr. Phys. Org. Chem.*, **6**, 1 (1968).
264. Tannebaum, E., Myers, R.J. and Gwinn, N.D., *J. Chem. Phys.*, **25**, 42 (1956).
265. Hirschfelder, J.O., Curtiss, C.F. and Bird, R.B., "Molecular Theory of Gases and Liquids", Wiley, New York, N.Y., 1954.
266. Hirschfelder, J.O., *Intermolecular Forces*, *Adv. Chem. Phys.*, **12** (1967).
267. Nakagawa, I. and Shimanouchi, T., *Spectrochim. Acta*, **22**, 759, 1707 (1966).
268. Fujita, J., Martell, A.E. and Nakamoto, K., *J. Chem. Phys.*, **36**, 339 (1962).
269. Thomas, O., *Discuss. Faraday Soc.*, No. 9, 339 (1950).  
Jensen, H.H. and Cyvin, S.Y., *Acta Chem. Scand.*, **23**, 3168 (1969).
270. Liquori, A.M., Damiani, A. and Elefante, G., *J. Mol. Biol.*, **33**, 439 (1968).
271. De Coen, J.L., Elefante, G., Liquori, A.M. and Damiani, A., *Nature*, **216**, 910 (1967).
272. Hilderbrandt, R.L., *J. Chem. Phys.*, **51**, 1654 (1969).
273. Nomura, T., Marumo, F. and Saito, Y., *Bull. Chem. Soc. Japan*, **42**, 1016 (1969).
274. Keene, F.R., Searle, G.H., Yoshikawa, Y., Imai, A. and Yamasaki, K., *Chem. Comm.*, 784 (1970).
275. Keene, F.R., Searle, G.H. and Mason, S.F., *Chem. Comm.*, 893 (1970).
276. Keene, F.R. and Searle, G.H., *Inorg. Chem.*, **11**, 148 (1972).
277. Kobayashi, M., Marumo, F. and Saito, Y., *Acta Cryst.*, **B28**, 470 (1972).
278. Konno, M., Marumo, F. and Saito, Y., *Acta Cryst.*, **B29**, 739 (1973).

279. Delépine, M., Bull. Soc. Chim. France, Series 5, 1, 1256 (1934).
280. Delépine, M. and Charronat, R., Bull. Soc. France Mineral, 53, 73 (1930).
281. Werner, A., Ber., 45, 1228 (1912).
282. Jaeger, F.M., Bull. Soc. Chim. France, Series 5, 4, 1201 (1937).
283. O'Connor, B.H. and Hale, D.H., Acta Cryst., 21, 705 (1966).
284. Beevers, C.A. and Lipson, H., Z. Krist., 83, 123 (1932).
285. Snow, M.R., personal communication.
286. "FORTRAN Reference Manual for Control Data 6000 Series Computer Systems operating under SCOPE Version 3.4", Control Data Corporation (CDC) Sunnyvale, California, 1972.
287. "SCOPE Reference Manual Version 3.4 for Control Data 6000 Series Computer Systems", CDC, Sunnyvale, California, 1974.
288. "LOADER Reference Manual under SCOPE Version 3.4 for Control Data 6000 Series Computer Systems", CDC, Sunnyvale, California, 1974.
289. "SUBROUTINE GELS", IBM Scientific Subroutines Package, IBM Corporation, Poughkeepsie, N.Y.
290. "International Tables for X-ray Crystallography", Vol. IV, Ed. J.A. Ibers and W.C. Hamilton, Kynoch Press, Birmingham, England, 1974.
-